THE BEHAVIOUR OF WIRE ROPE

by

Mohd. Amin Bin Mohd. Sura

A thesis submitted in accordance with the requirements
of the University of Liverpool for the
Degree of Doctor in Philosophy

Department of Mechanical Engineering,
The University of Liverpool.

Liverpool August, 1984

بِسْمِ اللّٰهِ الرَّحْمٰنِ الرَّحِيْمِ

اِقْرَاْ بِاسْمِ رَبِّكَ الَّذِيْ خَلَقَ ۚ ① خَلَقَ الْاِنْسَانَ مِنْ عَلَقٍ ۚ ②
اِقْرَاْ وَرَبُّكَ الْاَكْرَمُ ۙ ③ الَّذِيْ عَلَّمَ بِالْقَلَمِ ۙ ④ عَلَّمَ الْاِنْسَانَ
مَا لَمْ يَعْلَمْ ۗ ⑤

In the name of Allah, the Beneficient,
the Merciful.

Read : In the name of thy Lord Who createth.

Createth man from a clot.

Read : And thy Lord is the most Bounteous,

Who teacheth by the pen,

Teacheth man that which he knew not.

ACKNOWLEDGEMENTS

I would like to register my gratitude towards my supervisor, Professor Norman Jones, for his patient guidance and encouragement and above all for the concern and sympathy he showed particularly during the period of my illness.

I am grateful to the staff of the Computer Laboratory, University of Liverpool, for the advice and assistance that I received during the period of my research.

I would like to thank Dr. W.S Utting for the useful discussions that I had with him on the experimental aspects of the work on wire rope.

My thanks are also due to Miss E. Mooney who typed a large proportion of the thesis and to Mrs. B. Lussey who finished it off from where Miss Mooney left off.

I am also indebted to the University of Malaya, Malaysia, for giving me the necessary study leave and also to the Public Services Department, Malaysia, for providing me with the grant to complete this course of research.

Last but not least, I am particularly grateful to my wife, Rohana and children Aishah, Aiman and Kauthar for the encouragement, support and patience which helped a great deal in ensuring the completion of this thesis.

NOMENCLATURE

a	Semi-minor axis of an ellipse.
b	Semi-major axis of an ellipse.
c	Constant defined by equation (4.1).
h	Pitch of a helical wire.
k	Ratio of Semi-major axis to semi-minor axis of an ellipse.
l	Length of a helical wire.
m	Number of wires in a strand.
n	Defined by equation (3.25).
r	Helix radius.
s	Constant defined in equation (4.2).
x,y,z	Coordinates defined by equation (2.1) and shown in Fig 2.2.
z_1	Perpendicular distance from the tangent plane to any point on the surface of the body near the point of contact.
A	Defined by equation (5.27).
A,B	Constants defined by equations (3.18)a-b.
B,C	Constants defined by equations (2.15)a-b.
D_1	Defined by Equation (3.57).
$\overline{E}$	Generalised strain rate vector.
E(k')	Elliptic integral.
F	Axial load on a strand as illustrated in Fig 2.4a.
F_T	Total axial load.
F(φ',k')	Elliptic integral.
G,G'	Bending moments per unit length in the direction shown in

Fig 2.3.

G_o Defined by equation (5.4)a.

G'_* Defined by equation (5.24)a.

H Twisting moment.

H_{co} Defined by equation (5.39)a.

H_o Defined by equation (5.4)b.

H_* Defined by equation (5.24)b.

$H(\phi',k')$ Elliptic integral.

J Defined by equation (3.24).

K,K' External bending moments per unit length about the x and y axis, respectively.

L Length of strand or core wire.

M Torsional moment.

M_T Total torsional moment.

N,N' Transverse shear forces per unit length.

Q Line contact force per unit length.

Q' Point contact force defined by equation (3.29).

R Radius of an individual wire in a strand.

R_c Radius of core wire.

$\overline{R}$ Radius of wire in the outer layer.

R_1, R_1' Minimum and maximum radii of curvature of the surface of body 1, respectively.

R_2, R_2' minimum and maximum radii of curvature of the surface of body 2, respectively.

T Axial force in a wire.

T_o Defined by equation (3.43).

T_* Defined by equation (7.2)a.

T_{co} Defined by equation (5.39)b.

U_1, U_2 Lines lying in plane sections containing the maximum radii

R_1' and R_2', respectively.

V_1, V_2 Lines lying in plane sections containing the minimum radii R_1 and R_2, respectively.

X, Y, Z External forces per unit length acting in the x,y and z directions, respectively.

X Resultant normal distributed line load acting on the inner strand.

α Helix angle.

α_0 Initial helix angle.

β Angle made by line of action of contact force with line of action of line load X.

β Angle defined in Fig 2.2.

γ Defined by equation (2.29)b.

δ Axial extension of a single pitch of a strand.

ϵ Defined by equation (2.29)a.

ϵ_ω Centre line strain of a wire.

η Displacement of a wire parallel but in a sense opposite to the principal normal vector of a helix. (i.e η is positive in negative x direction).

Θ External twisting moment per unit length.

θ Angle as shown in Fig 2.6b.

κ, κ' Curvatures defined by equations (2.4) and (2.10), respectively.

λ Defined by equation (5.15).

μ Non-dimensionalised external twisting moment.

μ_1, μ_2 Poisson's ratio for bodies 1 and 2, respectively.

ν Poisson's ratio.

ρ Defined by equation (2.29)c.

σ_0 Uniaxial yield stress.

$\sigma_x, \sigma_y, \sigma_z$ Principal stresses at a point on the z-axis and at a distance z from the origin which lies in the surface of contact of two bodies.

τ Twist defined by equation (2.12).

τ_{oc} Octahedral shearing stress.

ϕ Non-dimensionalised axial force defined by equation (5.6).

ω Angle defined in equation (3.2) and shown in Fig 3.3.

χ Non-dimensionalised contact force defined by equation (3.42)

Δ Angular rotation of a single pitch of a strand.

Δs Distance between contact points along the inner lines.

Λ Defined by equation (3.26).

Φ Angle shown in Fig 3.3.

ψ Angle V_1 makes with V_2.

$(\dot{\ })$ $\partial(\ )/\partial t$

$(\bar{\ })$ Refers to the outer strand.

$(^*)$ Derivative with respect to s.

Subscript c Refers to the core.

Subscript T Refers to total values.

TABLE OF CONTENTS

INTRODUCTION

Without doubt wire rope has been recognised as an important engineering component. It plays an important part in our daily lives : we have only to look at our skyscrapers where we are whisked from floor to floor by lifts using wire rope - indeed the construction of such buildings would be very difficult without the use of hoisting equipment utilising this product. Wire rope has found extensive use in the marine environment(1) due to its high flexibility and availability in long lengths as well as superior handling and storage characteristics. It is used in the mooring and towing of ships and exploration rigs, in cranes, power shovels, slings for cargo handling and in construction nets. In fact, wherever a combination of high resistance to tensile loads with low resistance to bending is required, a wire rope is a prime candidate.

From historical evidence, ropes are known to have been used since as early as the Paleolithic Period(2). The art of rope making developed through the centuries, which led eventually to the making of wire ropes which are considerably stronger, will respond to load with little stretch, are much stiffer and are proportionately heavier than the natural or man-made fibre ropes of a given size. A copper cable found in the ruins of Nenevah near Babylon indicates that wire rope was used as a structural element in about 700 B.C(3,4).

Eventhough, wire rope has been around for many centuries, there is still a large area of research required, especially in

developing theoretical methods that can confidently be used to predict the stresses in a wire rope. The knowledge of these stresses is necessary for the proper design of a wire rope. So far, very little has been done to understand the theoretical behaviour of wire rope subjected to plastic loads. Only Jones and Christodoulides(64) have attempted work in this area. The knowledge of the maximum possible load that a rope can support prior to failure would allow an estimate of the reserve strength beyond the elastic range and aid in the selection of a meaningful factor of safety or in the appropriate rope construction. Due to the importance that is placed on the rope breaking load by rope manufacturers and users of wire rope, it is thus necessary to explore further the characteristics of wire rope loaded beyond the elastic limit.

The object of the present work is to extend the work by Jones and Christodoulides(64) and study ropes with more realistic configurations. The assumption that the rope is made of rigid inextensible wires will be removed and the influence of the contact stresses on the strength of the wire rope will be explored.

In Chapter 1, a literature survey of the research done on wire rope is presented.

The basic equations governing a helical wire and a strand are presented in Chapter 2.

Chapters 3 and 4 introduce the contact problem in wire rope and provide values of contact force for line and point contacts

that will cause yield and indentation in the wires. The contact force to produce indentation in the wire is taken as an approximation to the collapse value of χ, which is used to predict the plastic collapse of wire rope in Chapters 5 and 7.

Static plastic collapse of wire rope in which the helical wires are inextensible is presented in Chapter 5 for a single strand, a strand with core wire, a 1X19 rope and a rope with n-layers of strand. A similar analysis but with the inextensible assumption removed, is presented in Chapter 7.

In Chapter 6, equilibrium equations governing helical wires with finite extension is developed and using The Principle of Virtual Work, consistent strain relations are obtained. The results obtained are compared with work by Costello and Phillips(55), which is for a linear elastic case.

In Chapter 8, the theoretical results obtained from the plastic collapse analysis are compared with experimental results, and the conclusions and suggestions for further work are presented in Chapter 9.

CHAPTER 1

Research on wire rope - A literature survey.

One of the earliest works related to wire ropes was carried out by Thomson and Tait(5), who looked at the behaviour of curved wires and applied it in the study of spiral springs. Later Love(6) made an analysis on the kinematics of thin curved rods and the governing equilibrium equations. Basset(7) commented that Love's treatment of the physical portion of the subject was not satisfactory and himself provided a further exposition on the theory of wires.

Apart from the above, the early works on wire rope have been, on the main, experimental in nature. One of the earliest organised research programmes on wire rope was carried out by the Wire Rope Research Committee(8,9,10,11,12) set-up by the British Institution of Mechanical Engineers, with W.A. Scoble as its reporter. It was appointed to investigate the repeated bending of wire ropes over pulleys, sheaves, drums and the like(10). In its first report(8), a thorough literature review was carried out and one of the conclusions arrived at by the committee was that the calculation of the bending stress for design, then, did not appear to be satisfactory. It was suggested that an attempt should be made at an analysis which will separate the three destructive effects, namely, outside wear, wear between the wire and bending fatigue. In the same report, there was also a mention of a work by Howe(13), who developed a method for calculating the Modulus of Elasticity of any strand or rope. In the rest of the reports(9,10,11,12), numerous test results were presented for tests carried out with various sizes and types of wire ropes, running over pulleys with different diameters. A long list of references to the subject could be found in the first(8) and the fifth(12) reports. At about the same time, there was a similar

research programme carried out in Germany under the direction of Dr. Richard Woernle(14). Drucker and Tachau(15) analysed the experimental data obtained by Scoble and Woernle and concluded that the bearing pressure is of far greater importance than nominal bending and direct tensile stresses, in the choosing of wire rope. They demonstrated this by a plot of number of cycles to failure against the dimensionless bearing pressure ratio. Additional test results on the bending of wire ropes are reported in (16,17).

Besides the above experiments, there are various other tests that were carried out on wire rope. De Forest and Hopkins(18) developed test methods for the study of fatigue properties of wire rope. Layland(19) carried out torsion tests on stranded mining wire ropes and arrived at several conclusions including equations for the relationship between tension and torque for a 6/7 ropes. Their validity was checked and confirmed by experiment at different dimensions. Hind(20) determined the transmission losses due to the bending of loaded wire ropes over sheaves in term of rope variables and sheave thread diameter. He found that the transmission loss at a sheave is usually about 1 per cent of rope load and in the worst case, it is about 1.6 per cent of the rope load. Laura, Vanderveldt and Gaffney(21,22) introduced a method of detection of wire rope failure by means of monitoring stress waves emitted during the loading cycle of the cable. Vanderveldt, Chung and Reader(23) described experimental and analytical results on the absorption characteristics of wire rope during the propagation of transverse waves.

In a theoretical paper, Hall(24) developed equations for

axial load on a rope, on a strand and on a wire in terms of rope variables such as lay angle and the number of wires and strands in the rope. But, various assumptions were made : (i) all rope loads are equally distributed amongst the several strands, and all strand loads are equally distributed over the individual wires, (ii) all strands and wires are free from friction and binding, one against the other, (iii) all strands and wires are in full and complete contact with each other and (iv) there is no stretch under load. From the results, he found that stresses in the outer wires for any given load on the rope, are greater than those in the inner wires, so that the outer wires tend to break first. Inspired by the above-mentioned paper, Hruska produced a series of three papers(25,26,27). The first paper(25) is concerned with the calculation of stresses in wire ropes due to tension only. He noted a few disagreements with Hall(24) including the assertion that the wire cores are less stressed. In the second paper(26), he dealt with the radial forces in wire ropes and in the third(27), with tangential forces.

The importance of compressive contact stresses began to be appreciated through the work of Messrs. Drucker, Tachau and Hruska(28). Leissa(28) investigated the contact stresses in wire rope. In his analysis, he used the expression for the radial force derived by Hruska(26) which is expressed as a function of the tensile loading and geometry of the rope, and also the equations obtained by Seely and Smith(29), which relate the three principal compressive stresses due to the compressive radial force, to the load, geometry and elastic properties of the material. He then applied the two failure theories - the maximum-shear-stress theory and the maximum-normal-stress theory, and looked at two critical

regions : (1) along the lines of contact between the individual wires in a strand, and (2) between adjacent wires in neighbouring strands of the wire rope. Starkey and Cress(30) pursued the work by Leissa(28) and his analysis shows that the critical stresses in a wire rope are due largely to contact stresses and are much higher than direct-tensile-stress, the stress which is often used as the primary criterion of failure of wire rope. They performed experiments to investigate fretting and proposed a probable mode of failure of wire rope i.e. propagation of fretting-induced fatigue cracks. Karamchetty and Yuen(31) approached the contact problem geometrically. Contact points developed due to geometry changes while laying and due to loading of the rope are determined and calculations of contact stresses follow the method described by Seely and Smith(29). Karamchetty(32) also considered a small element of a wire as a portion of a torus. An element of the torus containing the contact point is described and tangential sections are obtained which can be used in numerical methods of calculating contact stresses and deformations. The problem of contact is also discussed by Bert and Stein(33) and Durelli, Machida and Parks(34). Dong and Steidel(35) has carried out an experimental study of interstrand contact stresses using the stress-freezing photoelastic technique.

The study of the geometrical characteristics of wires in wire ropes is reported in the work by Karamchetty(36). When a rope is bent into a circular arc, geometrical characteristics of an individual wire are defined and simple strain calculations for such cases are presented. Wire ropes make use of strands with circular and non-circular cross sections. For the wire rope designer, the determination of wire sizes is necessary for all the

elements to fit together easily. Hobbs(37) presented a method of calculation for circular strands and Karamchetty(38) provided a procedure for non-circular strands.

The behaviour of continuous filament yarn has been investigated by many authors. Review of their work is contained in a paper by Hearle(39). Even though these yarns are not used frequently in practice, they are particularly convenient for theoretical and experimental investigations, and could provide valuable insight into the mechanics of wire rope(40). Huang and Funk(41) listed the assumptions made by earlier investigators on small extension of linearly elastic continuous filament yarns with circular cross-sections. In their paper, several assumptions were removed and in the analysis, the equations of equilibrium of curved rods obtained by Huang(42) were employed. This curved rod approach is also used by Huang in his investigation of small deformation of two-ply filament yarn subjected to axial extension(43) and bending(44), finite viscoelastic deformation of two-ply filament yarns(45) and finite extension of elastic strand with a central core(46).

Machida and Durelli(47) carried out a theoretical study on the response of a strand to axial and torsional displacements. Their study is based on the strength of materials approach. They developed explicit expressions for the determination of axial force, bending and twisting moments in the helical wires, and for axial force and twisting moment in the core of a 7-wire strand subjected to axial and torsional displacements. Measurements of strains, stresses and displacements using mechanical and electrical strain gauges, dial gauges and brittle coatings on

oversized epoxy models of strand (48), show good correlation with the theory(47). The above approach is also employed in (49) in the study of a single helix with end load.

An analysis of multiwire strands in tension and combined tension and torsion is reported in the work by Chi(50). A geometrical relationship of deformed and undeformed wire strands is derived. In conjunction with balance laws of forces and moments, the governing equations for computing the strains, elongations, and end rotations of a strand with free or fixed ends and with tensile and torsional loadings are derived.

Of all the study on wire ropes, the analyses performed by Phillips and Costello(51,52,53), like that of Huang's(46), is probably the most rigorous. In their analyses, the rope or strand is separated into thin helical wires and for each wire, Phillips and Costello solved the six equations of equilibrium obtained by Love(6), with Huang using the equations he developed using the principle of virtual work(42). In the work of Phillips and Costello, it is assumed that the cable is loaded by an axial force and an axial twisting moment ; that there are no frictional forces between the wires ; and that in the initial unloaded configuration of the rope, the wires are just touching each other. For the calculation of stresses due to line contact loads(51,52), the equations derived by Lubkin(54) for Hertz contact problem of two parallel cylinders of infinite extent, are employed.

In (55), Costello and Phillips studied the elongation and rotation of a wire rope or strand subjected to an axial force and an axial twisting moment. Even though the inextensibility

assumption is removed, the wire strain is still assumed small, so that the equations of equilibrium for infinitesimal displacements with no finite deflection are valid. A plot of the effective modulus is shown as a function of the original helix angle of a wire where the effective modulus is determined by investigating the slope of the load deflection curve at the origin. Two common types of end-condition are considered i.e. cable ends free to rotate and no end-rotation.

The works by Phillips and Costello reported above are pursued and extended by Phillips, Costello, Miller and Sinha(56,57,58,59,60,61). Phillips and Costello(56) investigated the axial impact of wire cables. The longitudinal impact of a finite length wire rope fixed at one end is considered in detail, and numerical results for this case are presented. Costello and Sinha(57) looked at torsional stiffness in twisted wire cables and in (58), determined the axial, bending and torsional stiffnesses for a strand and then treating this strand as a wire with these properties in the more-complex-cross-section wire rope. The bending stiffness is determined by a theory presented in the work of Costello(62) for the large deflections of a helical spring subjected to bending. Costello and Miller(59) investigated the effect of winding and unwinding of a strand due to twisting moments on the torsional stiffness of the strand. It is found that in the right lay - regular lay rope under tension, a tightening up of wires in the strand is produced resulting in a stiffer rope when compared with the right lay - lang lay rope. Costello and Miller(60) then extended the work above(59) to determine the initial configuration of a rope which will not rotate under an axial load. Phillips, Miller and Costello(61) investigated, in

particular, the localised stresses due to the contact forces between wires in adjacent layers of a stretched, multi layer, cross-lay 1X19 wire rope. In the computation of the contact stresses, the work of Boresi, Sidebottom, et al.(29) has been used. The works above(51,53,55,56,57,59) have also been the basis of the theory developed by Costello and Butson(63) to predict the static response of wire rope subjected to tension, torsion and bending i.e. those loads associated with a rope wrapped around a sheave.

All theoretical works on wire ropes have been studying the behaviour of ropes which are loaded within the elastic range. Only Jones and Christodoulides(64) haveattempted to explore the characteristics of the rope when loaded beyond the elastic limit. The knowledge of the maximum possible load that a rope can support prior to failure would allow an estimate of the reserve strength beyond the elastic range and aid in the selection of a meaningful factor of safety or in the appropriate rope construction. In examining the static plastic collapse of a single strand, the limit theorems of plasticity for infinitesimal displacements are employed.

CHAPTER 2

The strand - Basic equations.

2.1 Definitions

The wire is the basic element of a wire rope. They are laid into a strand and several such strands are laid to form a wire rope. Fig. 2.1 shows the elements of a typical wire rope.

Some ropes may have a strand for a core while others may have some flexible hemp rope or another wire rope.

Wires may be laid either right-handed or left-handed into the strand and the strands in turn are laid either right-handed or left-handed into the rope. Depending on the way they are laid, the ropes are classed as right-hand or left-hand and ordinary or lang's lay.

2.2 Geometry of a Helical Wire

The centre-line of a helical wire may be described by the equations of a right circular helix.

If we define the orthogonal cartesian co-ordinates XYZ as shown in Fig. 2.2, with the radius of the cylinder on which the centre-line of the helical wire is wrapped being r and the pitch being h, the governing equations are [65]:

$$x = r\cos\beta, \quad y = r\sin\beta, \quad z = \frac{h\beta}{2\pi} \qquad (2.1\ a\text{-}c)$$

The helix angle α is defined as

$$\alpha = \tan^{-1}\left(h/2\pi r\right) \qquad (2.2)$$

(2.1 c) can now be rewritten as

$$z = r\beta\tan\alpha \qquad (2.3)$$

2.2.1 Curvatures of a Helical Wire

In a helical wire, when the principal axes of the cross-section are coincident with its principal normal and binormal vectors [65], curvature

$$\kappa = 0 \tag{2.4}$$

Curvature, κ' is defined as [65],

$$\kappa' = \sqrt{\left(\frac{d^2x}{ds^2}\right)^2 + \left(\frac{d^2y}{ds^2}\right)^2 + \left(\frac{d^2z}{ds^2}\right)^2} \tag{2.5}$$

where

$$ds = \sqrt{dx^2 + dy^2 + dz^2} \tag{2.6}$$

Using (2.1 a-b) and (2.3)

$$dx = -r\sin\beta d\beta,\ dy = r\cos\beta d\beta,\ dz = r\tan\alpha d\beta \tag{2.7 a-c}$$

and

$$d^2x = -r\cos\beta d\beta^2,\ d^2y = -r\sin\beta d\beta^2,\ d^2z = 0 \tag{2.8 a-c}$$

From (2.6) and (2.7 a-c),

$$ds = \frac{rd\beta}{\cos\alpha} \tag{2.9}$$

substituting (2.8) and (2.9) into (2.5)

$$\kappa' = \left[\frac{r^2\cos^2\beta d\beta^4\cos^4\alpha}{r^4 d\beta^4} + \frac{r^2\sin^2\beta d\beta^4\cos^4\alpha}{r^4 d\beta^4}\right]^{\frac{1}{2}}$$

or the curvature, $\kappa' = \dfrac{\cos^2\alpha}{r}$ (2.10)

2.2.2 Twist of a Helical Wire

Twist is defined and can be written in determinant form as [65],

$$\tau = \frac{1}{\kappa^2}\begin{vmatrix} \frac{dx}{ds} & \frac{dy}{ds} & \frac{dz}{ds} \\ \frac{d^2x}{ds^2} & \frac{d^2y}{ds^2} & \frac{d^2z}{ds^2} \\ \frac{d^3x}{ds^3} & \frac{d^3y}{ds^3} & \frac{d^3z}{ds^3} \end{vmatrix} \tag{2.11}$$

Using (2.7), (2.8), (2.9) and (2.10) in (2.11),

$$\tau = \frac{r^2}{\cos^4\alpha} \begin{vmatrix} -\sin\beta\cos\alpha & \cos\beta\cos\alpha & \sin\alpha \\ -\frac{\cos\beta\cos^2\alpha}{r} & -\frac{\sin\beta\cos^2\alpha}{r} & 0 \\ \frac{\sin\beta\cos^3\alpha}{r^2} & -\frac{\cos\beta\cos^3\alpha}{r^2} & 0 \end{vmatrix}$$

or the twist of the helical wire

$$\tau = \frac{\sin\alpha\cos\alpha}{r} \qquad (2.12)$$

2.3 Equilibrium Equations for a Helical Wire

Consider a curved bar as shown in Fig. 2.3. The axis of Z, of the orthogonal cartesian co-ordinates XYZ is directed along the tangent to the centre-line, and the axes of X and Y are coincident with its principal normal and binormal vectors.

The forces N and N' are shearing forces, the force, T is the tension, the couples G and G' are flexural couples and the couple H is the torsional couple.

Let us apply forces to the rod which are estimated by means of their force and couple resultants per unit length of the central-line. The components of these resultants referred to the principal torsion-flexure axes of the bar are X, Y, Z and K, K',θ respectively.

If we disregard the extension of the bar, and assume that the resultant components of curvature and twist are κ, κ' and τ respectively, then the force and moment equilibrium of the curved bar is given by [6],

$$\frac{dN}{ds} - N'\tau + T\kappa' + X = 0$$

$$\frac{dN'}{ds} - T\kappa + N\tau + Y = 0$$

$$\frac{dT}{ds} - N\kappa' + N'\kappa + Z = 0$$

$$\frac{dG}{ds} - G'\tau + H\kappa' - N' + K = 0 \qquad (2.13\ a\text{-}f)$$

$$\frac{dG'}{ds} - H\kappa + G\tau + N + K' = 0$$

$$\frac{dH}{ds} - G\kappa' + G'\kappa + \theta = 0$$

By a generalisation of the 'Bernoulli-Eulerian'[¥] theory, the stress-couples G, G' and H are connected with the curvature and twist of the curved bar by the equations of the form [7],

$$G = A\,d\kappa,\quad G' = B\,d\kappa',\quad H = C\,d\tau \qquad (2.14\ a\text{-}c)$$

where A, B and C are constants depending on the elastic quality of the material and the shape and dimensions of the cross-section.

In the case of a helical wire, which in most wire ropes has a circular cross-section, the cross-section of the wire has kinetic symmetry, and therefore A = B.

For a helical wire with circular cross-section, the constant B and C are

$$B = \frac{\pi E R^4}{4}, \qquad C = \frac{\pi E R^4}{4(1+\nu)} \qquad (2.15\ a\text{-}c)$$

where E is the Young's modulus of elasticity, ν is the Poisson ratio and R is the radius of the wire.

¥ This theory attributes the resistance to flexure of beams entirely to extension and contraction of the longitudinal filaments. Saint-Venant then brought the problems of the torsion and flexure of beams under a general theory. (For a historical development of the theory on beams, see Reference (6)).

Therefore (2.14) becomes,

$$G = \frac{\pi ER^4}{4} d\kappa, \qquad G' = \frac{\pi ER^4}{4} d\kappa', \qquad H = \frac{\pi ER^4}{4(1+\nu)} d\tau \tag{2.16}$$

If the helical wire is not subjected to external bending and torsional moments per unit length, i.e. $K = K' = \Theta = 0$, and that when loaded behaves identically at all sections (which requires the vanishing of all derivatives with respect of s), (2.13) and (2.4) gives

$$G = N = Z = Y = 0 \tag{2.17}$$

and

$$-N'\tau + T\kappa' + X = 0 \tag{2.18}$$

$$-G'\tau + H\kappa' - N' = 0 \tag{2.19}$$

As derived in Section 2.2, the curvature, κ' and twist, τ are given by

$$\kappa' = \frac{\cos^2\alpha}{r} \tag{2.20}$$

$$\tau = \frac{\sin\alpha\cos\alpha}{r} \tag{2.21}$$

where α is the helix angle and r is the helix radius of the helical wire.

2.4 Axial and Torsional Equilibrium of a Strand

Let us now lay these helical wires to form a strand, as shown in Fig. 2.4a. We apply, at its ends, an axial load, F and a torsional moment, M. The direction of the moments G' and H and the forces N' and T in one of the wires is shown in Fig. 2.4b.

The axial and torsional equilibrium of the entire strand in Fig. 2.4a will then require

$$F = m(T\sin\alpha + N'\cos\alpha) \tag{2.22}$$

and

$$M = m(H\sin\alpha + G'\cos\alpha + rT\cos\alpha - rN'\sin\alpha) \tag{2.23}$$

respectively, where m is the number of wires in the strand.

2.5 Consistent Strain Relations

If we define δ and Δ as the axial extension and the angular rotation of one pitch (h) of a strand, respectively, η, as the displacement of a wire parallel but in a sense opposite to the principal normal direction (X) (Fig. 2.5), and ε_ω as the centre-line strain of a single wire, then by the principle of virtual work, we can write

$$\dot{F}\dot{\delta} + \dot{M}\dot{\Delta} - m\int_o^{\ell} X\dot{\eta}\, ds = m\int_o^{\ell}(T\dot{\varepsilon}_\omega + G'\dot{\kappa}' + H\dot{\tau})ds \tag{2.24}$$

since $\kappa = 0$ (equation 2.4).

Here, we will consider a case where there is no axial extension of the wire and in arriving at the equilibrium equations (2.13) we have also disregarded this extension.

Therefore,

$$\varepsilon_\omega = 0$$

Referring to Fig. 2.2b,

$$\ell = \sqrt{h^2 + (2\pi r)^2} = h/\sin\alpha \tag{2.25}$$

If the wires in the strand behave identically at all sections, and we use (2.18),(2.19),(2.20), (2.21),(2.22),(2.23) and (2.25) in (2.24), we will have

$$\left[T\sin\alpha + H\frac{\cos^3\alpha}{r} - G'\frac{\sin\alpha\cos^2\alpha}{r}\right]\dot{\delta}$$

$$+ \left[H\sin\alpha + G'\cos\alpha + rT\cos\alpha + G'\sin^2\alpha\cos\alpha - H\sin\alpha\cos^2\alpha\right]\dot{\Delta}$$

$$= \frac{h}{\sin\alpha}\left\{\left[H\frac{\sin\alpha\cos^3\alpha}{r^2} - G'\frac{\sin^2\alpha\cos^2\alpha}{r^2} - T\frac{\cos^2\alpha}{r}\right]\dot{\eta}\right.$$

$$\left. + G'\dot{\kappa}' + H\dot{\tau}\right\} \tag{2.26}$$

If G', H and T are non-zero, we can group their coefficients together and make them equal zero. Thus, collecting the coefficients of T, we have

$$\frac{\sin^2\alpha}{h}\dot{\delta} + \frac{r\sin\alpha\cos\alpha}{h}\dot{\Delta} + \frac{\cos^2\alpha}{r}\dot{\eta} = 0 \qquad (2.27)$$

Therefore,

$$\dot{\varepsilon}\sin^2\alpha + \dot{\gamma}\cos^2\alpha + \dot{\rho}\cos^2\alpha = 0 \qquad (2.28)$$

where

$$\varepsilon = \delta/h,\ \gamma = \Delta/2\pi,\ \rho = \eta/r \qquad (2.29)$$

collecting the coefficients of G', we have

$$-\frac{\sin^2\alpha\cos^2\alpha}{hr}\dot{\delta} + \frac{\sin\alpha\cos\alpha}{h}\dot{\Delta} + \frac{\sin^3\alpha\cos\alpha}{h}\dot{\Delta}$$

$$+\frac{\sin^2\alpha\cos^2\alpha}{r^2}\dot{\eta} - \dot{\kappa}' = 0 \qquad (2.30)$$

By virtue of (2.29), (2.30) becomes

$$\dot{\kappa}' = -\dot{\varepsilon}\frac{\sin^2\alpha\cos^2\alpha}{r} + \dot{\gamma}\frac{\cos^2\alpha}{r} + \dot{\gamma}\frac{\sin^2\alpha\cos^2\alpha}{r}$$

$$+\dot{\rho}\frac{\sin^2\alpha\cos^2\alpha}{r}$$

Therefore,

$$\dot{\kappa}' = \frac{\sin^2\alpha\cos^2\alpha}{r}(\dot{\gamma} - \dot{\varepsilon} + \dot{\rho}) + \dot{\gamma}\frac{\cos^2\alpha}{r} \qquad (2.31)$$

Similarly, collecting the coefficients of H, we have

$$\frac{\sin\alpha\cos^2\alpha}{hr}\dot{\delta} + \frac{\sin^2\alpha}{h}\dot{\Delta} - \frac{\sin^2\alpha\cos^2\alpha}{h}\dot{\Delta}$$

$$-\frac{\sin\alpha\cos^3\alpha}{r^2}\dot{\eta} - \dot{\tau} = 0$$

and therefore

$$\dot{\tau} = -\frac{\sin\alpha\cos^3\alpha}{r}(\dot{\gamma} - \dot{\varepsilon} + \dot{\rho}) + \dot{\gamma}\frac{\sin\alpha\cos\alpha}{r} \qquad (2.32)$$

Equations (2.28), (2.31) and (2.32) are therefore consistent with the equilibrium equations (2.13), according to the Principle of

virtual work. These relations can also be derived geometrically by considering an axial extension, an angular rotation and a change in the helix radius when the helical wire is loaded (Appendix 1).

2.6 Geometrical Relation Between α and r for an m-Strand

We will consider a strand made up of m wires and the wires are touching each other. A transverse section of the strand yields wire cross-sections that are approximately elliptical¥ (Fig. 2.4c).

We can therefore define the cross-section of the wire (Fig. 2.6) by

$$\left(\frac{x}{a}\right)^2 + \left(\frac{y}{b}\right)^2 = 1 \qquad (2.33)$$

Therefore,

$$\frac{x}{y} = \sqrt{\left(\frac{a}{y}\right)^2 - \left(\frac{a}{b}\right)^2} \qquad (2.34)$$

Differentiating (2.33) with respect to x, we have

$$\frac{2x}{a^2} + \frac{2y}{b^2} \cdot \frac{dy}{dx} = 0$$

therefore,

$$\frac{dy}{dx} = -\frac{x}{y}\left(\frac{b}{a}\right)^2 \qquad (2.35)$$

But referring to Fig. 2.6,

$$\frac{dy}{dx} = -\tan\theta \qquad (2.36)$$

substituting (2.34) and (2.36) into (2.35) we have,

$$\tan\theta = \left(\frac{b}{a}\right)^2 \sqrt{\left(\frac{a}{y}\right)^2 - \left(\frac{a}{b}\right)^2}$$

¥ It should be noted that this is only valid for certain values of α. For the special cases when α = 0° and α=90°, the cross-sections are as shown in Fig. 2.7.

$$\left(\frac{a}{b}\right)^4 \tan^2\theta = \left(\frac{a}{y}\right)^2 - \left(\frac{a}{b}\right)^2$$

$$\frac{1}{y^2} = \frac{1}{b^2}\left[1 + \left(\frac{a}{b}\right)^2 \tan^2\theta\right]$$

therefore,

$$y = \frac{b}{\sqrt{1 + \left(\frac{a}{b}\right)^2 \tan^2\theta}} \tag{2.37}$$

substituting (2.37) into (2.34) we have

$$x = a\sqrt{\frac{\left(\frac{a}{b}\right)^2 \tan^2\theta}{1+\left(\frac{a}{b}\right)^2 \tan^2\theta}} \tag{2.38}$$

From Fig. 2.6b, if (x,y) are the co-ordinates of the point of contact between the wires,

$$\tan\theta = \frac{r-y}{x} \tag{2.39}$$

substituting (2.37) and (2.38) into (2.39)

$$r = \frac{b + a\sqrt{\left(\frac{a}{b}\right)^2 \tan^4\theta}}{\sqrt{1 + \left(\frac{a}{b}\right)^2 \tan^2\theta}} \tag{2.40}$$

But $a = \frac{R}{\sin\alpha}$, $b = R$ and since there are m wires $\theta = \frac{\pi}{2} - \frac{\pi}{m}$

therefore

$$\frac{r}{R} = \sqrt{1 + \frac{\tan^2\left(\frac{\pi}{2} - \frac{\pi}{m}\right)}{\sin^2\alpha}} \tag{2.41}$$

Equation (2.41) is the same equation obtained by Phillip and Costello [51].

CHAPTER 3

Contact problem in wire rope.

3.1 Introduction

The importance of the role that contact stresses play in determining the failure of a wire rope cannot be over-emphasised. A number of works directed in this area have been described in Chapter 1.

The theory on contact stresses is attributed to Hertz [66], who derived mathematical expressions for the distribution of pressure on the contact area of bodies having an initial point contact. He was able to determine the limiting size of the axes of the elliptical contact area and the relative displacements of the bodies. For circular areas of contact, he was able to determine the stress in the centre of the area and for bodies having initial line contact, he obtained expressions defining the width of the contact strip and the pressure distribution across the strip. Hertz verified his analysis by determining the areas of contact between a spherical glass lens and a glass plate at various loads and also between crossed cylindrical glass rods. Since the measured areas showed good agreement with those calculated, he took this as a check also of the stress components.

For over 100 years, since the theory was first developed, it has been a basis for the many studies related to contact problems [67]. Thomas and Hoersch [68] extended Hertz's work and determined the law of distribution for the stress components along the z-axis in the plane of symmetry of the loading curve (Fig. 3.1). They were able to express the expressions obtained by Hertz in terms of $F(\varphi',k')$ and $E(\varphi',k')$, the elliptic integrals of the first and second kind for which tables have been computed. They found that the maximum

shearing stress in the zone of contact is at some distance below the contact surface. By using Fry-strain-etch method¥, they were able to verify the mathematical computation for crossed cylinders.

Seely and Smith [29] utilise Thomas and Hoersch's work in one of the chapters in their book. They were able to present the theory in a more comprehensive manner and probably due to this, their book has become a common reference used by investigators studying contact stresses in wire ropes (see Chapter 1).

In wire ropes, primarily there are two types of contact:

1) line contact - produced by contact between individual wires in a strand and,
2) point contact - produced by contact between adjacent wires in neighbouring strands of the wire rope.

In this chapter, both types of contact will be looked at and values of contact force that will cause the wire to yield will be obtained.

3.2 Contact Theory (based largely upon Thomas and Hoersch's(68) work)

3.2.1 Principal Radii of Curvature

Consider two bodies being pressed together by forces Q', as shown in Fig. 3.2. The load Q' lies along the axis which passes through the centres of the bodies and through the point of contact and is perpendicular to a plane which is tangent to both bodies at the point of contact. The two bodies are initially in contact at a single point, and the effect of the load Q' is to cause the surface

¥ After the material has been subjected to a stress exceeding the yield point, it is heated for half an hour at approximately 400°F. The specimen may then be cut and then etched with a solution of cupric chloride in hydrochloric acid and water. Regions which have been overstressed will etch darker than the remainder of the section.

of the bodies to be deformed elastically over a region surrounding the initial point of contact, thereby bringing the two bodies into contact over a small area as shown in Fig. 3.2. The points which come into contact simultaneously are points on the two surfaces which were initially equal distances apart.

Let the minimum and maximum radii of curvature of the surface of the body 1 at the point of contact be R_1 and R_1' respectively and for the body 2 be R_2 and R_2' respectively. These are called the principal radii of curvature of the surface.

Now consider only body 1 assuming that the bodies are free from loads and are in contact at a point as shown in Fig. 3.3. In Fig. 3.2a, lines V_1 and V_2 lie in the plane sections containing the minimum radii R_1 and R_2, respectively and lines U_1 and U_2 lie in the plane sections containing the maximum radii R_1' and R_2' respectively. Line V_1 makes an angle ϕ with line V_2.

From Fig. 3.3

$$JP = {}^{u_1}/\tan \Phi \tag{3.1}$$

$$\tan \omega = \frac{R_1' - JP}{u_1} \tag{3.2}$$

$$\therefore \quad \tan \omega = \frac{R_1'}{u_1} - \frac{1}{\tan \Phi}$$

$$= \frac{1}{\sin \Phi} - \frac{1}{\tan \Phi}$$

$$= \frac{1 - \cos \Phi}{\sin \Phi}$$

Therefore,

$$\tan \omega = \frac{2 \sin^2 (\frac{1}{2}\Phi)}{2 \sin(\frac{1}{2}\Phi)\cos(\frac{1}{2}\Phi)}$$

$$= \tan({}^{\Phi}/2)$$

therefore, $$\omega = \Phi/2 \tag{3.3}$$

and $$z_1 = u_1 \tan(\Phi/2) \tag{3.4}$$

where z_1 is the perpendicular distance from the tangent plane to any point on the surface of the body near the point of contact. If Φ is small,

$$z_1 = \frac{1}{2} u_1 \Phi \tag{3.5}$$

Since JP is approximately equal to R_1'

$$\tan \Phi = \Phi = u_1/R_1' \tag{3.6}$$

From (3.5) and (3.6)

$$z_1 = \frac{1}{2} \frac{u_1^2}{R_1'} \tag{3.7}$$

Similarly, for distance z_1 to points K and N lying in the plane of radius R_1,

$$z_1 = \frac{1}{2} \frac{v_1^2}{R_1} \tag{3.8}$$

Now assume that the distance z_1 to any point H not lying in either plane of principal curvature is given by

$$z_1 = u_1^2/2R_1' + v_1^2/2R_1 \tag{3.9}$$

The assumption is justified since when $u_1 = 0$, (3.9) reduces to (3.8) and when $v_1 = 0$, (3.9) reduces to (3.7). Also, when z_1 is a constant, (3.9) is an ellipse and if u_1v_1 terms are present, the centre of the ellipse will be displaced from the line of action of the forces acting on the bodies, which is not the case expected.

Similarly, the distance z_2 from the tangent plane to any point in the surface of body 2 near the point of contact is given by

$$z_2 = {u_2}^2/2R_2' + {v_2}^2/2R_2 \qquad (3.10)$$

where u_2 and v_2 are co-ordinates with respect to axes lying in the tangent plane and also in the planes of the principal radii of curvature R_2' and R_2 respectively.

$$z = z_1 + z_2 = {u_1}^2/2R_1' + {v_1}^2/2R_1 + {u_2}^2/2R_2' + {v_2}^2/2R_2 \qquad (3.11)$$

where z is the distance between points on the two surfaces near the point of contact.

The co-ordinates u_2 and v_2 can be eliminated by using the transformation (Fig. 3.4)

$$u_2 = u_1 \cos\psi + v_1 \sin\psi$$
$$v_2 = -u_1 \sin\psi + v_1 \cos\psi \qquad (3.12\ a\text{-}b)$$

Therefore,

$$z = A'{u_1}^2 + H'u_1v_1 + B'{v_1}^2 \qquad (3.13)$$

where

$$2A' = (1/R_1') + (1/R'_2)\cos^2\psi + (1/R_2)\sin^2\psi$$
$$2H' = [(1/R_2' - (1/R_2)]\sin\psi\ \cos\psi \qquad (3.14\ a\text{-}c)$$
$$2B' = (1/R_1) + (1/R'_2)\sin^2\psi + (1/R_2)\cos^2\psi$$

The product term u_1v_1 in (3.13) can be eliminated by the transformation

$$u_1 = x \cos z - y \sin z$$
$$v_1 = x \sin z + y \cos z \qquad (3.15\ a\text{-}b)$$

where z is the angle through which the axes u_1 and v_1 must be rotated to eliminate the product term u_1v_1 (Fig. 3.2a).

From (3.13) and (3.15 a-b),

$$z = Ax^2 + By^2 \tag{3.16}$$

where

$$A = \frac{1}{4}\left(\frac{1}{R_1} + \frac{1}{R_2} + \frac{1}{R_1'} + \frac{1}{R'_2}\right)$$

$$- \frac{1}{4}\sqrt{\left[\left(\frac{1}{R_1} - \frac{1}{R_1'}\right) + \left(\frac{1}{R_2} - \frac{1}{R_2'}\right)\right]^2 - 4\left(\frac{1}{R_1} - \frac{1}{R_1'}\right)\left(\frac{1}{R_2} - \frac{1}{R_2'}\right)\sin^2\psi}$$

$$B = \frac{1}{4}\left(\frac{1}{R_1} + \frac{1}{R_2} + \frac{1}{R_1'} + \frac{1}{R'_2}\right)$$

$$+ \frac{1}{4}\sqrt{\left[\left(\frac{1}{R_1} - \frac{1}{R_1'}\right) + \left(\frac{1}{R_2} - \frac{1}{R_2'}\right)\right]^2 - 4\left(\frac{1}{R_1} - \frac{1}{R_1'}\right)\left(\frac{1}{R_2} - \frac{1}{R_2'}\right)\sin^2\psi} \tag{3.17 a-b}$$

Therefore the constants A and B depend upon the principal radii of curvature of the two bodies and upon the angle ψ between the corresponding planes of the minimum (or maximum) principal curvatures.

If the lines V_1 and V_2 (Fig. 3.2a) are parallel, $\psi = 0$ and eqns. (3.17 a-b) reduce to

$$A = \frac{1}{2}\left[\left({}^1/R_1'\right) + \left({}^1/R_2'\right)\right]$$

$$B = \frac{1}{2}\left[\left({}^1/R_1\right) + \left({}^1/R_2\right)\right] \tag{3.18 a-b}$$

3.2.2 Expressions for Principal Stresses - General Case

The expressions for the principal stresses σ_x, σ_y and σ_z at a point on the Z-axis and at a distance z from the origin which lies in the surface of contact of the two bodies were obtained by Thomas and Hoersch [68].

In the expressions, there are 4 elliptic integrals. They are:

$$F(\varphi',k') = \int_o^{\varphi'} \frac{d\theta}{\sqrt{1 - k'^2 \sin^2\theta}}$$

$$H(\varphi',k') = \int_o^{\varphi'} \sqrt{1 - k'^2 \sin^2\theta}\, d\theta$$

$$K(k') = F(\tfrac{\pi}{2},k') = \int_o^{\pi/2} \frac{d\theta}{\sqrt{1 - k'^2 \sin^2\theta}} \qquad (3.19\ a\text{-}d)$$

$$E(k') = H(\tfrac{\pi}{2},k') = \int_o^{\pi/2} \sqrt{1 - k'^2 \sin^2\theta}\, d\theta$$

where $k' = \sqrt{1 - k^2}$ (3.20)

where k is the ratio of the semi-minor axis of ellipse of contact to the semi-major axis of ellipse of contact, i.e.

$$k = {}^{b}/_{a} \qquad (3.21)$$

$$\cot\varphi' = k({}^{z}/_{b}) \qquad (3.22)$$

where z is the depth below the surface of contact to the point on Z-axis at which stresses are to be calculated.

The principal stresses are given by,

$$\sigma x = [J(\Omega x + \mu\Omega' x)]\frac{b}{\Lambda}$$

$$\sigma y = [J(\Omega y + \mu\Omega' y)]\frac{b}{\Lambda} \qquad (3.23\ a\text{-}c)$$

$$\sigma z = [\frac{J}{2}(\frac{1}{n} - n)]\frac{b}{\Lambda}$$

in which

$$J = \frac{2k}{k'^2 E(k')} \qquad (3.24)$$

$$n = \sqrt{\frac{k^2 + k^2({}^{z}/_{b})^2}{1 + k^2({}^{z}/_{b})^2}} \qquad (3.25)$$

$$\Lambda = \frac{1}{A+B}\left(\frac{1 - \mu_1^2}{E_1} + \frac{1 - \mu_2^2}{E_2}\right) \qquad (3.26)$$

where E_1, E_2 are tensile (or compressive) moduli of elasticity for bodies 1 and 2 respectively. μ_1, μ_2 are Poisson's ratio for bodies 1 and 2 respectively.

$$\Omega x = -\frac{1-n}{2} + k^{z}/b[F(\varphi',k') - H(\varphi',k')]$$

$$\Omega' x = -\frac{n}{k^2} + 1 + k^{z}/b[\frac{1}{k^2} H(\varphi',k') - F(\varphi',k')]$$

$$\Omega y = \frac{1}{2n} + \frac{1}{2} - \frac{n}{k^2} + k^{z}/b[\frac{1}{k^2} H(\varphi',k') - F(\varphi',k')]$$

$$\Omega' y = -1 + n + k^{z}/b[F(\varphi',k') - H(\varphi',k')] \qquad (3.27\ a\text{-}d)$$

When the principal radii of curvature of the surfaces near the point of contact are known, the value of k can be found from

$$\frac{B}{A} = \frac{(1/k^2)E(k') - K(k')}{K(k') - E(k')} \qquad (3.28)$$

Also, if the value of b can be found, the contact force Q' can be worked out from

$$Q' = \frac{2\pi b^3}{3k\Lambda E(k')} \qquad (3.29)$$

3.2.3 Special Case, k = 0

From (3.21), if $a = \infty$, $k = 0$. This is a case when 2 straight parallel cylinders are in contact where the contact area forms a long narrow rectangle.

For this case, Thomas and Hoersch [68] obtained the expressions for the principal stresses as follows:

$$\sigma x = -2\mu[\sqrt{1 + (z/b)^2} - z/b]\frac{b}{\Lambda}$$

$$\sigma y = -\left[\frac{(\sqrt{1 + (z/b)^2} - z/b)^2}{\sqrt{1 + (z/b)^2}}\right]\frac{b}{\Lambda} \qquad (3.30\ a\text{-}c)$$

$$\sigma z = -\left[\frac{1}{\sqrt{1 + (z/b)^2}}\right]\frac{b}{\Lambda}$$

If b can be found, the contact force Q¥ per unit length of the cylinders can be evaluated using

¥ See Reference (68) for derivation.

$$Q = \frac{\pi b^2}{2\Lambda} \tag{3.31}$$

3.3 Contact Between Wires in the Same Strand

3.3.1 Depth Below Contact Surface where Shear Stress is Maximum

Assume that the contact between wires in the same strand approaches that for the case of two long straight parallel cylinders in line contact.

Thomas and Hoersch [68] found that the maximum shearing stress in the zone of contact occurs at some distance below the contact surface. Seely and Smith [29] also found that the maximum octahedral shearing stress in the zone of contact occurs at the same distance as the maximum shearing stress reaches its maximum value.

Octahedral shearing stress, τ_{oc} is given by

$$\tau_{oc} = \frac{1}{3}\sqrt{(\sigma_x - \sigma_y)^2 + (\sigma_y - \sigma_z)^2 + (\sigma_z - \sigma_x)^2} \tag{3.32}$$

where σ_x, σ_y and σ_z are principal stresses.

Using (3.30) in (3.32), the distance z_{max} below the contact surface where the octahedral shearing stress reaches its maximum value can be found.

From (3.32),

$$\begin{aligned}\frac{d\tau_{oc}}{dz} = \frac{1}{6}&[(\sigma_x - \sigma_y)^2 + (\sigma_y - \sigma_z)^2 + (\sigma_z - \sigma_x)^2]^{-1/2} \\ &\times \{2(\sigma_x - \sigma_y)(\frac{d\sigma_x}{dz} - \frac{d\sigma_y}{dz}) \\ &+ 2(\sigma_y - \sigma_z)(\frac{d\sigma_y}{dz} - \frac{d\sigma_z}{dz}) \\ &+ 2(\sigma_z - \sigma_x)(\frac{d\sigma_z}{dz} - \frac{d\sigma_x}{dz})\}\end{aligned} \tag{3.33}$$

For maximum τ_{oc}, $\frac{d\tau_{oc}}{dz} = 0$.

Therefore,

$$(\sigma_x - \sigma_y)(\frac{d\sigma_x}{dz} - \frac{d\sigma_y}{dz}) + (\sigma_y - \sigma_z)(\frac{d\sigma_y}{dz} - \frac{d\sigma_z}{dz})$$

$$+ (\sigma_z - \sigma_x)(\frac{d\sigma_z}{dz} - \frac{d\sigma_x}{dz}) = 0 \qquad (3.34)$$

From (3.30 a-c)

$$\sigma_x = - 2\mu(\sqrt{1 + D^2} - D)\frac{b}{\Lambda}$$

$$\sigma_y = - \frac{(\sqrt{1 + D^2} - D)^2}{\sqrt{1 + D^2}}\frac{b}{\Lambda} \qquad (3.35\ a\text{-}c)$$

$$\sigma_z = - \frac{1}{\sqrt{1 + D^2}}\frac{b}{\Lambda}$$

where $D = z/b$ (3.36)

and

$$\frac{d\sigma_x}{dz} = - \frac{2\mu}{\Lambda}[\frac{D}{\sqrt{1 + D^2}} - 1]$$

$$\frac{d\sigma_y}{dz} = - \frac{1}{(1 + D^2)\Lambda}[2((\sqrt{1 + D^2} - D)D - \sqrt{1 + D^2})$$

$$- \frac{D(\sqrt{1 + D^2} - D)^2}{\sqrt{1 + D^2}}] \qquad (3.37\ a\text{-}c)$$

$$\frac{d\sigma_z}{dz} = - \frac{1}{\Lambda}[- \frac{D}{(1 + D^2)\sqrt{1 + D^2}}]$$

If (3.35) and (3.37) are substituted into (3.34) the value of D that satisfies (3.34) can be computed.

3.3.2 Contact Force that will Cause Wire to Yield

Using the octahedral shearing stress theory of failure which gives the same result as the energy distortion theory (von Mises), yielding

is expected to start at a point where the octahedral shearing stress is a maximum, i.e. at a distance z_{max} below the contact surface.

Using von Mises' theory of failure

$$2\sigma_o^2 = (\sigma_x - \sigma_y)^2 + (\sigma_y - \sigma_z)^2 + (\sigma_z - \sigma_x)^2 \qquad (3.38)$$

where σ_o is the uniaxial yield stress and σ_x, σ_y and σ_z are principal stresses.

If the value of D obtained from the computation is substituted into (3.35) and (3.35) is substituted into (3.38), the value of b, which is the width of the contact area, can be evaluated.

The contact force, Q per unit length of the wire that will produce yield in the wire may then be found from (3.31) where A in the equation is given by

$$A = \frac{2}{A+B} \left(\frac{1-\mu^2}{E}\right) \qquad (3.39)$$

since the wires are made of the same material. Since $R_1' = R_2' = \infty$ and $R_1 = R_2 = R$, where R is the radius of the wire, A = 0 and B = 1/R.

3.3.3 Dimensionless Force χ to Cause Yield

In Fig. 3.5, let β_o be the angle that the line of action of the contact force Q makes with the line of action of the force X. Therefore,

$$X = -2Q\cos\beta_o \qquad (3.40)$$

From geometrical consideration, Costello and Phillips [47] found that

$$\cos\beta_o = \frac{1}{\cos^2\alpha}\sqrt{1 + \frac{\tan^2(\frac{\pi}{z} - \frac{\pi}{m})}{\sin^2\alpha}} - \sqrt{\tan^2(\frac{\pi}{z} - \frac{\pi}{m})\left[1 + \frac{1}{\tan^2\alpha\cos^2(\frac{\pi}{z} - \frac{\pi}{m})[\sin^2\alpha + \tan^2(\frac{\pi}{z} - \frac{\pi}{m})] + \sin^4\alpha}\right]} \quad (3.41)$$

where α is the helix angle of the wire in the strand and m is the number of wires in the strand.

Now define a dimensionless force, χ such that

$$\chi = \frac{Xr}{To} \quad (3.42)$$

where r is the helix radius of the wire in the strand and To is the fully plastic axial load, T given by

$$To = \pi\sigma_o R^2 \quad (3.43)$$

where σ_o is the uniaxial yield stress and R is the radius of the wire.

The helix radius, r can be calculated from Eqn. (2.44).

Using (3.43), (2.44) and (3.40) in (3.42) the value of χ can be calculated. Fig. 3.7 shows the variation of χ with helix angle and Fig. 3.8 shows the variation of χ with the number of wires in the strand.

3.4 Contact Between Adjacent Wires in Neighbouring Strands

3.4.1 Spacing of Contact Zones

When two layers of strand with different helix angles are in contact, point contacts will occur at equally spaced distance along

each of the wires in the strands.

If the wires in both strands are developed onto a flat plane, the contact points can be located and thus the distance between the contact points along the inner and outer wires can be obtained. Superscript bar ($\bar{}$) will be used to denote variables associated with the outer layer.

Fig. 3.6 gives

$$\Delta s \sin(\bar{\alpha} - \alpha) = \frac{2\pi(r + R)}{\bar{m}} \sin \bar{\alpha} \tag{3.44}$$

$$\Delta \bar{s} \sin(\bar{\alpha} - \alpha) = \frac{2\pi(r + R)\sin\alpha}{m} \tag{3.45}$$

where Δs is the distance between contact points along the inner wires,

α is the helix angle for inner strand

m is the number of wires in inner strand

r is the helix radius of inner strand

R is the radius of the wires.

3.4.2 Principal Radii of Curvature at Contact

Consider one of the points of contact as shown in Fig. 3.9

$$R_1 = R \; ; \; R_2 = \bar{R} \tag{3.46}$$

$$\psi = \bar{\alpha} - \alpha \tag{3.47}$$

Fig. 3.10a shows a plane containing the centre-line of a strand, and Fig. 3.10b shows a view perpendicular to the normal direction of a wire in the inner strand.

From Fig. 3.10b

$$\frac{r}{\sqrt{r^2 + y^2}} = \frac{\sqrt{r^2 + y^2}}{2\mathbb{R}_1'}$$

$$\therefore \quad \mathbb{R}_1 = \frac{1}{2r}(r^2 + y^2) \tag{3.48}$$

But from Fig. 3.10a,

$$y = \frac{r}{\cos\alpha} \tag{3.49}$$

Therefore

$$\mathbb{R}_1 = \frac{r}{2}\left(1 + \frac{1}{\cos^2\alpha}\right) \tag{3.50}$$

Similarly,

$$\mathbb{R}_2 = \frac{\bar{r}}{2}\left(1 + \frac{1}{\cos^2\bar{\alpha}}\right) \tag{3.51}$$

where $\bar{r} = r + R + \bar{R}$ (3.52)

$$R_1' = \mathbb{R}_1 + R \tag{3.53}$$

and $$R_2' = \mathbb{R}_2 - R \tag{3.54}$$

since $\mathbb{R}_1$ and $\mathbb{R}_2$ are radii of curvature of the centre-line of the wires in the inner and outer strands, respectively.

3.4.3 Depth Below Contact Surface Where Shear Stress is Maximum

The principal stresses at each of the contact points are given by (3.23).

To find the depth below the contact surface where shear stress is maximum, the procedure as in section 3.3 i.e. using calculus, will not be adopted since in this case, the expressions for the principal stresses involve elliptic integrals $F(\varphi',k')$ and $H(\varphi',k')$. Instead,

a plot of the octahedral shear stress against the ratio $^{kz}/b$ will be produced as shown in Fig. 3.12 a-c so that a value of $^{kz}/b$ at which the octahedral shear stress is a maximum can be found.

The procedure for plotting the graph is as follows:

1. A graph of k versus $^{B}/A$ as shown in Fig. 3.11 is plotted using eqn. (3.28). Thus, when $^{B}/A$ is known from the geometry of the surface at contact, k can be determined.
2. With the value of k, k' can be obtained using (3.20).
3. Eqns. (3.25) and (3.27) are rewritten as

$$n = \sqrt{\frac{k^2 + D_1'}{1 + D_1^2}} \tag{3.55}$$

and

$$\Omega x = -\frac{1-n}{2} + D_1 [F(\varphi',k') - H(\varphi',k')]$$

$$\Omega' x = -\frac{n}{k^2} + 1 + D_1 [\frac{1}{k^2} H(\varphi',k') - F(\varphi',k')]$$

$$\Omega y = \frac{1}{2n} + \frac{1}{2} - \frac{n}{k^2} + D_1 [\frac{1}{k^2} H(\varphi',k') - F(\varphi',k')]$$

$$\Omega' y = -1 + n + D_1 [F(\varphi',k') - H(\varphi',k')] \tag{3.56 a-d}$$

where

$$D_1 = {}^{kz}/b \tag{3.57}$$

Since all wires are of the same material, eqn. (3.26) becomes

$$\Lambda = \frac{2}{A+B} (\frac{1 - \mu^2}{E}) \tag{3.58}$$

Values of A and B can be obtained by substituting (3.46),(3.47), (3.53) and (3.54) into (3.17).

4. Assume a value of D_1. From (3.22), φ' can be determined.
5. With the values of k' and φ', values of $F(\varphi',k')$ and $H(\varphi',k')$ can be looked up from Tables of Elliptic Integrals [69].

Procedure 1-5 with (3.24) will give σ_x, σ_y and σ_z in terms of $^b/_\Lambda$. These values can then be substituted into (3.32) to give a value of τ_{oc} for a given value of $^{kz}/_b$ (or D_1).

3.4.4 Contact Force that will Cause Yield

The von Mises theory of failure will again be used which gives equation (3.38).

Values of σ_x, σ_y and σ_z in terms of $^b/_\Lambda$ for which the octahedral shear stress is maximum can be calculated using procedure 1-5 in section 3.4.3 when the associated value of $^{kz}/_b$ has been found. These values can then be substituted into (3.38), so that the value of b can be obtained when Equations (3.35) are used.

The contact force Q' can be found by substituting the value of b into (3.29).

3.4.5 Dimensionless Force $\bar{X}$ to Cause Yield

The resultant normal distributed line load acting on the outer wire, $\bar{X}$ is related solely to the point contact loads Q' which are applied at regular intervals $\Delta\bar{s}$ along the inside of the outer layer as illustrated in Fig. 3.14.

This gives

$$\bar{X} = -\frac{Q'}{\Delta\bar{s}} \tag{3.59}$$

Therefore the value of the line load $\bar{X}$ can be obtained by substituting (3.29) and (3.45) into (3.58).

As in section (3.3.3), a dimensionless line load $\bar{\chi}$ will be defined as

$$\bar{\chi} = \frac{\bar{\bar{X}}\bar{r}}{To} \qquad (3.60)$$

The rope considered is a 1X6X12 rope, the cross-section of which is shown in Fig. 3.14. The wires are of the same size.

The values of $\bar{\chi}$ that will cause yield in the wire of the outer strand are shown in Fig. 3.13, for various values of inner and outer strand helix angles.

3.5 DISCUSSION

Contact stresses should no doubt be an important consideration in the design of wire rope. Starkey and Cress(30) have shown that the critical stresses in a wire rope are due largely to contact stresses and are much higher than direct-tensile-stress. Similarly, Phillips, Miller and Costello(61) show that for a 1X6X12 rope, the maximum contact stress due to the inter layer contact force is about 7.4 times as large as the tensile stress due to the tension in the outer wires of the rope.

In this chapter, two types of contact that occur in wire ropes have been described - (i) line contact which is produced by contact between individual wires in a strand and (ii) point contact which is produced by contact between adjacent wires in neighbouring strands. Comparing Figures 3.7 and 3.8 with figure 3.13, it is obvious that point contact is more critical between the two. The contact force required to initiate yield in the contacting wires is about a hundred times higher in line contact as compared to point contact (in the range of contact angles $(\bar{\alpha}-\alpha)$ as shown in figure 3.13).

Figure 3.7 shows that for line contact, as the helix angle α increases, the value of χ also increases but the increase becomes smaller as the helix angle approaches 90^0. The value of contact force Q is the same irrespective of the value of α since the contact has been assumed to approach that for the case of two straight parallel cylinders. Thus, from equations (3.40) and (3.42), the value of χ, the dimensionless line force X for a given size of wire and number of wires in a strand m, will depend on $\cos\beta_0$, where β_0 is the angle that the line of action of the contact force Q makes

with the line of action of X, and also r, the helix radius. $\cos\beta_o$ is given by equation (3.41) and r, by equation (2.44).

The value of χ decreases as the number of wires in the strand increases as can be seen in Figure 3.8. But, for value of m>9, the decrease becomes very small that χ is almost constant.

With point contact, χ, the dimensionless line force X required to initiate yield in the wires, depends on the contact angle, the difference in the helix angle between the inner and the outer strand. As the contact angle increases from 0^0 to 90^0, the contact area will decrease from a maximum to a minimum. Thus, it is expected that χ will decrease as the contact angle increases. This is illustrated in figure 3.13 which shows the variation in χ for various combinations of helix angle between the inner and the outer strand.

CHAPTER 4

Improved approximation on χ to cause collapse derived from plasticity consideration.

4.1 Introduction

It is well known that in elastic contact of solids, the yield point is first reached beneath the surface of contact. Hence, for loads not greatly in excess of the elastic limit, plastic deformation will be fully "contained" by elastic material and the order of magnitude of both elastic and plastic strains will be the same. Due to this, Johnson [70] argued that the departure of the mean contact pressure from its 'elastic' value in the early stages of plastic deformation is fairly gradual and thus Hertz's [66] original suggestion that the point of first yield could be used as a rational measure of hardness proved to be impractical. ¥

With the above viewpoint as a basis, we seek to find a better approximation on the collapse value for χ, than that obtained in Chapter 3, that will be used in the subsequent chapters (i.e. Chapters 5 and 7) to predict the static plastic collapse of a wire rope.

4.2 Rigid-Plastic Deformation

A rigid plastic solid is a hypothetical solid which, under any stress system, would be rigid when stressed below the yield point, that is, the elastic modulus is infinitely large. The yield point of a rigid plastic body is that load in the loading sequence for which deformation first becomes possible. For materials, such as metals, with a high ratio of Young's modulus of elasticity to uniaxial yield stress (E/σ_o), the theory of rigid perfectly-plastic solids has been successful in predicting the indentation pressure in terms of the yield stress of the material, except when the indentation is very shallow.

¥ It is appreciated that during the manufacture of wire ropes, residual stresses will occur. It is acknowledged that the present analysis does not take this into account.

Thus, the problem of indentation may be used to provide a better estimate on the collapse value for χ.

Most studies of indentation problems have been made in terms of plane strain which makes the mathematical aspects very much simpler. In plane flow, the velocity vector is everywhere parallel to a certain plane and is independent of the distance from the plane. Plane plastic flow is in fact one of the most highly developed branches of plasticity theory, largely as a result of the work by Hill [71] in developing and applying the theory of the "slip-line field", a theory whose simplicity is derived largely from the restrictions imposed by plane strain conditions.

The indentation of a rigid-plastic semi-infinite medium was first investigated by Prandtl [72]. For ductile metals, Tabor [73] has shown that the mean contact pressure can be related to the yield stress of the material in simple compression, σ_c by an expression based on the theory of indentation of a rigid perfectly-plastic solid, viz.

$$P_m = c\sigma_c \tag{4.1}$$

where c is a constant whose value is about 3, depending to some extent upon the geometry of the indenter.

Levin [74] used the limit design theorem of Drucker, Prager and Greenberg [75] to compute an upper bound for the indentation pressure of a smooth circular punch. He found that 5.84s is an upper bound on the indentation pressure where s is the yield stress in simple shear.

Shield and Drucker [76] obtained a lower bound of 5s for the indentation pressure for any convex area of indentation.

Spencer [77] used perturbation methods in plasticity to study the problem of indentation of a semi-infinite solid by the curved surface of a smooth circular cylinder. He obtained a value of $s(2 + \pi)$ for the initial contact pressure which is the same as the upper bound value for the indentation pressure due to a punch whose cross-section is a very long rectangle.

The problem of mutual indentation of crossedcylinders and wedges of various metals in various states of work-hardening was investigated by Atkins and Tabor [78]. For mutual indentation of highly work-hardened crossed cylinders, they found that the mean contact pressure was 2.3 times the uniaxial yield stress as compared to 2.8 for ball indentation of a flat. The reason they gave for the difference is that, compared with a ball in a flat, there is less constraint to deformation with crossed cylinders, because of the material "missing" from the flanks of the cylinders.

4.3 Contact Between Wires in the Same Strand

As in Chapter 3, assume that the contact between wires in the same strand approaches that for the case of two long straight parallel cylinders in line contact.

Indentation pressure obtained by indenting the curved surface of a smooth circular cylinder on a semi-infinite solid is $s(2 + \pi)$ (section 4.2).

Using the von Mises criterion

$$s = \sigma_o/\sqrt{3} \tag{4.2}$$

where σ_o is the uniaxial yield stress. Therefore the indentation pressure is $2.97\ \sigma_o$.

For the same reason given for the difference in the value for the indentation pressure of a ball in a flat and the crossed cylinders, the indentation pressure for the case of a mutual indentation of two straight parallel cylinders is expected to be less than $2.97\ \sigma_o$.

Atkins and Tabor [78] also found that the difference between the two indentation pressures (ball in a flat and mutual indentation of two crossed cylinders) is by a factor 1.2. Therefore, if it is assumed that the difference in this case (mutual indentation of two straight parallel cylinders and indentation of the curved surface of a smooth circular cylinder on a semi-infinite solid) is of the same order, then the indentation pressure is $\approx 2.5\ \sigma_o$.

The contact force to cause collapse, Q per unit length of the wires can be found if the width of the contact area (indentation) due to the indentation pressure is known, viz.

$$Q \approx 5b\sigma_o \tag{4.3}$$

where b is half the width of the indentation.

Provided that the plastic layer is small compared to the radius of the wire, the Hertz contact theory may be employed to determine the values of b and Q when the indentation pressure is known.

Using the Hertz theory, it was found that the plastic layer is about 1.5% of the radius of the wire (Appendix 2). Therefore, the value of Q associated with the indentation pressure $\approx 2.5\sigma_o$, is evaluated using the Hertz contact theory.

Substituting (4.3) into (3.31)

$$b \approx \frac{2\Lambda}{\pi} (5\sigma_o) \tag{4.4}$$

therefore, substituting (4.4) into (4.3),

$$Q \approx \frac{2\Lambda}{\pi} (5\sigma_o)^2 \tag{4.5}$$

The corresponding value of χ to cause collapse of the wire may be evaluated following the procedure outlined in Section (3.3.3). i.e. assuming that the wire remains elastic up to Q given by Equation (4.3) even though the wire is actually behaving in an elastic-plastic manner.

Fig. 4.1 shows the variation of the collapse value of χ with helix angle and Fig. 4.2 shows its variation with the number of wires in the strand. The changes in the values of χ should the factor c chosen is other than 2.5 is shown in Fig. 4.3. From the figure for a change of 1% in the value of c, there is a change of 1.9% in the value of χ.

4.4 Contact Between Adjacent Wires in Neighbouring Strands

Assume that the contact of adjacent wires in neighbouring strands approaches that of two crossed cylinders. Atkins and Tabor [78] found that the indentation pressure for the case of mutual indentation of highly work-hardened crossed cylinders was 2.3 σ_o.

For fully work-hardened metals, the yield stress is essentially constant and thus unaffected by the indentation process. By contrast, with annealed or partially work-hardened materials, the deformation produced by an indentation will cause the local yield stresses to increase.

If it is assumed that the wires are fairly highly work-hardened due to the process they undergo during rope manufacture, then it is expected that the indentation pressure is $> 2.3\ \sigma_o$. Also the results of Shield and Drucker [76] indicate that the upper bound of the indentation pressure increases as the ratio of indentation area to perimeter increases. Compared to the mutual indentation of two parallel cylinders (whose indentation area is that of a very long rectangle), the mutual indentation of two crossed cylinders (whose indentation area is circular) should have a larger area to perimeter ratio. Thus, it is expected that the indentation pressure for the mutual indentation of crossed cylinders to be $> 2.5\ \sigma_o$ (i.e. greater than that for the case of parallel cylinders). If it is assumed that the difference is of the same order to that for the case of indentation by a punch on a semi-infinite solid, then the indentation pressure for the mutual indentation of two crossed cylinders is $\approx 2.8\ \sigma_o$.

For the same reason given in section (4.3), the Hertz contact theory will again be employed to determine the value of contact force Q'.

$$Q' \approx 2.8\pi ab\sigma_o \qquad (4.6)$$

where a is the semi-major axis of the ellipse of contact and b, its semi-minor axis.

When the ratio $^{B}/A$ is known from the geometry of the surface at contact, k can be determined from Fig. 3.11.

Since $k = {}^{b}/a$ (eqn. 3.21), a can be written in terms of b, viz.

$$a = {}^{b}/k \tag{4.7}$$

Substituting (4.7) into (4.6)

$$Q' \approx \frac{2.8\pi b^2 \sigma_o}{k} \tag{4.8}$$

Substituting (4.8) into (3.29),

$$b \approx 4.2\Lambda E(k')\sigma_o \tag{4.9}$$

The value of E(k') can be found from the Tables of Elliptic Integral [69].

By substituting (4.9) into (4.8), Q' can be found, viz.

$$Q' \approx \frac{2.8\pi}{k} \sigma_o^3 [4.2\Lambda E(k')]^2 \tag{4.10}$$

The corresponding values of $\bar{\chi}$ to cause collapse of the wires may be found following the procedure outlined in Section 3.4.5.

The values of $\bar{\chi}$ to cause collapse of wires for various combinations of inner and outer strand helix angles are shown in Fig. 4.4.

The changes in the values of χ for factor c being slightly greater or smaller than 2.8 is shown in Fig. 4.5. The figure shows that for a change of 1% in the value of c, there is a change of 0.96% in the value of $\bar{\chi}$.

4.5 DISCUSSION

It has been assumed that the mean contact pressure to produce an indentation will provide a better approximation on the collapse value of χ due to the reason given in Section 4.1.

For line contact, Figs. 4.1 and 4.2 show that the value of χ to produce an indentation is about twice that to initiate yield in the wires(Figs. 3.7 and 3.8). But, Fig. 4.4 shows that for point contact, the value of χ to produce an indentation is about 16 times that to initiate yield in the wires(Fig. 3.13). This result is not unexpected since for line contact, the contact force Q is proportional to c^2(Equation 4.5), where $c\sigma_0$ is the indentation pressure. From the contact force to produce yield in the wires, c is equivalent to ≈ 1.7 whereas the value of c to produce an indentation is ≈ 2.5. For point contact, the equivalent value of c at yield is ≈ 1.1 and its value to produce an indentation is ≈ 2.8, and from Equations (4.8), (3.29), (4.9) and (4.10), the contact force Q' is proportional to c^3.

The results shown in Fig. 4.4 agrees well with the experimental results obtained by Hamlet(90) (see Fig. 4.7) for tests carried out on crossed-cylinders. Both show that a large contact load is required to produce a given indentation when the contact angle is small and as the contact angle approaches 90^0, the contact load drops sharply and then levels off.

Using the size of the rods used by Hamlet(90), it is found that the load required to produce an indentation in the rods, when it is in line contact, is 19kN/m. When this value is checked against the

load-deflection curve obtained by Hamlet (see Fig 4.6), it shows a very close agreement as it lies in the region of the curve where plastic deformation has occurred.

CHAPTER 5

Static plastic collapse - No axial strain in individual wire.

5.1 Limit Analysis

5.1.1 Introduction

Limit analysis is not a new concept. It has been around for a couple of centuries but only in this century has it received popularity. In [79], using examples, Prager traces the slow development of the concept in the 18th and 19th centuries, its temporary eclipse by the emerging theory of elasticity and its final establishment in the 20th century.

An important consideration in an engineering structure is not whether the yield stress is exceeded at some point, but whether the structure will carry the intended loads or perform its intended function, and there is no reason for assuming that the stress in the structure should never exceed the elastic limit. The practice is therefore becoming more widespread to design structures into the plastic range, where the materials are assumed to behave in an elastic-perfectly plastic manner. In this type of design practice, no attempt is made to determine the stresses and strains in the structure, but rather what is sought is the load-carrying capacity or limiting load at which the structure will collapse. This load at collapse is called the plastic collapse load.

Theoretical research on wire ropes has been, in the main, concentrated on the behaviour of the wire ropes which are subjected to loads within the elastic range (see Chapter 1). By performing a limit analysis on wire ropes, one would be in a position to estimate the reserve strength beyond the elastic range and this would help in the selection of a meaningful factor of safety or in making an

appropriate rope construction. Work in this area has been started by Jones [64]. Due to the contributions that it would offer to the proper design of wire ropes, the present work will pursue and extend the above work to include an analysis on wire rope with configurations which are more realistic.

5.1.2 The Limit Theorems

The theorems were first presented by Gvozdev [80] and independently proved by Hill [81, 82] for rigid-perfectly plastic material and by Drucker, Greenberg and Prager [83, 84] for the elastic perfectly-plastic material with the conventional small displacement assumption.

The theorems are complementary principles which permit us to compute load parameters which lie respectively within or outside the limit surface in load space. The two theorems are obtained by comparing first the constraints imposed on the solution by equilibrium requirements and the yield condition (Lower Bound), and second the constraints imposed by kinematic requirements including the normality requirements of the constitutive equations (Upper Bound).

The theorems may be stated in several equivalent ways. One of the ways of stating them is as follows:-

a) Lower Bound Theorem.

A statically admissible state can be associated with a load state if and only if the load state is on or within the yield interaction surface.

A statically admissible stress state is defined as a generalised

stress distribution such that the generalised stress distribution is in internal equilibrium, is in equilibrium with the external loads and satisfies the yield condition.

b) Upper Bound Theorem

A kinematically admissible state can be associated with a load state if and only if the load state is outside of or on the yield-point interaction surface.

A kinematically admissible state is defined as one where the total external rate of work done by the actual loads on a velocity field is positive and that the velocity field satisfies the velocity (or displacement) constraints.

5.1.3 Exact Solution

The limit theorems can be used as a tool by which the exact limit surface can be found. This happens when the lower bound to the limit surface coincides with the upper bound.

If the limit surface cannot be found exactly, we can attempt to find bounds on the limit surface by determining a series of points within the limit surface and a series of points outside the limit surface. This may sometimes be sufficient depending upon the purposes that we have at hand.

5.2 Yield Criterion

The law that defines the limit of elasticity under any possible combination of loads is known as the criterion of yielding.

For bars with circular cross-sections and subjected to combined

bending and torsional loads, Hill and Siebel [85] found

$$\left(\frac{G'}{G_o}\right)^2 + \left(\frac{H}{H_o}\right)^2 = 1 \qquad (5.1)$$

where G' and H are defined in Fig. 2.3.

When the bars are subjected to combined loads of torsion and tension, they found that

$$\left(\frac{H}{H_o}\right)^2 + \left(\frac{T}{T_o}\right)^2 = 1 \qquad (5.2)$$

where T is defined in Fig. 2.3.

For the case of bars subjected to combined torsion, bending and tension, the yield criterion is given as

$$\left(\frac{T}{T_o}\right)^2 + \left(\frac{H}{H_o}\right)^2 + \frac{G'}{G_o}\left[1 - \left(\frac{H}{H_o}\right)^2\right]^{\frac{1}{2}} = 1 \qquad (5.3)$$

If the rods are of radius R and are made from a perfectly plastic material with a uniaxial yield stress σ_o, then

$$G_o = 4\sigma_o R^3/3 \quad \text{and} \quad H_o = \pi\sigma_o R^3/3 \qquad (5.4\ a,b)$$

are the fully plastic generalised forces when G' and H act alone, respectively, while

$$T_o = \pi\sigma_o R^2 \qquad (5.4\ c)$$

is the fully plastic tangential load T.

5.3 Plastic Collapse Load for a Single Strand (mainly based on Reference(64)

5.3.1 Approximation from Below

For a helical wire which is inextensible, the moments G' and H control its plastic yielding. For this case, the tensile force T in a sense tangential to the helical wire is a reaction. The influence of the transverse shear force N' on yielding is disregarded, which is customary when considering plastic yielding of structural members with cross-sectional dimensions much smaller than the overall length.

Therefore, in order to obtain a lower bound to the exact values of F (axial force on a strand) and M (torsional moment on a strand) required for the collapse of an elastic perfectly plastic strand, it is necessary to seek a statically admissible generalised stress field which satisfies the equilibrium equations (2.21) and (2.22) and lies wholly inside or on the yield surface described by equation (5.1) [86, 87].

Eliminating N' from equations (2.21) and the expression for F (2.25) and using equations (2.23) and (2.24) gives,

$$\frac{T}{T_o} = \varphi \sin \alpha - \chi \tag{5.5}$$

where

$$\varphi = {}^{F}/_{mT_o} \tag{5.6}$$

and

$$\chi = rX/T_o \tag{5.7}$$

Eliminating T from the same equations above gives

$$N' = \frac{F}{m}\cos\alpha + Xr\tan\alpha \tag{5.8}$$

Using (2.22) and (2.21) to eliminate G' and T, respectively from (2.26) gives

$$H = \frac{M}{m}\sin\alpha + Xr^2\tan\alpha + N'r \tag{5.9}$$

Substitute (5.8) into (5.9)

$$H = \frac{M}{m}\sin\alpha + \frac{F}{m}r\cos\alpha + 2Xr^2\tan\alpha \tag{5.10}$$

Using (5.4 b,c) in (5.10) gives

$$\frac{H}{H_o} = \mu\sin\alpha + 3r\varphi\cos\alpha/R + 6r\chi\tan\alpha/R \tag{5.11}$$

where

$$\mu = \frac{M}{mH_o} \tag{5.12}$$

Similarly, by eliminating H from (2.26)

$$\frac{G'}{G_o} = (\pi/4)[\mu\cos\alpha - (3r/R)\{\varphi\sin\alpha + \chi(\tan^2\alpha - 1)\}] \tag{5.13}$$

Finally, substituting equations (5.11) and (5.13) into equation (5.1) gives

$$\begin{aligned}&(\sin^2\alpha + \pi^2\cos^2\alpha/16)\mu^2 + 9(\cos^2\alpha + \pi^2\sin^2\alpha/16)\varphi^2\lambda^2\\ &+ \sin\alpha\cos\alpha\,(6 - 3\pi^2/8)\mu\varphi/\lambda + 9\{4\sin\alpha + \pi^2\sin\alpha(\tan^2\alpha\\ &- 1)/8\}\chi\varphi/\lambda^2 + 3\{4\tan\alpha\sin\alpha - \pi^2\cos\alpha(\tan^2\alpha\\ &- 1)/8\}\chi\mu/\lambda + \{36\tan^2\alpha + 9\pi^2(\tan^2\alpha - 1)^2/16\}\chi^2/\lambda^2 - 1 = 0\end{aligned} \tag{5.14}$$

where

$$\lambda = R/r \tag{5.15}$$

Equations (5.5)-(5.15) are identical to equations (9)-(15) in [64].

A lower bound to the exact non-dimensionalised collapse moment μ for given values of φ, α and m^* can be obtained from equation (5.14). Alternatively, the lower bound to the exact non-dimensionalised collapse load φ for given values of μ, α and m may be obtained. Thus, an interaction curve lying in a φ-μ plane may be constructed given the values of α and m.

5.3.2 Approximation from Above

An upper bound to the exact values of F and M (equations 2.25 and 2.26) associated with the collapse of an elastic perfectly plastic strand is obtained by equating the external work rate to the corresponding internal energy dissipation. This is achieved by selecting any kinematically admissible displacement field and employing the normality requirements of plasticity to seek the relevant active portions of the yield surface (equation 5.1) [86, 87].

Thus, equating the external work rate to the internal energy dissipation of a strand gives

$$\dot{F}\dot{\delta} + \dot{M}\dot{\Delta} - m\int_0^{\sqrt{(h^2 + (2\pi r)^2)}} X\dot{\eta}ds = m\int_0^{\sqrt{(h^2 + (2\pi r)^2)}} (T\,\dot{\varepsilon}_\omega + G'\dot{\kappa}' + H\dot{\tau})ds \qquad (5.16)$$

where δ and Δ are the axial extension and angular rotation of one pitch (h) of a strand, respectively, η is the displacement of a wire parallel but in a sense opposite to the principal normal direction,

---

* λ as defined by equation (5.15) may be calculated from equation (2.41) with given values of α and m and for the same values of α and m, the value of χ can be obtained from Figs. 4.1 and 4.2.

and ε_ω is the centre-line strain of a single wire. $\dot{\kappa}'$ and $\dot{\tau}$ are given by equations (2.31) and (2.32) respectively.

Now, the wire was assumed inextensible and T was taken as a reaction in the lower bound calculations. Thus, $\dot{\varepsilon}_\omega = 0$.

From equation (2.28),

$$\dot{\rho} = - \dot{\varepsilon} \tan^2\alpha - \dot{\gamma} \tag{5.17}$$

Substituting equations (2.31) and (2.32) into equation (5.16) with $\dot{\varepsilon}_\omega = 0$ and using equation (2.29 c) gives

$$\frac{\dot{F}\dot{\delta} + \dot{M}\dot{\Delta}}{m\{h^2 + (2\pi r)^2\}^{\frac{1}{2}}} = \frac{G'\sin^2\alpha\cos^2\alpha}{r}(\dot{\gamma} - \dot{\varepsilon} + \dot{\rho}) + G'\dot{\gamma}\frac{\cos^2\alpha}{r}$$

$$- \frac{H\sin\alpha\cos^3\alpha}{r}(\dot{\gamma} - \dot{\varepsilon} + \dot{\rho}) + H\dot{\gamma}\frac{\sin\alpha\cos\alpha}{r} + Xr\dot{\rho} \tag{5.18}$$

With the aid of equations (2.31), (2.32) and $\dot{\varepsilon}_\omega = 0$, the generalised strain rate vector $\overline{E} = \dot{\kappa}'\underline{i} + \dot{\tau}\,\underline{j} + \dot{\varepsilon}_\omega\,\underline{k}$ can be recast in the form

$$\overline{E} = \{\frac{\sin^2\alpha\cos^2\alpha}{r}(\dot{\gamma} - \dot{\varepsilon} + \dot{\rho}) + \dot{\gamma}\frac{\cos^2\alpha}{r}\}\,\underline{i}/r$$

$$- \{\frac{\sin^2\alpha\cos^3\alpha}{r}(\dot{\gamma} - \dot{\varepsilon} + \dot{\rho}) - \dot{\gamma}\frac{\sin\alpha\cos\alpha}{r}\}\,\underline{j}/r \tag{5.19}$$

In order to satisfy the normality requirements of plasticity, $\overline{E}$ must be parallel to $\nabla\Phi$ where $\Phi = 0$ represents the yield condition (equation 5.1).

$$\nabla\Phi = \underline{i}\frac{\partial\Phi}{\partial G'} + \underline{j}\frac{\partial\Phi}{\partial H} + \underline{k}\frac{\partial\Phi}{\partial T} \tag{5.20}$$

thus,

$$\nabla\Phi = \underline{i}\frac{2G'}{Go^2} + \underline{j}\frac{2H}{Ho^2} \tag{5.21}$$

For $\bar{E}$ to be parallel to $\nabla\Phi$.

$$\bar{E} \otimes \nabla\Phi = 0 \tag{5.22}$$

Therefore

$$\frac{2H^*}{Ho}\left\{\frac{\sin^2\alpha\cos^2\alpha}{r}(\dot{\gamma} - \dot{\varepsilon} + \dot{\rho}) + \dot{\gamma}\frac{\cos^2\alpha}{r}\right\}$$

$$+ \frac{2G^*}{Go}\left\{\frac{\sin\alpha\cos^3\alpha}{r}(\dot{\gamma} - \dot{\varepsilon} + \dot{\rho}) - \dot{\gamma}\frac{\sin\alpha\cos\alpha}{r}\right\} = 0 \tag{5.23}$$

where

$$G'^* = \frac{G'}{Go} \quad \text{and} \quad H^* = \frac{H}{Ho} \tag{5.24 a,b}$$

Substituting (5.17) into (5.23) gives

$$\frac{Go(\dot{\gamma}\cos^3\alpha - \dot{\varepsilon}\sin^2\alpha)}{G'^*} = \frac{Ho\sin\alpha\cos\alpha(\dot{\gamma} + \dot{\varepsilon})}{H^*} \tag{5.25}$$

Substituting (5.4) into (5.25) gives

$$\frac{4H^*\cos^2\alpha/\pi - G^{*\prime}\sin\alpha\cos\alpha}{4H^*\sin^2\alpha/\pi + G^{*\prime}\sin\alpha\cos\alpha} = A \tag{5.26}$$

where

$$A = \dot{\varepsilon}/\dot{\gamma} \tag{5.27}$$

Using equations (5.4), (5.6), (5.7), (5.12), (5.15), (2.29), (5.24) and (5.27), and $\tan\alpha = h/2\pi r$, equation (5.18) can be rewritten as

$$\Phi A\sin\alpha + \mu\lambda\cos\alpha/3 = -(1 + A\tan^2\alpha)\chi$$

$$+ 4\lambda G^{*\prime}(\cos^2\alpha - A\sin^2\alpha)/3\pi + \lambda H^*\sin\alpha\cos\alpha(1 + A)/3 \tag{5.28}$$

Equation (5.28) is the same as equation (27) in [64].

5.3.3 Exact Solution

It may be shown (Appendix 3) that equation (5.28) reduces to equation (5.14). Therefore, the lower and upper bound calculations lead to identical predictions so that the theoretical solution is

exact according to the classical theory of plasticity.

5.3.4 Analysis for Computation and Results

Substituting (5.24) into (5.1) and eliminating H* from equations (5.26) and (5.1) gives

$$G^{*\prime} = \frac{4(1 - A\tan^2\alpha)}{[\pi^2\tan^2\alpha(A + 1)^2 + 16(1 - A\tan^2\alpha)^2]^{\frac{1}{2}}} \tag{5.29}$$

and therefore

$$H^* = \frac{\pi\tan\alpha(A + 1)}{[\pi^2\tan^2\alpha(A + 1)^2 + 16(1 - A\tan^2\alpha)^2]^{\frac{1}{2}}} \tag{5.30}$$

Substituting (2.23) and (2.24) into (2.22) gives

$$N' = - G' \frac{\sin\alpha\cos\alpha}{r} + H \frac{\cos^2\alpha}{r} \tag{5.31}$$

Substituting (5.31) into (2.21) and using equations (2.23) and (2.24) gives

$$T = - \frac{\chi r}{\cos^2\alpha} + \frac{G'\sin^2\alpha}{r} - \frac{H\sin\alpha\cos\alpha}{r} \tag{5.32}$$

Therefore, using (5.4 a-c) in (5.32)

$$\frac{T}{T_o} = - \frac{\chi}{\cos^2\alpha} + \frac{4G^{*\prime}\lambda\sin^2\alpha}{3\pi} - \frac{H^*\lambda\sin\alpha\cos\alpha}{3} \tag{5.33}$$

For given values of α and m, λ may be calculated from equation (2.41) and χ can be obtained from Chapter 4. Then for a given value of A, $G^{*\prime}$ and H^* can be found from equations (5.29) and (5.30), respectively. Values of χ, G'^* and H^* can then be substituted into equation (5.33) to obtain value for T/T_o. Thus, φ can be calculated from equation (5.5) and μ from equation (5.11) or (5.13). This procedure is repeated for values of $-\infty < A < \infty$ to obtain an interaction curve lying in a φ-μ plane.

Fig. 5.1 shows the exact interaction curves in the dimensionless axial load φ and bending moment μ space for various values of α while Figs. 5.2a and 5.2b[¥] show that for various numbers of wires, m.

5.4 Plastic Collapse Load for a Single Strand with Core Wire

5.4.1 Relationship between the Strand and the Core

It will be assumed that the strand and the core extend and rotate as a unit. Therefore, if subscript c refers to variables for the core,

$$\delta_c = \delta \tag{5.34}$$

and

$$\Delta_c = \Delta \tag{5.35}$$

where δ is the axial extension and Δ, the angular rotation on one pitch of the strand. Also, it is obvious that,

$$F_T = F_c + F \tag{5.36}$$

and

$$M_T = M_c + M \tag{5.37}$$

where F_T is the total axial load and M_T, the total torsional moment acting on the rope.

5.4.2 The Core

It is assumed that when the rope is subjected to axial and torsional loads, no bending occurs in the core wire. Thus, the tension T_c and twisting moment H_c will control plastic yielding in the core wire. Therefore, from equation (5.2), the yield criterion can be written as

$$\left(\frac{H_c}{H_{co}}\right)^2 + \left(\frac{T_c}{T_{co}}\right)^2 = 1 \tag{5.38}$$

¥ Fig. 5.2a shows the average axial collapse load in an individual wire and Fig. 5.2b shows the total axial collapse load of the strand.

where

$$H_{co} = \pi \sigma_{co} R_c^3/3 \text{ and } T_{co} = \pi \sigma_{co} R_c^2 \qquad (5.39\ a,b)$$

where σ_{co} is the uniaxial yield stress of the material for the core and R_c is the radius of the core wire.

Since the core wire is straight,

$$F_c = T_c \qquad (5.40)$$

and

$$M_c = H_c \qquad (5.41)$$

Therefore, the lower bound to the exact values of F_c and M_c required for the collapse of an elastic perfectly plastic core wire is given by

$$\left(\frac{F_c}{T_{co}}\right)^2 + \left(\frac{M_c}{H_{co}}\right)^2 = 1 \qquad (5.42)$$

The upper bound to the exact values of F_c and M_c associated with the collapse of an elastic perfectly plastic core wire is obtained by equating the external work rate to the corresponding internal energy dissipation, viz.

$$F_c \dot{\delta}_c + M_c \dot{\Delta}_c = \int_o^L (T_c \dot{\varepsilon}_c + H_c \dot{\tau}_c)\, ds \qquad (5.43)$$

where L is the length of the rope, ε_c, the axial strain of the core wire and τ_c its twist per unit length.

To satisfy the normality requirements of plasticity, the generalised strain rate vector $\overline{E}$ must be parallel to $\nabla\Phi$ where $\Phi = 0$ represents the yield condition (equation 5.38)

$$\nabla\Phi = \underline{j}\,\frac{2H_c}{H_{co}^2} + \underline{k}\,\frac{2T_c}{T_{co}^2} \tag{5.44}$$

$$\bar{E} = \underline{j}\,\dot{\tau}_c + \underline{k}\,\dot{\varepsilon}_c \tag{5.45}$$

Therefore,

$$\frac{2H_c}{H_{co}^2}\,\dot{\varepsilon}_c - \frac{2T_c}{T_{co}^2}\,\dot{\tau}_c = 0$$

$$\dot{\tau}_c = \frac{H_c}{T_c}\left(\frac{T_{co}}{H_{co}}\right)^2 \dot{\varepsilon}_c \tag{5.46}$$

substituting equation (5.46) into equation (5.43) gives

$$\dot{F}_c\dot{\delta}_c + \dot{M}_c\dot{\Delta}_c = \dot{\delta}_c\left[T_c + \frac{H_c^2}{T_c}\left(\frac{T_{co}}{H_{co}}\right)^2\right] \tag{5.47}$$

since

$$\delta_c = L\varepsilon_c \tag{5.48}$$

Relating the core to the strand by Equation (5.47) gives the upper bound to the exact values of F_c and M_c required for the collapse of an elastic perfectly plastic core wire.

It can be shown (Appendix 4) that equation (5.47) reduces to equation (5.42) with the aid of equations (5.27), (5.38), (5.40), (5.41), (2.29) and (5.48). Therefore, exact values of F_c and M_c required for the collapse of an elastic perfectly plastic core wire can be obtained.

Using equations (5.27), (5.34), (5.35) and (2.29 a,b) and $h/2\pi r = \tan\alpha$, equation (5.47) can be written as

$$M_c = r\,A\tan\alpha\left[\frac{T_c^2H_{co}^2 + H_c^2T_{co}^2}{T_cH_{co}^2} - F_c\right] \tag{5.49}$$

Also, using equations (2.29 a,b), (5.27), (5.48) and $\Delta_c = L\tau_c$, equation (5.46) can be written as

$$rA\tan\alpha = \frac{T_c}{H_c}\left(\frac{H_{co}}{T_{co}}\right)^2 \tag{5.50}$$

Substituting equations (5.40) and (5.41) into equation (5.50) and eliminating M_c using equation (5.42) gives

$$F_c = \frac{rA\tan\alpha T_{co}^2}{[T_{co}^2 r^2 A^2 \tan^2\alpha + H_{co}^2]^{\frac{1}{2}}} \tag{5.51}$$

Alternatively, eliminating F_c from these equations gives

$$M_c = \frac{H_{co}^2}{[T_{co}^2 r^2 A^2 \tan^2\alpha + H_{co}^2]^{\frac{1}{2}}} \tag{5.52}$$

5.4.3 Exact Solution for the Plastic Collapse of a Single Strand with Core Wire.

Since exact solutions are obtained for a single strand (section 5.3) and a core wire (section 5.4.2), it follows from equations (5.36) and (5.37) that exact values of F_T (total axial force on the rope) and M_T (total torsional moment on the rope) required for the collapse of an elastic perfectly plastic rope can be found.

From equations (5.36) and (5.37),

$$\Phi_T = \Phi + \Phi_c \tag{5.53}$$

$$\mu_T = \mu + \mu_c$$

where

$$\Phi_T = F_T/mT_o$$

$$\Phi_c = F_c/mT_o$$

and

$$\mu_T = M_T/mH_o \tag{5.55 a-d}$$

$$\mu_c = M_c/mH_o$$

From equations (5.5), (5.51), (5.53) and (5.55 a,b)

$$\Phi_T = \frac{(T/T_o + \chi)}{\sin\alpha} + \frac{rA\tan\alpha T_{co}^2}{mT_o[r^2A^2\tan^2\alpha T_{co}^2 + H_{co}^2]^{\frac{1}{2}}} \quad (5.56)$$

Also, from equations (5.5), (5.11), (5.52), (5.54) and (5.55 c,d),

$$\mu_T = \frac{H^*}{\sin\alpha} - \frac{3\cos\alpha}{\lambda\sin^2\alpha}\left(\frac{T}{T_o}\right) - \frac{3\chi\cos\alpha}{\lambda\sin^2\alpha}(1 + 2\sin^2\alpha)$$

$$+ \frac{H_{co}^2}{mH_o[r^2A^2\tan^2\alpha T_{co}^2 + H_{co}^2]^{\frac{1}{2}}} \quad (5.57)$$

From equations (5.4 b,c) it can be deduced that

$$H_{co} = \pi\sigma_{co}R_c^3/3 \quad \text{and} \quad T_{co} = \pi\sigma_{co}R_c^2 \quad (5.58\ a\text{-}b)$$

If the core wire and the helical wires in the strand are made of the same material and are of the same diameter,

$$H_{co} = H_o \quad (5.59\ a)$$

and

$$T_{co} = T_o \quad (5.59\ b)$$

Therefore equations (5.56) and (5.57) become

$$\Phi_T = \frac{(T/T_o + \chi)}{\sin\alpha} + \frac{rA\tan\alpha\, T_o}{m[r^2A^2\tan^2\alpha T_o^2 + H_o^2]^{\frac{1}{2}}} \quad (5.60)$$

and

$$\mu_T = \frac{H}{H_o\sin\alpha} - \frac{3\cos\alpha}{\lambda\sin^2\alpha}\left(\frac{T}{T_o}\right) - \frac{3\chi\cos\alpha}{\lambda\sin^2\alpha}(1 + 2\sin^2\alpha)$$

$$+ \frac{H_o}{m[r^2A^2\tan^2\alpha T_o^2 + H_o^2]^{\frac{1}{2}}} \quad (5.61)$$

However, if the diameters of the core wire and the wires in the strand are different, H_{co} and T_{co} in equations (5.56) and (5.57) become

$$H_{co} = H_o \left(\frac{R_c}{R}\right)^3 \quad \text{and} \quad T_{co} = T_o \left(\frac{R_c}{R}\right)^2 \qquad (5.62\ a,b)$$

respectively.

5.4.4 Analysis for Computation and Results

For given values of α and m, r may be calculated from equation (2.41), and χ may be found from Figs. 4.1 and 4.2. When the value of A is given, H and T may be found from equations (5.30) and (5.33) respectively. Thus, Φ_T and μ_T can be calculated from equation (5.56) and (5.57), when the ratio of radii R_c/R in equations (5.62 a,b) is given. This may be repeated for values of $-\infty < A < \infty$ and an interaction curve lying in a $\Phi_T - \mu_T$ plane can thus be constructed.

Fig. 5.3 shows the exact interaction curves in the dimensionless total axial load, Φ_T and total bending moment μ_T space for various values of α while Fig. 5.4 shows that for various numbers of wires, m. Fig. 5.5 shows the curves for various radii ratio, R_c/R.

5.5 Plastic Collapse Load for a Rope Made Up of Two Layers of Strand and a Core Wire

5.5.1 The Rope-Governing Equations

The rope considered is a 1 x 19 rope whose cross-section is shown in Fig. 3.14. The method however, can be easily adapted to ropes with different number of wires in each strand.

It will be assumed that the two layers of strand and the core wire extend and rotate as a unit. Therefcre,

$$\bar{\delta} = \delta_c = \delta \qquad (5.63)$$

and $$\bar{\Delta} = \Delta_c = \Delta \tag{5.64}$$

where the superscript bar ($\bar{}$) denotes variables associated with the outer strand. Also, for equilibrium,

$$F_T = F + \bar{F} + F_c \tag{5.65}$$

and $$M_T = M + \bar{M} + M_c \tag{5.66}$$

5.5.2 The Outer Strand

Unlike the inner strand, the wires in the outer strand are not in contact with each other. Instead, contacts only occur with wires in the inner strand. When the two strands are of different helix angles, point contacts will occur at equally spaced distance along each of the wires in the strands. These distances are given by equations (3.44) and (3.45).

The resultant normal distributed line load acting on each of the wires in the outer strand $\bar{X}$ is given by equation (3.58) and its corresponding dimensionless value is given by equation (3.59) where

$$\bar{r} = r + R + \bar{R} \tag{5.67}$$

The equations that govern the outer strand are similar in form to that of a single strand (Section 5.3). Thus

$$\frac{\bar{T}}{T_o} = \bar{\varphi} \sin \bar{\alpha} - \bar{\chi} \tag{5.68}$$

where

$$\bar{\varphi} = \bar{F}/\bar{m}T_o \tag{5.69}$$

and $$\chi = \bar{r}\bar{X}/T_o \tag{5.70}$$

$$\frac{\bar{H}}{H_o} = \bar{\mu}\sin\bar{\alpha} + 3\bar{r}\bar{\varphi}\cos\bar{\alpha}/\bar{R} + 6\bar{r}\bar{\chi}\tan\bar{\alpha}/\bar{R} \tag{5.71}$$

where $$\bar{\mu} = \bar{M}/\bar{m}H_o \tag{5.72}$$

$$\frac{\bar{G}'}{G_o} = (\tfrac{\pi}{4})[\bar{\mu}\cos\bar{\alpha} - (3\bar{r}/\bar{R})\{\bar{\varphi}\sin\bar{\alpha} + \bar{\chi}(\tan^2\bar{\alpha} - 1)\}] \tag{5.73}$$

when the wires are made of the same material.

Also,

$$\bar{G}^* = \frac{4(1 - \bar{A}\tan^2\bar{\alpha})}{[\pi^2\tan^2\bar{\alpha}\,(\bar{A} + 1)^2 + 16(1 - \bar{A}\tan^2\bar{\alpha})^2]^{\frac{1}{2}}} \tag{5.74}$$

and

$$\bar{H}^* = \frac{\pi\tan\bar{\alpha}\,(\bar{A} + 1)}{[\pi^2\tan^2\bar{\alpha}\,(\bar{A} + 1)^2 + 16(1 - \bar{A}\tan^2\bar{\alpha})^2]^{\frac{1}{2}}} \tag{5.75}$$

where $$\bar{A} = \bar{\dot{\epsilon}}/\bar{\dot{\gamma}} \tag{5.76}$$

Using equations (2.29 a,b)

$$\bar{A} = \frac{\bar{\dot{\delta}}}{\bar{h}}\cdot\frac{2\pi}{\bar{\dot{\gamma}}} \tag{5.77}$$

substituting equations (5.63) and (5.64) into equation (5.77) and using equations (2.29 a,b)

$$\bar{A} = \frac{h}{\bar{h}}A \tag{5.78}$$

where $$A = \dot{\epsilon}/\dot{\gamma} \tag{5.79}$$

Equation (5.78) can be rewritten as

$$\bar{A} = \frac{r\tan\alpha}{\bar{r}\tan\bar{\alpha}}A \tag{5.80}$$

since $$\tan\alpha = h/2\pi r$$

and $$\tan\bar{\alpha} = \bar{h}/2\pi\bar{r}$$

It has been defined that [equation (5.15)],

$$\lambda = \frac{R}{r} \tag{5.81}$$

Thus, similarly,

$$\bar{\lambda} = \bar{R}/\bar{r} \tag{5.82}$$

Substituting equation (5.67) into equation (5.82) and eliminating r using equation (5.81) gives

$$\bar{\lambda} = \frac{\bar{R}}{R}\left[\frac{1}{\frac{1}{\lambda} + 1 + \bar{R}/R}\right] \tag{5.83}$$

Substituting equations (5.81) and (5.82) into equation (5.83) gives

$$\frac{r}{\bar{r}} = \frac{1}{\lambda}\left[\frac{1}{\frac{1}{\lambda} + 1 + \bar{R}/R}\right] \tag{5.84}$$

Therefore, substituting equation (5.84) into equation (5.80) gives

$$\bar{A} = \frac{\tan\alpha}{\lambda\tan\bar{\alpha}}\left[\frac{1}{\frac{1}{\lambda} + 1 + \bar{R}/R}\right]A \tag{5.85}$$

5.5.3 Exact Solution

Since it has been found (section 5.3) that an exact solution exists for the plastic collapse of a single strand, exact values of $\bar{F}$ (axial load on the outer strand) and $\bar{M}$ (torsional moment on the outer strand) for the plastic collapse of the outer strand can also be found. Therefore, from equations (5.65) and (5.66) it follows that exact values of F_T and M_T for the plastic collapse of a rope made of two layers of strand and a core wire can be found.

5.5.4 Analysis for Computation and Results

The procedure for constructing the interaction curves are similar to that mentioned in the previous sections.

Substituting equations (5.55 a,b) and (5.69) into equation (5.65) gives

$$\varphi_T = \varphi + \frac{\bar{m}}{m}\bar{\varphi} + \varphi_c \qquad (5.86)$$

Similarly, substituting equations (5.55 c,d) and (5.72) into equation (5.66) gives

$$\mu_T = \mu + \frac{\bar{m}}{m}\bar{\mu} + \mu_c \qquad (5.87)$$

For given values of α, m and A, φ_c and μ_c can be found from section (5.4.4) $\bar{X}$ can be obtained from Figs. 4.4 when values of $\bar{\alpha}$ and $\bar{m}$ are known. $\bar{A}$ can be calculated from equation (5.80) and following the same procedure as for a single strand, values of $\bar{\varphi}$ and $\bar{\mu}$ can be found.

For the wires in the inner strand, the line load $\bar{X}$ due to contact with wires in the outer strand may be regarded as an additional normal line load. Thus (see Fig 5.13)

$$X = X_I - \bar{X} \qquad (5.88)$$

where X_I is the line load on the inner wire due to the contact that occurs between wires in the inner strand. X is the resultant normal line load acting on the wires in the inner strand.

For the given values of α and m, X_I can be obtained from Figs. 4.1 and 4.2. Finally, following the same procedure as in section (5.3.4), values of φ and μ can be calculated.

Thus, for given values of α, $\bar{\alpha}$, m, $\bar{m}$ and A exact values of φ_T and μ_T for the plastic collapse of the rope can be found.

Figures 5.7, 5.8 and 5.9 show the exact interaction curves for the plastic collapse of rope with two layers of strand. When the wires are of the same size and Figures 5.10[¥] and 5.11 show the curves for various values of ratios of radii $^{R}c/R$ and $^{R}/R$.

5.6 Rope with n-Layers of Strand

The previous analyses can easily be extended to study plastic collapse of a rope with any number of layers of strand.

The total axial force on the rope will be the sum of forces on the core wire (if it is present) and the layers of strand, viz.

$$F_T = F_c + F_1 + F_2 \ldots\ldots + F_n \tag{5.89}$$

Similarly, the total torsional moment acting on the rope will be the sum of the moments on the core wire (if it is present) and the layers of strand, viz.

$$M_T = M_c + M_1 + M_2 \ldots\ldots + M_n \tag{5.90}$$

Equations (5.89) and (5.90) can be written in dimensionless form such that

$$\varphi_T = \varphi_c + \varphi_1 + \frac{m_2}{m_1}\varphi_2 + \ldots\ldots\frac{m_n}{m_1}\varphi_n \tag{5.91}$$

and

$$\mu_T = \mu_c + \mu_1 + \frac{m_2}{m_1}\mu_2 + \ldots\ldots\frac{m_n}{m_1}\mu_n \tag{5.92}$$

where

$$\begin{aligned} \varphi_T &= {}^{FT}/_{m_1 T_o} \\ \varphi_c &= {}^{F_c}/_{m_1 T_o} \\ \varphi_1 &= {}^{F_1}/_{m_1 T_o} \\ \varphi_2 &= {}^{F_2}/_{m_2 T_o} \\ \varphi_n &= {}^{F_n}/_{m_n T_o} \end{aligned} \tag{5.93}$$

¥ This is considering the values of $^{R}c/_{R}$ less than one and increasing from that value.

and

$$\mu_T = {}^{M_T}/_{m_1 H_o}$$

$$\mu_c = {}^{M_c}/_{m_1 H_o}$$

$$\mu_1 = {}^{M_1}/_{m_1 H_o} \qquad (5.94)$$

$$\mu_2 = {}^{M_2}/_{m_2 H_o}$$

$$\mu_n = {}^{M_n}/_{m_n H_o}$$

where m_i is the number of wires in the strand.

It may be assumed that rotationally and axially, the core wire and the layers of strand move as a unit so that

$$\delta_c = \delta_1 = \delta_2 = \ldots \delta_n \qquad (5.95)$$

and

$$\Delta_c = \Delta_1 = \Delta_2 = \ldots \Delta_n \qquad (5.96)$$

It is defined that

$$A = {}^{\dot{\varepsilon}_1}/_{\dot{\gamma}_1} \qquad (5.97)$$

Therefore, since $\varepsilon = {}^{\delta}/_{n}$ and $\gamma = {}^{\Delta}/_{2\pi}$

$$A = \frac{\dot{\delta}_1}{\dot{\Delta}_1 r_1 \tan\alpha_1} \qquad (5.98)$$

where $\tan\alpha_1 = {}^{h_1}/_{2\pi r_1}$

If it is also defined that

$$A_i = {}^{\dot{\varepsilon}_i}/_{\dot{\gamma}_i} \qquad (5.99)$$

it can be shown using equations (5.95) (5.96) and (5.98) that

$$A_i = \frac{r_1 \tan\alpha_1}{r_i \tan\alpha_i} A \qquad (5.100)$$

where $\tan\alpha_i = {}^{h_i}/_{2\pi r_i}$ (5.101)

Using equation (5.85), equation (5.95) can be written as

$$A_i = \frac{\tan\alpha_1}{\lambda_1 \tan\alpha_i} \left[\frac{1}{\frac{1}{\lambda_1} + 1 + \frac{Ri}{R_1}}\right] \qquad (5.102)$$

The collapse value of the normal line load X_i acting on the wires in each layer of strand will depend on the nature of contacts experienced by each of the wires and that of the wires in the outer layers. It will be assumed that apart from the first layer, the wires in the other layers are in contact with wires in neighbouring layers and they are not in contact with wires in the same layer. Thus, there will be an interaction between the various layers. If X_1 is the normal line load for wires in the first layer due to contact between wires in the same layer, X_2, its equivalent in the second layer due to contact between wires in the second and first layer, X_3, its equivalent in the third layer due to contact between wires in the third and second layer, etc.

$$X'_i = X_i - X_{i+1} - X_{i+2} \ldots\ldots X_n \qquad (5.103)$$

where X'_i is the resultant normal line load acting on the wires in the i^{th} layer.

The values of X_i can be calculated from equations (4.5) and (4.10). Since it has been shown that exact solution exists for the plastic collapse of a single strand and also that for a core wire, it is possible to obtain exact values of φ_T and μ_T for the plastic collapse of a rope with n layers of strand from equations (5.91) and (5.92).

Value of φ_i can be calculated from

$$\varphi_i = \frac{1}{\sin\alpha_i}\left(\frac{T_i}{T_o} + \chi_i\right) \tag{5.104}$$

where $\frac{T_i}{T_o}$ is obtained from

$$\frac{T_i}{T_o} = -\frac{\chi_i}{\cos^2\alpha_i} + \frac{4G'^*_i R_i \sin^2\alpha_i}{3\pi r_i} - \frac{H^*_i R_i \sin\alpha_i \cos\alpha_i}{3r_i} \tag{5.105}$$

where

$$r_1 = R_1\left\{1 + \frac{\tan^2(\pi/2 - \pi/m_1)}{\sin^2\alpha_1}\right\}^{\frac{1}{2}}$$

$$r_2 = r_1 + R_1 + R_2$$

$$r_3 = r_1 + R_1 + 2R_2 + R_3$$

$$r_n = r_1 + R_1 + 2(R_2 + R_3 \ldots + R_n - 1) + R_n \tag{5.106}$$

when the wires are of the same diameters. From equations (5.29) and (5.30),

$$G'^*_i = \frac{4(1 - A_i\tan^2\alpha_i)}{[\pi^2\tan^2\alpha_i(A_i + 1) + 16(1 - A_i\tan^2\alpha_i)^2]^{\frac{1}{2}}} \tag{5.107}$$

$$H^*_i = \frac{\pi\tan\alpha_i(A_i + 1)}{[\pi^2\tan^2\alpha_i(A_i + 1) + 16(1 - A_i\tan^2\alpha_i)^2]^{\frac{1}{2}}} \tag{5.108}$$

value of μ_i can then be calculated from

$$\mu_i = \frac{1}{\sin\alpha_i}\left\{H^*_i - \frac{3r_i\varphi_i\cos\alpha_i}{R_i} - \frac{6r_i\chi_i\tan\alpha_i}{R_i}\right\} \tag{5.109}$$

Thus, with values of φ_c and μ_c calculated from section (5.4), for given values of helix angles of the layers of strand, the radius and the number of wires in each layer of strand, and A, the exact values of φ_T and μ_T for the plastic collapse of the rope with n layers of strand can be calculated. By repeating the procedure with values of $-\infty < A < \infty$, and interaction curve lying in the φ_T-μ_T plane may be constructed.

5.7 DISCUSSION

5.7.1 Normality

Figure 5.12 shows a typical dimensionless load interaction curve. The ellipse can be divided into two halves - the curve PQR is obtained with the positive values of the square root in equations (5.29) and (5.30) and the curve PSR constructed using the negative values of the square root. The directions of the strain rate vector are shown at points P,Q,R and S. At points P and R, A has the value $+\infty$, and $-\infty$ respectively. Thus, they show the direction of the strain rate vector, $\dot{\epsilon}$ (i.e = $\dot{\delta}/h$) which must be parallel to the ϕ axis. Since, the direction is also normal to the interaction curve at P and R, the normality requirement has been satisfied. Similarly, at points Q and S, A has the value zero and thus the arrows show the direction of the strain rate vector, $\dot{\gamma}$ (i.e = $\dot{\Delta}/2\pi$) which must be parallel to the μ axis.

Figure 5.12 is the interaction curve for a single strand where m=6 and $\alpha=75^0$. In this example, the axial collapse load ($\phi>0$, $\mu=0$) is associated with either axial stretching ($\dot{\delta}>0$) and a slight winding ($\dot{\Delta}>0$) or with axial contraction ($\dot{\delta}<0$) and unwinding ($\dot{\Delta}<0$).

5.7.2 Effect of the change in helix angle.

It is evident from Figure 5.1 that the maximum axial collapse load increases as the helix angle approaches 90^0, but the difference between the maximum and the minimum values of the dimensionless twisting moment μ decreases. Also, the maximum axial collapse load is associated with an axial stretching ($\dot{\delta}>0$) and winding ($\dot{\Delta}>0$) when $\alpha=60^0$, and as α increases, the winding diminishes until eventually when $\alpha=80^0$, the axial collapse load is associated with an axial

stretching ($\dot{\delta}>0$) and a slight unwinding ($\dot{\Delta}>0$).

5.7.3 Effect of the number of wires in the strand.

Figures 5.2a and 5.2b show the dimensionless load interaction curves for a single strand with $\alpha=75^{\circ}$ but with varying number of wires in the strand. As expected the collapse load for any particular end condition increases as the number of wires increases, but doubling the number of wires does not make the axial collapse load twice as large as can be seen in figure 5.2b. However, the maximum value of μ, does increase by more than a factor of two. Thus, this result suggests that if a strand is to undergo a lot of twisting, then it is more efficient to have it made with larger number of wires. Figure 5.2a explains further this point - as the number of wires in the strand increases, the average axial collapse load in an individual wire decreases but the maximum value of the collapse load μ, increases.

5.7.4 Effect of introducing a core wire.

Comparing Figures 5.1 and 5.2 with figures 5.3 and 5.4, it can be seen that by introducing a core wire in a single strand, the maximum axial collapse load is increased by 0.17 which is equivalent to 18.5% of the axial collapse load for a strand with core wire with $\alpha=80^{\circ}$. The difference between maximum and minimum collapse load ϕ, is also increased by a factor of two. However, there is little change in μ except for a slight increase in its minimum collapse load. Figure 5.5 shows the effect of the size of the core wire on the load interaction curve. When the diameter of the core wire is larger than that of the wires in the strand, contact will no longer occur between wires in the strand. Instead, contact will occur

between the wires in the strand and the core wire. This is illustrated in Figure 5.6. Figure 5.5 shows that the maximum axial collapse load increases as the diameter of the core increases but when the core wire is larger than the wires in the strand, the maximum axial collapse load drops to a lower value. This is due to the fact that the contact stresses are more critical between the core and the wires in the strand than between adjacent wires in the strand. It has to be noted here that the rope in which the core wire is smaller than the wires in the strand is a hypothetical one since the core wire will not be held together in the rope. This can however be overcome by introducing soft fibres around the core wire which helps little in improving the rope strength but does hold the core wire in place.

5.7.5 Rope with two layers of strand.

In a rope with two layers of strand, the inter-strand-wire-contact greatly influence the strength of the rope. This is because the contact stresses developed from point contact is more critical than that developed from line contact as shown in Chapters 3 and 4.

It is evident from Figures 5.7, 5.8 and 5.9 that as the contact angle between the wires in the inner strand and that of the outer strand ($\bar{\alpha}$-α) increases, the collapse load decreases. This is due mainly to the reduction in the contact area which increases the critical contact stresses for a given contact force. Figures 5.7, 5.8 and 5.9 also suggest a suitable configuration for rope with two layers of strand. When compared to the load interaction curve for a single strand with core wire (dashed curve), it can be seen that the

helix angle for the second strand should be less than $\simeq 105^{0}$. Also, for the rope to withstand a higher axial load, the helix angles of the strands have to be a value approaching 90^{0}.

Effect of the size of the core wire on the load interaction curve is similar to that discussed in Section 5.7.4 for a rope with a single strand. This is shown in Figure 5.10.

Figure 5.11 shows that when the radius of the wires in the outer strand is increased by a factor of 0.1R, the axial collapse load ($\phi_T>0$, $\mu_T=0$) is increased by 1.3%. Thus, since the increase is small, the variation in the size of the wires in the outer strand from its nominal size (when $\bar{R}=R$) is not very critical.

CHAPTER 6

Finite extension of helical wires.

6.1 Equilibrium Equations

Consider an element of a curved rod with finite extension as shown in Fig. 6.1. The length of the rod is initially ds and due to the forces and moments as shown, the rod extends by an amount $\varepsilon_\omega ds$, where ε_ω is the axial strain in the rod. There are also rotations κds, $\kappa' ds$ and τds which are positive about the -G, -G' and -H sense, respectively.

6.1.1 Equilibrium of Forces

For equilibrium in the T direction.

$$(T + \frac{\partial T}{\partial s} ds)\cos(\kappa' ds)\cos \kappa ds - T$$

$$+ (N' + \frac{\partial N'}{\partial s} ds)\cos(\tau ds)\sin(\kappa ds)\cos(\kappa' ds)$$

$$- (N + \frac{\partial N}{\partial s} ds)\cos(\tau ds)\sin(\kappa' ds)\cos(\kappa ds)$$

$$+ Z ds = 0 \qquad (6.1\ a)$$

For equilibrium in the N' direction.

$$(N' + \frac{\partial N'}{\partial s} ds)\cos(\tau ds)\cos(\kappa ds) - N'$$

$$+ (N + \frac{\partial N}{\partial s} ds)\sin(\tau ds)\cos(\kappa' ds)\cos(\kappa ds)$$

$$- (T + \frac{\partial T}{\partial s} ds)\cos(\kappa' ds)\sin(\kappa ds)\cos(\tau ds)$$

$$+ Y ds = 0 \qquad (6.1\ b)$$

For equilibrium in the N direction.

$$(N + \frac{\partial N}{\partial s} ds)\cos(\tau ds)\cos(\kappa' ds) - N$$

$$+ (T + \frac{\partial T}{\partial s} ds)\cos(\kappa ds)\sin(\kappa' ds)\cos(\tau ds)$$

$$- (N' + \frac{\partial N'}{\partial s} ds)\sin(\tau ds)\cos(\kappa' ds)\cos(\kappa ds)$$

$$+ X ds = 0 \qquad (6.1\ c)$$

Using the MacLaurin's series expansion,

$$\cos(x) = 1 - \frac{x^2}{2!} + \frac{x^4}{4!} - \frac{x^6}{6!} + \ldots.$$

$$\sin(x) = x - \frac{x^3}{3!} + \frac{x^5}{5!} - \frac{x^7}{7!} + \ldots. \qquad (6.2\ a,b)$$

Neglecting terms of second order and higher and dividing equations (6.1 a-c) throughout by ds gives

$$\frac{\partial T}{\partial s} + N'\kappa - N\kappa' + Z = 0$$

$$\frac{\partial N'}{\partial s} - T\kappa + N\tau + Y = 0$$

$$\frac{\partial N}{\partial s} + T\kappa' - N'\tau + X = 0 \qquad (6.3\ a\text{-}c)$$

6.1.2 Equilibrium of Moments

For equilibrium in H direction.

$$(H + \frac{\partial H}{\partial s} ds)\cos(\kappa' ds)\cos(\kappa ds) - H$$
$$+ (G' + \frac{\partial G'}{\partial s} ds)\cos(\tau ds)\sin(\kappa ds)\cos(\kappa' ds)$$
$$- (G + \frac{\partial G}{\partial s} ds)\cos(\tau ds)\sin(\kappa' ds)\cos(\kappa ds)$$
$$+ \theta ds = 0 \qquad (6.4\ a)$$

For equilibrium in the G' direction.

$$(G' + \frac{\partial G'}{\partial s} ds)\cos(\tau ds)\cos(\kappa ds) - G'$$
$$+ (G + \frac{\partial G}{\partial s} ds)\sin(\tau ds)\cos(\kappa' ds)\cos(\kappa ds)$$
$$- (H + \frac{\partial H}{\partial s} ds)\cos(\kappa' ds)\sin(\kappa ds)\cos(\tau ds)$$
$$+ Nds(1 + \varepsilon_\omega) + K'ds = 0 \qquad (6.4\ b)$$

For equilibrium in the G direction.

$$(G + \frac{\partial G}{\partial s} ds)\cos(\tau ds)\cos(\kappa' ds) - G$$
$$+ (H + \frac{\partial H}{\partial s} ds)\cos(\kappa ds)\sin(\kappa' ds)\cos(\tau ds)$$
$$- (G' + \frac{\partial G'}{\partial s} ds)\sin(\tau ds)\cos(\kappa' ds)\cos(\kappa ds)$$

$$- N'ds(1 + \varepsilon_\omega) + Kds = 0 \qquad (6.4\ c)$$

Again using equation (6.2) in equation (6.4), neglecting terms of second order and higher, and dividing throughout by ds gives

$$\frac{\partial H}{\partial s} + G'\kappa - G\kappa' + \theta = 0$$

$$\frac{\partial G'}{\partial s} + G\tau - H\kappa + N(1 + \varepsilon_\omega) + K' = 0 \qquad (6.5\ a\text{-}c)$$

$$\frac{\partial G}{\partial s} + H\kappa' - G'\tau - N'(1 + \varepsilon_\omega) + K = 0$$

It should be noted here that equations (6.3) and (6.5) are the same as equations obtained by Reissner [88] when the transverse strains in his equations are made to vanish and due allowance made for the difference in signs.

Also, it should be noted that when $\varepsilon_\omega = 0$, equations (6.3) and (6.5) reduce to equation (2.18), the equilibrium equations for the case of infinitesimal extension.

6.1.3 Equilibrium of a Helical Wire

Now, consider a helical wire governed by equations (6.3) and (6.5). When $\kappa = 0$ (the principal axes (x,y) of the cross-section are coincident with the principal normal and binormal vectors of the helix) and that when loaded, behaves identically at all sections (which requires the vanishing of all derivatives with respect to s), equations (6.3) and (6.5) become

$$T\kappa' - N'\tau + X = 0$$

$$H\kappa' - G'\tau - N'(1 + \varepsilon_\omega) = 0 \qquad (6.6\ a,b)$$

where κ' and τ are given by equations (2.23) and (2.24) respectively.

6.1.4 Axial and Torsional Equilibrium of a Strand

When m helical wires are placed together to make up a strand, the resultant line contact force per unit length, X becomes an internal force in the strand.

The total axial force and the total axial twisting moment are respectively given by

$$F = m(T \sin\alpha + N'\cos\alpha) \tag{6.7}$$

and

$$M = m(H\sin\alpha + G'\cos\alpha + Tr\cos\alpha - N'r\sin\alpha) \tag{6.8}$$

which are the same as equations (2.25) and (2.26).

6.2 Consistent Strain Relations

Strain relations which are consistent with the equilibrium equations (6.6), (6.7) and (6.8) can be obtained using the principle of virtual work [89]. Therefore, equating external work rate to internal energy dissipation of a strand, gives

$$F\dot{\delta} + M\dot{\Delta} - m\int_0^L X\dot{\eta}\, ds = \int_0^L m\,(T\dot{\varepsilon}_\omega + G'\dot{\kappa}' + H\dot{\tau})ds \tag{6.9}$$

substituting (6.6 a), (6.7) and (6.8) into (6.9) gives

$$\int_0^L (T\dot{\varepsilon}_\omega + G'\dot{\kappa}' + H\dot{\tau})ds = -\int_0^L (N'\tau - T\kappa')\dot{\eta}\, ds$$

$$+ [T\sin\alpha + N'\cos\alpha]\dot{\delta} + [H\sin\alpha + G'\cos\alpha$$

$$+ rT\cos\alpha - rN'\sin\alpha]\dot{\Delta} \tag{6.10}$$

Using integration by parts.

$$\int_0^L N'^{*}\dot{\delta}ds = [N'\dot{\delta}]_0^L - \int_0^L N'\dot{\delta}^{*}\, ds$$

where superscript $(^{*})$ is derivative with respect to s.

Therefore,

$$N'\dot{\delta} = \int_0^L (N'^{*}\dot{\delta} + N'\dot{\delta}^{*})\, ds \tag{6.11}$$

Since it has been assumed that the helical wires behave identically at all sections,

$$N'^{*} = 0 \tag{6.12}$$

substituting (6.12) into (6.11) gives

$$\dot{N'\delta} = \int_0^L N'\dot{\delta}^{*}ds \tag{6.13 a}$$

similarly,

$$\begin{aligned}
\dot{T\delta} &= \int_0^L T\dot{\delta}^{*}ds \\
\dot{H\Delta} &= \int_0^L H\dot{\Delta}^{*}ds \\
\dot{G'\Delta} &= \int_0^L G'\dot{\Delta}^{*}ds \\
\dot{T\Delta} &= \int_0^L T\,\dot{\Delta}^{*}ds \\
\dot{N'\Delta} &= \int_0^L N'\dot{\Delta}^{*}ds
\end{aligned} \tag{6.13 b-f}$$

From equation (2.29)

$$\dot{\eta} = r\dot{\rho} \; ; \quad \dot{\delta} = h\dot{\varepsilon} \; ; \quad \dot{\Delta} = 2\pi\dot{\gamma} \tag{6.14 a-c}$$

substituting (6.13) and (6.14) into (6.10) gives

$$\begin{aligned}
&\int_0^L (T\dot{\varepsilon}_{\omega} + G'\dot{\kappa}' + H\dot{\tau})ds = -\int_0^L r(N'\tau - T\kappa')\dot{\rho}ds \\
&+ \int_0^L \{(T\sin\alpha + N'\cos\alpha)h\dot{\varepsilon}^{*} + (H\sin\alpha + G'\cos\alpha \\
&+ rT\cos\alpha - rN'\sin\alpha)\,2\pi\dot{\gamma}^{*}\}ds
\end{aligned} \tag{6.15}$$

From equation (6.6 b)

$$N' = \frac{H\kappa' - G'\tau}{(1 + \varepsilon_{\omega})} \tag{6.16}$$

Substituting (6.16) into (6.15), and if G', H and T are non-zeros, we can deduce the following equations.

$$\dot{\varepsilon}_{\omega} = \cos^2\alpha\dot{\rho} + h\sin\alpha\,\dot{\varepsilon}^{*} + 2\pi r\cos\alpha\,\dot{\gamma}^{*} \tag{6.17}$$

$$\dot{\kappa}' = \frac{\sin\alpha\cos\alpha\tau}{1 + \varepsilon_{\omega}}\dot{\rho} - \frac{\tau\cos\alpha h\dot{\varepsilon}^{*}}{1 + \varepsilon_{\omega}} + (\cos\alpha + \frac{\sin^2\alpha\cos\alpha}{1 + \varepsilon_{\omega}})2\pi\dot{\gamma}^{*} \tag{6.18}$$

$$\dot{\tau} = -\frac{\sin\alpha\cos\alpha\kappa'}{1+\varepsilon_\omega}\dot{\rho} + \frac{h\cos\alpha\kappa'}{1+\varepsilon_\omega}\dot{\varepsilon}^* + (\sin\alpha - \frac{\sin\alpha\cos^2\alpha}{1+\varepsilon_\omega})2\pi\dot{\gamma}^* \quad (6.19)$$

If the helical wire is developed onto a flat plane, it can be shown that

$$\frac{h}{2\pi r} = \tan\alpha \quad (6.20)$$

and

$$\frac{2\pi r}{\cos\alpha} = ds(1+\varepsilon_\omega) \quad (6.21)$$

Substituting (6.20) into (6.17) gives

$$\dot{\varepsilon}_\omega = \cos^2\alpha\dot{\rho} + 2\pi r(\frac{\sin^2\alpha}{\cos\alpha}\dot{\varepsilon}^* + \cos\alpha\,\dot{\gamma}^*) \quad (6.22)$$

Substituting (6.21) into (6.22) gives

$$\dot{\varepsilon}_\omega = \cos^2\alpha\dot{\rho} + (1+\varepsilon_\omega)(\sin^2\alpha d\dot{\varepsilon} + \cos^2\alpha d\dot{\gamma}) \quad (6.23)$$

If $\dot{\varepsilon}$ and $\dot{\gamma}$ are initially zero, (6.23) can be written as

$$\dot{\varepsilon}_\omega = \cos^2\alpha\dot{\rho} + (1+\varepsilon_\omega)(\sin^2\alpha\dot{\varepsilon} + \cos^2\alpha\dot{\gamma}) \quad (6.24)$$

Substituting (2.23) and (2.24) into (6.18)

$$\dot{\kappa}' = \frac{\sin^2\alpha\cos^2\alpha}{r(1+\varepsilon_\omega)}\dot{\rho} + 2\pi\{[\cos\alpha + \frac{\sin^2\alpha\cos\alpha}{1+\varepsilon_\omega}]\dot{\gamma}^*$$

$$- \frac{\sin\alpha\cos^2\alpha}{1+\varepsilon_\omega}\cdot\frac{h}{2\pi r}\dot{\varepsilon}^*\} \quad (6.25)$$

Using equation (6.20) and (6.21) in (6.25)

$$\dot{\kappa}' = \frac{\sin^2\alpha\cos^2\alpha}{r(1+\varepsilon_\omega)}\dot{\rho} + \frac{\cos\alpha(1+\varepsilon_\omega)}{r}\{\frac{\sin^2\alpha\cos\alpha}{1+\varepsilon_\omega}(\dot{\gamma} - \dot{\varepsilon})$$

$$+ \cos\alpha\,\dot{\gamma}\}$$

Therefore,

$$\dot{\kappa}' = \frac{\sin^2\alpha\cos^2\alpha}{r}\{\dot{\gamma} - \dot{\varepsilon} + \frac{\dot{\rho}}{1+\varepsilon_\omega}\} + \frac{\cos^2\alpha(1+\varepsilon_\omega)}{r}\dot{\gamma} \quad (6.26)$$

similarly,

$$\dot{\tau} = -\frac{\sin\alpha\cos^3\alpha}{r}\{\dot{\gamma} - \dot{\varepsilon} + \frac{\dot{\rho}}{1+\varepsilon_\omega}\} + \frac{\sin\alpha\cos\alpha}{r}(1+\varepsilon_\omega)\dot{\gamma} \quad (6.27)$$

It can be shown that when $\varepsilon_\omega = 0$ (helical wire inextensible), equations (6.24), (6.26) and (6.27) reduce to the equations for the inextensible case, (2.28), (2.31) and (2.32), respectively. Equations (6.24), (6.26) and (6.27) are therefore consistent according to the principle of virtual work [89] with the equilibrium equations (6.6), (6.7) and (6.8) for the case of finite extension.

6.3 Comparison with Work by Costello and Phillips for Linear Elastic Case

6.3.1 Introduction

In the work of Costello and Phillips [55] the inextensibility assumption imposed on the wires in the wire rope was removed. However, the wire strain was considered small so that Love's [6] equilibrium equations which they used were valid.

In section (6.1), equilibrium equations for helical wires with finite extension have been developed. Thus, in this section, with the aid of the equilibrium equations developed, the extent to which the analysis by Costello and Phillips [55] is valid will be explored.

6.3.2 Analysis for Computation

The rope that will be looked at is the same as that used by Costello and Phillips [55] which is a single-lay cable or a strand with m-wires.

The axial strain of the strand, ε, is defined as $(\ell-\ell_o)/\ell_o$, in which ℓ_o = the original length of the strand and ℓ = final length of the strand. The rotational strain of the strand, ξ, is defined as $r_o(\theta-\theta_o)/\ell_o$ in which θ_o = the original total angle that a given helical wire sweeps out in a plane perpendicular to the axis of the strand; θ = the final total angle the same wire sweeps out in a plane perpendicular to the axis of the strand and r_o = initial helix radius of the strand.

From Fig. 6.2, which shows the initial and final configurations of a developed wire helix,

$$\ell_o = L \sin\alpha_o \tag{6.28}$$

$$\ell = L(1 + \varepsilon_\omega)\sin\alpha \tag{6.29}$$

Therefore the axial strain of the rope,

$$\varepsilon = (1 + \varepsilon_\omega)\frac{\sin\alpha}{\sin\alpha_o} - 1 \tag{6.30}$$

Also,

$$\theta_o = \frac{\ell_o}{r_o \tan\alpha_o} \tag{6.31}$$

$$\theta = \frac{\ell}{r\tan\alpha} \tag{6.32}$$

Therefore, the rotational strain of the rope

$$\xi = \frac{r_o}{\ell_o}\left(\frac{\ell}{r\tan\alpha} - \frac{\ell_o}{r_o\tan\alpha_o}\right) \tag{6.33}$$

$$\xi = \frac{r_o}{r}(1 + \varepsilon)\frac{1}{\tan\alpha} - \frac{1}{\tan\alpha_o} \tag{6.34}$$

Equations (6.30) and (6.34) are the same as equations (20) and (21) in [55]. From equation (6.30),

$$\sin\alpha = \frac{\sin\alpha_o(1 + \varepsilon)}{(1 + \varepsilon_\omega)} \tag{6.35}$$

Therefore,

$$\cos\alpha = 1 - \sqrt{\frac{\sin^2\alpha_o(1 + \varepsilon)^2}{(1 + \varepsilon_\omega)^2}} \tag{6.36}$$

and

$$\tan\alpha = \frac{\sin\alpha_o(1 + \varepsilon)}{(1 + \varepsilon_\omega)\sqrt{1 - \dfrac{\sin^2\alpha_o(1 + \varepsilon)^2}{(1 + \varepsilon_\omega)^2}}} \tag{6.37}$$

The bending and twisting couples, G' and H respectively are related to curvature, κ' and twist, τ by (equation 2.15),

$$G' = \frac{\pi E R^4}{4} (\kappa' - \kappa'_o) \tag{6.38}$$

and

$$H = \frac{\pi E R^4}{4(1+\nu)} (\tau - \tau_o) \tag{6.39}$$

where E = the Young's Modulus; R = radius of the helical wire; and ν = the Poisson's ratio; and the wire tension, T, is related to the wire strain, ε_ω, by

$$T = \pi E R^2 \varepsilon_\omega \tag{6.40}$$

The initial curvature and twist are given by

$$\kappa'_o = \frac{\cos^2 \alpha_o}{r_o} ; \quad \tau_o = \frac{\sin\alpha_o \cos\alpha_o}{r_o} \tag{6.41 a,b}$$

and the configuration is given by

$$\kappa' = \frac{\cos^2 \alpha}{r} ; \quad \tau = \frac{\sin\alpha\cos\alpha}{r} \tag{6.42 a,b}$$

Equation (2.41) gives a geometrical relation between α and r, viz.

$$r = R\sqrt{1 + \frac{\tan^2 (\pi/2 - \pi/m)}{\sin^2 \alpha}} \tag{6.43 a}$$

where m is the number of helical wires in the strand.

It also follows that

$$r_o = R\sqrt{1 + \frac{\tan^2 (\pi/2 - \pi/m)}{\sin^2 \alpha_o}} \tag{6.43 b}$$

If equations (6.43 a,b) are substituted into equations (6.41) and (6.42), and the resulting equations are substituted into equations (6.38) and (6.39), with the aid of equations (6.35), (6.36) and (6.37), it can be shown that G' and H are functions of ε_ω alone for given values

of ε, α_o, m, R, E and ν.

Costello and Phillips [55] employed Love's [6] equilibrium equations for curved bars in their analysis which as shown in section (2.3) reduce to

$$-N'\tau + T\kappa' + X = 0 \tag{6.44}$$

$$-G'\tau + H\kappa' + N' = 0 \tag{6.45}$$

for helical wires.

In section (6.13), when the helical wires are treated with finite extension, it was found that

$$-N'\tau + T\kappa' + X = 0 \tag{6.46}$$

$$-G'\tau + H\kappa' - N'(1 + \varepsilon_\omega) = 0 \tag{6.47}$$

Therefore, the only difference in the equilibrium equations, is the presence of the ε_ω term in equation (6.47).

When m helical wires are laid together to form a strand, the total axial force and the total axial twisting moment of the strand are given by equations (6.7) and (6.8) which are the same as the equations obtained by Costello and Phillips [55].

From equation (6.47),

$$N' = (-G'\tau + H\kappa')/(1 + \varepsilon_\omega) \tag{6.48}$$

It has been shown earlier that G' and H are functions of ε_ω alone and with the aid of equations (6.35), (6.36), (6.37), (6.42) and (6.43), it can also be shown that τ and κ' are functions of ε_ω alone for given values of ε, α_o, m, R, E and ν. Thus, it follows from equation (6.48)

that N' is also a function of ε_ω alone for given values of ε, α_o, m, R, E and ν.

a) Strand ends free to rotate

In this case, no moment will be generated at the strand ends. Therefore,

$$M = 0 \tag{6.49}$$

Substituting equations (6.40) and (6.49) into equation (6.8) yields

$$H\sin\alpha + G'\cos\alpha + \pi ER^2 \varepsilon_\omega r\cos\alpha - N'r\sin\alpha = 0 \tag{6.50}$$

From equations (6.35) and (6.36), it can be seen that $\sin\alpha$ and $\cos\alpha$ are functions of ε_ω for given values of α_o and ε. Also by substituting equation (6.35) into equation (6.43 a), it can be shown that r is also a function of ε_ω. Therefore, since it has been shown earlier that H and G' are also functions of ε_ω alone, equation (6.50) can be written in the form

$$f(\varepsilon_\omega) = 0 \tag{6.51}$$

For given values of ε, α_o, m, R, E and ν, value of ε_ω can be computed from equation (6.51). The corresponding value of F can be calculated from equation (6.7) when equations (6.35), (6.36), (6.38) (6.39), (6.40), (6.41), (6.42), (6.43 a,b) and (6.48) are used.

The results for a strand with 3 wires, of initial helix angles 60°, 70° and 80° are shown in Fig. 6.3. Similar curves for strand with 6 wires are shown in Fig. 6.4.

b) Strand ends constrained against rotation

In this case, the rotational strain of the strand, $\xi = 0$. Thus, equation (6.34) becomes

$$\frac{r_o}{r}(1 + \varepsilon)\frac{1}{\tan\alpha} - \frac{1}{\tan\alpha_o} = 0 \qquad (6.52)$$

By virtue of equations (6.43 a,b), ε can be obtained directly from equation (6.52) when, for given values of m and α_o, the value of α is specified. Value of ε_ω may be calculated from equation (6.30) and the wire tension T can then be calculated using equation (6.40). Using the equations (6.38), (6.39), (6.41), (6.42) and (6.43 a,b), the value of N' can be obtained from equation (6.48). Thus, the corresponding value of F can be determined from equation (6.7).

The plot of dimensionless axial load $F/(ER^2)$ against the axial strain of the strand is shown in Figs. 6.3 and 6.4 for 3 and 6-wire strands, respectively, when the initial helix angles are 60^o, 70^o and 80^o.

6.3.3 Discussion

Figures (6.5) and (6.6 a-c) show the difference between axial loads obtained by Costello and Phillips [55] and that obtained using equilibrium equations developed in section (6.1) for helical wires with finite extension. Fig. 6.5 shows the difference when there is no end-moment acting on the strand while Figs. 6.6 a-c show the curves for the case in which there is no end-rotation.

When there is no end-moment acting on the strand, the axial loads

calculated from the present analysis are smaller than that obtained by Costello and Phillips [55], but when there is no end-rotation in the strand, the axial loads obtained are larger than that obtained by Costello and Phillips [55].

For the two types of end-condition, the difference increases when the number of wires in the strand becomes smaller and when the initial helix angle of the strand gets smaller than 90^{o}. For given values of α_{o}, m and ε, the difference is larger when there is no end-moment acting on the strand as compared to when there is no rotation at the strand ends. As one would expect, for both types of end-condition, the difference increases as the axial strain, ε, increases but when there is no end-moment acting on the strand, a maximum value is reached at a particular value of ε and further increase in ε will result in a reduction in the difference. The maximum difference occurs at a larger value of ε as the value of initial helix angle gets smaller than 90^{o}.

The main point to note is that for the values of parameters considered, the difference in axial loads obtained by Costello and Phillips [55] and that of the present analysis is small, being less than one-half percent. Since wire ropes normally have large helix angles ($> 60^{o}$), Love's [6] equilibrium equations, which were used by Costello and Phillips [55] is adequate, when performing elastic analysis on wire ropes. However, in plastic analysis which naturally involves large strains, it will be shown in Chapter 7 that there is a marked difference in the collapse loads predicted when the wire is considered rigid ($\varepsilon_{\omega} = 0$) and when there is finite extension in the wire.

CHAPTER 7

Static plastic collapse - Finite extension.

7.1 Introduction

In Chapter 5, static plastic collapse of wire ropes in which the strands consist of rigid helical wires ($\varepsilon_\omega = 0$) was considered. In practice, the wires will extend, the extension of which will depend upon the load applied on the wire rope and the physical properties of the wires. This extension may be small when the rope is subjected to elastic loads, but when the rope becomes plastic, the value of the extension is such that it cannot be ignored.

Thus, in the present chapter, the static plastic collapse of wire rope with finite extension will be analysed. The analysis will be on wire ropes with configurations similar to the ropes used in Chapter 5.

7.2 Plastic collapse load for a single strand

7.2.1 Approximation from below

If a helical wire extends when loaded its plastic yielding is controlled by the moments G' and H and the tensile force, T in the wire. The yield criterion is thus given by equation (5.3), viz

$$T_*^2 + H_*^2 + G_*' \left[1 - H_*^2 \right]^{\frac{1}{2}} = 1 \qquad (7.1)$$

where

$$T_* = \frac{T}{T_o} \; ; \quad H_* = \frac{H}{H_o} \; ; \quad G_*' = \frac{G'}{G_o} \qquad (7.2a\text{-}c)$$

and T_o, H_o and G_o are defined by equations (5.4a-c).

To obtain a lower bound to the exact values of F, the axial force on a strand and M, the torsional moment on a strand, required for the collapse of an elastic perfectly plastic strand which consists of extensible helical wires, it is necessary to seek a statically admissible generalised stress field which satisfies the equilibrium equations (6.3) and (6.5) and lies wholly inside or on the yield surface described by

equation (7.1) [86,87]+

Eliminating N' from equations (6.6a) and (6.7) and using equations (2.23) and (2.24) gives

$$T_* = \phi \sin\alpha - \chi \tag{7.3}$$

where

$$\phi = \frac{F}{mT_o} \quad ; \quad \chi = \frac{X_r}{T_o} \tag{7.4a,b}$$

Eliminating T from the same equations above gives

$$\frac{N'}{T_o} = \left(\phi + \frac{\chi \sin\alpha}{\cos^2\alpha} \right) \cos\alpha \tag{7.5}$$

Eliminating G' from equations (6.6b) and (6.8) and using equations (7.2a-c) and (5.4a-c) gives

$$\mu = \frac{H_*}{\sin\alpha} + \frac{3rT_*\cos\alpha}{R} - \frac{3rN'\sin\alpha}{RT_o}\left(1 + \frac{1 + \varepsilon_\omega}{\sin^2\alpha}\right) \tag{7.6}$$

where $\mu = \dfrac{M}{mH_o}$ (7.7)

Substituting equations (7.3) and (7.5) into equation (7.6) gives

$$\mu = \frac{H_*}{\sin\alpha} + \frac{3r\cos\alpha}{R}\left\{ \phi\sin\alpha - \chi - \sin\alpha\left(\phi + \frac{\chi\sin\alpha}{\cos^2\alpha}\right)\left(1 + \frac{1 + \varepsilon_\omega}{\sin^2\alpha}\right) \right\} \tag{7.8}$$

Therefore,

$$H_* = \mu\sin\alpha + \frac{3r\cos\alpha}{R}\left\{(1 + \varepsilon_\omega)\phi + \frac{\chi(2 + \varepsilon_\omega)\sin\alpha}{\cos^2\alpha}\right\} \tag{7.9}$$

Using equations (7.2b,c) and (5.4a-c),

$$G_*' = \frac{\pi}{4}\left[H_* \frac{\cos\alpha}{\sin\alpha} - \frac{3r}{R\sin\alpha\cos\alpha}\frac{N'}{T_o}(1 + \varepsilon_\omega) \right] \tag{7.10}$$

+ It should be noted that the limit theorems have been developed for a case of infinitesimal deflections. Therefore, the lower bound and also the upper bound calculations will not be exact.

Thus, substituting equations (7.5) and (7.9) into (7.10) and simplifying yields

$$G_*' = \frac{\pi}{4}\{\mu\cos\alpha - \frac{3r}{R}[\phi(1+\varepsilon_\omega)\sin\alpha + \chi(\tan^2\alpha(1+\varepsilon_\omega) - 1)]\} \qquad (7.11)$$

The equation for the lower bound to the exact non-dimensionalised collapse moment μ for given values of ϕ, ε^+, α and m^* may now be obtained by substituting equations (7.3), (7.9) and (7.11) into equation (7.1). Alternatively, when the value of μ is known, the lower bound to the exact non-dimensionalised collapse load, ϕ, for given values of ε, α and m may be obtained. Thus, an interaction curve lying in a $\phi - \mu$ plane may be constructed given the values of ε, α and m.

The lower bound equation can be written as

$$\begin{aligned}
&\{\sin^2\alpha + [3(1+\varepsilon_\omega)\cos\alpha/\lambda]^2\}\phi^2 \\
&+ \sin^2\alpha\,\mu^2 + \{1 + [3(2+\varepsilon_\omega)\tan\alpha/\lambda]^2\}\lambda^2 \\
&+ 6(1+\varepsilon_\omega)\sin\alpha\cos\alpha\,\phi\mu/\lambda + 2\sin\alpha\{9(1+\varepsilon_\omega)(2+\varepsilon_\omega)/\lambda^2 \\
&- 1\}\phi\chi + 6(2+\varepsilon_\omega)\sin^2\alpha\mu\chi/\lambda\cos\alpha \\
&+ \pi/4\{\mu\cos\alpha - \frac{3}{\lambda}[\phi(1+\varepsilon_\omega)\sin\alpha \\
&+ \chi(\tan^2\alpha(1+\varepsilon_\omega) - 1)]\}\{1 - 9(1+\varepsilon_\omega)^2\cos^2\alpha\,\phi^2/\lambda^2 \\
&- \sin^2\alpha\mu^2 - 9(2+\varepsilon_\omega)^2\sin^2\alpha\chi^2/\lambda^2\cos^2\alpha \\
&- 6(1+\varepsilon_\omega)\sin\alpha\cos\alpha\,\phi\mu/\lambda \\
&- 18(1+\varepsilon_\omega)(2+\varepsilon_\omega)\sin\phi\chi/\lambda^2 \\
&- 6(2+\varepsilon_\omega)\sin^2\alpha\mu\chi/\lambda\cos\alpha\}^{\frac{1}{2}} - 1 = 0
\end{aligned} \qquad (7.12)$$

+ The corresponding value of ε_ω can be calculated using the procedure in Appendix 6.

* λ (= R/r) may be calculated from equation (2.41) with the given values of α and m, and for the same values of α and m, the value of χ can be obtained from Figures (4.1) and (4.2).

When $\varepsilon_\omega = 0$ and thus tension T regarded as a reaction, the above equation (equation 7.12) reduces to equation (5.14) for the infinitesimal case.

7.2.2 Approximation from above

An upper bound to the exact values of F and M associated with the collapse of an elastic perfectly plastic strand with finite extension is obtained by equating the external work rate to the corresponding internal energy dissipation. This is achieved by selecting any kinematically admissible displacement field and employing the normality requirements of plasticity to seek the relevant active portions of the yield surface (equation 7.1) [86,87].+

In order to satisfy the normality requirements of plasticity, $\overline{E}$, the generalised strain rate vector ($= \dot{\kappa}'\underline{i} + \dot{\tau}\underline{j} + \dot{\varepsilon}_\omega \underline{k}$) must be parallel to $\nabla\Phi$ where $\Phi = 0$ represents the yield condition (equation 7.1) and $\nabla\Phi = \underline{i}\frac{\partial\Phi}{\partial G} + \underline{j}\frac{\partial\Phi}{\partial H} + \underline{k}\frac{\partial\Phi}{\partial T}$. Therefore,

$$\nabla\Phi = \frac{(1 - H_*^2)^{\frac{1}{2}}}{G_o}\,\underline{i} + \left(\frac{2H_*}{H_o} - \frac{G_*H_*}{H_o(1 - H_*^2)^{\frac{1}{2}}}\right)\underline{j} + \frac{2T_*}{T_o}\,\underline{k} \qquad (7.13)$$

$$\overline{E} \otimes \nabla\Phi = (aB - bA)\,\underline{k} + (cA - aC)\,\underline{j} + (bC - cB)\,\underline{i} \qquad (7.14)$$

where

$$a = \dot{\kappa}' \;;\quad b = \dot{\tau} \;;\quad c = \dot{\varepsilon}_\omega \qquad (7.15a\text{-}c)$$

and

$$A = \frac{(1 - H_*^2)^{\frac{1}{2}}}{G_o} \;;\quad B = \left(\frac{2H_*}{H_o} - \frac{G_*H_*}{H_o(1 - H_*^2)^{\frac{1}{2}}}\right) \;;$$

$$C = \frac{2T_*}{T_o} \qquad (7.16a\text{-}c)$$

+ See footnote on page 98.

Therefore, for $\bar{E}$ and $\nabla\Phi$ to be parallel,

$$(aB - bA)\,\underline{k} + (cA - aC)\,\underline{j} + (bC - cB)\,\underline{i} = 0 \tag{7.17}$$

For equation (7.17) to be valid

$$aB = bA \;;\; cA = aC \;;\; bC = cB \tag{7.18a-c}$$

Therefore,

$$\left(\frac{2H_*}{H_o} - \frac{G_*H_*}{H_o(1 - H_*^2)^{\frac{1}{2}}}\right)\dot{\kappa}' = \frac{(1 - H_*^2)^{\frac{1}{2}}}{G_o}\,\dot{\tau} \tag{7.19a}$$

$$\frac{\dot{\kappa}'}{\dot{\varepsilon}_\omega} = \frac{T_o(1 - H_*^2)^{\frac{1}{2}}}{2T_*G_o} \tag{7.19b}$$

$$\frac{\dot{\tau}}{\dot{\varepsilon}_\omega} = \frac{T_o}{2T_*}\left(\frac{2H_*}{H_o} - \frac{G_*H_*}{H_o(1 - H_*^2)^{\frac{1}{2}}}\right) \tag{7.19c}$$

When $\varepsilon_\omega = 0$ and thus tension T regarded as a reaction (and does not appear in the yield condition), equations (7.19 a-c) reduce to equation (5.26) for the case of infinitesimal deflection.

Using equations (5.4 a-c), equations (7.19 a-c) become

$$\frac{\dot{\tau}}{\dot{\kappa}'} = \frac{4H_*}{\pi(1 - H_*^2)^{\frac{1}{2}}}\left(2 - \frac{G_*'}{(1 - H_*^2)^{\frac{1}{2}}}\right) \tag{7.20a}$$

$$\frac{\dot{\kappa}'}{\dot{\varepsilon}_\omega} = \frac{3\pi(1 - H_*^2)^{\frac{1}{2}}}{8T_*R} \tag{7.20b}$$

$$\frac{\dot{\tau}}{\dot{\varepsilon}_\omega} = \frac{3H_*}{T_*R}\left(1 - \frac{G_*'}{2(1 - H_*^2)^{\frac{1}{2}}}\right) \tag{7.20c}$$

From equation (6.24)

$$\dot{\rho} = \frac{\dot{\varepsilon}_\omega}{\cos^2\alpha} - (1 + \varepsilon_\omega)(\tan^2\alpha\,\dot{\varepsilon} + \dot{\gamma}) \tag{7.21}$$

Substituting equation (7.21) into equation (6.26) gives

$$\dot{\kappa}' = \frac{\sin^2\alpha\cos^2\alpha}{r}\{\dot{\gamma} - \dot{\varepsilon}\} + \frac{\cos^2\alpha(1+\varepsilon_\omega)}{r}\dot{\gamma}$$

$$+ \frac{\sin^2\alpha\cos^2\alpha}{r(1+\varepsilon_\omega)}\left\{\frac{\dot{\varepsilon}_\omega}{\cos^2\alpha} - (1+\varepsilon_\omega)[\tan^2\alpha\dot{\varepsilon} + \dot{\gamma}]\right\}$$

$$= \frac{\sin^2\alpha\cos^2\alpha}{r}\dot{\gamma} - \frac{\sin^2\alpha\cos^2\alpha}{r}\dot{\varepsilon} + \frac{\cos^2\alpha(1+\varepsilon_\omega)}{r}\dot{\gamma}$$

$$+ \frac{\sin^2\alpha}{r(1+\varepsilon_\omega)}\dot{\varepsilon}_\omega - \frac{\sin^4\alpha}{r}\dot{\varepsilon} - \frac{\sin^2\alpha\cos^2\alpha}{r}\dot{\gamma}$$

Therefore,

$$\dot{\kappa}' = \frac{\sin^2\alpha}{r(1+\varepsilon_\omega)}\dot{\varepsilon}_\omega - \frac{\sin^2\alpha}{r}\dot{\varepsilon} + \frac{\cos^2\alpha(1+\varepsilon_\omega)}{r}\dot{\gamma} \qquad (7.22)$$

and

$$\frac{\dot{\kappa}'}{\dot{\varepsilon}_\omega} = \frac{\sin^2\alpha}{r(1+\varepsilon_\omega)} - \frac{\sin^2\alpha}{r}\frac{\dot{\varepsilon}}{\dot{\varepsilon}_\omega} \quad \frac{\cos^2\alpha(1+\varepsilon_\omega)}{r}\frac{\dot{\gamma}}{\dot{\varepsilon}_\omega} \qquad (7.23)$$

Substituting equation (7.20b) into equation (7.23) gives

$$\frac{\dot{\varepsilon}}{\dot{\varepsilon}_\omega} = \frac{1}{1+\varepsilon_\omega} - \frac{3\pi r(1-H_*^2)^{\frac{1}{2}}}{8T_*R\sin^2\alpha} + \frac{(1+\varepsilon_\omega)\dot{\gamma}}{\tan^2\alpha\,\dot{\varepsilon}_\omega} \qquad (7.24)$$

Substituting equation (7.21) into equation (6.27) gives

$$\dot{\tau} = -\frac{\sin\alpha\cos^3\alpha}{r}\{\dot{\gamma} - \dot{\varepsilon}\} + \frac{\sin\alpha\cos\alpha}{r}(1+\varepsilon_\omega)\dot{\gamma}$$

$$- \frac{\sin\alpha\cos^3\alpha}{r(1+\varepsilon_\omega)}\left\{\frac{\dot{\varepsilon}_\omega}{\cos^2\alpha} - (1+\varepsilon_\omega)[\tan^2\alpha\dot{\varepsilon} + \dot{\gamma}]\right\}$$

$$= \frac{\sin\alpha\cos^3\alpha}{r}\dot{\varepsilon} - \frac{\sin\alpha\cos^3\alpha}{r}\dot{\gamma} + \frac{\sin\alpha\cos\alpha}{r}(1+\varepsilon_\omega)\dot{\gamma}$$

$$- \frac{\sin\alpha\cos\alpha}{r(1+\varepsilon_\omega)}\dot{\varepsilon}_\omega + \frac{\sin^3\alpha\cos\alpha}{r}\dot{\varepsilon} + \frac{\sin\cos^3\alpha}{r}\dot{\gamma}$$

Therefore

$$\frac{\dot{\tau}}{\dot{\varepsilon}_\omega} = \frac{\sin\alpha\cos\alpha}{r}\left\{(1+\varepsilon_\omega)\frac{\dot{\gamma}}{\dot{\varepsilon}_\omega} + \frac{\dot{\varepsilon}}{\dot{\varepsilon}_\omega} - \left(\frac{1}{1+\varepsilon_\omega}\right)\right\} \qquad (7.25)$$

Substituting equations (7.20c) and (7.24) into equation (7.25) gives

$$\frac{3H_*}{T_*R} - \frac{3G_*H_*}{3T_*R(1 - H_*^2)^{\frac{1}{2}}} = \frac{\sin\alpha\cos\alpha}{r}\left\{ (1 + \varepsilon_\omega)\ \frac{\dot{\gamma}}{\dot{\varepsilon}_\omega} - \frac{1}{(1 + \varepsilon_\omega)} + \frac{1}{(1 + \varepsilon_\omega)} - \frac{3\pi r(1 - H_*^2)^{\frac{1}{2}}}{8T_*R\sin^2\alpha} \right.$$

$$\left. + \frac{\cos^2\alpha}{\sin^2\alpha}(1 + \varepsilon_\omega)\ \frac{\dot{\gamma}}{\dot{\varepsilon}_\omega} \right\} \qquad (7.26)$$

Therefore

$$\frac{\dot{\gamma}}{\dot{\varepsilon}_\omega} = \frac{3\alpha r\ (1 - H_*^2)^{\frac{1}{2}}}{8T_*R(1 + \varepsilon_\omega)} + \frac{3r\tan\alpha}{2T_*R(1 + \varepsilon_\omega)}\left[2H_* - \frac{G_*H_*}{(1 + H_*^2)^{\frac{1}{2}}} \right] \qquad (7.27)$$

Finally, substituting equation (7.27) into equation (7.24) gives

$$\frac{\dot{\varepsilon}}{\dot{\varepsilon}_\omega} = \frac{1}{(1 + \varepsilon_\omega)} - \frac{3\pi r(1 - H_*^2)^{\frac{1}{2}}}{8T_*R\sin^2\alpha} + \frac{(1 + \varepsilon_\omega)}{\tan^2\alpha}\left\{ \frac{3\pi r\ (1 - H_*^2)^{\frac{1}{2}}}{8T_*R\ (1 + \varepsilon_\omega)} \right.$$

$$\left. + \frac{3r\tan\alpha}{2T_*R(1 + \varepsilon_\omega)}\left[2H_* - \frac{G_*H_*}{(1 + H_*^2)^{\frac{1}{2}}} \right] \right\} \qquad (7.28)$$

Therefore

$$\frac{\dot{\varepsilon}}{\dot{\varepsilon}_\omega} = \frac{1}{1 + \varepsilon_\omega} - \frac{3\pi r(1 - H_*^2)^{\frac{1}{2}}}{8T_*R} + \frac{3r}{2T_*R}\left[2H_* - \frac{G_*H_*}{(1 - H_*^2)^{\frac{1}{2}}} \right]\frac{1}{\tan\alpha} \qquad (7.29)$$

Equating the external work rate to the internal energy dissipation of a strand gives

$$\frac{F}{m}\dot{\delta} + \frac{M}{m}\dot{\Delta} - \int_o^L X\dot{\eta}\,ds = \int_o^L (T\dot{\varepsilon}_\omega + G'\dot{\kappa}' + H\dot{t})\,ds \qquad (7.30)$$

As in equations (6.13 a-f),

$$\frac{F}{m}\dot{\delta} = \frac{1}{m}\int_o^L F\,\dot{\delta}^*\,ds \qquad (7.31a)$$

and

$$\frac{M}{m}\dot{\Delta} = \frac{1}{m}\int_{o}^{L} M\dot{\Delta}^{*}\, ds \qquad (7.31b)$$

where the superscript (*) is derivative with respect to s.

Substituting equation (6.21) into equations (7.31 a,b) gives

$$\frac{F}{m}\dot{\delta} = \frac{1}{m}\int F\, d\dot{\delta}\, \frac{(1+\varepsilon_{\omega})\cos\alpha}{2\pi r}\, ds \qquad (7.32a)$$

$$\frac{M}{m}\dot{\Delta} = \frac{1}{m}\int M\, d\dot{\Delta}\, \frac{(1+\varepsilon_{\omega})\cos\alpha}{2\pi r}\, ds \qquad (7.32b)$$

If $\dot{\delta}$ and $\dot{\Delta}$ are initially zero, equations (7.32 a,b) can be written as

$$\frac{F}{m}\dot{\delta} = \frac{1}{m}\int F\dot{\delta}\, \frac{(1+\varepsilon_{\omega})\cos\alpha}{2\pi r}\, ds \qquad (7.33a)$$

$$\frac{M}{m}\dot{\Delta} = \frac{1}{m}\int M\dot{\Delta}\, \frac{(1+\varepsilon_{\omega})\cos\alpha}{2\pi r}\, ds \qquad (7.33b)$$

Substituting equations (7.33 a,b) into equation (7.30) and using equations (2.29 b,c)

[i.e. $\dot{\delta} = h\dot{\varepsilon}$; $\dot{\Delta} = 2\pi\dot{\gamma}$] gives

$$\frac{F}{m}\sin\alpha(1+\varepsilon_{\omega})\dot{\varepsilon} + \frac{M}{m}\frac{\cos\alpha}{r}(1+\varepsilon_{\omega})\dot{\gamma}$$

$$= T\dot{\varepsilon}_{\omega} + G'\dot{\kappa}' + H\dot{\tau} + Xr\dot{\rho} \qquad (7.34)$$

Using equations (5.4 a-c), equation 97.34) becomes

$$\phi \sin (1+\varepsilon_{\omega})\frac{\dot{\varepsilon}}{\dot{\varepsilon}_{\omega}} + \mu\frac{R}{3r}\cos\alpha\,(1+\varepsilon_{\omega})\frac{\dot{\gamma}}{\dot{\varepsilon}_{\omega}}$$

$$= T_{*} + G_{*}'\frac{4R}{3\pi}\frac{\dot{\kappa}'}{\dot{\varepsilon}_{\omega}} + H_{*}\frac{R}{3}\frac{\dot{\tau}}{\dot{\varepsilon}_{\omega}} + X\frac{\dot{\rho}}{\dot{\varepsilon}_{\omega}} \qquad (7.35)$$

where

$$\phi = \frac{F}{mT_{o}} \quad ; \quad \mu = \frac{M}{mH_{o}} \quad ; \quad X = \frac{Xr}{T_{o}} \qquad (7.36\ a\text{-}c)$$

Finally, substituting equations (7.20 b,c) and (7.21) into equation (7.35) gives

$$\phi \sin\alpha\,(1+\varepsilon_\omega)\frac{\dot{\varepsilon}}{\dot{\varepsilon}_\omega} + \mu\frac{R}{3r}\cos\alpha(1+\varepsilon_\omega)\frac{\dot{\gamma}}{\dot{\varepsilon}_\omega}$$

$$+ \chi\left[(1+\varepsilon_\omega)\frac{\dot{\gamma}}{\dot{\varepsilon}_\omega} + (1+\varepsilon_\omega)\tan^2\alpha\,\frac{\dot{\varepsilon}}{\dot{\varepsilon}_\omega} - \frac{1}{\cos^2\alpha}\right]$$

$$= \frac{1}{2T_*}\left[2T_*^2 + 2H_*^2 + G_*'(1+H_*^2)^{\frac{1}{2}} - \frac{G_*'H_*^2}{(1-H_*^2)^{\frac{1}{2}}}\right] \qquad (7.37)$$

It may be shown that when $\varepsilon_\omega = 0$ and tension T regarded as a reaction (and thus does not appear in the yield condition) equation (7.37) reduces to equation (5.28) which is the upper bound equation for the case of infinitesimal deflection.

7.2.3 Exact solution

It may be shown (Appendix 5) that the upper bound equation (equation 7.37) reduces to the lower bound equation (equation 7.12). Therefore, the lower and upper bound calculations lead to identical predictions so that the theoretical solution is exact according to the classical theory of plasticity.

7.2.4 Analysis for computation, and results

Dividing equation (7.29) by equation (7.27) gives

$$A\left\{\frac{\pi(1-H_*^2)^{\frac{1}{2}}}{4} + \left[2H_*\frac{G_*'H_*(1-H_*^2)^{\frac{1}{2}}}{(1-H_*^2)}\right]\tan\alpha\right\}$$

$$= (1+\varepsilon_\omega)\frac{2T_*R}{3r(1+\varepsilon_\omega)} - \frac{\pi(1-H_*^2)^{\frac{1}{2}}}{4} + \left[2H_* - \frac{G_*'H_*(1-H_*^2)^{\frac{1}{2}}}{(1-H_*^2)}\right]\frac{1}{\tan\alpha}\Bigg\} \qquad (7.38)$$

where $A = \dot{\varepsilon} / \dot{\gamma}$.

Thus,

$$\frac{2T_*\lambda}{3} = \left[\frac{\pi}{4}(1 - H_*^2)^{\frac{1}{2}}\right]\left[A + (1 + \varepsilon_\omega)\right]$$

$$+ \left[2H_* - \frac{H_*G_*'(1 - H_*^2)^{\frac{1}{2}}}{(1 - H_*^2)}\right]\left[A\tan\alpha - \frac{(1 + \varepsilon_\omega)}{\tan\alpha}\right] \qquad (7.39)$$

where

$$\lambda = R/r \qquad (7.40)$$

From equation (7.10),

$$\frac{N'}{T_o} = \left(-\frac{4G_*'}{\pi} + H_*\frac{\cos\alpha}{\sin\alpha}\right)\frac{\sin\alpha\cos\alpha}{3(1 + \varepsilon_\omega)} \qquad (7.41)$$

Substituting equation (7.41) into equation (7.5) gives

$$\phi = \frac{\lambda}{3(1 + \varepsilon_\omega)}\left(H_*\cos\alpha - \frac{4G_*'\sin\alpha}{\pi}\right) - \frac{\chi\sin\alpha}{\cos^2\alpha} \qquad (7.42)$$

Substituting equation (7.42) into equation (7.3) then gives

$$T_* = \frac{\lambda}{3(1 + \varepsilon_\omega)}\left(H_*\sin\alpha\cos\alpha - \frac{4G_*'\sin^2\alpha}{\pi}\right) - \frac{\chi}{\cos^2\alpha} \qquad (7.43)$$

Eliminating T_* from equations (7.39) and (7.43) gives

$$\frac{8G_*'^2\sin^2\alpha}{9\pi(1 + \varepsilon_\omega)} - \frac{H_*G_*'(1 - H_*^2)^{\frac{1}{2}}}{(1 - H_*^2)}\left[A\tan\alpha - \frac{(1 + \varepsilon_\omega)}{\tan\alpha}\right]$$

$$= \left\{\frac{2H_*\lambda^2\sin\alpha\cos\alpha}{9(1 + \varepsilon_\omega)} - \frac{2\lambda^*}{3\cos^2\alpha} - \left[\frac{\pi}{4}(1 - H_*^2)^{\frac{1}{2}}\right]\left[A + (1 + \varepsilon_\omega)\right] - 2H_*\left[A\tan\alpha - \frac{(1 + \varepsilon_\omega)}{\tan\alpha}\right]\right\} \qquad (7.44)$$

Therefore,

$$\left\{\begin{array}{l} \dfrac{2H_*\lambda^2\sin\alpha\cos\alpha}{9(1 + \varepsilon_\omega)} - \dfrac{2\lambda\chi}{3\cos^2\alpha} - \left[\dfrac{\pi}{4}(1 - H_*^2)^{\frac{1}{2}}\right]\left[A + (1 + \varepsilon_\omega)\right] \\ - 2H_*\left[A\tan\alpha - \dfrac{(1 + \varepsilon_\omega)}{\tan\alpha}\right] \end{array}\right\}$$

$$G_*' = \frac{\left\{ \text{from the bottom of previous page} \right\}}{\frac{8\lambda^2 \sin^2\alpha}{9\pi(1+\varepsilon_\omega)} - \frac{H_*(1-H_*^2)^{\frac{1}{2}}}{(1-H_*^2)} \left[A\tan\alpha - \frac{(1+\varepsilon_\omega)}{\tan\alpha}\right]} \qquad (7.45)$$

For given values of A, ε_ω^*, H_*, m and α^+, G_*' may be found from from equation (7.45). T_* can then be calculated from equation (7.43). The values of H_*, G_*' and T_* may then be substituted into the yield condition (equation 7.1) to check whether it is satisfied. Thus, a value of H_* that satisfies the yield condition may be computed using an iterative procedure. Therefore, the value of ϕ for given values of A, ε_ω, m and α may be found from equation (7.42). The corresponding value of μ may then be found from equation (7.8). The procedure is repeated for values of $-\infty < A < +\infty$, and this yields an exact interaction curve in dimensionless axial load ϕ and bending moment μ space for given values of ε_ω, m and α.

Figs. 7.1, 7.2 and 7.3 show the exact interaction curves in dimensionless axial load ϕ and bending moment μ space for various values of α, m and ε, respectively.

7.3 Plastic collapse load for a single strand with core wire

7.3.1 Plastic collapse of a core wire

It has been shown in section 5.4 that for the core wire, the lower bound and the upper bound calculations led to identical predictions. Thus, exact values of axial load, F_c and torsional moment M_c required for the collapse of an elastic perfectly plastic core wire can be obtained. When linked to the strand, these values are given by equations (5.51) and (5.52), viz.

---

* The corresponding value of ε can be calculated using procedure m, Appendix 6.

\+ λ (= R/r) may be calculated from equation (2.41) with the given values of α and m, and for the same values of α and m, the value of χ can be obtained from figures (4.1) and (4.2).

$$F_c = \frac{rA\tan\alpha T_{co}^{\,2}}{[T_{co}^{\,2} r^2 A^2 \tan^2\alpha + H_{co}^{\,2}]^{\frac{1}{2}}} \tag{7.46}$$

$$M_c = \frac{H_{co}^{\,2}}{[T_{co}^{\,2} r^2 A^2 \tan^2\alpha + H_{co}^{\,2}]^{\frac{1}{2}}} \tag{7.47}$$

where T_{co} = the fully plastic tangential load T_c,

H_{co} = the fully plastic generalised moment H_c,

r = the helix radius of the wires in the strand.

α = the helix angle of the wires in the strand.

and $A = \dot{\varepsilon}/\dot{\gamma}$.

When the core wire and the wires in the strand are made of the same material, the values of H_{co} and T_{co} are given by equations (5.62 a,b), viz.

$$H_{co} = H_o \left(\frac{R_c}{R}\right)^3 \tag{7.48}$$

$$T_{co} = T_o \left(\frac{R_c}{R}\right)^2 \tag{7.49}$$

where

H_o = the fully plastic generalised moment, H of the wire in the strand,

T_o = the fully plastic tangential load T of the wire in the strand,

R_c = the radius of the core wire,

and R = the radius of the wires in the strand.

7.3.2 Exact solution for the plastic collapse of a single strand with core wire

Since exact solutions are obtained for a single strand, in which the wires experience finite extension (Section 7.2), and a core wire (Section 5.4.2), it follows from equations (5.36) and (5.37) that exact

values of F_T (total axial load on the rope) and M_T (total torsional moment on the rope) required for the collapse of an elastic perfectly plastic rope consisting of a single strand with core wire can be found.

7.3.3. Analysis for computation and results

Equations (5.36) and (5.37) can be written in dimensionless form as follows :

$$\phi = \phi + \phi_c \tag{7.50}$$

$$\mu_T = \mu + \mu_c \tag{7.51}$$

where

$$\phi_T = F_T/mT_o$$
$$\phi_c = F_c/mT_o$$
$$\mu_T = M_T/mH_o \tag{7.52a-d}$$
$$\mu_c = M_c/mH_o$$

From Section (7.2.4), it has been shown that for given values of A, $\varepsilon\omega$, m and α, value of H_* and thus G_*' and T_* that satisfy the yield condition (equation 7.1), may be computed using an iterative procedure. The value of ϕ may then be obtained from equation (7.42), and the corresponding value of μ from equation (7.8). For the same given values above, ϕ_c and μ_c can be found using equations (7.46), (7.47), (7.48), (7.49) and (7.52 b,d) when the ratio of radii, R_c/R is known. Thus, the total dimensionless axial load ϕ_T and torsional moment μ_T can be obtained from equations (7.50) and (7.51). An interaction curve lying in a ϕ_T - μ_T plane can be constructed if the procedure is repeated with values of A from $-\infty$ to $+\infty$.

Fig. 7.4 shows the exact interaction curves for various values of α, Fig. 7.5 for various values of m, Fig. 7.6 for various values of ε,

and Fig. 7.7 for various values of ratio of radii R_c/R.

7.4 Plastic collapse load for a rope made up of two layers of strand and a core wire

7.4.1 The rope - governing equations

As in Chapter 5, the rope considered is a 1 x 19 rope which consists of a core wire, 6 wires in the inner strand and 12 wires in the outer strand. The method, however, can be easily adapted to ropes with different numbers of wires in each strand.

It will be assumed that the two layers of strand and the core wire extend and rotate as a unit. Therefore,

$$\bar{\delta} = \delta_c = \delta \tag{7.53}$$

and

$$\bar{\Delta} = \Delta_c = \Delta \tag{7.54}$$

where the superscript bar ($\bar{}$) denotes variables associated with the outer strand.

For equilibrium

$$F_T = F + \bar{F} + F_c \tag{7.55}$$

$$M_T = M + \bar{M} + M_c \tag{7.56}$$

where F_T is the total axial load on the rope and M_T is the total torsional moment.

Equations (7.55) and (7.56) can be written in dimensionless form as

$$\phi_T = \phi + \frac{\bar{m}}{m}\,\bar{\phi} + \phi_c \tag{7.57}$$

$$\mu_T = \mu + \frac{\bar{m}}{m}\,\bar{\mu} + \mu_c \tag{7.58}$$

respectively, where

$$\phi_T = F_T/mT_o$$

$$\phi = F/mT_o \tag{7.59 a-d}$$

$$\phi_c = F_c/mT_o$$

$$\bar{\phi} = \bar{F}/\bar{m}T_o$$

and

$$\mu_T = M_T/mH_o$$
$$\mu = M/mH_o$$
$$\mu_c = M_c/mH_o \qquad (7.59\ e\text{-}h)$$
$$\bar{\mu} = \bar{M}/\bar{m}H_o$$

when the wires are made of the same material.

7.4.2 The outer strand

Unlike the inner strand, the wires in the outer strand are not in contact with each other. Instead, contacts only occur with wires in the inner strand. When the two strands are of different helix angles, point contacts will occur at equally spaced distance along each of the wires in the strands. These distances are given by equations (3.44) and (3.45).

The helix radius of the wires in the outer strand is given by

$$\bar{r} = r + R + \bar{R} \qquad (7.60)$$

The equations that govern the outer strand are similar in form to that of a single strand (Section 7.2). Therefore, from equation (7.42)

$$\bar{\phi} = \frac{\bar{\lambda}}{3(1+\bar{\epsilon}_\omega)}\left(\bar{H}_* \cos\bar{\alpha} - \frac{4\bar{G}_* \sin\bar{\alpha}}{\pi} - \frac{\bar{\chi}\sin\bar{\alpha}}{\cos^2\bar{\alpha}}\right) \qquad (7.61)$$

where $\bar{H}_* = \frac{\bar{H}}{\bar{H}_o}$; $\bar{G}_* = \frac{\bar{G}'}{\bar{G}_o}$ (7.62 a,b)

and $\bar{\lambda}$ is given by equation (5.83), i.e.

$$\bar{\lambda} = \frac{\bar{R}}{\bar{R}}\left[\frac{1}{\frac{1}{\bar{\lambda}} + 1 + \frac{\bar{R}}{\bar{R}}}\right] \qquad (7.63)$$

From equation (7.8),

$$\bar{\mu} = \frac{\bar{H}_*}{\sin\bar{\alpha}} + \frac{3\cos\bar{\alpha}}{\bar{\lambda}}\left\{\bar{\phi}\sin\bar{\alpha} - \bar{\chi} - \sin\bar{\alpha}\left(\bar{\phi} + \frac{\bar{\chi}\sin\bar{\alpha}}{\cos^2\bar{\alpha}}\right)\left(1 + \frac{1+\bar{\epsilon}_\omega}{\sin^2\bar{\alpha}}\right)\right\} \qquad (7.64)$$

From equation (7.45)

$$\bar{G}'_* = \frac{\{\frac{2\bar{H}_*\bar{\lambda}^2 \sin\bar{\alpha}\cos\bar{\alpha}}{9(1+\bar{\varepsilon}_\omega)} - \frac{2\bar{\lambda}\bar{\chi}}{3\cos^2\bar{\alpha}} - [\frac{\pi}{4}(1-\bar{H}_*^2)^{\frac{1}{2}}][\bar{A} + (1+\bar{\varepsilon}_\omega)] - 2\bar{H}_*[\bar{A}\tan\bar{\alpha} - \frac{(1+\bar{\varepsilon}_\omega)}{\tan\bar{\alpha}}]\}}{\{\frac{8\bar{\lambda}^2\sin^2\bar{\alpha}}{9\pi(1+\bar{\varepsilon}_\omega)} - \frac{\bar{H}_*(1-\bar{H}_*^2)^{\frac{1}{2}}}{(1-\bar{H}_*^2)}[\bar{A}\tan\bar{\alpha} - \frac{(1+\bar{\varepsilon}_\omega)}{\tan\bar{\alpha}}]\}}$$

where $\bar{A}$ is given by equation (5.85), i.e. (7.65)

$$\bar{A} = \frac{\tan\alpha}{\lambda\tan\bar{\alpha}}\left[\frac{1}{\frac{1}{\bar{\lambda}} + 1 + \frac{\bar{R}}{R}}\right] A \qquad (7.66)$$

From equation (7.43)

$$\bar{T}_* = \frac{\bar{\lambda}}{3(1+\bar{\varepsilon}_\omega)}\left(\bar{H}_* \sin\bar{\alpha}\cos\bar{\alpha} - \frac{4\bar{G}_*\sin^2\bar{\alpha}}{\pi}\right) - \frac{\bar{\chi}}{\cos^2\bar{\alpha}} \qquad (7.67)$$

Finally, from equation (7.1)

$$\bar{T}_*^2 + \bar{H}_*^2 + \bar{G}_*'(1-\bar{H}_*^2)^{\frac{1}{2}} = 1 \qquad (7.68)$$

7.4.3 Exact solution

Since it has been shown than an exact solution exists for the plastic collapse of a single strand in which the wires experience finite extension (Section 7.2), exact values of $\bar{F}$ (axial load on the outer strand) and $\bar{M}$ (torsional moment on the outer strand) for the plastic collapse of the outer strand can also be found. Therefore, from equations (7.55) and (7.56) it follows that exact values of F_T, the total axial load and

M_T, the total torsional moment for the plastic collapse of a rope made of two layers of strand and a core wire can be found.

7.4.4 Analysis for computation and results

The procedure for constructing the interaction curves are similar to that mentioned in the previous sections.

For given values of α, m and A, ϕ_c and μ_c can be found from Section (7.3.2).

The value of $\bar{\chi}$ can be obtained from Fig. 4.4 when values of $\bar{\alpha}$ and $\bar{m}$ are known. A can be calculated from equation (7.66) and following the same procedure as for a single strand, values of $\bar{\phi}$ and $\bar{\mu}$ can be found from equations (7.61) and (7.64) respectively.

For the wires in the inner strand, the line load $\bar{X}$ due to contact with wires in the outer strand may be regarded as an additional normal line load. Thus, X, the resultant normal line load. Thus, X, the resultant normal line load acting on the wires in the inner strand is given by

$$X = X_I - \bar{X} \tag{7.69}$$

where X_I is the line load on the inner wire due to the contact that occurs between wires in the inner strand (Fig. 5.13).

For the given values of α and m, the dimensionless value of X_I (i.e. $\chi_I = \frac{X_I r}{T_o}$) can be obtained from Figures 4.1 and 4.2. Finally, following the same procedure as in Section (7.2.4), the values of ϕ and μ can be computed.

Thus, for given values of α, $\bar{\alpha}$, m, $\bar{m}$, ε^+ and A, exact values of

---

+ The corresponding value of ε_ω and $\bar{\varepsilon}_\omega$ can be calculated using procedure in Appendix 6.

ϕ_T and μ_T for the plastic collapse of the rope can be found from equations (7.57) and (7.58), respectively.

Figures (7.8) - (7.10) show the exact interaction curves in ϕ_T - μ_T plane for values of α being 60^o, 70^o and 80^o, and $\bar{\alpha}$ with values of 95^o, 105^o and 115^o. Figures (7.11) and (7.12) show the effect of different sizes of core wire and wires in the outer strand, respectively, with respect to the wires in the inner strand while Figure (7.13) shows the effect of ϵ , on the interaction curves.

7.5 Rope with n-layers of strand

The previous analyses can easily be extended to study plastic collapse of a rope with any number of layers of strand.

The total axial force on the rope will be the sume of the forces on the core wire (if it is present) and the layers of strand, viz.

$$F_T = F_c + F_1 + F_2 \ldots\ldots + F_n \tag{7.70}$$

Similarly, the total torsional moment acting on the rope will be the sum of the moments on the core wire (if it is present) and the layers of strand, viz.

$$M_T = M_c + M_1 + M_2 \ldots\ldots + M_n \tag{7.71}$$

Equations (7.70) and (7.71) can be written in dimensionless form such that

$$\phi_T = \phi_c + \phi_1 + \frac{m_2}{m_1}\phi_2 + \ldots\ldots + \frac{m_n}{m_1}\phi_n \tag{7.72}$$

and

$$\mu_T = \mu_c + \mu_1 + \frac{m_2}{m_1}\mu_2 + \ldots\ldots + \frac{m_n}{m_1}\mu_n \tag{7.73}$$

where

$$\phi_T = F_T/m_1T_o$$

$$\phi_c = F_c/m_1T_o$$

$$\phi_1 = F_1/m_1T_o$$

$$\phi_2 = F_2/m_2T_o \qquad (7.74)$$

$$\vdots \quad \vdots$$

$$\phi_n = F_n/m_nT_o$$

and

$$\mu_T = M_T/m_1H_o$$

$$\mu_c = M_c/m_1H_o$$

$$\mu_1 = M_1/m_1H_o \qquad (7.75)$$

$$\mu_2 = M_2/m_1H_o$$

$$\vdots \quad \vdots$$

$$\mu_n = M_n/m_nH_o$$

where m_i is the number of wires in the strand.

It may be assumed that rotationally and axially, the core wire and the layers of strand move as a unit so that

$$\delta_c = \delta_1 = \delta_2 = \ldots\ldots = \delta_n \qquad (7.76)$$

and $$\Delta_c = \Delta_1 = \Delta_2 = \ldots\ldots = \Delta_n \qquad (7.77)$$

A is defined as

$$A = \dot{\epsilon}_1/\dot{\gamma}_1 \qquad (7.78)$$

where $\epsilon_1 = \delta_1/h_1$ and $\gamma_1 = \Delta_1/2\pi$.

From equation (7.66) A_i can be written in terms of A, viz.

$$A_i = \frac{\tan\alpha_1}{\lambda_1\tan\alpha_i}\left[\frac{1}{\frac{1}{\lambda_1} + 1 + \frac{Ri}{R}}\right] A \qquad (7.79)$$

The collapse value of the normal line load X_i acting on the wires in each layer of strand will depend on the nature of contacts experienced by a wire on a strand and that of the wires in the outer strands. It will be assumed that apart from the first layer, the wires in the other layers are in contact with wires in neighbouring layers and they are not in contact

with wires in the same layer. Thus, there will be an interaction between the various layers. If X_1 is the normal line load for wires in the first layer due to contact between wires in the same layer, X_2, its equivalent in the second layer due to contact between wires in the second and first layer, X_3, its equivalent in the third layer due to contact between wires in the third and second layer, etc.

$$X_i' = X_i - X_{i+1} - X_{i+2} \cdots\cdots - X_n \tag{7.80}$$

where X_i' is the resultant normal line load acting on the wires in the ith layer.

The values of X_i can be calculated from equations (4.5) and (4.10).

Since it has been shown that exact solution exists for the plastic collapse of a single strand and also that for a core wire, it is possible to obtain exact values of ϕ_T and μ_T for the plastic collapse of a rope with n- layers of strand from equations (7.72) and (7.73), respectively.

The value of ϕ_i can be calculated from

$$\phi_i = \frac{\lambda_i}{3(1 + \varepsilon_{\omega i})} \left(H_{*i} \cos\alpha_i - \frac{4G'_{*i} \sin\alpha_i}{\pi}\right) - \frac{\chi_i \sin\alpha_i}{\cos^2\alpha_i} \tag{7.81}$$

where $H_{*i} = \frac{H_i}{H_o}$; $G'_{*i} = \frac{G_i}{G_o}$ (7.82 a-b)

and $\lambda_i = \frac{R_i}{R} \left[\frac{1}{\frac{1}{\lambda} + 1 + \frac{R_i}{R}}\right]$ (7.83)

Also,

$$\left\{ \frac{2H_{*i}\lambda_i^2 \sin\alpha_i\cos\alpha_i}{9(1 + \varepsilon_{\omega_i})} - \frac{2\lambda_i \chi_i}{3\cos^2\alpha_i} - \left[\frac{\pi}{4}(1 - H_{*i}^2)^{\frac{1}{2}}\right][A_i + (1 + \varepsilon_{\omega i})] - 2H_{*i}\left[A_i \tan\alpha_i - \frac{(1 + \varepsilon_{\omega i})}{\tan\alpha_i}\right] \right\}$$

$$G'_{*i} = \frac{\left\{ \text{from the bottom of previous page} \right\}}{\left\{ \frac{\delta\lambda_i^2 \sin^2\alpha_i}{9(1+\varepsilon_{\omega_i})} - \frac{H_{*i}(1-H_{*i}^2)^{\frac{1}{2}}}{(1-H_{*i}^2)} \left[A_i \tan\alpha_i - \frac{(1+\varepsilon_{\omega_i})}{\tan\bar{\alpha}} \right] \right\}} \tag{7.84}$$

$$T_{*i} = \frac{\lambda_i}{3(1+\varepsilon_{\omega_i})} \left(H_{*i} \sin\alpha_i \cos\alpha_i - \frac{4G'_{*i} \sin^2\alpha_i}{\pi} \right) \frac{\chi_i}{\cos^2\alpha_i} \tag{7.85}$$

$$T_{*i}^2 + H_{*i}^2 + G'_{*i}(1-H_{*i}^2)^{\frac{1}{2}} = 1 \tag{7.86}$$

Thus, the value of μ_i can be obtained from

$$\mu_i = \frac{H_{*i}}{\sin\alpha_i} + \frac{3\cos\alpha_i}{\lambda_i} \left\{ \phi_i \sin\alpha_i - \chi_i \right.$$

$$\left. - \sin\alpha_i \left(\phi_i + \frac{\chi_i \sin\alpha_i}{\cos^2\alpha_i} \right) \left(1 + \frac{1+\varepsilon_{\omega_i}}{\sin^2\alpha_i} \right) \right\} \tag{7.87}$$

7.6 DISCUSSION

7.6.1 Effect of extension.

The results obtained are generally similar and follow the same trend as that obtained for the case of infinitesimal extension(Chapter 5), but with finite extension, there is an increase in the maximum value of the axial collapse load as shown in Figs. 7.3,7.6 and 7.13. The increase in the maximum axial collapse load depends on the extension at collapse and as the extension increases, the maximum axial collapse load becomes larger. For a strand, the maximum axial collapse load when $\epsilon = 0.01$ is 10% higher than that when there is no extension.

For a single strand and a strand with core wire(Figs. 7.3 and 7.6, respectively), the interaction curve shifts to the left about the ϕ axis as the extension increases, but for a rope with two layers of strand, the interaction curve shifts to the right. The reason for this difference is that in a rope with two layers of strand, the second layer is made up of twelve wires as compared to six in the inner layer and they are wound in the opposite direction. Thus, the second layer is about twice as strong in torsion in one direction as compared to the inner layer in the other direction. The resultant effect is that the maximum torsional collapse load becomes larger for the rope with two layers of strand.

7.6.2 Normality

A typical dimensionless load interaction curve is shown in Fig. 5.12. The ellipse can be divided into two halves - the curve PQR is obtained with the negative values of the square root in equation (7.45) and the curve PSR constructed using the positive

values of the square root. The directions of the strain rate vector are shown at points P,Q,R and S. At points P and R, A has the value $+\infty$, and $-\infty$ respectively. Thus, they show the direction of the strain rate vector, $\dot{\epsilon}$(i.e = $\dot{\delta}/h$) which must be parallel to the ϕ axis. Since, the direction is also normal to the interaction curve at P and R, the normality requirement has been satisfied. Similarly, at points Q and S, A has the value zero and thus the arrows show the direction of the strain rate vector, $\dot{\gamma}$(i.e = $\dot{\Delta}/2\pi$) which must be parallel to the μ axis.

7.6.3 Effect of the change in helix angle.

As shown in Fig. 7.1, the maximum axial collapse load increases as the helix angle approaches 90^0, but the difference between the maximum and the minimum torsional collapse load decreases. This result justifies the choice of large helix angles($>73^0$) on wire rope by manufacturers since a larger helix angle would mean a higher collapse load.

7.6.4 Effect of the number of wires in the strand.

As the number of wires in a strand increases, the maximum axial collapse load increases as shown in Fig. 7.2b, but the axial collapse load in an individual wire decreases as illustrated in Fig. 7.2. Thus doubling the number of wires does not make the axial collapse load twice as large. However, Fig. 7.2b shows that the maximum value of ϕ, does increase by more than a factor of two. Thus, if a strand is to undergo a lot of twisting, then it is more efficient to have it made with larger number of wires.

7.6.5 Effect of introducing a core wire.

Comparing Figures 7.1 and 7.2 with Figures 7.4 and 7.5, it can be seen that by introducing a core wire in a single strand, the maximum axial collapse load when $\varepsilon=0.01$ is increased by 0.17 which is equivalent to 16.7% of the axial collapse load for a strand with core wire with $\alpha=80^{0}$. However, there is little change in the maximum and the minimum values of μ_T.

When the diameter of the core wire is larger than that of the wires in the strand, contact will no longer occur between wires in the strand. Instead, contact will occur between the wires in the strand and the core wire. This is illustrated in Figure 5.6. Figure 7.7 shows that the maximum axial collapse load increases as the diameter of the core increases but when the core wire is larger than the wires in the strand, the maximum axial collapse load drops to a lower value. This is due to the fact that the contact stresses is more critical between the core and the wires in the strand than between adjacent wires in the strand. It has to be noted here that the rope in which the core wire is smaller than the wires in the strand is a hypothetical one since the core wire will not be held together in the rope. This can however be overcome by introducing soft fibres around the core wire which helps little in improving the rope strength but hold the core wire together.

7.6.6 Rope with two layers of strand.

Figures 7.8, 7.9 and 7.10 suggest a suitable configuration for rope with two layers of strand. When compared to the load interaction curve for a single strand with core wire (dashed curve), it can be seen that the helix angle for the second strand should be

less than ≈105°. Also, for the rope to withstand a higher axial load, the helix angles of the strands should be a value approaching 90°.

Effect of the variation in the size of the wires in the outer strand is small as can be seen in Fig. 7.12. This is particularly obvious as an increase in the size of the wires produces only a small increase in the maximum axial collapse load. Thus, the variation in the size of the wires in the outer strand from its nominal size (when $\bar{R}$=R) is not very critical.

CHAPTER 8

Comparison of theoretical and experimental results.

8.1 Comparison with experimental results.

8.1.1 Introduction.

There have been many tests carried out on wire ropes(Chapter 1) but those tests were either carried out within the elastic range (except for bending tests) or the ropes used were different in configurations than those described in the present work. However, at the University of Liverpool in the recent years, there have been extensive tensile tests carried out on wire rope with similar configuration to that described here(91,92). The results obtained by W.S Utting(92) will be used to check the validity of the theoretical analysis presented in this thesis.

8.1.2 Comparison of theoretical and experimental results.

Fig 8.1 shows the results obtained from tensile tests by W.S Utting(92) on wire rope with cross-section as shown in Fig 5.6b and specifications as follows:-

Diameter of helical wire = 3.73mm.

Diameter of core wire = 3.91mm.

Grade of wire = 180kgf/mm² minimum breaking load to BS2763.

Since the load-extension curves do not have distinct yield points, the 0.1% proof load will be used to calculate the stress at which the rope becomes plastic. From Fig 8.1, the loads that are required to make the rope plastic are as follows :-

Helix Angle	Load to yield (0.1% proof load) (kN)	0.2% proof load (kN)	Failure Load (kN)
75.4°	89 (ε=0.0055)	96 (ε=0.0065)	130.5
76.01°	99 (ε=0.0082)	110 (ε=0.011)	139.6
77.8°	106 (ε=0.0075)	116 (ε=0.009)	145.4
78.9°	107.5 (ε=0.0074)	119 (ε=0.0085)	136.7
80.9°	109 (ε=0.007)	122 (ε=0.008)	137.9

Table 8.1

The above values are obtained from tests in which the rope ends are fixed. Thus, in this case, there will be no angular rotation and γ becomes zero. Therefore, A ($=\dot{\varepsilon}/\dot{\gamma}$) is ∞ and the yield load is equivalent to the load at point P on the interaction curve as shown in Fig 5.12.

Using the characteristics (dimensions, helix angle and material) of the rope used in the tests, the dimensionless line load χ to cause indentation in the wires is obtained following the procedure described in Chapter 4. This value of χ is then used to determine the axial collapse load of the wire rope following the procedure described in Section 7.3. The values of the axial collapse load obtained are as follows:-

Helix Angle	χ	Theoretical Axial Collapse Load (kN)
75.4°	-0.018955	8.7
76.01°	-0.0189571	8.9
77.8°	-0.018959	10.06
78.9°	-0.018962	11.5
80.9°	-0.018964	13.1

Table 8.2

It can be seen that the theoretical values for collapse in Table 8.2 are less than 10% of the experimental failure loads reported in Table 8.1. This is much too small and the possible source of discrepancy could be the assumption that the contact load at collapse is equivalent to that load required to produce an indentation in the wires. Thus, presumably, whilst the area near the contact points is plastic, the rest of the cross-section may still remain elastic. Therefore, it is now desirable to determine the combined loading (line load, axial force and torsional moment) required to produce full plastic condition throughout the cross-section of the wire, which will then be in a state of full plastic collapse.

8.1.3 Determination of collapse load by considering stress at a point due to tension, torsion, bending and contact.

Consider a section of a wire as shown in Fig 8.2 being acted upon by the tension T, bending G', torsion H and contact force Q. At point O in the cross-section of the wire, the stresses σ_{ox} σ_{oy} and σ_{oz} due to the contact force Q can be found as shown in Chapter 3. There will also be direct stresses σ_{xt} and σ_{xg} due to tension and bending, respectively and a shear stress τ_h due to torsion. Therefore, there will be resultant stresses $\sigma_x(=\sigma_{ox} + \sigma_{xt} + \sigma_{xg})$, $\sigma_y(=\sigma_{oy})$ and $\sigma_z(=\sigma_{oz})$ and a shear stress $\tau(=\tau_h)$. From these stresses, the principal stresses σ_1, $\sigma_2$and σ_3 can be found from(93)

$$\sigma^3 - (\sigma_x + \sigma_y + \sigma_z)\sigma^2 + (\sigma_x\sigma_y + \sigma_y\sigma_z + \sigma_z\sigma_x - \tau^2)\sigma - (\sigma_x\sigma_y\sigma_z - \sigma_x\tau^2) = 0 \qquad (8.1)$$

Using the von Mises' theory of failure

$$2\sigma_o^2 = (\sigma_1 - \sigma_2)^2 + (\sigma_2 - \sigma_3)^2 + (\sigma_3 - \sigma_1)^2 \qquad (8.2)$$

Thus, for a given contact force Q, which will yield values of tension T, bending G' and torsion H when the configuration of the rope and value of $A(=\dot{\epsilon}/\dot{\gamma})$ are known, it is possible to determine whether a point in the cross-section of the wire has become plastic.

A block diagram of the procedure for calculating the axial load at which the cross-section of the wire has become plastic is shown in Fig 8.3. A value c in equation (4.1) is assumed and this yields the value of χ following the procedure described in Chapter 4. The value of χ, together with the rope variables (dimensions, helix angle, material and $A=\infty$) are then used to obtain values of ϕ_T, μ_T, T_*

G'_* and H_* using method of computation described in Section 7.3.2.

With the aid of equations (5.4)a-c and (7.2)a-c, the values of T, G' and H can be found. viz.

$$T = T_* \pi \sigma_0 R^2 \tag{8.3}$$

$$G' = 4G'_* \sigma_0 R^3/3 \tag{8.4}$$

$$H = H_* \pi \sigma_0 R^3/3 \tag{8.5}$$

For a given point O in Fig 8.2, z is its distance from the contact surface. Thus, the stress at that point due to bending is given by

$$\sigma_{xg} = \frac{G'y}{I} \tag{8.6}$$

where $y = R - z$

and I = moment of inertia $\left(= \frac{\pi R^4}{2}\right)$

and the shear stress due to torsion is given by

$$\tau_h = \frac{Hr}{J} \tag{8.7}$$

where $r = R - z$

and J = Polar moment of inertia. $\left(= \frac{\pi R^4}{4}\right)$

The stress due to tension is given by

$$\sigma_{xt} = T/\pi R^2 \tag{8.8}$$

where R is the radius of the wire.

The distance z also determines the stresses σ_{ox}, σ_{oy} and σ_{oz} due to contact which can be calculated following the procedure in Chapter 3. Thus, the stresses σ_x, σ_y, σ_z and τ can be found and the

principal stresses σ_1, σ_2 and σ_3 evaluated by iterative computation from equation (8.1). Using equation (8.2), it will be known if the point O has become plastic. This procedure is repeated for values of z that cover the cross-section of the wire and a value of c that will determine the value of χ can be found for which full plasticity has just been achieved (i.e minimum stress in the cross-section is equal to the yield stress of the material). The values of collapse loads obtained by the above procedure are as follows:-

Helix Angle	Machida and Durelli's predictions† (kN)	Theoretical Collapse Load(kN)			
		$\epsilon = 0$	$\epsilon = 0.01$	$\epsilon = 0.025$	$\epsilon = 0.03$
75.4	74.53	84	93.8	123.1	130.7
76.01	74.70	91	102	131.2	139
77.8	75.16	104	112	140	148.4
78.9	75.41	108	120	147.3	155
80.9	75.80	119	128	155.2	163

(see Appendix 8 for detailed results)

Table 8.3

† These are an estimate of the plastic collapse loads. See Appendix 7.

8.1.4 Discussion.

Comparing the results obtained in the above section to the experimental values shown in Table 8.1, it can be seen that the theoretical collapse loads(ϵ=0.025)[¥] are about 4-11% lower than the failure loads obtained experimentally. The largest deviations are with helix angles 78.9° and 80.9°, where the difference are 9% and 11%, respectively. The theoretical predictions(Table 8.3) show that the failure loads should increase as the helix angle approaches 90° and this agrees with the failure loads obtained for helix angles from 75.4° to 77.8°. However, the failure loads for helix angles 78.9° and 80.9° obtained experimentally(Table 8.1) are lower than that for 77.8° even though the 0.1% and 0.2% proof loads show the same trend as predicted theoretically i.e the loads increase as the helix angle approaches 90°. Thus, it may be suspected that the deviations from the theoretical predictions for wire ropes with helix angles 78.9° and 80.9° may be largely due to experimental discrepancies. For the rope with helix angle 80.9°, one helical wire broke at the end grip and shook loose from the remaining wires over the whole length(92), but for the rope with helix angle 78.9°, apparently the nature of failure is the same as the rest of the rope.

Again comparing with the experimental results(Table 8.1), it can be seen that the load to cause initial elastic yielding in the rope using Machida and Durelli's(47) prediction is about 40% lower than the actual failure load. It is also about 17% lower than the load to cause experimentally detectable yielding in the rope.

¥ This is approximated by comparing the load-extension curves with the load-surface-strain curves obtained by W.S Utting(92). This is done by considering the differences in the strain and extension values as the load is increased. A relationship is established between them and the load-extension curves are extrapolated up to the failure loads. The actual value of extension at collapse was not obtained since the extensometer had to be removed before failure occurred.

Looking at the theoretical results(Table 8.3), it can be seen that the theoretical predictions obtained with infinitesimal extensions are about 20-35% lower that that when the extension is finite(ε=0.025). Thus, the collapse theory for infinitesimal deflection(Chapter 5) will predict collapse loads which are more than 20-35% lower than the actual failure loads. In fact, the collapse loads predicted by that theory lie in the region of the 0.1% proof loads obtained experimentally. Therefore, if the 0.1% proof load is used as the safe working load, then the collapse theory for infinitesimal deflection may be used to predict this.

8.2 Rope with two layers of strand and a core wire.

The analysis presented in Section 8.1.3 may be extended to include an additional layer of strand. In this case, two contact areas will have to be considered - (i)contact between the outer and the inner layer of strand and (ii)contact between the core wire and the inner layer. For the former, the type of contact(line or point) will depend on the helix angles of the wires in the inner and the outer layers. If the helix angles are different, point contact will occur and for the special case in which the helix angles are the same, line contact will result. Depending on the type of contact, either Section 3.3 or Section 3.4 will be used to evaluate the stresses due to contact.

In evaluating the value of χ to cause full plasticity in each layer of the strand in this type of rope, the analysis can either start from the outer layer and then proceeding towards the core or start from the core wire and work towards the outer wires. Here, the former is considered. Thus, the first contact area to be considered is the contact between the inner and the outer layers. The analysis

here is similar to that described in Section 8.1.3 except that if it is a point contact(i.e the helix angles of the wires in the inner and the outer layers are different), Section 3.4 will be used to evaluate the stresses due to contact. From the iterations, a value of $\bar{X}$ will be established for which full plasticity is achieved throughout the cross-section of the wires in the outer layer.

Next, the wires in the inner layer will be considered. They will experience contact with the outer wires and the core wire(Fig. 8.4). Since $\bar{X}$ has already been found, a value of X_I (line force due to contact between the core wire and the inner layer) can be found for which full plasticity is achieved throughout the cross-section of the wires in the inner layer using the procedure described in Section 8.1.3. In this case however, there will be additional stresses $\bar{\sigma}_{ox}$, $\bar{\sigma}_{oy}$ and $\bar{\sigma}_{oz}$ due to contact with the outer wires. Thus, the resultant stresses at a point O, in the cross-section of the inner wire are:-

$$\begin{aligned} \sigma_x &= \sigma_{ox} + \sigma_{xt} + \sigma_{xg} + \bar{\sigma}_{ox} \\ \sigma_y &= \sigma_{oy} + \bar{\sigma}_{oy} \\ \sigma_z &= \sigma_{oz} + \bar{\sigma}_{oz} \end{aligned} \qquad (8.9)a\text{-}c$$

Finally, using equation (7.69), the resultant normal line load acting in the inner strand, X can be found.

The value of X_I obtained will then be used to check if the core wire has become plastic. For the core wire, contacts occur at equally spaced points with the wires in the inner layer(Fig. 8.5). For a given value of A, the values of F_c and M_c can be found from equations (7.46) and (7.47), respectively. The stresses due to these

can be evaluated using equations (8.7) and (8.8) but with H and T replaced by M_c and F_c, respectively. Thus, following Section 8.1.3, it may be found if the core wire has become plastic. In obtaining the results given in the next section, it is found that the core wire reached full plasticity after it has been achieved in the inner and the outer wires.

8.2.1 Results and discussion.

Currently, at the Mechanical Engineering Department, University of Liverpool, preparations for tensile tests on ropes with two layers of strand and a core wire has just begun. Details of the rope used are as follows:-

Diameter of wires in the inner and the outer strand - 1.27mm.

Diameter of the core wire - 1.41mm.

overall diameter of the rope - 6.40mm.

Helix angle of the inner and the outer wires - 74.75°.

Using the above dimensions and following the procedure described in the previous section, the theoretical axial collapse load for the rope are as follows:-

Inner Helix Angle	Outer Helix Angle	Theoretical Axial Collapse Load(kN)					
		$\epsilon = 0$	$\epsilon = 0.01$	$\epsilon = 0.02$	$\epsilon = 0.03$	$\epsilon = 0.05$	$\epsilon = 0.1$
	75°	30.3	36.2	40.7	43	47.3	54.2
75°	80°	29	35.7	38	42.4	45.9	50.1
	105°	27.2	32.4	35.3	40.1	40.5	47

(see Appendix 9 for detailed results)

Table 8.4

It has to be noted here that the 'rope' used is an element of a 6X19 rope(i.e one of the strands of the rope). It has been removed from the rope and thus it is not straight but is initially bent in a helical manner. Also, it is observed that the helix angles of the wires in the inner and the outer layers are the same and thus, line contact instead of point contact occurs between the wires in the inner and the outer layers. This is a desired configuration since line contact is less critical than point contact. This can also be seen from the above results in which the collapse load at a given extension is highest when the helix angle of the outer wires is the same as that for the inner wires.

When the helix angles for the inner and the outer wires are different, point contact will occur and the contact stresses for a given load will increase as the contact angle($\bar{\alpha}-\alpha$) increases. This results in the collapse load being higher when the contact angle is smaller as can be seen from the results above in which the 'rope' with an outer layer helix angle of 80° has a collapse load about 3-9% higher than that when the helix angle is 105°.

CHAPTER 9

Conclusions and suggestions for further work.

As wire rope finds widespread use, particularly in the offshore industry, the need to understand its behaviour becomes a concern to designers, manufacturers and users of wire rope. Various research programmes(as reported in Chapter 1 and also by the SERC Marine Technology Directorate, U.K) have been undertaken to study the various facets of its behaviour. Also, since the size of wire ropes has grown steadily in the recent years, which will make it difficult, if not impossible, for it to be tested to failure in tension, a theoretical model that is able to predict its strength is desirable.

The present work has been an attempt to understand further the behaviour of wire rope loaded beyond the elastic limit where very little work has been done. It has been inspired by the work by Jones and Christodoulides(64), where in their analysis, extension in the wires has been assumed infinitesimal and the actual evaluation of the line load X due to contact between the wires has not been attempted. Also, in the present analysis, besides the 'rope' with a single strand, analysis is also done for a 'rope' with a single strand and a core wire, a rope with two layers of strand and a core wire, and also a rope with n-layers of strand and a core wire.

The work in Chapters 3 and 4 has been useful in understanding the contact stresses in wire rope and in evaluating the value of line load X at collapse. Chapter 6 introduces finite extension and the analysis for the plastic collapse of wire rope is presented in Chapter 5, for extension assumed infinitesimal and in Chapter 7 for finite extension. Finally, in Chapter 8, a further analysis on contact is attempted which provides values of collapse load which are about 4-11% lower than the actual failure loads obtained

experimentally(Section 8.1.4).

9.1 Conclusions.

The importance of a study of rope behaviour beyond the elastic limit need no further mentioning. It does not only provide an estimate of the reserve strength beyond the elastic limit, which will help in the selection of a meaningful factor of safety, but the knowledge of the theoretical behaviour of wire ropes loaded beyond the elastic limit can also help in the proper design and construction of a wire rope.

In the present work, an analysis that would be able to predict the plastic collapse load of a wire rope has been presented. The results obtained from the analysis has been able to predict to a reasonable degree of accuracy, the collapse load of a 1X7 rope. However, the experimental results available are still too few to fully confirm the theory and more experimental results with wire rope of different sizes, helix angles and end conditions would have been useful.

In the analysis, the effect of contact stresses and extension in the wire have been given particular attention. As the results suggest, contact stresses play an important part in determining the collapse load for a given rope. The contact stresses depend on the manner the wires are laid in the rope and the analysis provide a rope configuration for which the contact stresses are minimised and the collapse load increased. Also, it has been shown that with the extension assumed infinitesimal, the collapse load predicted is about 20-35% lower than the actual collapse load in wire strands having $\epsilon=0.025$ at failure.

9.1.1 Role of inter-wire contact.

The problem of contact in wire rope has been and will be a concern to investigators attempting work on wire rope. It is not difficult to realise this as can be seen in the present work where contact stresses play a major part in determining the collapse load of a wire rope.

Since contact stresses depend on the manner in which the wires are laid in a rope, the knowledge of contact behaviour in wire rope will help to reduce these stresses and thus produce a rope which is capable of withstanding a larger load. It can be seen in Chapters 3 and 4 that for a single strand with core wire, the contact force required to produce an indentation increases as the helix angle of the wires in the strand approaches 90^0, and for a rope with two layers of strand, this contact force increases as the contact angle $(\bar{\alpha}-\alpha)$ approaches 0^0. Thus, to reduce the stresses due to contact in a wire rope, the helix angle of the helical wires should be a value approaching 90^0 and for a rope with two layers of strand, the difference in the helix angle between the inner and the outer wires should be small, and preferably the helix angles should be the same.

It has been seen that the contact load at collapse is much larger than the load required to produce an indentation in the wire. Thus, this further strengthens the fact that the stresses developed from contact in a rope are very large and cannot be ignored(61).

9.1.2 Effect of wire extension.

It has been seen in Chapter 6 that wire extension has a very small effect and may be ignored when performing elastic analysis on

wire ropes. However, in plastic analysis, it has been shown that there is substantial increase in collapse load with extension and thus, it has to be considered in the analysis.

9.1.3 Suitable helix angle for wire rope.

It has been a practice of wire rope manufacturers to produce wire ropes with helix angles approaching 90°. This practice is justified as can be seen that the collapse load of a wire rope increases as the helix angle approaches 90°. Also, from the experimental results obtained from the work of W.S. Utting(92) as shown in Section 8.1.2, it can be seen that as the helix angle approaches 90°, the failure load and the load to cause yielding in the wire rope also increase except for the failure loads for rope with helix angles 78.9° and 80.9° , which may be due to experimental discrepancies(Section 8.1.4).

9.1.4 Effect of a core wire.

Wire ropes may have a metal core or a soft fibre core and a metal core would obviously increase the strength of a wire rope. In a 1x7 rope, the core wire diameter would normally be slightly larger than the diameter of the helical wires. It has been found that the collapse load for this rope is smaller than a rope in which the core wire is of the same size or slightly smaller than the helical wire. However, the latter rope is an hypothetical one as the core wire will not be held together in the rope unless soft fibres are introduced between the core wire and the strand.

9.1.5 Suitable rope configuration for a rope with two layers of strand.

From the results obtained for a rope with two layers of strand,

the present work has been able to show that the best configuration for this type of rope is to have the helix angle for the inner and the outer strands approaching 90° and the helix angle for the outer strand should be less than ≈105°.

9.2 Suggestions for further work.

1. It has been realised that more experimental results are required to check the theoretical analysis that has been presented. Thus, a next stage to the present work is to carry out tensile tests to failure of a similar configuration rope but with varying sizes and helix angles, and also with various end conditions. The theoretical predictions of the collapse load should then be computed following the analysis described in Section 8.1.3 and the values compared with that obtained experimentally.

2. As wire ropes may also be bent over and around pulleys and drums during operation, the present analysis may also be extended to include the effect of bending. This may be done by studying the changes in curvature and twist of the wires in the rope and also their effect on the contact stresses when the rope is bent, and incorporating them in the analysis. Such analysis on a simple rope(1x7), which forms an element of a strand in a complex rope, will help greatly in the analysis for wire ropes with complex configurations.

3. With the knowledge of the effect of bending, the analysis may be extended to study wire ropes with more complex configurations such as that shown in Fig. 2.1, in which the core wire in the strand forms a 'double helix'. Here however, it is more

difficult to locate the contact points and thus to evaluate the contact stresses, but Karamchetty and Yuen(31,32) have produced an analysis for which this may be done.

REFERENCES

1. D.M. SHARP, "Rope in the Marine Environment", Proceedings of The Institution of Mechanical Engineers, Vol. 190, pp. 45-57.

2. The New Encyclopaedia Britannica, Vol. 15, pp. 1144-1150.

3. G.A. COSTELLO, "Analytical Investigation of Wire Rope," Applied Mechanics Reviews, Vol. 31, no. 7, pp. 897-900.

4. G.A COSTELLO, "Mechanics of Wire Rope," AIchE Symposium, Ser. n. 194, Vol. 76, 1980, pp. 107-112.

5. W. THOMSON and P.G. TAIT, "Treatise on Natural Philosophy," Vol.I, 1867.

6. LOVE, A.E.H., "A Treatise on the Mathematical Theory of Elasticity," Dover Publications, Inc., New York, NY 1944, Chapters 18 and 19.

7. BASSET, A.B, "On The Deformation of Thin Elastic Wires," American Journal of Mathematics, Vol.17, 1895, pp. 281-317.

8. W.A. SCOBLE, "Wire Ropes Research," Proceedings of the Institution of Mechanical Engineers, Vol. 115, 1920, pp. 835-868.

9. W.A. SCOBLE, "Wire Ropes Research," Proceedings of the Institution of Mechanical Engineers, Vol. 119, 1924, pp. 1193-1290.

10. W.A. SCOBLE, "Wire Ropes Research," Proceedings of the Institution of Mechanical Engineers, Vol. 123, 1928, pp. 353-404.

11. W.A. SCOBLE, "Wire Ropes Research," Proceedings of the Institution of Mechanical Engineers, Vol. 125, 1930, pp. 553-602.

12. W.A. SCOBLE, "Wire Ropes Research," Proceedings of the Institution of Mechanical Engineers, Vol. 130, 1935, pp. 373-478.

13. J.F. HOWE, "Determination of Stresses in Wire Rope as Applied to Modern Engineering Problems," Transaction of ASME, Vol. 40, No. 1680, 1918, pp. 1043-1095.

14. R. WOERNLE , "Wire Rope Research," Z.V.D.I., 1931, Vol. 75, Part 1, pp. 206 ; Part 2, pp. 1485. Translated in Colliery Guardian, 1932.

15. D.C DRUCKER and H. TACHAU, "A New Design Criterion for Wire Rope," Journal of Applied Mechanics, Vol.12, March 1945, pp. A-33 - A-38.

16. F.C. CARSTARPHEN, "Effects of Bending Wire Rope," Transactions of ASCE, Vol.98, 1933, pp. 562-621.

17. R.W. CHAPMAN, "The Stress in Wire Ropes Due to Bending," Engineering Review, Oct. 1908.

18. A.V DE FOREST and L.W. HOPKINS, "The Testing of Rope Wire and Wire Rope," Proceedings of ASTM, Vol. 32 (Part II), 1932, pp. 398-412.

19. C.L. LAYLAND, "Experimental Investigation of Torsion in Stranded Mining Wire Ropes," Proceedings (B) of the Institution of Mechanical Engineers, Vol. 1B, 1952-53, pp. 323-342.

20. E.C. HIND, "Wire Rope Transmission Losses," Proc. of the Institution of Mechanical Engineers, Vol. 178,

Part. 1, No. 30, pp. 815-829.

21. P.A. LAURA, H.H. VANDERVELDT and P.G. GAFFNEY, "Mechanical Behaviour of Stranded Wire Rope," Marine Technology Society Journal, Vol. 4, Part. 3, pp. 19-38.

22. P.A. LAURA, H.H. VANDERVELDT and P.G. GAFFNEY, "Acoustic Detection of Structural Failure of Mechanical Cables," Journal of Acoust. Soc. Amer., Vol.45, 1969, pp. 791-792.

23. H.H. VANDERVELDT, B.S. CHUNG and W.T. READER, "Some Dynamic Properties of Axially Loaded Wire Ropes," Experimental Mechanics, Vol. 13, 1973, pp. 24-30.

24. HALL, H. M., "Stresses in Small Wire Ropes," Wire and Wire Products, 26, 1951, pp. 228, 257-259.

25. F.H. HRUSKA, "Calculation of Stresses in Wire Ropes," Wire and Wire Products, Vol. 26, Sept. 1951, pp. 766-767, 799-801.

26. F.H. HRUSKA, "Radial Forces in Wire Ropes," Wire and Wire Products, Vol. 27, No.5, May 1952, pp. 459-463.

27. F.H. HRUSKA, "Tangential Forces in Wire Ropes," Wire and Wire Products, Vol. 28, No.5, May 1953, pp. 455-460.

28. A.W. LEISSA, "Contact Stresses in Wire Ropes," Wire and Wire Products, Vol. 34, No. 3, Mar. 1959, pp.307-314, 372-373.

29. F.B SEELY and J.O SMITH, "Advanced Mechanics of Materials," John Wiley and Sons, 1952.

30. W.L STARKEY and H.A CRESS, "An Analysis of Critical Stresses and Mode of Failure of a Wire Rope," Journal of Engineering for Industry, Trans. ASME, Vol. 81, 1959, pp. 307-316.

31. S.D.S.R. KARAMCHETTY and W.Y. YUEN, "Contact Problems in Wire Ropes," Journal of Mechanical Design, Trans. of the ASME, Paper No. 79-DE-2, 1979.

32. S.D.S.R. KARAMCHETTY, "Sections of a Torus - Application to Contact Stress Problems in Wire Rope," to be published.

33. BERT, C.W. and STEIN, R. A., "Stress Analysis of Wire Rope in Tension and Torsion," Wire and Wire Products, 37, 1962, pp. 769-770.

34. A.J DURELLI, S. MACHIDA and V.J PARKS, "Strains and Displacements on a Steel Wire Strand," Naval Engineers Journal, Vol.84, No.6, Dec.1972, pp. 85-93.

35. R.G DONG and R.F STEIDEL, "Contact Stress in Stranded Cable," Experimental Mechanics, May 1965, pp.142-147.

36. S.D.S.R. KARAMCHETTY, "Some Geometrical Characteristics of Wires in Wire Ropes," Proceedings of the Ninth SECTAM, Developments in Theoretical and Applied Mechanics, Vol. 9, Ed. by R.M. HACKETT, Vanderbilt University, May 1978, pp. 519-541.

37. Jr. W. HOBBS, "Calculating Wire Sizes for Wire Rope," Wire and Wire Products, Vol. 11, Nov. 1970, pp. 40-44.

38. S.D.S.R. KARAMCHETTY, "A Method for Determining the Geometry of Non-Circular Wire Rope Strands," Wire

Journal, February 1978, pp. 81-88.

39. J.W.S. HEARLE, "Theory of the Extension of Continuous Filament Yarns" in "Structural Mechanics of Fibers, Yarns and Fabrics" by J.W.S. HEARLE, P. GROSBERG and S. BACKER, Wiley, New York, 1969, pp.175-212.

40. N. JONES, "Elastic-Plastic and Viscoelastic Behaviour of a Continuous Filament Yarn," Int. Journal of Mech. Science, Vol. 16, 1974, pp. 679-687.

41. N.C. HUANG and G.E. FUNK, "Theory of Extension of Elastic Continous Filament Yarns," Textile Research Journal, Vol. 45, 1975, pp. 14-24.

42. N.C. HUANG, "Theories of Elastic Slender Curved Rcds" Journal of Applied Math. and Physics (ZAMP), vol. 24, 1973, pp. 1-19.

43. HUANG, N. C., "On the Extension of Elastic Two-Ply Filament Yarns," Journal of Applied Mechanics, Vol. 42, 1975, pp. 821-824.

44. HUANG, N.C., "On the Flexure of Elastic Two-Ply Filament Yarns," Textile Research Journal, Vol.47, 1977, pp. 73-76.

45. HUANG, N.C., "On Finite Extension of a Viscoelastic Two-Ply Filament Yarn," Textile Research Journal, Vol. 48, 1978, pp. 61-67.

46. HUANG N. C., "Finite Extension of an Elastic Strand with a Central Core," Journal of Applied mechanics, Transactions, ASME, 45, 1978, pp. 852-858.

47. MACHIDA, S. and DURELLI, A. J.,"Response of a Strand

to Axial and Torsional Displacements," Journal of Mechanical Eng. Science, 15, 1973, pp. 241-251.

48. A.J DURELLI and S. MACHIDA, "Response of Epoxy Oversized Models of Strands to Axial and Torsional Loads" Experimental Mechanics, Vol.13, No.8, Aug. 1973, pp. 313-321.

49. A.J DURELLI, V.J PARKS and H.M HASSEEM, "Helices Under Load," Journal of Engineering for Industry, Aug. 1975, pp. 853-858.

50. CHI, M., "Analysis of Multi-wire Strands in Tension and Torsion," Developments in Theoretical and Applied Mechanics, Proceedings of the Seventh Southeastern Conference on Theoretical and Applied Mechanics, Vol. 7, 1974, pp. 599-639.

51. J.W PHILLIPS and G.A COSTELLO, "Contact Stresses in Twisted Wire Cables," Journal Eng. Mech. Div. Proc. ASCE, EM2, Apr.1973, pp. 331-341.

52. COSTELLO, G. A. and PHILLIPS, J. W., "Contact Stresses in Thin Twisted Rods," Journal of Applied Mechanics, Transactions, ASME, Series E, 40, 1973, pp.629-630.

53. G.A COSTELLO and J.W PHILLIPS, "A More Exact Theory for Twisted Wire Cables," Journal Eng. Mech. Div. Proc. ASCE, Vol.100, EM5, Oct.1974, pp. 1096-1099.

54. J.L. LUBKIN, "Contact Problems," Chap. 42, "Handbook of Engineering Mechanics," Edited by W. FLUGGE, 1962, pp. 42-1 - 42-12.

55. G.A COSTELLO and J.W PHILLIPS, "Effective Modulus of

Twisted Wire Cables," Journal Eng. Mech. Div. Proc. ASCE, Vol.102, EM1, Feb.1976, pp. 171-181.

56. J.W. PHILLIPS and G.A. COSTELLO, "Axial Impact of Twisted Wire Cables," Journal of App. Mech., ASME, Mar.1977, pp. 127-131.

57. G.A COSTELLO and SUNIL K SINHA, "Torsional Stiffness of Twisted Wire Cables," Journal Eng. Mech. Div. Proc. ASCE, Vol.103, EM4, Aug.1977, pp. 766-770.

58. G.A COSTELLO and SUNIL K. SINHA, "Static Behaviour of Wire Rope," Journal Eng. Mech. Div. Proc. ASCE, Vol. 103, EM6, Dec.1977, pp. 1011-1022.

59. COSTELLO, G. A. and MILLER, R. E., "Lay Effect of Wire Rope," TAM Report No. 422, Department of Theoretical and Applied Mechanics, University of Illinois at Urbana-Champaign, Urbana, Illinois, 1977, pp.1-23.

60. G.A. COSTELLO and J.W. PHILLIPS, "Static Response of Stranded Wire Helical Springs," Int. Journal of Mech. Sci., Vol.21, 1979, pp. 171-178.

61. PHILLIPS, J. W., MILLER, R. E. and COSTELLO, G. A., "Contact Stresses in a Straight Cross-lay Wire Rope," Proceedings of the 1st. Annual Wire Rope Symposium, 1980, pp. 177-199.

62. G.A. COSTELLO, "Large Deflections of Helical Spring due to Bending," Journal Eng. Mech. Div. Proc. ASCE, Vol.103, EM3, Jun.1977, pp. 481-487.

63. COSTELLO, G.A. and BUTSON, G. J., "Simplified Bending Theory for Wire Rope," Journal of the Engineering

Mechanics Division, Proceedings of ASCE, Vol. 108, No. EM2, April, 1982, pp. 219-227.

64. N. JONES and J.C CHRISTODOULIDES, "Static Plastic Behaviour of a Strand," International Journal of Mechaical Science, Vol. 22, 1980, pp.185-195.

65. F.B HILDEBRAND, "Advance Calculus for Applications, Prentice-Hall, 1962.

66. H.R HERTZ, "Miscellaneous Papers," Translated by D.E JONES and G.A SCHOTT, Mac Millan, London, 1896.

67. K.L JOHNSON, "One Hundred Years of Hertz Contact," Proceedings of the Institute of Mechanical Engineers, Vol. 196, No. 39, 1982, pp. 363-378.

68. H.R THOMAS and V.A HOERSCH, "Stresses Due to the Pressure of One Elastic Solid Upon Another," Bulletin No. 212, Univ. of Illinois Engineering Expt. Station, July 1930.

69. ABRAMOWITZ and STEGUN, "Handbook of Mathematical Functions," Dover Publication, N.Y., 1965.

70. K.L JOHNSON, "The Correlation of Indentation Experiments," J. Mech. Phys. Solids, Vol.18, 1970, pp.115-126.

71. R. HILL, "The Mathematical Theory of Plasticity," Oxford University Press, 1950.

72. W. JOHNSON, R. SOWERBY and J.B HADDOW, "Plane-strain Slip-Line Fields : Theory and Bibliography," Edward Arnold, 1970, pp. 64.

73. D. TABOR, "Hardness of metals," Clarendon Press,

Oxford, 1951.

74. E. LEVIN, "Indentation Pressure of a Smooth Circular Punch," Quarterly of Applied Maths., Vol. 13, 1955, pp. 133-137.

75. DRUCKER, PRAGER and GREENBERG, "Extended Limit Design Theorems for continuous Media," Quarterly of Applied Maths., Vol. 9, 1952, pp. 381-389.

76. R.T SHIELD and D.C DRUCKER, "The Application of Limit Analysis to Punch Indentation Problems," Journal of Applied Mechanics, Vol. 20, 1953, pp. 453-460.

77. A.J.M SPENCER, "Perturbation Methods in Plasticity - II, Plane Strain of Slightly Irregular Bodies," Journal Mech. Phy. Solids, Vol. 10, 1962, pp. 17-26.

78. A.G ATKINS and D. TABOR, "The Plastic Deformation of Crossed Cylinders and Wedges," Journal of the Institute of Metals, Vol. 94, 1966, pp. 107-115.

79. W. PRAGER, "Limit Analysis : The Development of a Concept," pp. 3-25 in Problems of Plasticity edited by A. SAWCZUK, 1974.

80. A.A GVOZDEZ, "The Determination of the Value of the Collapse load for Statically Indeterminate Systems Undergoing Plastic Deformation," Int. J. Mech. Sci., Vol. 1, 1960, pp.322-355.

81. R. HILL, "On the State of Stress in a Plastic-Rigid Body at the Yield Point," Phil. Mag., Vol. 42, 1951, pp. 868-875.

82. R. HILL, "A Note on Estimating the Yield-Point Loads

in a Plastic-Rigid Body," Phil. Mag., Vol. 43, 1952, pp. 353-355.

83. D.C DRUCKER, H.J GREENBERG and W. PRAGER, "The Safety Factor for an Elastic-Plastic Body in Plane Strain," Journal of Applied Mechanics, Vol. 18, 1951, pp. 371-378.

84. D.C DRUCKER, W. PRAGER and H.J GREENBERG, "Extended Limit Design Theorems for Continuous Media," Quarterly Applied Maths., Vol. 9, 1952, pp. 381-389.

85. R. HILL and M.P.L. SIEBEL, "On the Plastic Distortion of Solid Bars by Combined Bending and Twisting," Journal of the Mechanics and Physics of Solids, Vol.1 1953, pp. 207-214.

86. W. JOHNSON and P.B MELLOR, "Engineering Plasticity," Van Nostrand, 1973.

87. J.B MARTIN, "Plasticity : Fundamentals and General Results, M.I.T Press, 1975.

88. E. REISSNER, "On One-Dimensional Large - Displacement Finite-Strain Beam Theory," Studies in Applied Maths, Vol. LII, No.2, June, 1973, pp. 87-95.

89. N. JONES, "Consistent Equations for the Large Deflections of Structures," Bull. Mech. Engineering Education, Vol. 10, 1971, pp. 9-20.

90. C.D HAMLET, "Contact Stresses and Loads Between Individual Wires in a Stranded Wire Rope," Final Year Project, Mech. Eng. Dept., University of Liverpool, 1982/83.

91. G. RAINEY and D. MOXHAM, "An Investigation of the

Mechanical Behaviour of a Wire Strand in Tension," Final Year Project, Mech. Eng. Dept., University of Liverpool, 1980/81.

92. W.S UTTING, "Experimental and Theoretical Studies in the Deformation of Wire Ropes Under Axial Tensile Loads," Ph.D Thesis, University of Liverpool, March, 1984.

93. J.O SMITH and O.M. SIDEBOTTOM, "Elementary Mechanics of Deformable Bodies," The Macmillan Company, 1969.

APPENDICES

APPENDIX 1

Deriving strain relations (2.28), (2.31) and (2.32) geometrically

With the aid of Fig. 2.2a, the governing equations for a helical curve can be written as [65]

$$x = r\cos\beta\ ,\quad y = r\sin\beta\ ,\quad z = \frac{h\beta}{2\pi} \qquad \text{(A1.1a-c)}$$

where r and h are the radius and pitch of a circular helix, respectively. It is evident from Fig. 2.2b which shows a helical curve developed onto a flat plane that

$$\tan\alpha = \frac{h}{2\pi r} \qquad \text{(A1.2)}$$

$$\cos\alpha = \frac{2\pi r}{[h^2 + (2\pi r)^2\ ]^{\frac{1}{2}}} \qquad \text{(A1.3)}$$

and

$$\sin\alpha = \frac{h}{[h^2 + (2\pi r)^2\ ]^{\frac{1}{2}}} \qquad \text{(A1.4)}$$

where α is the helix angle.

If a helical curve with an initial length L along the z axis is loaded, then it elongates by an amount $\delta L/h$ and rotates through an angle $\Delta L/h$ about the z axis as shown in Fig. 2.5 (δ and Δ are the axial extension and angular rotation for one pitch (h), respectively). In addition, the radius r becomes $r + \eta$.

The initial arc length of the segment AB in Fig. 2.5 is

$$s = L\ [\ h^2 + (2\pi r)^2\ ]^{\frac{1}{2}} / h \qquad \text{(A1.5)}$$

while the deformed length A'B' is

$$s' = L[\ (h + \delta)^2 + (2\pi + \Delta)^2\ (r + \eta)^2\ ]^{\frac{1}{2}} \qquad \text{(A1.6)}$$

provided A'B' is part of a helical curve with a radius $r + \eta$. The centre-line engineering strain of the helical curve in Fig. 2.5 is therefore

$$\varepsilon_w = (s' - s)/s \tag{A1.7}$$

Substituting equations (A1.5) and (A1.6) into equation (A1.7) gives

$$0 = \varepsilon \sin^2\alpha + \gamma \cos^2\alpha + \rho \cos^2\alpha \tag{A1.8}$$

when

$$\varepsilon_w = 0, \quad \varepsilon = \delta/h \ , \ \gamma = \Delta/2\pi \quad \text{and } \rho = \eta/r \tag{A1.9 a-d}$$

and ε , γ and ρ are small compared to unity.

The pitch of the deformed helical curve in Fig. 2.5 is

$$h' = (h + \delta)2\pi / (2\pi + \Delta)$$

or
$$h' = h (1 + \varepsilon - \gamma) \tag{A1.10}$$

when ε , $\gamma \ll 1$.

With the aid of equations (A1.3) and (A1.4), equations (2.10) and (2.12) may be rewritten as

$$\kappa' = (2\pi)^2 r / \{ h^2 + (2\pi r)^2 \} \tag{A1.11}$$

and
$$\tau = 2\pi h / \{ h^2 + (2\pi r)^2 \} \tag{A1.12}$$

Equations (A1.11) and (A1.12) with h replaced by h' and r replaced by $r + \eta$ give the curvature and torsion of the deformed helical curve which is shown in Fig. 2.5. Thus

$$d\kappa' = (2\pi)^2 (r + \eta) / \{ h'^2 + (2\pi)^2 (r + \eta)^2 \} - (2\pi)^2 r / \{ h^2 + (2\pi r)^2 \} \tag{A1.13}$$

and

$$d\tau = 2\pi h' / \{ h'^2 + (2\pi)^2 (r + \eta)^2 \} - 2\pi h / \{ h^2 + (2\pi r)^2 \} \tag{A1.14}$$

Using equations (A1.3), (A1.4), (A1.10) and (A1.9), equations (A1.13) and (A1.14) become

$$d\kappa' = \frac{\sin^2\alpha \cos^2\alpha}{r} (\gamma - \varepsilon + \rho) + \gamma \frac{\cos^2\alpha}{r} \tag{A1.15}$$

$$d\tau = \frac{\sin\alpha \cos^3\alpha}{r} (\gamma - \varepsilon + \rho) + \gamma \frac{\sin\alpha \cos\alpha}{r} \tag{A1.16}$$

Therefore equations (A1.8), (A1.15) and (A1.16), given equations (2.28), (2.31) and (2.32), respectively.

Equations (A1.15) and (A1.16) are the same as Equations (A.12) and (A.13), respectively, in Reference(64) if Equation (A1.8) is used in Equations (A1.15) and (A1.16).

APPENDIX 2

Extent of the plastic layer due to indentation.

(i) Contact between wires in the same strand(line contact).

The indentation force, Q is given by Equation (4.5), viz.

$$Q = \frac{2\Lambda}{\pi} (5\sigma_0)^2 \qquad (A2.1)$$

where Λ is given by Equation (3.39).

Substituting Equation (A2.1) into Equation (3.31) gives

$$b = \frac{2\Lambda}{\pi} (5\sigma_0) \qquad (A2.2)$$

Substituting b into Equations (3.35) and using the resulting equations in Equation (3.38), a value of D (i.e =z/b) that satisfies the equation may be found by iteration.

Therefore, the extent of the plastic layer equivalent to the indentation force, Q

$$z = Db \qquad (A2.3)$$

From the computation the following results are obtained :-

$$Q = 6082.9 \text{ N/m.}$$

$$b = 5.793E\text{-}6 \text{ m.}$$

$$z = 0.0149R \text{ m.}$$

where R is the radius of the wires.

Therefore, the plastic layer is 1.49% of the radius of the wires.

(ii) Contact between adjacent wires in neighbouring strands (point contact).

The indentation force, Q' is given by Equation (4.8), viz.

$$Q' = \frac{2.8\pi b^2 \sigma_0}{k} \qquad (A2.4)$$

and b is given by Equation (4.9), viz.

$$b = 4.2\ E(k') \qquad \text{(A2.5)}$$

The value of b may be used to determine the value of D_1 (i.e $=\frac{kz}{b}$) that satisfies the Equation (3.38) where σ_x, σ_y and σ_z are given by Equations (3.23), following procedure 1-5 in Section 3.4.3.

Thus, the extent of the plastic layer equivalent to the indentation force, Q'

$$z = \frac{D_1 b}{k} \qquad \text{(A2.6)}$$

From the computation the following results are obtained :-

$Q' = 0.472$ N.

$b = 7.8283E\text{-}6$ m.

$k = 0.24$.

$z = 0.0238R$ m.

($\alpha = 75^\circ$; $\bar{\alpha} = 105^\circ$)

Therefore, the plastic layer is 2.38% of the radius of the wires.

APPENDIX 3

Showing Upper bound equation for a single strand (equation 5.28) reducing to the lower bound equation (equation 5.14)

(stated in Reference(64))

Rewriting equation (5.28),

$$A(\phi \sin\alpha + \tan^2\alpha\chi + 4\lambda G'_* \sin^2\alpha/3\pi - \lambda H_* \sin\alpha\cos\alpha/3)$$
$$= -\mu\lambda\cos\alpha/3 - \chi + 4\lambda G'_* \cos^2\alpha/3\pi + \lambda H_* \sin\alpha\cos\alpha/3 \qquad (A3.1)$$

Substituting equation (5.26) into equation (A3.1), gives

$$(4H_*\cos^2\alpha/\pi = G_\downarrow \sin\alpha\cos\alpha)(\phi \sin\alpha + \tan^2\alpha\chi + 4\lambda G_\downarrow \sin^2\alpha/3\pi - \lambda H_* \sin\alpha\cos\alpha/3)$$
$$= (4H_* \sin^2\alpha/\pi + G'_* \sin\alpha\cos\alpha)(-\mu\lambda\cos\alpha/3 - \chi$$
$$+ 4\lambda G'_* \cos^2\alpha/3\pi + \lambda H_* \sin\alpha\cos\alpha/3) \qquad (A3.2)$$

$$4H_*\phi \sin\alpha\cos^2\alpha/\pi - G'_*\phi \sin^2\alpha\cos\alpha + 4H_*\chi \sin^2\alpha/\pi$$
$$- G'_*\chi \sin^2\alpha\tan\alpha + 16\lambda H_* G'_* \sin^2\alpha\cos^2\alpha/3\pi^2$$
$$- 4\lambda G'^2_* \sin^3\alpha\cos\alpha/3\pi - 4\lambda H_*^2 \sin\alpha\cos^3\alpha/3\pi$$
$$+ \lambda G'_* H_* \sin^2\alpha\cos^2\alpha/3$$
$$= -4\lambda H_*\mu\sin^2\alpha\cos\alpha/3\pi - \lambda G'_*\mu\sin\alpha\cos^2\alpha/3$$
$$- 4H_*\chi\sin^2\alpha/\pi - G'_*\chi\sin\alpha\cos\alpha + 16\lambda G'_* H_* \sin^2\alpha\cos^2\alpha/3\pi^2$$
$$+ 4\lambda G'^2_* \sin\alpha\cos3\alpha/3\pi + 4\lambda H_*^2 \sin^3\alpha\cos\alpha/3\pi + \lambda G'_* H_* \sin^2\alpha\cos^2\alpha/3 \qquad (A3.3)$$

Simplifying (A3.3) and using equation (5.1) gives

$$3H_*\phi\cos\alpha/\lambda = \frac{3\pi}{4\lambda} G'_*\phi \sin\alpha + H_*\mu\sin\alpha$$
$$+ \frac{\pi}{4} G'_*\mu\cos\alpha + 6H_*\chi\tan\alpha/\lambda - \frac{3\pi}{4\lambda} G'_*\chi(\tan^2\alpha - 1) - 1 = 0 \qquad (A3.4)$$

Substituting equation (5.15) into equations (5.11) and (5.13) gives

$$H_* = \mu\sin\alpha + 3\phi\cos\alpha/\lambda + 6\chi\tan\alpha/\lambda \qquad (A3.5)$$

$$G_* = \frac{\pi}{4}\mu\cos\alpha - \frac{3\pi}{4\lambda}\phi\sin\alpha - \frac{3\pi}{4\lambda}\chi(\tan^2\alpha - 1) \qquad (A3.6)$$

Therefore, substituting equations (A3.5) and (A3.6) into equation (A3.4) gives

$$3\phi\mu\sin\alpha\cos\alpha/\lambda + 9\phi^2\cos^2\alpha/\lambda^2 + 18\phi\chi\sin\phi/\lambda^2$$

$$= \frac{3\pi^2}{16\lambda}\phi\mu\sin\alpha\cos\alpha + \frac{9\pi^2}{16\lambda^2}\phi^2\sin^2\alpha + \frac{9\pi^2}{16\lambda^2}\phi\chi\sin\alpha(\tan^2\alpha - 1)$$

$$+ \mu^2\sin^2\alpha + 3\phi\mu\sin\alpha\cos\alpha/\lambda + 6\mu\chi\sin\alpha\tan\alpha/\lambda$$

$$+\frac{\lambda^2}{16}\mu^2\cos^2\alpha - \frac{3\pi^2}{16\lambda}\phi\mu\sin\alpha\cos\alpha - \frac{3\pi^2}{16\lambda}\mu\chi\cos\alpha(\tan^2\alpha - 1)$$

$$+ 6\mu\chi\sin\alpha\tan\alpha/\lambda + 18\phi\chi\sin\alpha/\lambda^2 + 36\chi^2\tan^2\alpha/\lambda^2$$

$$- \frac{3\pi^2}{16\lambda}\mu\chi\cos\alpha(\tan^2\alpha - 1) + \frac{9\pi^2}{16\lambda^2}\phi\chi\sin\alpha(\tan^2\alpha - 1)$$

$$+ \frac{9\pi^2}{16\lambda^2}\chi^2(\tan^2\alpha - 1)^2 - 1 = 0 \qquad \text{(A3.7)}$$

Finally, simplifying equation (A3.7) gives the lower bound equation (equation 5.14) which is

$$(\sin^2\alpha + \pi^2\cos^2\alpha/16)\mu^2 + 9(\cos^2\alpha + \pi^2\sin^2\alpha/16)\phi^2/\lambda^2$$

$$+ \sin\alpha\cos\alpha(6 - 3\pi^2/8)\mu\phi/\lambda$$

$$+ 9[4\sin\alpha + \pi^2\sin\alpha(\tan^2\alpha - 1)/8]\phi\chi/\lambda^2$$

$$+ 3[4\tan\alpha\sin\alpha - \pi^2\cos\alpha(\tan^2\alpha - 1)/8]\mu\chi/\lambda$$

$$+ [36\tan^2\alpha + 9\pi^2(\tan^2\alpha - 1)^2/16]\chi^2/\lambda^2 - 1 = 0 \qquad \text{(A3.8)}$$

APPENDIX 4

Showing that the upper bound and lower bound calculations for the core wire lead to identical predictions

The upper bound equation for a core wire is given by equation (5.47)

i.e.

$$F_c\delta_c + M_c\Delta_c = \delta_c \left[T_c + \frac{H_c^2}{T_c} \left(\frac{T_{co}}{H_{co}} \right)^2 \right] \qquad \text{(A4.1)}$$

Substituting equation (5.38) into equation (A4.1) gives

$$F_c\delta_c + M_c\Delta_c = \delta_c \left[\frac{T_{co}^2}{T_c} \right] \qquad \text{(A4.2)}$$

Using equation (5.48) and $\Delta_c = L\tau_c$ equation (A4.2) becomes

$$F_c\varepsilon_c + M_c\tau_c = \varepsilon_c \left[\frac{T_{co}^2}{T_c} \right] \qquad \text{(A4.3)}$$

Substituting equation (5.46) into equation (A4.3) gives

$$F_c + \frac{M_c H_c}{T_c} \left(\frac{T_{co}^2}{H_{co}} \right) = \frac{T_{co}^2}{T_c} \qquad \text{(A4.4)}$$

Finally, substituting equations (5.40) and (5.41) into equation (A4.4) gives

$$F_c = \frac{M_c^2}{F_c} \left(\frac{T_{co}}{H_{co}} \right)^2 = \frac{T_{co}^2}{F_c}$$

$$F_c = \frac{T_{co}^2}{F_c} \left[1 - \frac{M_c^2}{H_{co}^2} \right]$$

$$\therefore \left(\frac{F_c}{T_{co}} \right)^2 + \left(\frac{M_c}{H_{co}} \right)^2 = 1 \qquad \text{(A4.5)}$$

Equation (A4.5) is the lower bound equation. Thus, the upper bound and lower bound calculations for the core wire lead to identical predictions.

APPENDIX 5

Showing that the upper bound and lower bound calculations lead to identical predictions for a single strand with finite wire extension

Substituting equation (7.3) into equation (7.9) gives

$$H_* = \mu\sin\alpha + \frac{3r\cos\alpha}{R}\{(1+\varepsilon\omega)\phi + \frac{(2+\varepsilon\omega)\sin\alpha}{\cos^2\alpha}[\phi\sin\alpha - T_*]\}$$

$$\therefore H_* = \mu\sin\alpha + \frac{3\phi r}{R\cos\alpha}[(1+\varepsilon\omega) + \sin^2\alpha] - \frac{3T_* r(2+\varepsilon\omega)\sin\alpha}{R\cos\alpha} \qquad \text{(A5.1)}$$

Substituting equation (7.3) into equation (7.11) gives

$$G_*' = \frac{\pi}{4}\{\mu\cos\alpha - \frac{3r}{R}[\phi(1+\varepsilon\omega)\sin\alpha + (\phi\sin\alpha - T_*)(\tan^2\alpha(1+\varepsilon\omega) - 1]\}$$

$$\therefore \mu = \frac{4G_*'}{\pi\cos\alpha} + \frac{3r\phi(1+\varepsilon\omega)\sin\alpha}{R\cos^3\alpha} - \frac{3r}{R}\phi\frac{\sin\alpha}{\cos\alpha} + \frac{3rT_*}{R\cos\alpha} - \frac{3rT_*}{R\cos\alpha}\tan^2\alpha(1+\varepsilon\omega) \qquad \text{(A5.2)}$$

Now, substituting equation (A5.2) into equation (A5.1) gives

$$H_* = \frac{4G_*'\sin\alpha}{\pi\cos\alpha} + \frac{3r\phi(1+\varepsilon\omega)\sin^2\alpha}{R\cos^3\alpha} - \frac{3r}{R}\phi\frac{\sin^2\alpha}{\cos\alpha} + \frac{3rT_*\sin\alpha}{R\cos\alpha} - \frac{3rT_*}{R}\tan^3\alpha(1+\varepsilon\omega) + \frac{3r\phi}{R\cos\alpha}(1+\varepsilon\omega) + \frac{3r\phi\sin^2\alpha}{R\cos\alpha} - \frac{3T*r}{R\cos\alpha}(2+\varepsilon\omega)\sin\alpha$$

which, after simplifying can be written as

$$\phi = \frac{H_*R\cos^3\alpha}{3r(1 + \varepsilon\omega)} - \frac{4G_*'R\sin\alpha\cos^2\alpha}{3\pi r\ (1 + \varepsilon\omega)} + T_* \sin\alpha \qquad \text{(A5.3)}$$

Substituting equation (A5.3) into equation (A5.2) gives

$$\mu = \frac{4G_*'}{\pi\cos\alpha} + \frac{3rT_*}{R\cos\alpha} - \frac{3rT_*}{R\cos\alpha} \tan^2\alpha\ (1 + \varepsilon\omega)$$

$$+ \frac{3r(1 + \varepsilon\omega)\sin\alpha}{R\cos^3\alpha} \left[\frac{H_*R\cos^3\alpha}{3r(1 + \varepsilon\omega)} + T_*\sin\alpha - \frac{4G_*'R\sin\alpha\cos^2\alpha}{3\pi r\ (1 + \varepsilon\omega)} \right]$$

$$- \frac{3r\sin\alpha}{R\cos\alpha} \left[\frac{H_*R\cos^3\alpha}{3r\ (1 + \varepsilon\omega)} + T_*\sin\alpha - \frac{4G_*'R\sin\alpha\cos^2\alpha}{3\pi r\ (1 + \varepsilon\omega)} \right]$$

and simplifying gives

$$\mu = \frac{4G_*'}{\pi} \left[\cos\alpha + \frac{\sin^2\alpha\cos\alpha}{(1 + \varepsilon\omega)} \right] + \frac{3rT_*\cos\alpha}{R}$$

$$+ H_*\sin\alpha\ (1 - \frac{\cos^2\alpha}{1 + \varepsilon\omega}) \qquad \text{(A5.4)}$$

Substituting equation (A5.3) into equation (7.3) gives

$$\chi = \frac{H_*R\sin\alpha\cos^3\alpha}{3r\ (1 + \varepsilon\omega)} - \frac{4G_*'R\sin^2\alpha\cos^2\alpha}{3\pi r(1 + \varepsilon\omega)} - T_*\cos^2\alpha \qquad \text{(A5.5)}$$

Finally, substituting equations (7.27), (7.29), (A5.3), (A5.4) and (A5.5) into the upper bound equation (equation (7.37)) gives

$$\left\{ \frac{H_*R\cos^3\alpha}{3r(1 + \varepsilon\omega)} - \frac{4G_*'R\sin\cos^2\alpha}{3\pi r\ (1 + \varepsilon\omega)} + T_*\sin\alpha + \frac{H_*R\sin^2\alpha\cos\alpha}{3r\ (1 + \varepsilon\omega)} \right.$$

$$\left. - \frac{4G_*'R\sin^3\alpha}{3\pi r\ (1 + \varepsilon\omega)} - T_*\sin\alpha \right\} \left\{ \sin\alpha - \frac{3\pi r\ (1 + \varepsilon\ )\sin\alpha(1 - H_*^2)^{\frac{1}{2}}}{8T_*R} \right.$$

$$+ \frac{3r\ (1 + \varepsilon\omega)H_*\cos\alpha}{T_*R} - \frac{3r\ (1 + \varepsilon\omega)G_*'\ H_*\cos\alpha}{2T_*R\ (1 - H_*^2)^{\frac{1}{2}}}$$

$$+\left\{\frac{4G_*R\cos\alpha}{3\pi r}\left[\cos\alpha+\frac{\sin^2\alpha\cos\alpha}{(1+\varepsilon\omega)}\right]+T_*\cos^2\alpha\right.$$

$$+\frac{H_*R\sin\alpha\cos\alpha}{3r}\left[1-\frac{\cos^2\alpha}{1+\varepsilon\omega}\right]+\frac{H_*R\sin\alpha\cos^3\alpha}{3r(1+\varepsilon\omega)}$$

$$\left.-\frac{4G_*'R\sin^2\alpha\cos^2\alpha}{3r(1+\varepsilon\omega)}-T_*\cos^2\alpha\right\}\left\{\frac{3\pi r(1-H_*^2)^{\frac{1}{2}}}{8T_*R}\right.$$

$$\left.+\frac{3rH_*\sin\alpha}{T_*R\cos\alpha}-\frac{3rG_*'H_*\sin\alpha}{2T_*R(1-H_*^2)^{\frac{1}{2}}}\cos\alpha\right\}$$

$$=\frac{H_*R\sin\alpha\cos\alpha}{3r(1+\varepsilon\omega)}-\frac{4G_*'R\sin^2\alpha}{3\pi r(1+\varepsilon\omega)}-T_*+T_*+\frac{H_*^2}{T_*}$$

$$+\frac{G_*(1-H_*^2)^{\frac{1}{2}}}{2T_*}-\frac{G_*H_*^2}{2T_*(1-H_*^2)^{\frac{1}{2}}} \qquad \text{(A5.6)}$$

Simplifying and introducing equation (7.1) gives

$$\frac{H_*R\sin\alpha\cos\alpha}{3r(1+\varepsilon\omega)}-\frac{H_*\pi\sin\alpha\cos\alpha(1-H_*^2)^{\frac{1}{2}}}{8T_*}+\frac{H_*^2\cos^2\alpha}{T_*}$$

$$-\frac{G_*H_*^2\cos^2\alpha}{2T_*(1-H_*^2)^{\frac{1}{2}}}-\frac{4G_*'R\sin^2\alpha}{3\pi r(1+\varepsilon\omega)}+\frac{G_*'\sin^2\alpha(1-H_*^2)^{\frac{1}{2}}}{2T_*}$$

$$-\frac{4G_*'H_*\sin\alpha\cos\alpha}{\pi T_*}+\frac{2G_*'H_*\sin\alpha\cos\alpha}{\pi T_*(1-H_*^2)^{\frac{1}{2}}}+\frac{G_*\cos^2\alpha(1-H_*^2)^{\frac{1}{2}}}{2T_*}$$

$$+\frac{4G_*'\cos\alpha\sin\alpha H_*}{\pi T_*}-\frac{2G_*^2H_*\sin\alpha\cos\alpha}{\pi T_*(1-H_*^2)^{\frac{1}{2}}}+H_*\sin\alpha\cos\alpha\pi\frac{(1-H_*^2)^{\frac{1}{2}}}{8T_*}$$

$$+\frac{H_*^2\sin^2\alpha}{T_*}-\frac{G_*H_*^2\sin^2\alpha}{2T_*(1-H_*^2)^{\frac{1}{2}}}$$

$$=\frac{H_*R\sin\alpha\cos\alpha}{3r(1+\varepsilon\omega)}\quad\frac{4G_*'R\sin^2\alpha}{3\pi r(1+\varepsilon\omega)}+G_*'(1-H_*^2)^{\frac{1}{2}}$$

$$=\frac{G_*H_*^2}{2T_*(1-H_*^2)^{\frac{1}{2}}}+\frac{1-T_*^2-G_*'(1-H_*^2)^{\frac{1}{2}}}{T_*} \qquad \text{(A5.7)}$$

Finally, substituting equations (7.3), (7.9) and (7.11) into equation (A5.7) gives equation (7.12) which is the lower bound equation.

APPENDIX 6

Relationship between ε_ω and ε_ω with ε

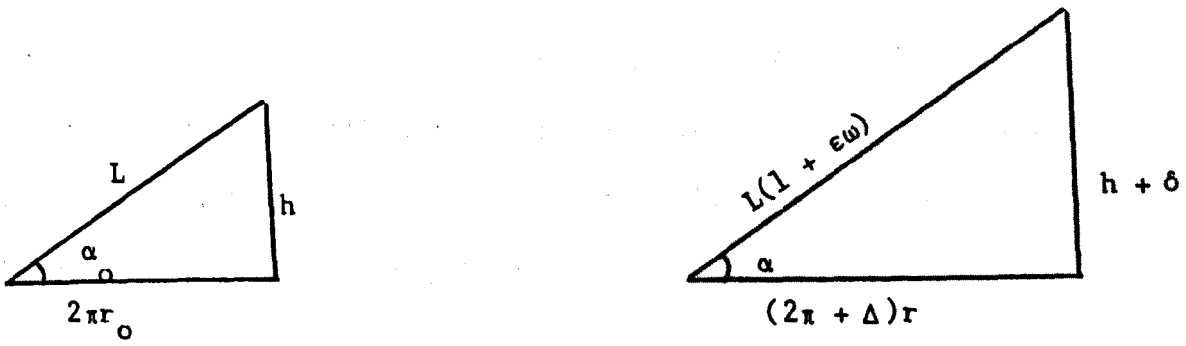

INITIAL FINAL

The figure shows a helical curve developed on a flat plane.

$$\sin\alpha = \frac{h + \delta}{L(1 + \varepsilon_\omega)} \qquad \text{(A6.1)}$$

But $L = h/\sin\alpha_o$ (A6.2)

Therefore, substituting equation (A6.2) into equation (A6.1) gives

$$\varepsilon_\omega = (1 + \varepsilon)\frac{\sin\alpha_o}{\sin\alpha} - 1 \qquad \text{(A6.3)}$$

where $\varepsilon = \delta/h$ (A6.4)

$$\cos\alpha = \frac{(2\pi + \Delta)r}{L(1 + \varepsilon_\omega)} \qquad \text{(A6.5)}$$

and $$L = \frac{2\pi r_o}{\cos\alpha_o} \qquad \text{(A6.6)}$$

Therefore, substituting equations (A6.3) and (A6.6) into equation (A6.5) gives

$$\gamma = (1 + \varepsilon)\frac{r_o \tan\alpha_o}{r \tan\alpha} - 1 \qquad \text{(A6.7)}$$

where $\gamma = \Delta/2\pi$ (A6.8)

If r_o is the helix radius when the wires in the strand are just touching each other, r will be the helix radius when the wires have undergone an indentation at the area of contact between the wires due

to the contact pressure resulting from the loads applied on the strand.

From Chapter 4 (Section 4.3), it has been found that the plastic layer is about 1.5% of the radius of the wire. Thus, the indentation will have to be less than 1.5% of the radius of the wire, and since the helix radius is more than twice the radius of the wire (i.e. for strand with m > 6), the indentation is very small compared to the helix radius. Therefore, it can be assumed that $r_o \approx r$.

Therefore, equation (A6.7) becomes

$$\gamma = (1 + \varepsilon) \frac{\tan\alpha_o}{\tan\alpha} - 1 \qquad \text{(A6.9)}$$

It has been defined that

$$A = \dot{\varepsilon}/\dot{\gamma} \qquad \text{(A6.10)}$$

$$\text{Thus, } A = \partial\varepsilon/\partial\gamma \qquad \text{(A6.11)}$$

If the initial extension and angular rotation are zero, then equation (A6.11) can be written as

$$A = \varepsilon/\gamma \qquad \text{(A6.12)}$$

Thus, for a given value of ε and A, γ can be found from equation (A6.12). The value of α_o can then be found from equation (A6.9) and finally, the corresponding value of ε_ω can be found from equation (A6.3).

Similarly, for a rope with two layers of strand, the value of ε_ω can be found if equations (A6.3), (A6.9) and (A6.12) are written as follows,

$$\bar{\varepsilon}_\omega = (1 + \bar{\varepsilon}) \frac{\sin\bar{\alpha}_o}{\sin\bar{\alpha}} - 1 \qquad \text{(A6.13)}$$

$$\bar{\gamma} = (1 + \bar{\varepsilon}) \frac{\tan\bar{\alpha}_o}{\tan\bar{\alpha}} - 1 \qquad \text{(A6.14)}$$

$$\text{and} \quad \bar{A} = \bar{\varepsilon}/\bar{\gamma} \qquad \text{(A6.15)}$$

For a given value of ε, the extension of the inner strand δ can be found from

$$\delta = 2\pi r \tan\alpha \qquad \text{(A6.16)}$$

From equation (7.53)

$$\bar{\delta} = \delta = 2\pi r \tan\alpha \qquad \text{(A6.17)}$$

Thus,

$$\bar{\varepsilon} = \frac{2\pi r \tan\alpha\varepsilon}{2\pi \bar{r} \tan\bar{\alpha}} \qquad \text{(A6.18)}$$

The value of $\bar{A}$ can be obtained from equation (7.66)

APPENDIX 7

An Estimate of Plastic Collapse Load following the work by Machida and Durelli(47).

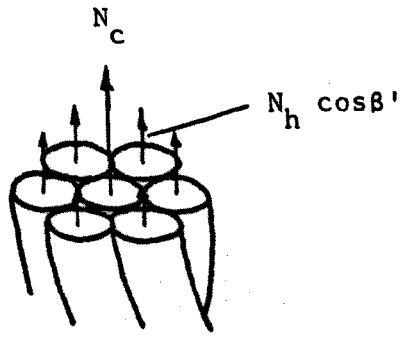

The external axial force acting on the strand,

$$N = N_c + 6N_h\cos\beta' \qquad \text{(A7.1)}$$

where N_c is the axial force acting in the core wire,

N_h is the axial force acting in the helical wire,

and β' is the helical wire lay angle after deformation.

$$\beta' = \tan^{-1}\left(\frac{1+\gamma}{1+\varepsilon}\tan\beta\right) \qquad \text{(A7.2)}$$

where γ is the normalised rotation per original one pitch length of the strand,

ε is the axial displacement of the strand per unit length.

For a fixed end case, $\gamma = 0$ and thus

$$\beta' = \tan^{-1}\left(\frac{1}{1+\varepsilon}\tan\beta\right) \qquad \text{(A7.3)}$$

If σ_y is the yield stress of the material, the axial forces to cause yielding in the core and the helical wire are

$$N_c = A_c\,\sigma_y \qquad \text{(A7.4)}$$

and

$$N_h = A_h\,\sigma_y \qquad \text{(A7.5)}$$

respectively, where A_c and A_h are the cross-sectional areas of the core wire and the helical wire, respectively.

The yield stress of the material for the rope used in the tests(92) is determined from the load-extension graphs obtained for the helical wires(Figs. A5.4 - A5.9 in (92)). The 0.1% proof load is used as there is no distinct yield point.

The average 0.1% proof load = 1100 kgf.

= 10.791 kN. (when $g=9.81 m/s^2$)

Therefore, the 0.1% proof stress

$$= \frac{10.791 \times 10^3}{\pi/4 \times 0.00373^2}$$

$$= 987.5 \text{ MN/m}^2.$$

Thus, the load to cause initial elastic yielding

$$= N_c + 6N_h \cos\beta'$$

$$= (11.86 + 64.76\cos\beta') \text{ kN.}$$

APPENDIX 8

Results associated with the theoretical collapse loads in Table 8.3

Helix Angle = 75.4°

ϵ	χ	G'_*	H_*	T_*	ϕ_T	σ_1 (N/m^2)	σ_2 (N/m^2)	σ_3 (N/m^2)
0	-0.977	53.125	3.8E-3	7.23	6.097	-2.032E8	-1.83E8	-3.33E4
0.01	-1.0953	55.375	3.5E-3	7.51	6.813	-2.140E8	-1.873E8	-6.312E6
0.025	-1.129	70.931	1.9E-3	8.53	8.935	-3.297E8	-2.413E8	-9.613E6
0.03	-1.195	73.134	1.7E-3	8.91	9.487	-3.52E8	-2.63E8	-1.27E7

Helix Angle = 76.01°

ϵ	χ	G'_*	H_*	T_*	ϕ_T	σ_1 (N/m^2)	σ_2 (N/m^2)	σ_3 (N/m^2)
0	-0.989	55.111	3.6E-3	7.39	6.605	-2.073E8	-1.852E8	-5.531E5
0.01	-1.103	61.715	3.3E-3	7.76	7.404	-2.341E8	-2.013E8	-7.73E6
0.025	-1.207	73.986	1.65E-3	8.97	9.523	-3.62E8	-2.81E8	-2.34E7
0.03	-1.241	75.012	1.42E-3	9.19	10.09	-3.84E8	-2.97E8	-2.741E7

Helix Angle = 77.8°

ϵ	χ	G'_*	H_*	T_*	ϕ_T	σ_1 (N/m^2)	σ_2 (N/m^2)	σ_3 (N/m^2)
0	-1.115	62.312	2.81E-3	7.87	7.55	-2.51E8	-2.143E8	-9.36E6
0.01	-1.127	66.93	2.39E-3	8.241	8.13	-2.86E8	-2.23E8	-1.23E7
0.025	-1.243	75.311	1.41E-3	9.21	10.16	-3.87E8	-3.01E8	-3.87E7
0.03	-1.26	77.125	1.19E-3	9.49	10.77	-4.01E8	-3.27E8	-5.53E7

Helix Angle = 78.9°

ϵ	χ	G'_*	H_*	T_*	ϕ_T	σ_1 (N/m^2)	σ_2 (N/m^2)	σ_3 (N/m^2)
0	-1.117	63.122	2.55E-3	7.93	7.839	-2.55E8	-2.22E8	-9.761E6
0.01	-1.134	68.517	2.17E-3	8.43	8.71	-3.061E8	-2.31E8	-8.55E6
0.025	-1.253	73.011	1.23E-3	9.41	10.69	-3.98E8	-3.11E8	-8.16E7
0.03	-1.29	79.012	1.01E-3	9.77	11.25	-4.55E8	-3.65E8	-1.27E8

Helix Angle = 80.9°

ϵ	χ	G'_*	H_*	T_*	ϕ_T	σ_1 (N/m^2)	σ_2 (N/m^2)	σ_3 (N/m^2)
0	-1.131	68.555	2.16E-3	8.41	8.637	-2.97E8	-2.24E8	-7.66E6
0.01	-1.187	71.911	1.71E-3	8.82	9.29	-3.34E8	-2.44E8	-1.01E7
0.025	-1.292	79.012	1.01E-3	9.77	11.26	-4.57E8	-3.72E8	-1.29E8
0.03	-1.302	80.713	0.98E-3	9.84	11.83	-4.82E8	-3.96E8	-2.24E8

APPENDIX 9

Results associated with the theoretical collapse load predictions in Table 8.4 for 1X6X12 wire ropes

$\alpha = 75°$; $\bar{\alpha} = 75°$

ε	χ	$\bar{\chi}$	G'_*	H_*	T_*	$\bar{G}'_*$	$\bar{H}_*$	$\bar{T}_*$	ϕ_T
0	-0.016	--0.043	3.731	0.147	1.503	1.743	0.287	0.831	2.201
0.01	-0.0173	-0.047	3.846	0.168	1.731	1.821	0.310	0.946	2.629
0.02	-0.0177	-0.057	3.878	0.181	2.037	1.855	0.355	1.112	2.956
0.03	-0.0181	-0.062	3.914	0.210	2.291	1.877	0.398	1.213	3.123
0.05	-0.0185	-0.069	4.021	0.281	2.544	1.902	0.432	1.330	3.436
0.10	-0.0192	-0.077	4.541	0.312	3.12	1.977	0.487	1.52	3.937

$\alpha = 75^\circ$; $\bar{\alpha} = 80^\circ$

ϵ	χ	$\bar{\chi}$	G'_*	H_*	T_*	$\bar{G}'_*$	$\bar{H}_*$	$\bar{T}_*$	ϕ_T
0	-0.0147	-0.038	3.641	0.127	1.433	1.692	0.261	0.811	2.106
0.01	-0.0165	-0.045	3.753	0.152	1.654	1.812	0.293	0.897	2.593
0.02	-0.049	-0.049	3.852	0.173	1.856	1.837	0.322	0.989	2.76
0.03	-0.0179	-0.059	3.905	0.187	2.145	1.860	0.365	1.154	3.08
0.05	-0.0182	-0.065	3.989	0.273	2.441	1.882	0.411	1.231	3.334
0.10	-0.0188	-0.072	4.121	0.289	2.846	1.952	0.444	1.473	3.639

$\alpha = 75°$; $\bar{\alpha} = 105°$

ϵ	χ	$\bar{\chi}$	G'_*	H_*	T_*	$\bar{G}'_*$	$\bar{H}_*$	$\bar{T}_*$	ϕ_T
0	-0.0144	-0.032	3.522	0.113	1.343	1.586	0.247	0.765	1.975
0.01	-0.0161	-0.044	3.742	0.151	1.621	1.767	0.292	0.867	2.353
0.02	-0.0163	-0.045	3.749	0.157	1.689	1.789	0.301	0.874	2.564
0.03	-0.0176	-0.052	3.867	0.177	1.973	1.810	0.347	1.080	2.912
0.05	-0.0177	-0.054	3.871	0.180	1.986	1.842	0.350	1.087	2.943
0.10	-0.0185	-0.069	4.016	0.274	2.592	1.898	0.421	1.361	3.414

FIGURES

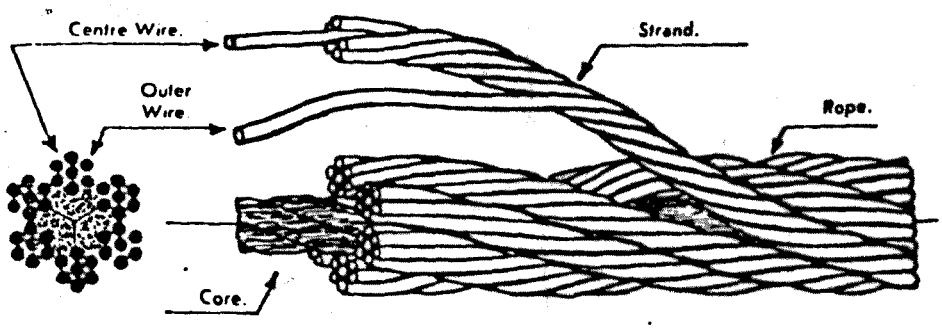

FIG 2.1 CHIEF COMPONENT PARTS OF A STRANDED WIRE ROPE.

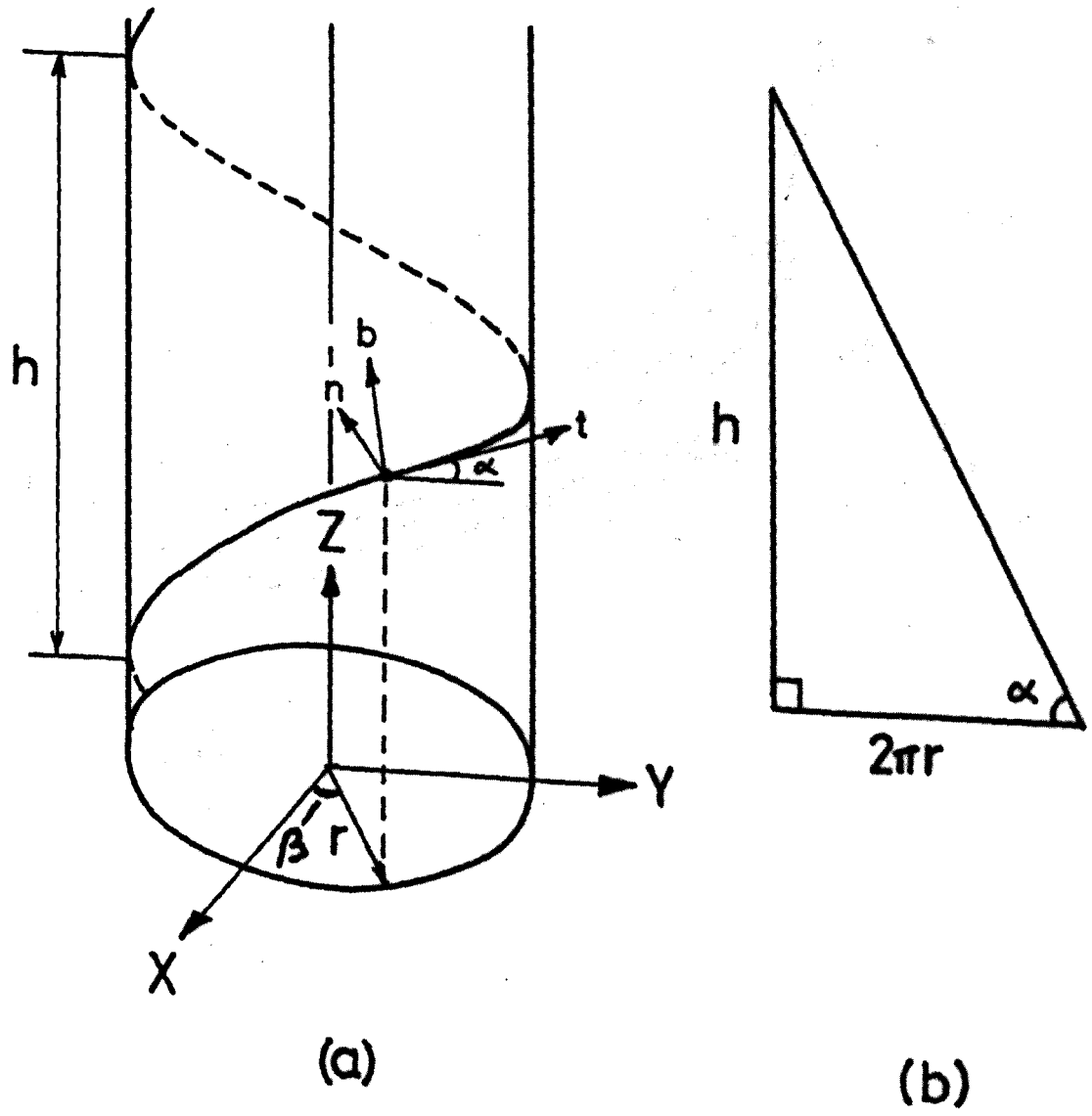

FIG 2.2 RIGHT CIRCULAR HELIX.

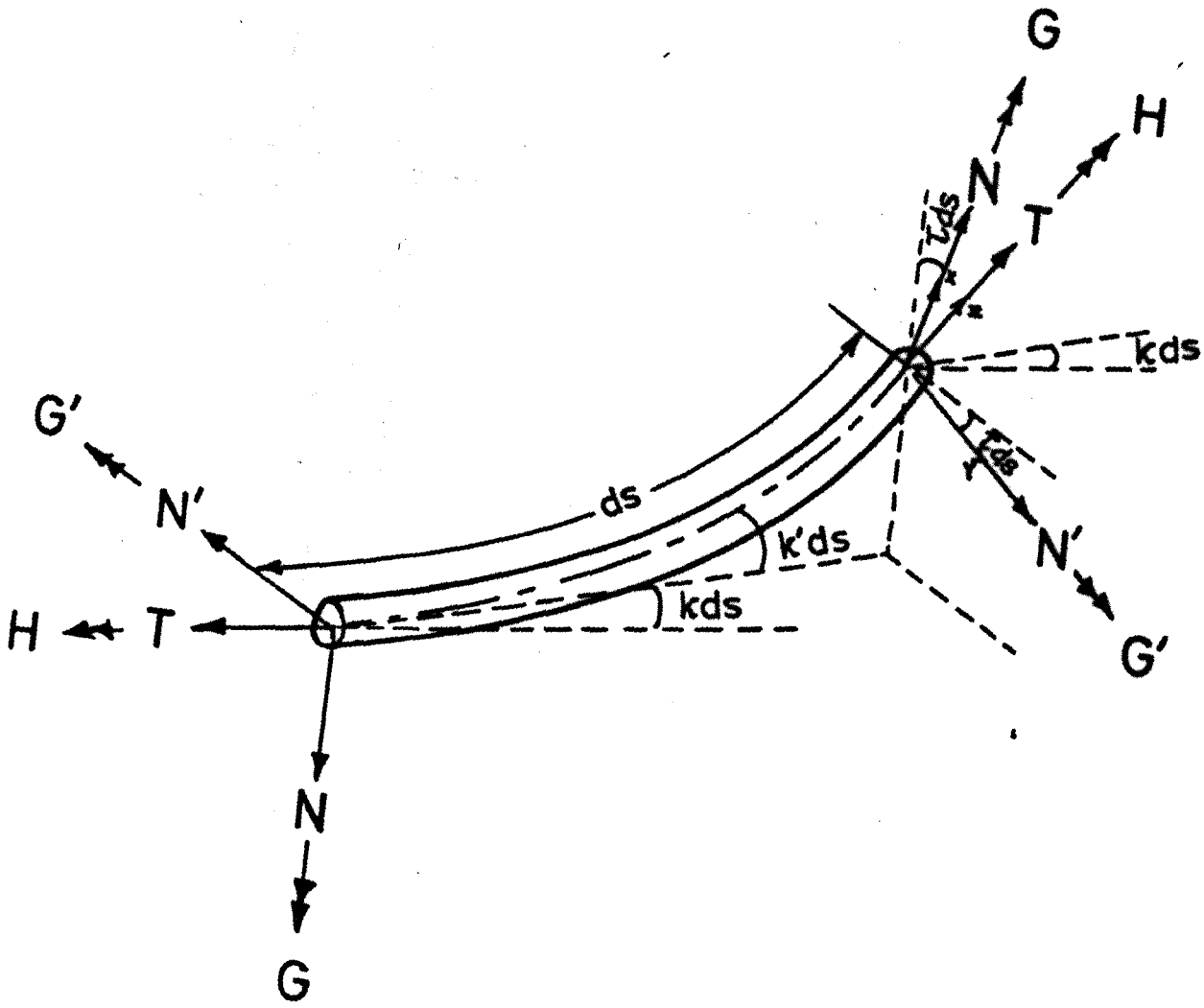

FIG 2.3 GENERALISED STRESS RESULTANTS IN A CURVED BAR.

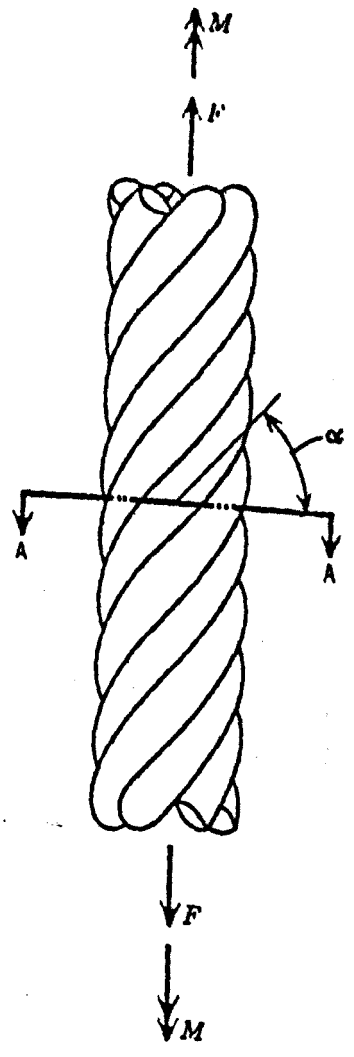

FIG 2.4a A STRAND.

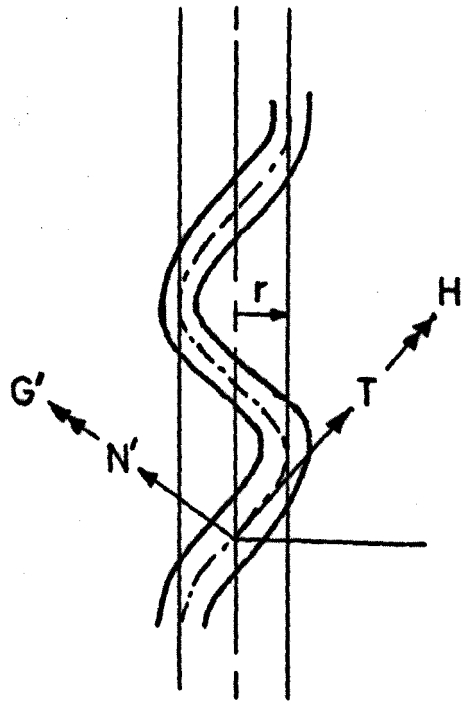

FIG 2.4b FORCES AND MOMENTS IN A HELICAL WIRE.

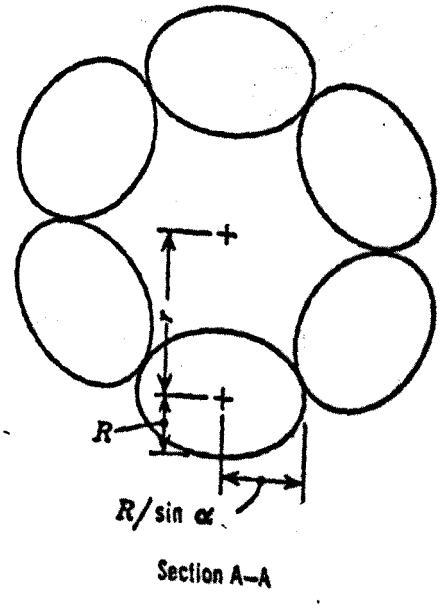

FIG 2.4c TRANSVERSE CROSS-SECTION OF A STRAND.

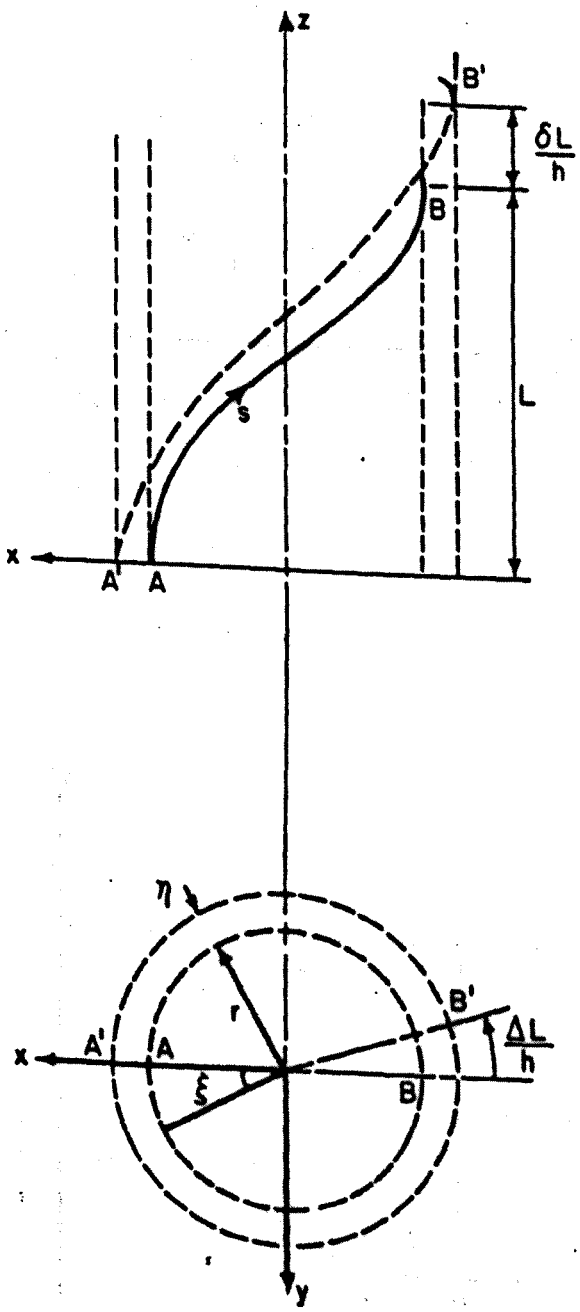

FIG 2.5 DEFORMATION OF AN INDIVIDUAL WIRE.

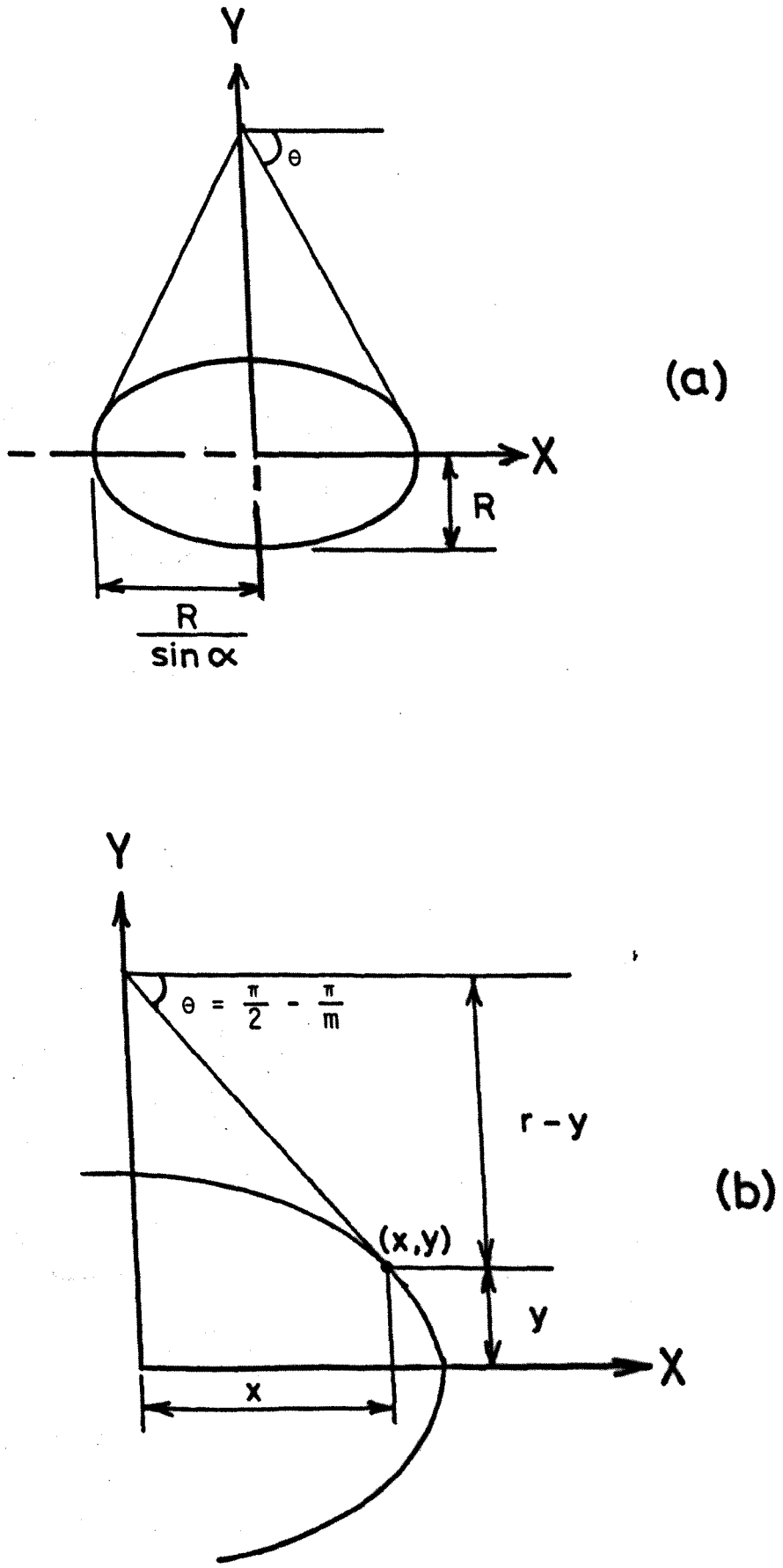

FIGURE 2.6 WIRE CROSS-SECTION FROM A TRANSVERSE CROSS-SECTION OF A STRAND.

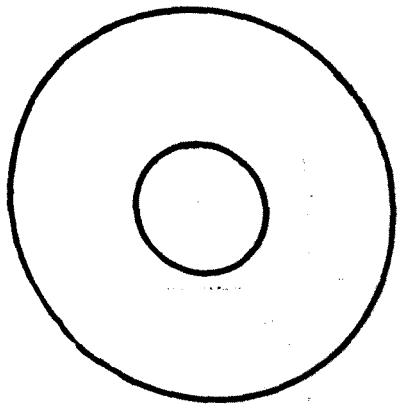

$\alpha = 0°$

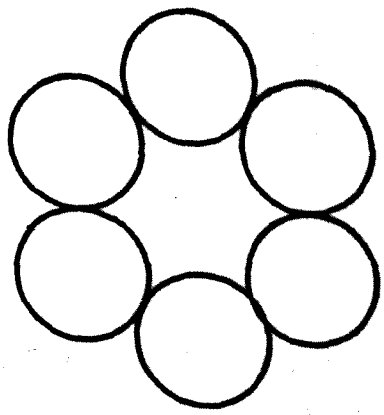

$\alpha = 90°$

Fig. 2.7 TRANSVERSE SECTION OF A STRAND WITH LIMITING VALUES OF α

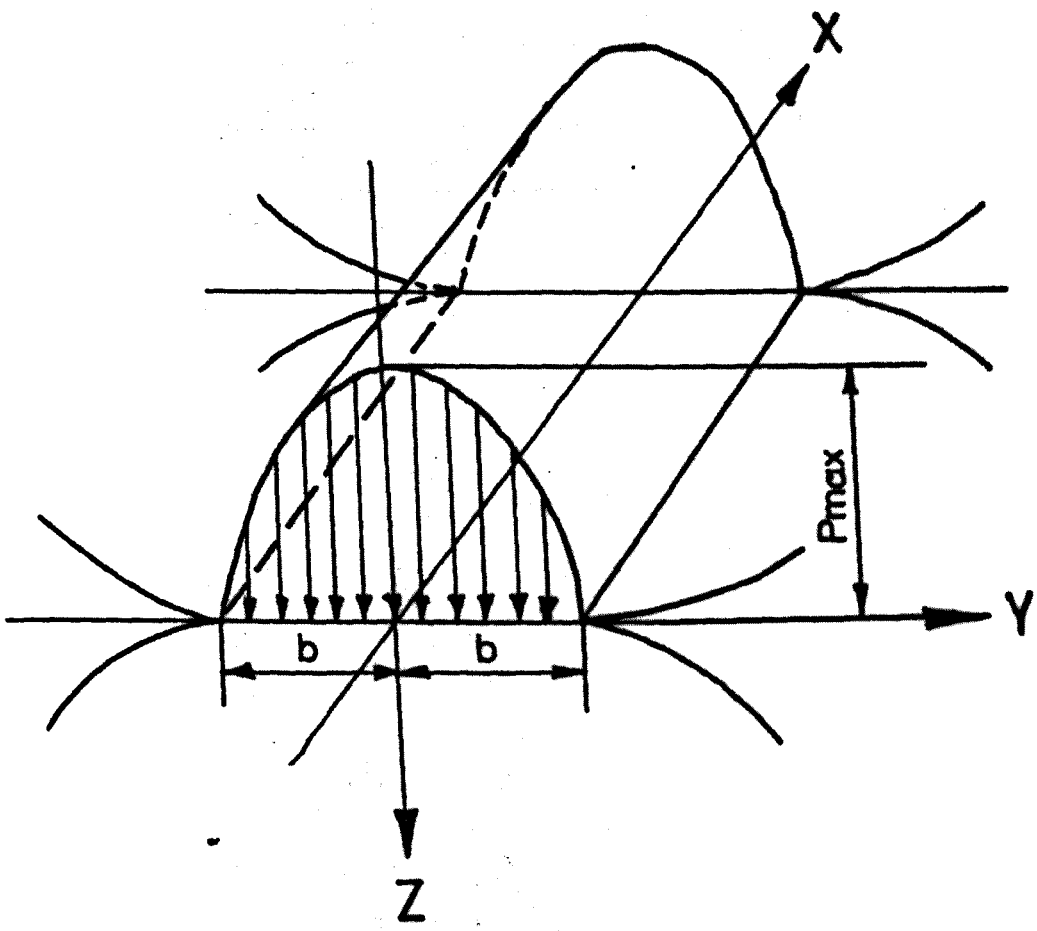

FIG 3.1 PRESSURE DISTRIBUTION ACROSS THE WIDTH OF THE CONTACT SURFACE.

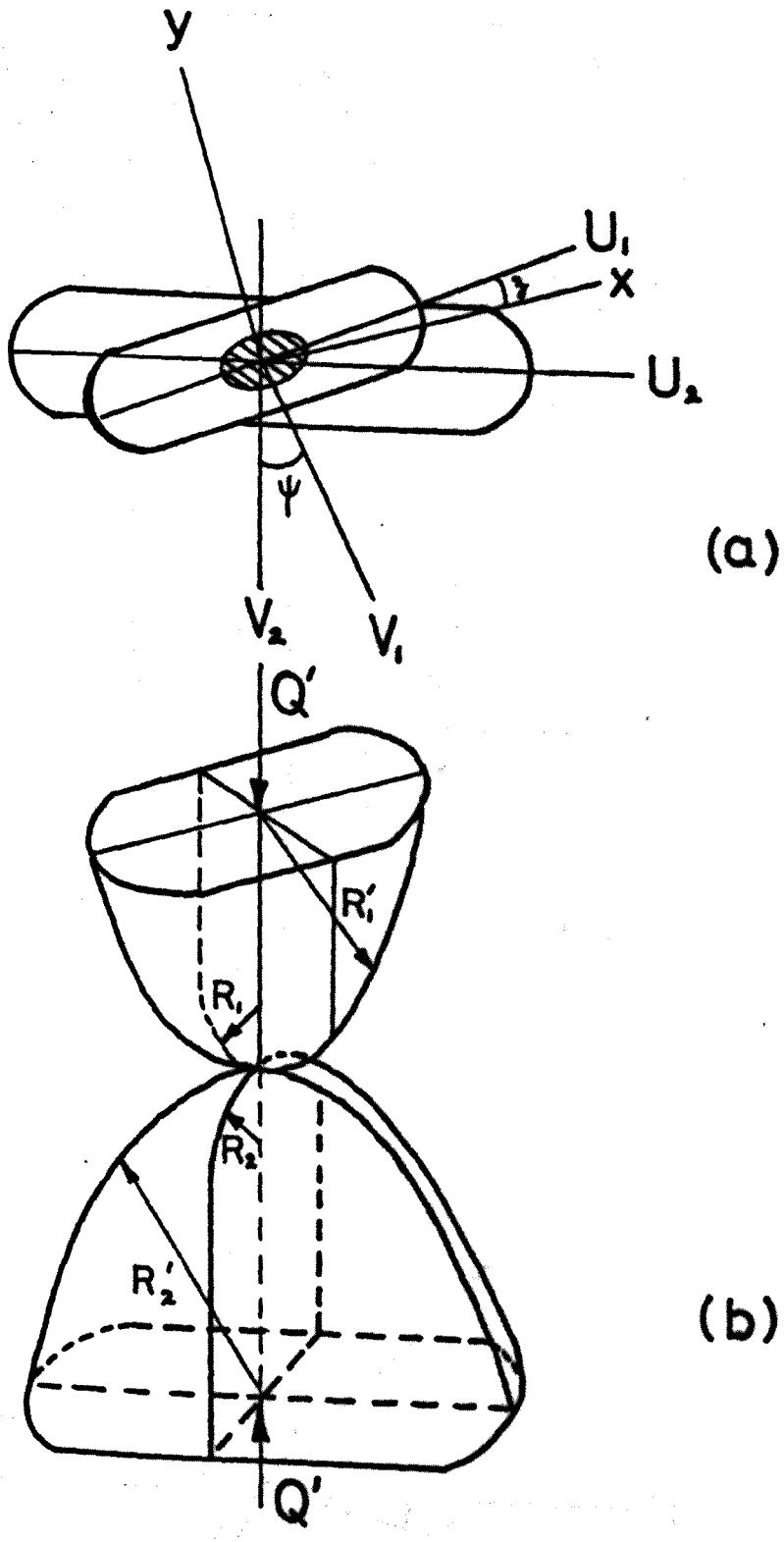

FIG 3.2 TWO BODIES IN CONTACT.

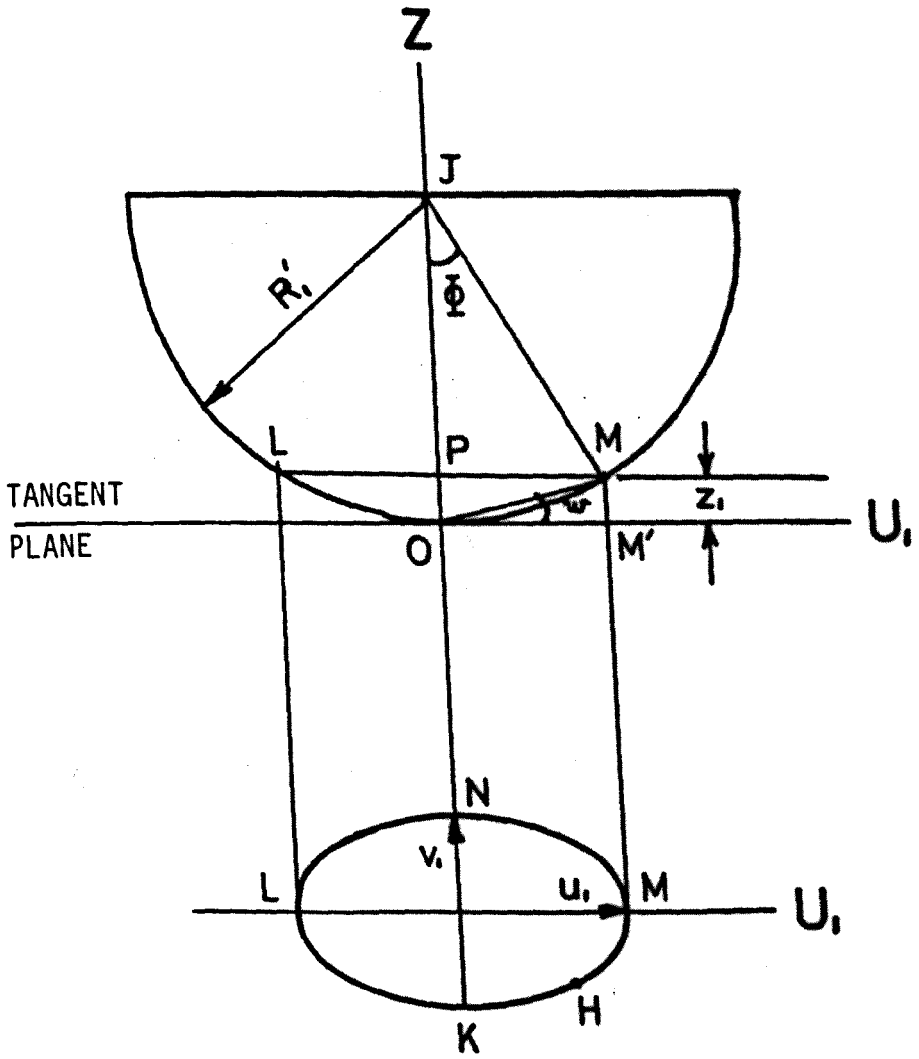

FIG 3.3 DISTANCE OF THE CONTACT SURFACE FROM THE TANGENT PLANE.

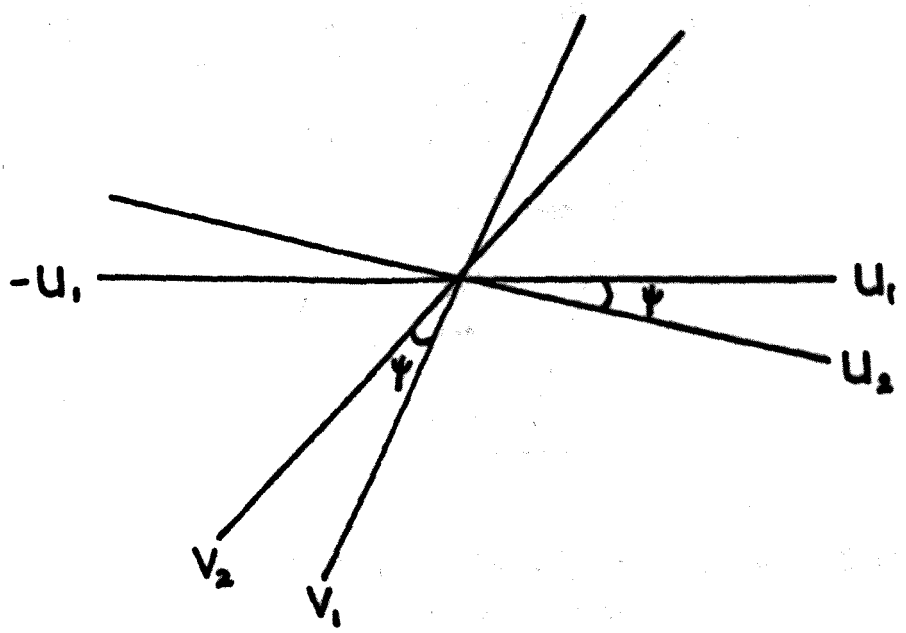

FIG 3.4 TRANSFORMATION OF COORDINATES.

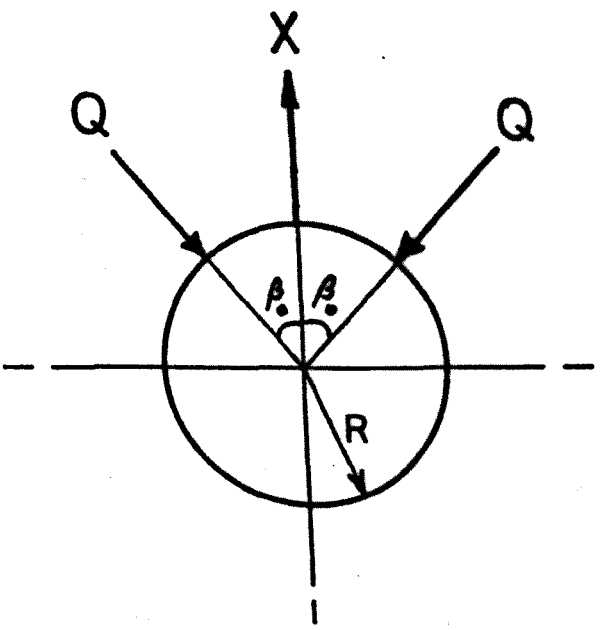

FIG 3.5 TRUE CROSS-SECTIONAL VIEW OF A WIRE SHOWING CONTACT ANGLE β_o

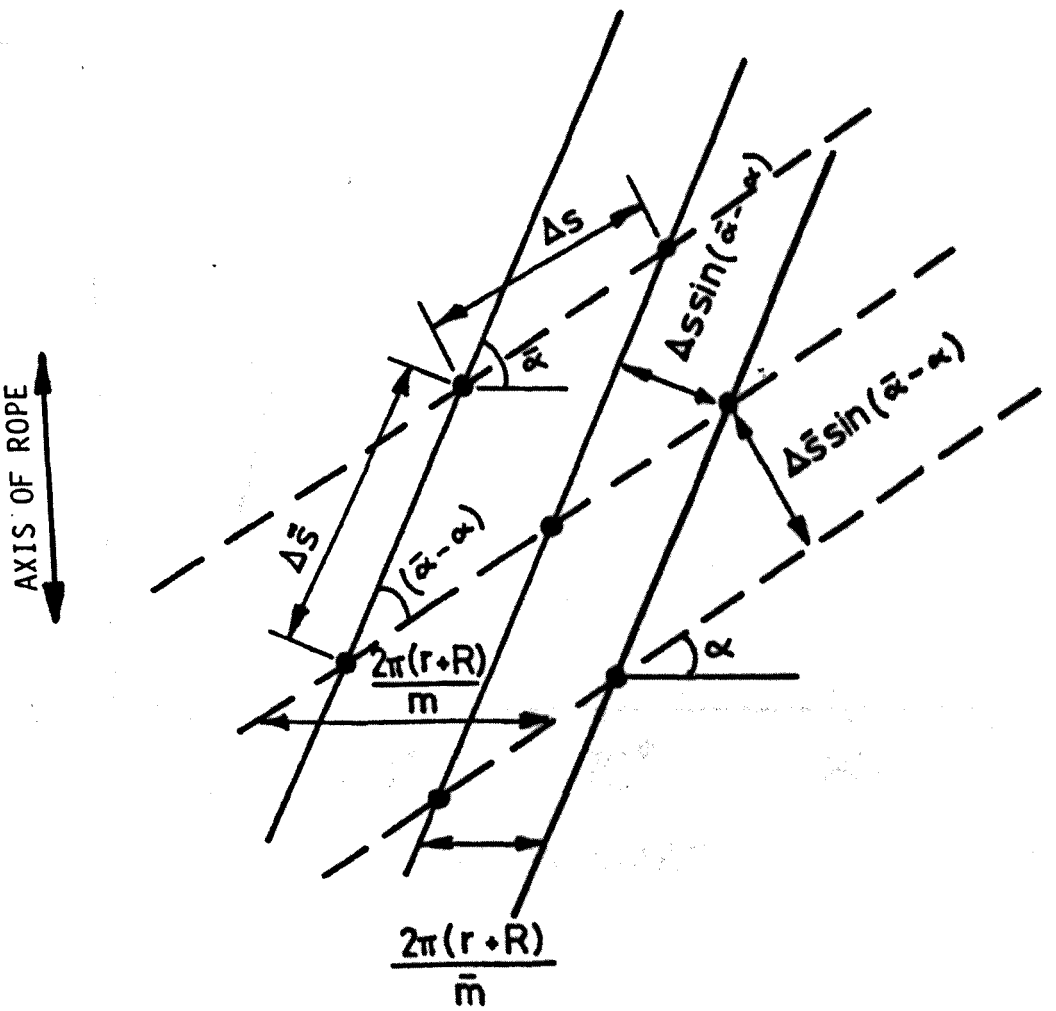

FIG 3.6 WIRES IN OUTER AND INNER STRAND DEVELOPED ON A FLAT PLANE.

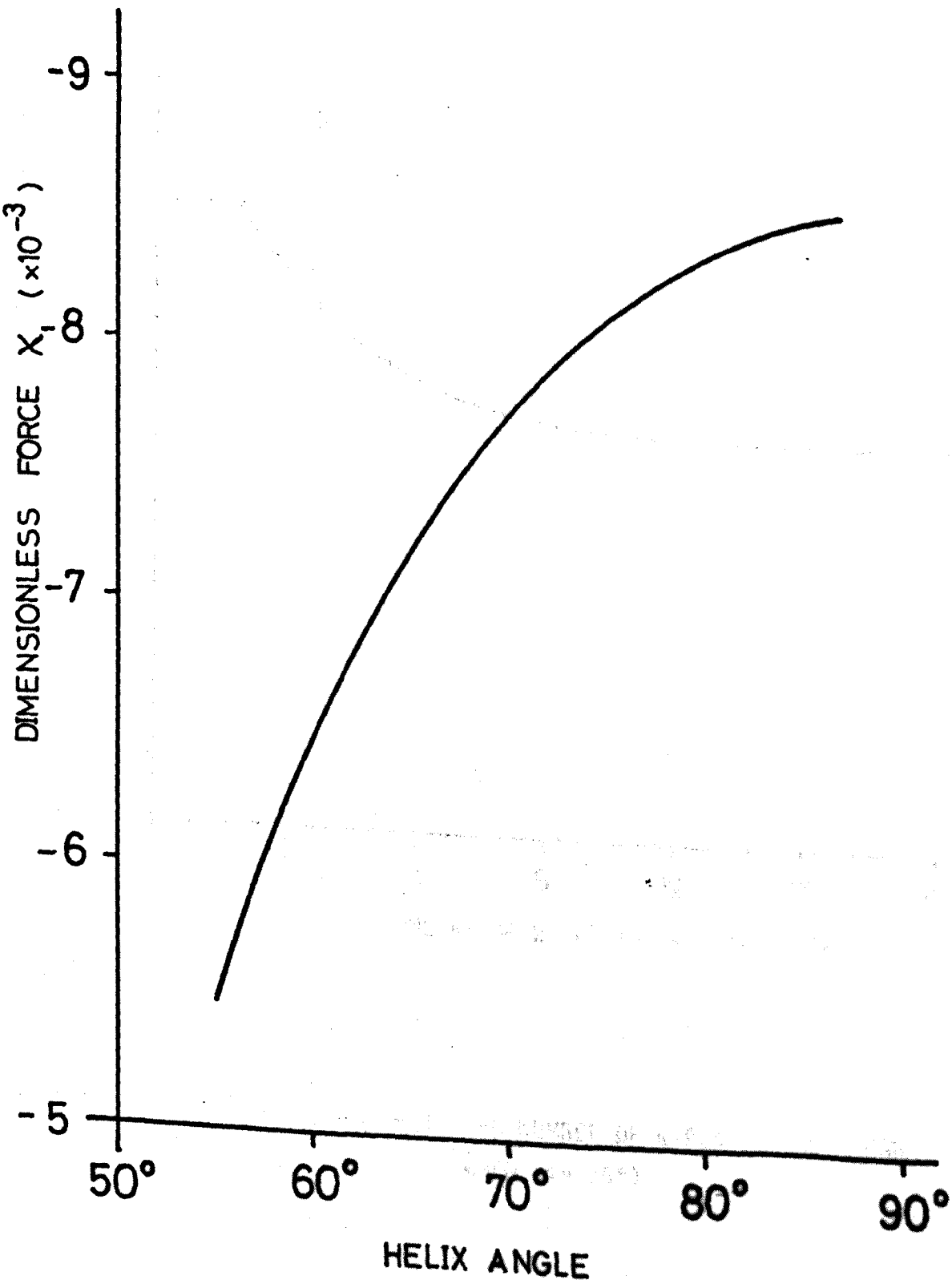

FIG 3.7 VARIATION OF χ WITH HELIX ANGLE. (m = 6)

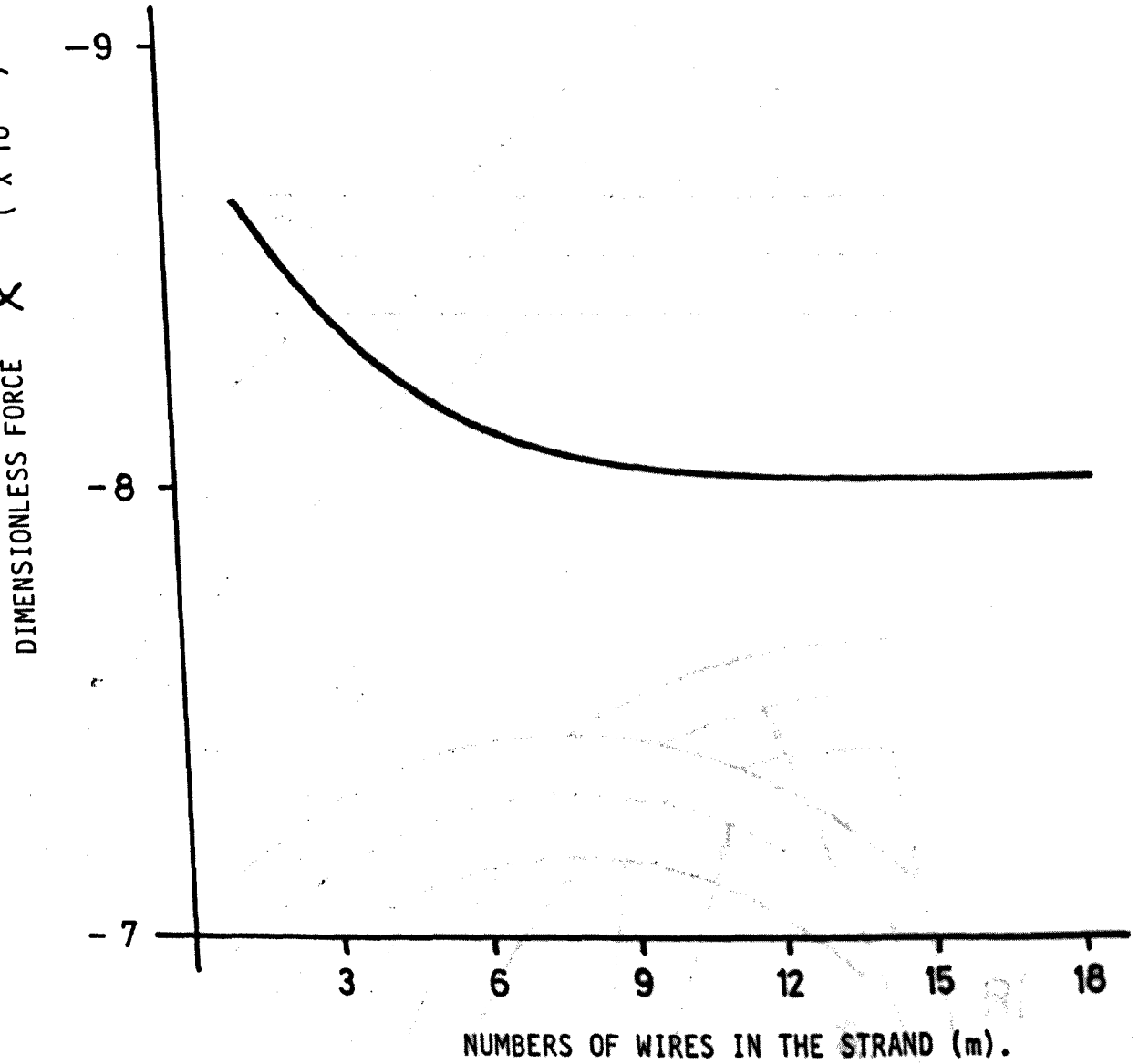

FIG 3.8 VARIATION OF χ WITH THE NUMBER OF WIRES IN THE STRAND. (WHEN $\alpha = 75°$)

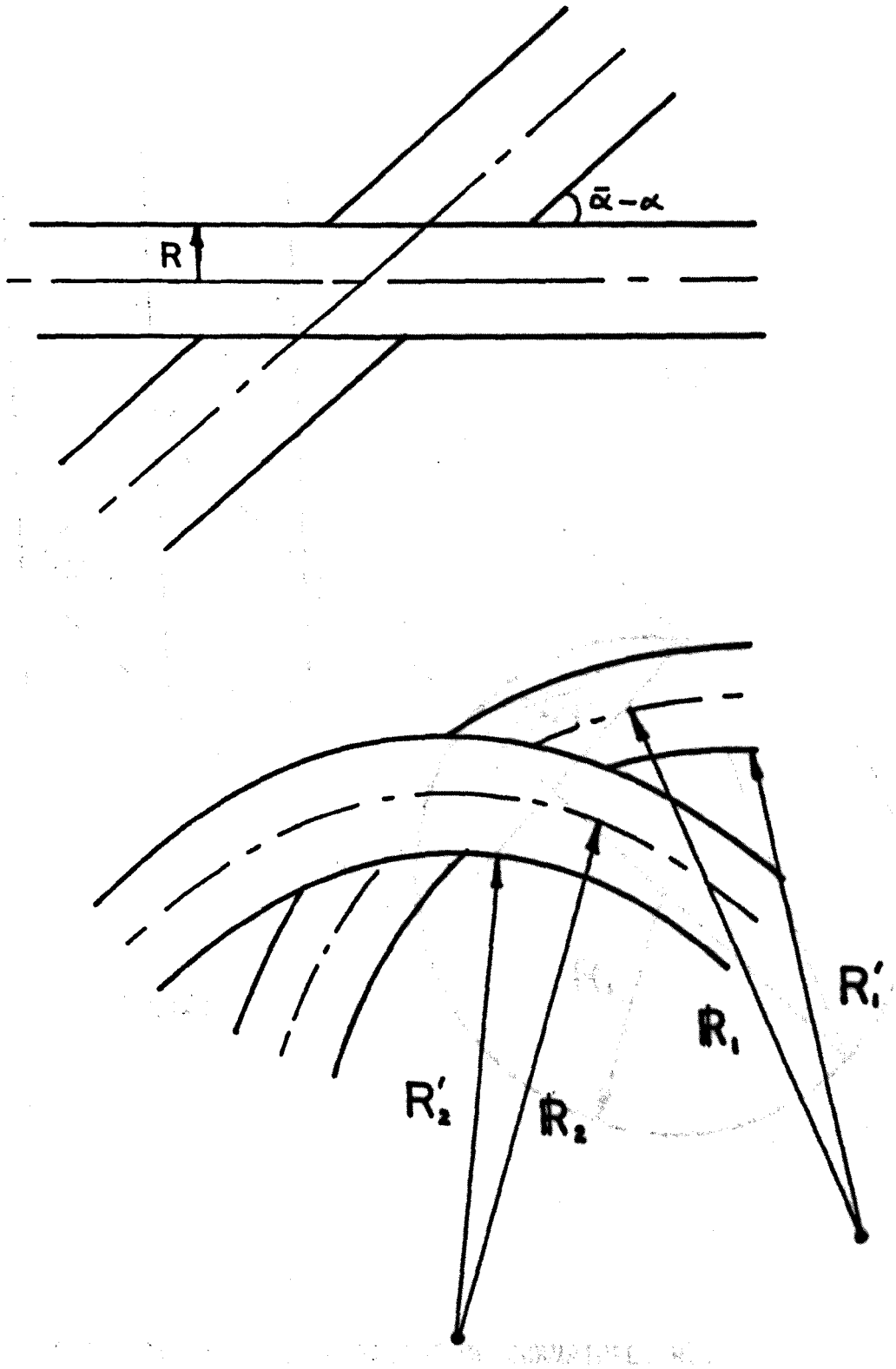

FIG 3.9 CONTACT BETWEEN WIRES IN NEIGHBOURING STRANDS.

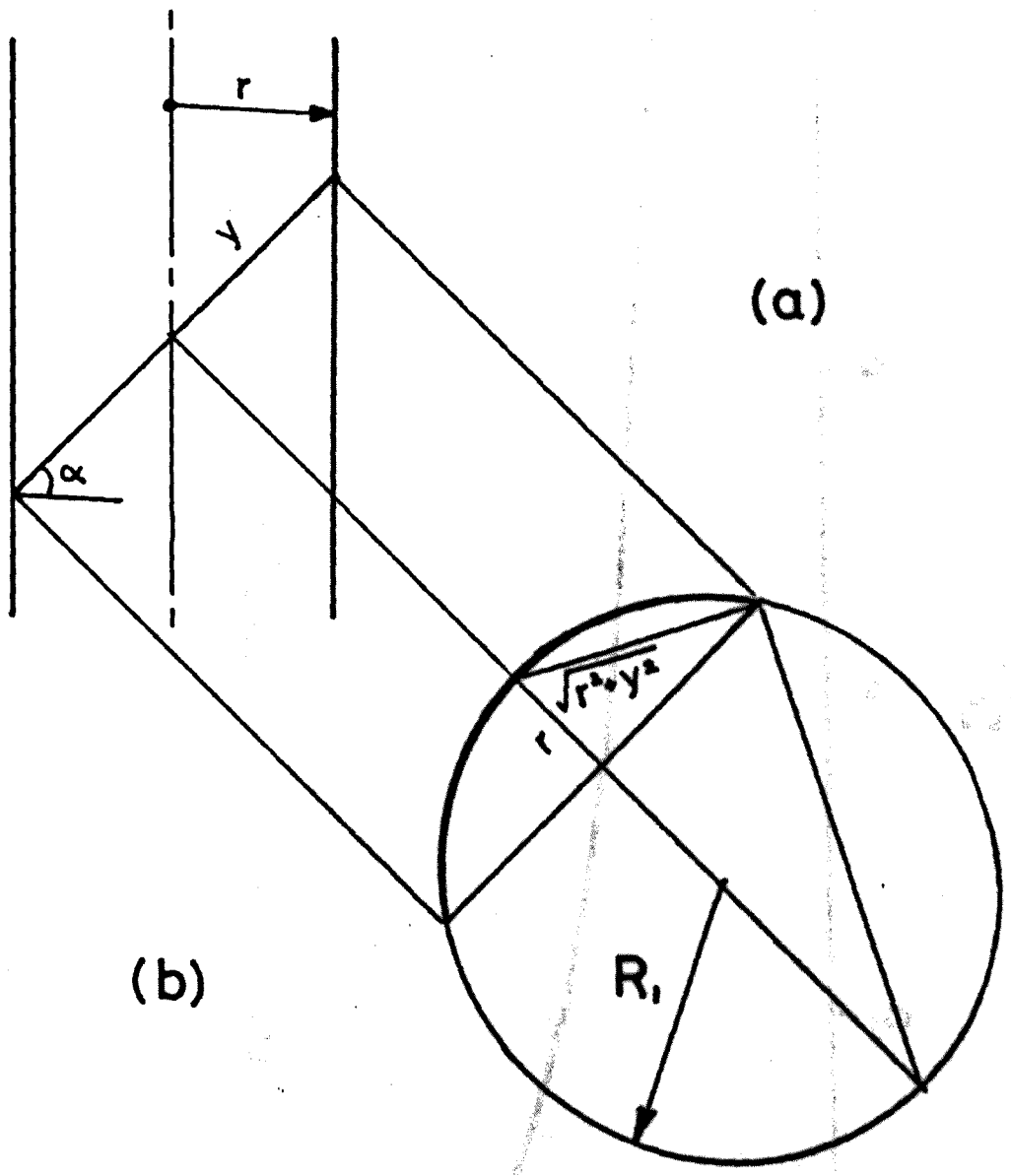

FIG 3.10 PRINCIPAL RADIUS OF CURVATURE, R_1.

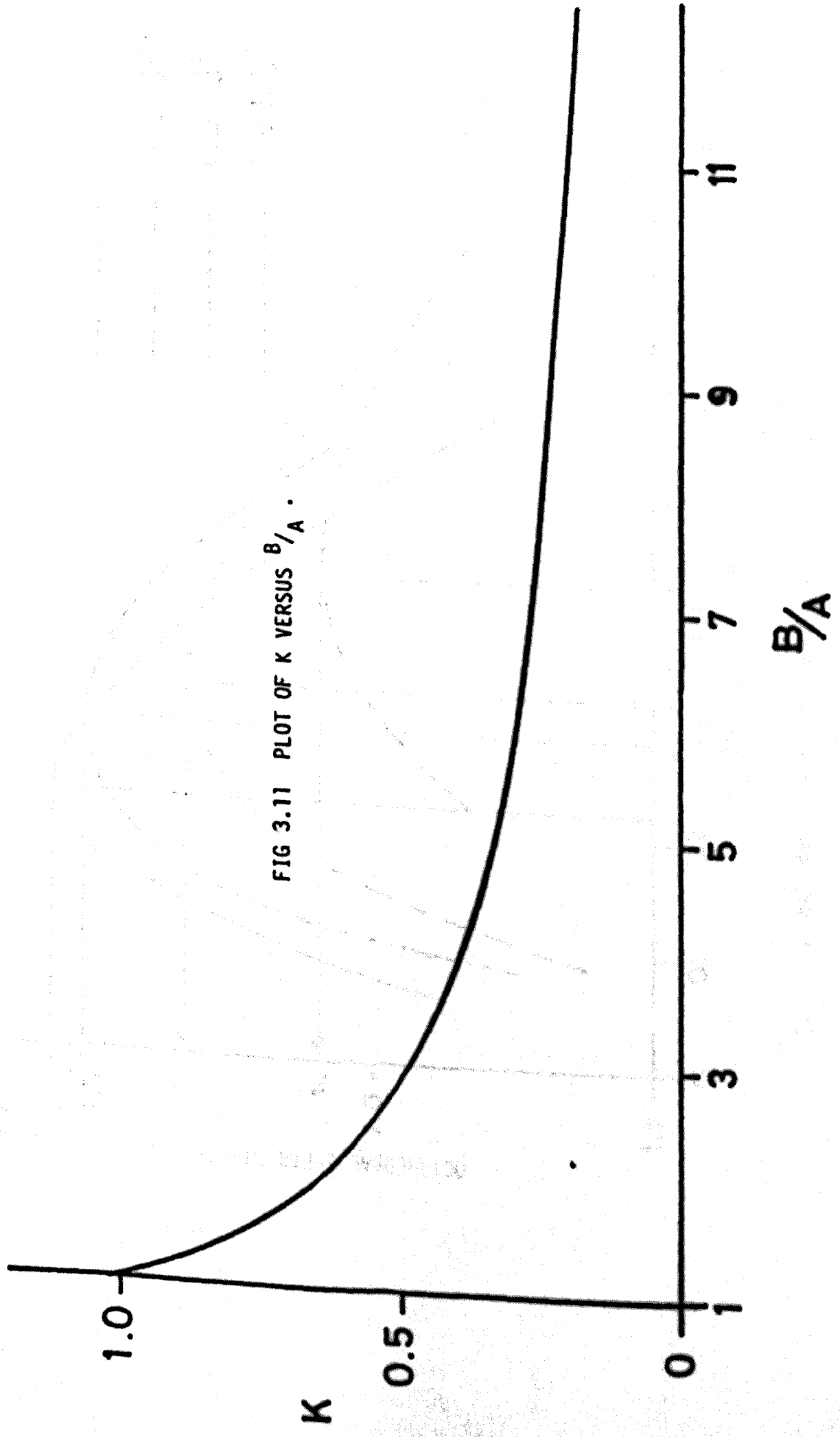

FIG 3.11 PLOT OF K VERSUS $^{B}/_{A}$.

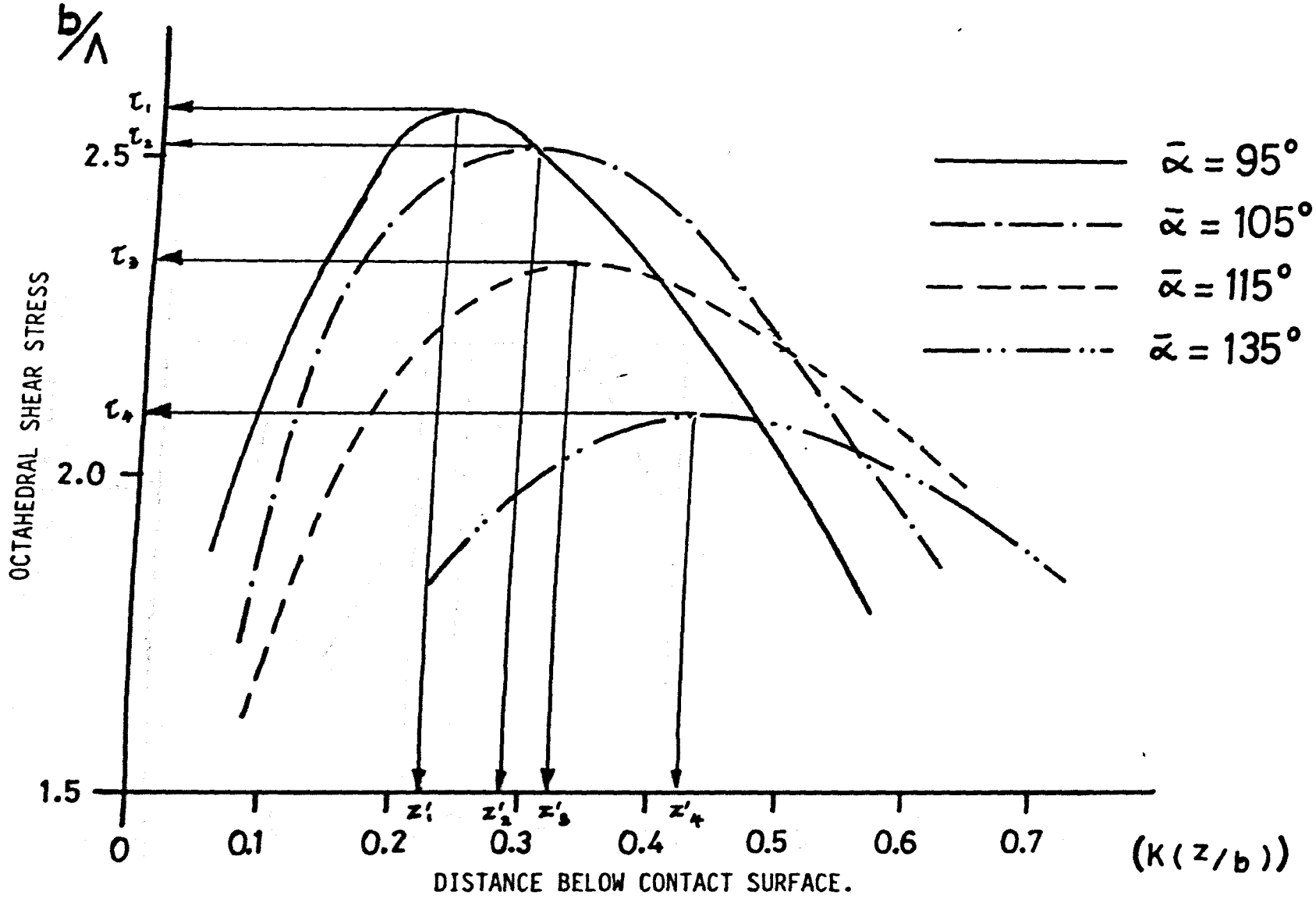

FIG 3.12a MAXIMUM OCTAHEDRAL SHEAR STRESS. (α = 60°)

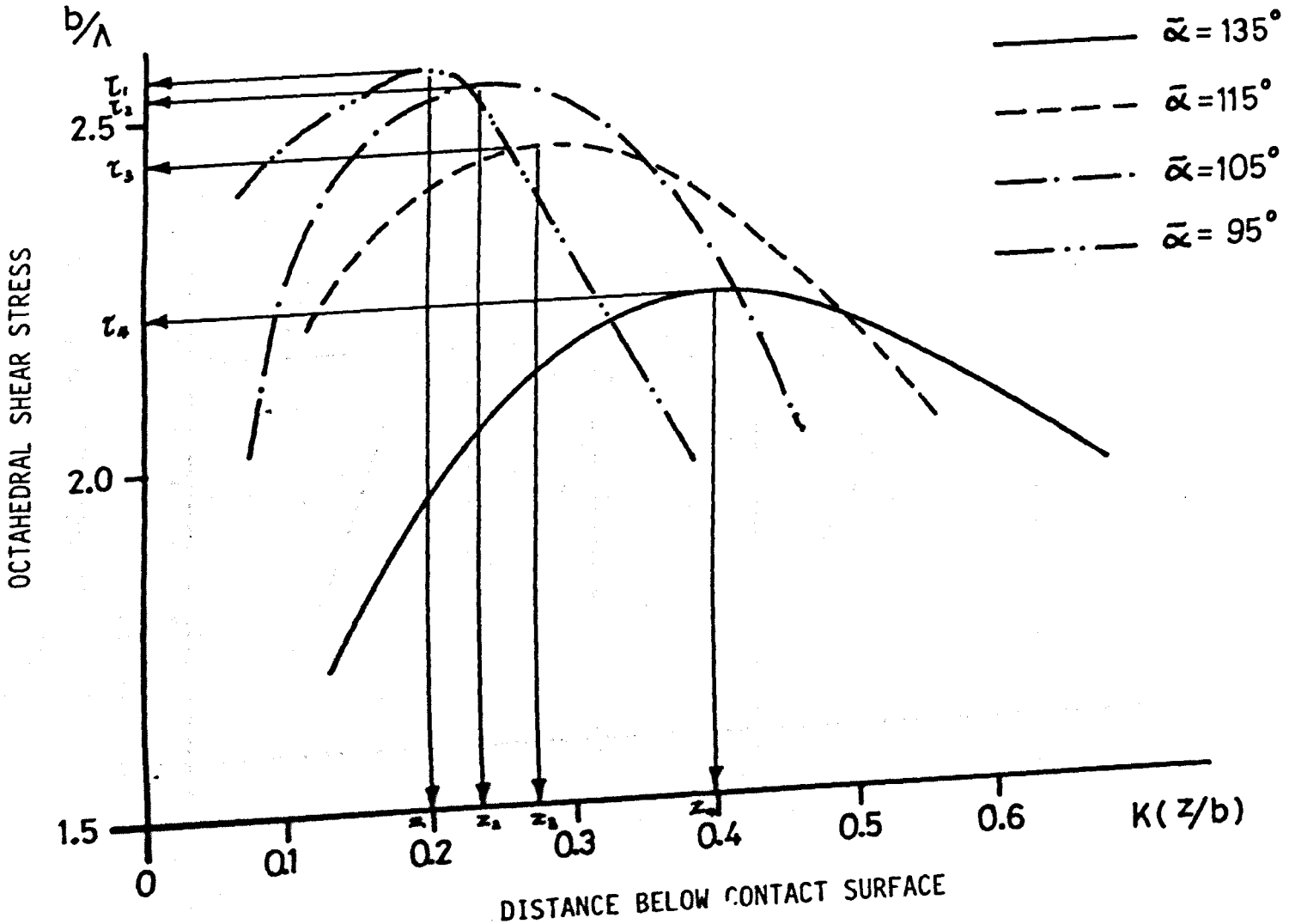

FIG 3.12b MAXIMUM OCTAHEDRAL SHEAR STRESS. (α = 70°)

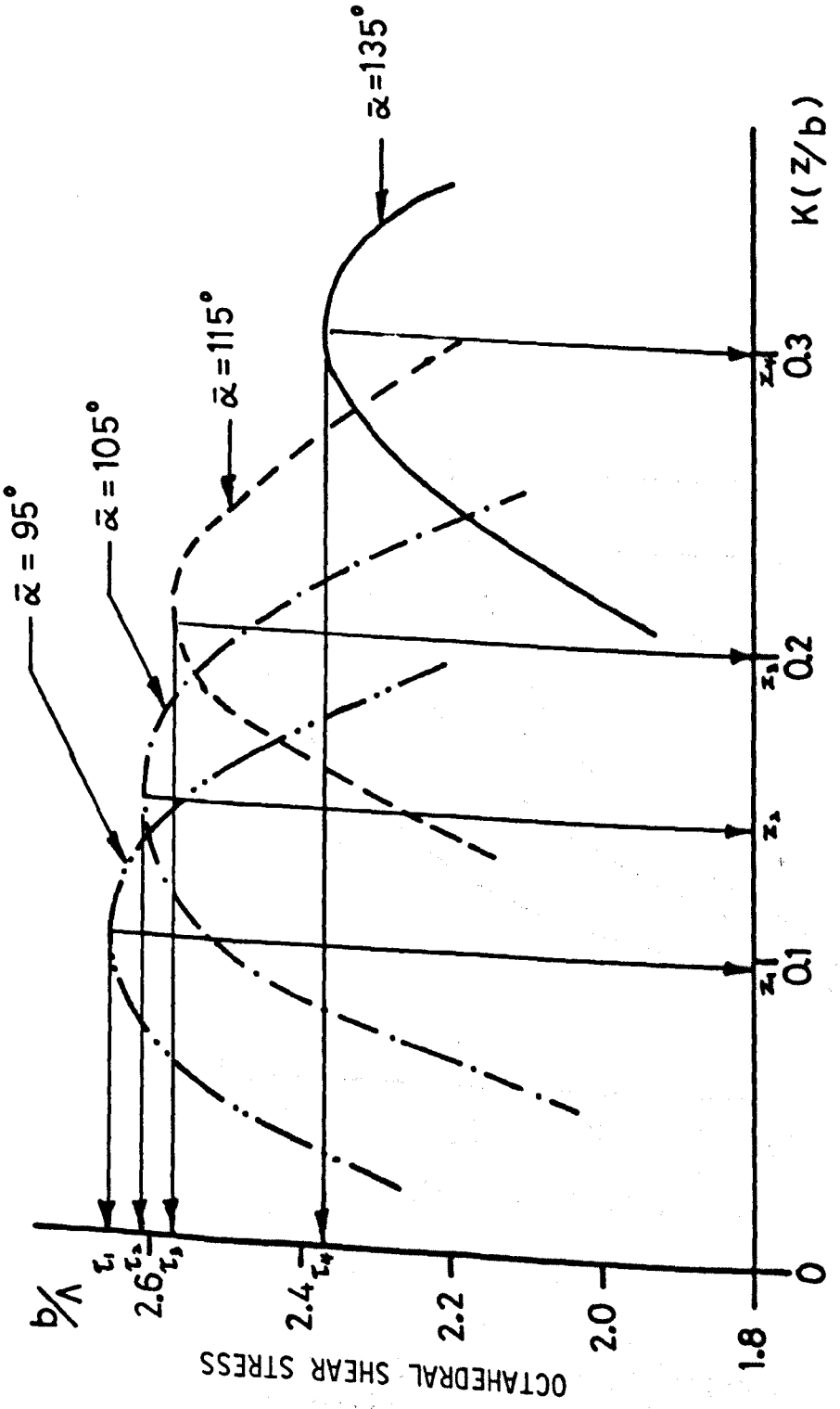

FIG 3.12c MAXIMUM OCTAHEDRAL SHEAR STRESS. ($\alpha = 80°$)

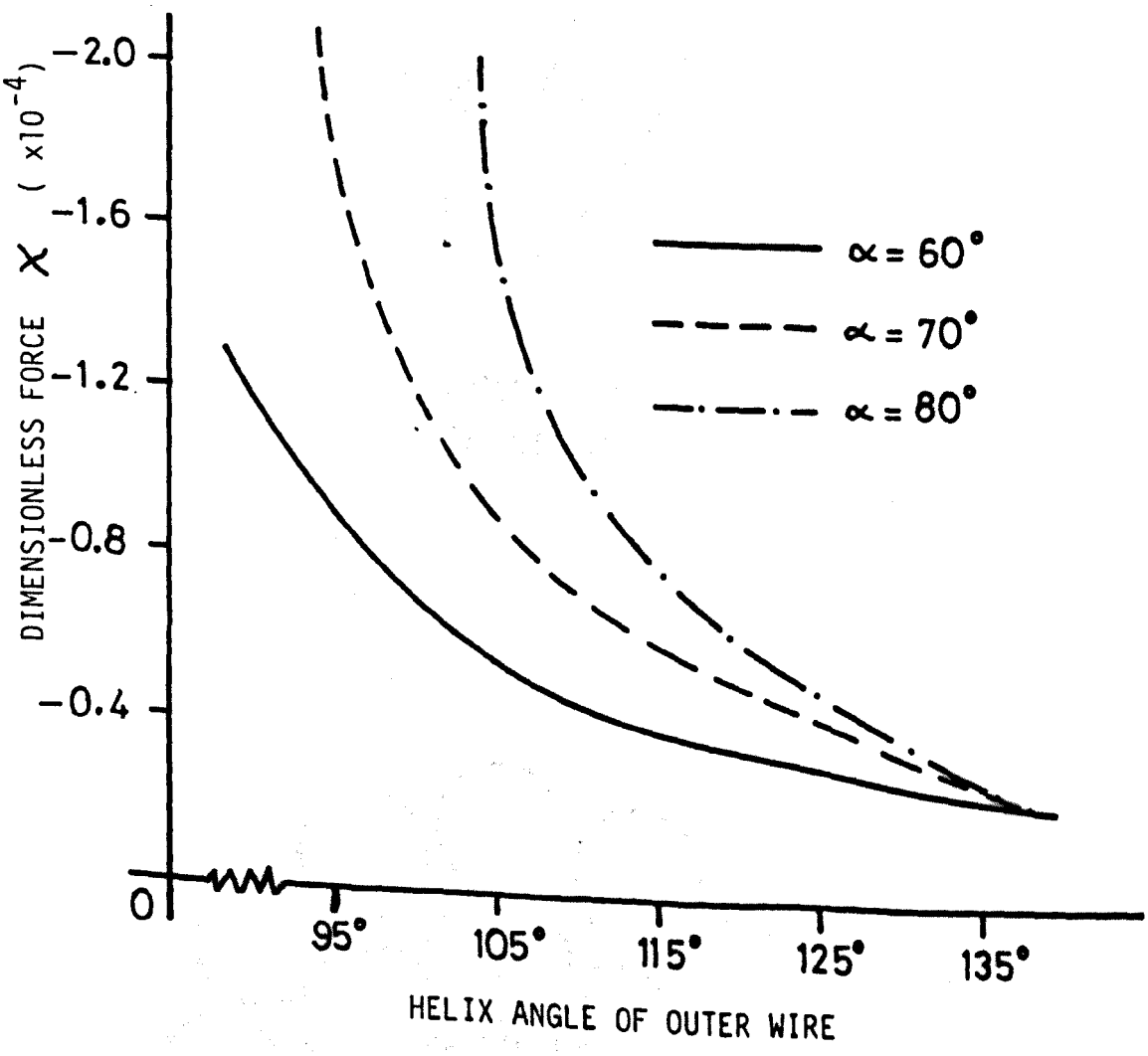

FIG 13.13 VALUES OF χ FOR DIFFERENT COMBINATION OF INNER AND OUTER HELIX ANGLE TO PRODUCE YIELD.

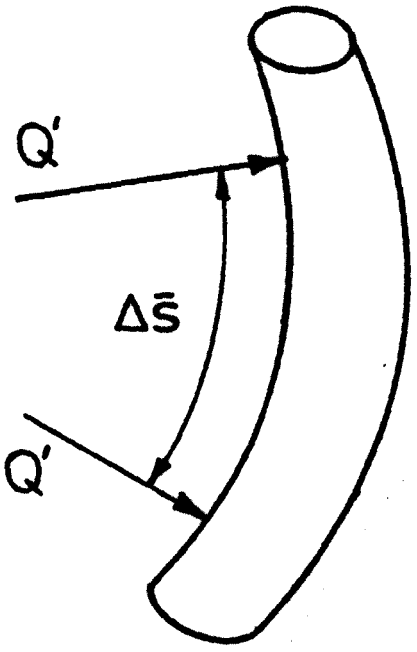

FIG 3.14 POINT CONTACT LOADS ON THE WIRE IN THE OUTER STRAND.

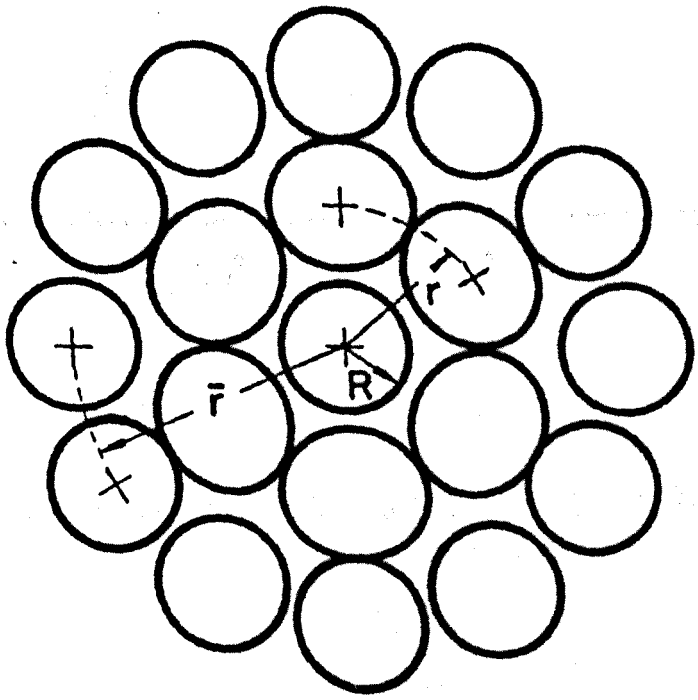

FIG 3.15 CROSS-SECTION OF A 1X19 ROPE SHOWING SOME OF THE WIRES.

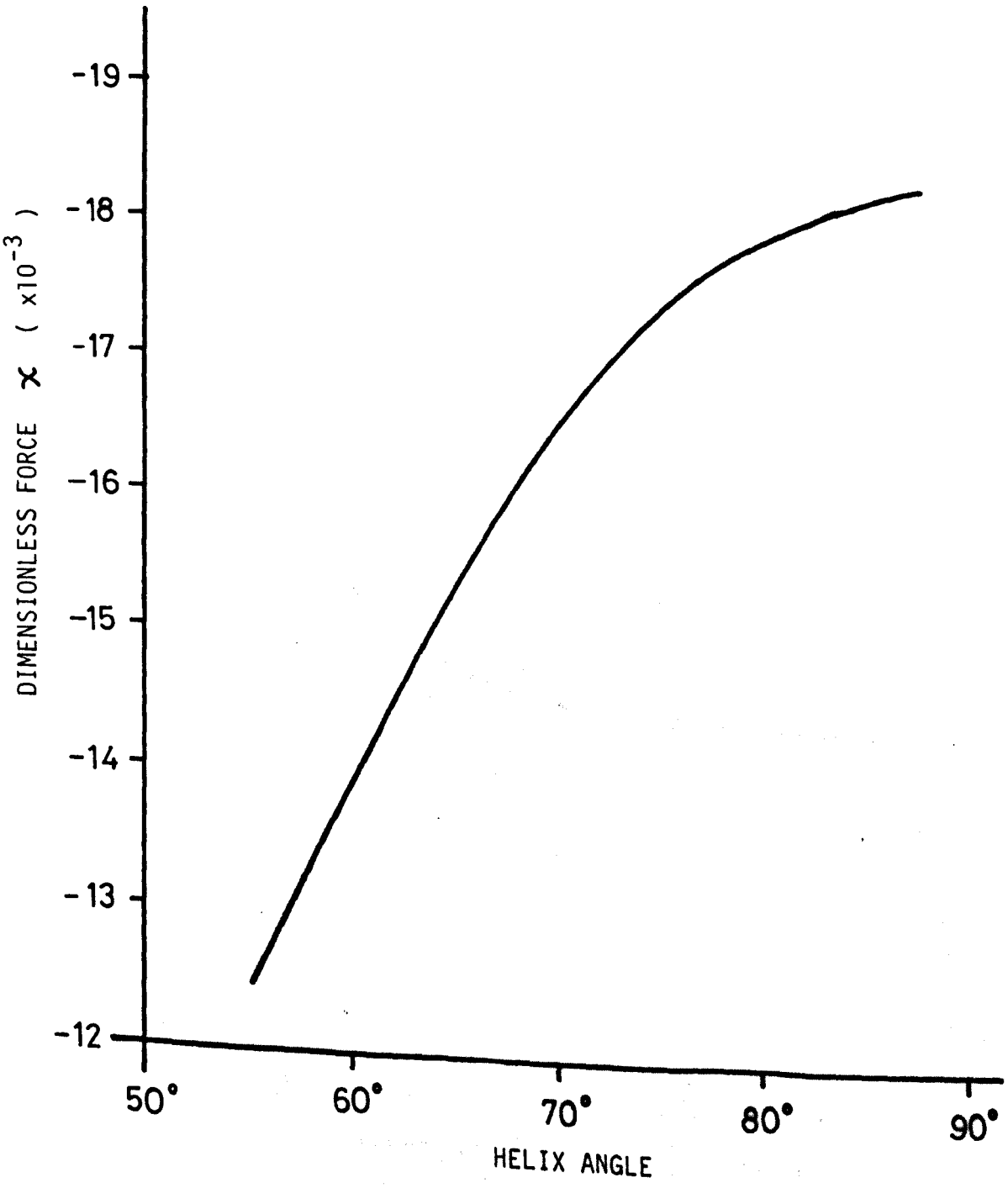

FIG 4.1 VARIATION OF COLLAPSE VALUE OF χ WITH HELIX ANGLE WHEN m=6.

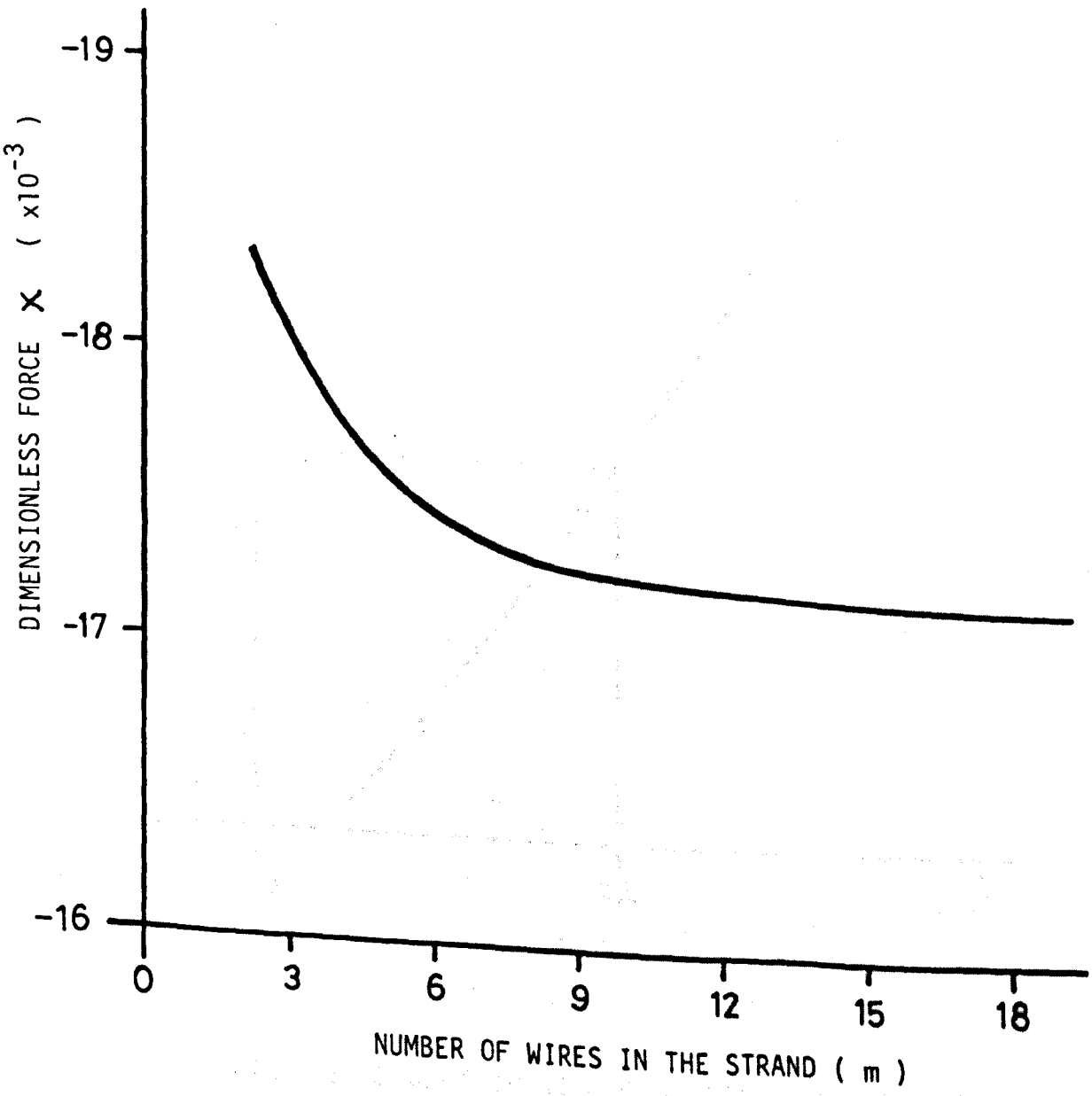

FIG 4.2 VARIATION OF COLLAPSE VALUE OF X WITH m WHEN HELIX ANGLE IS 75°.

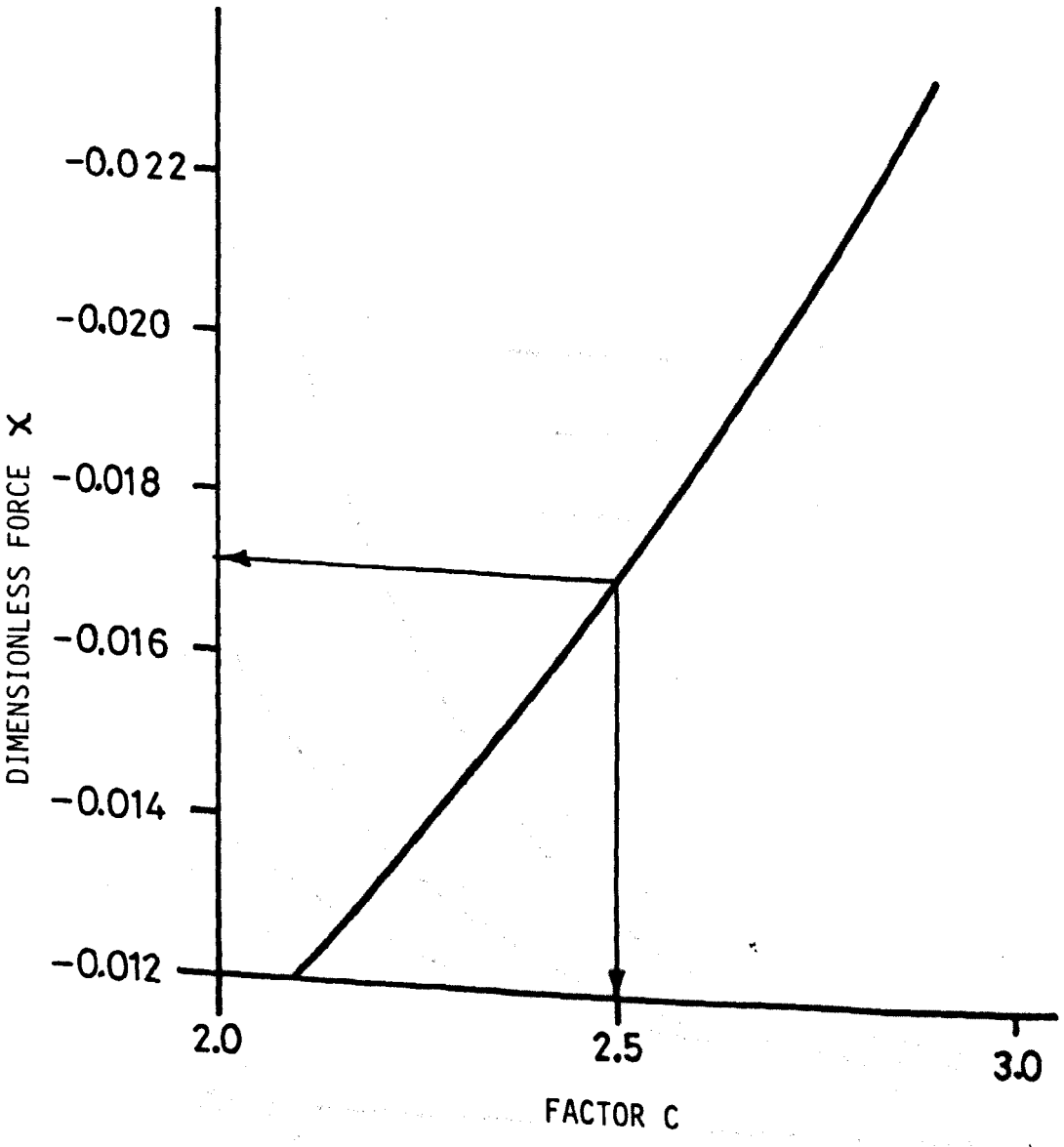

FIG 4.3 CHANGES IN X WITH A CHANGE IN FACTOR C.
(α = 75° , m = 6)

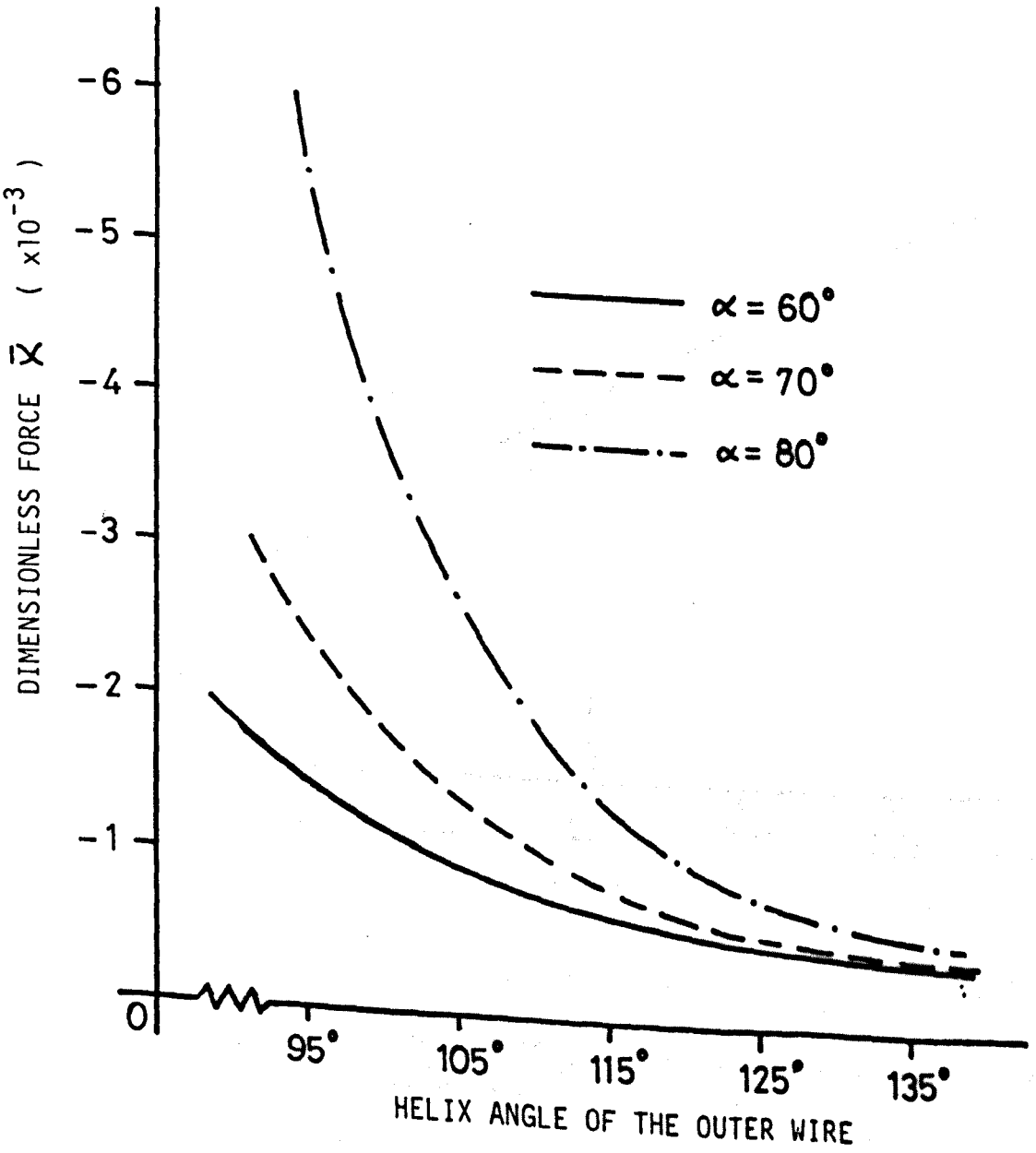

FIG 4.4 VALUES OF $\bar{\chi}$ DUE TO CONTACT BETWEEN WIRES IN NEIGHBOURING STRANDS.

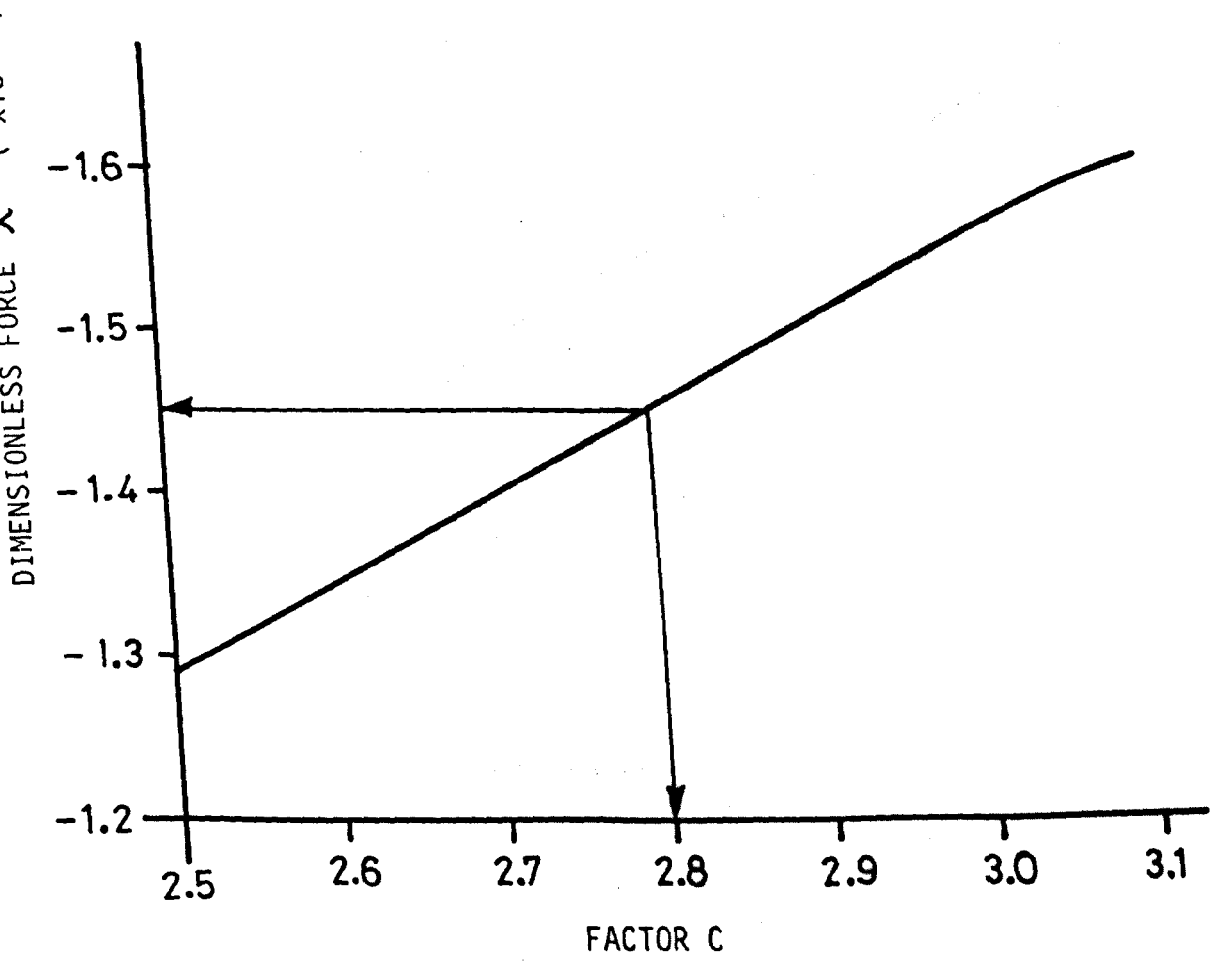

FIG 4.5 CHANGES IN $\bar{\chi}$ DUE TO CHANGES IN FACTOR C WHEN HELIX ANGLES ARE $\alpha = 60°$ AND $\bar{\alpha} = 95°$.

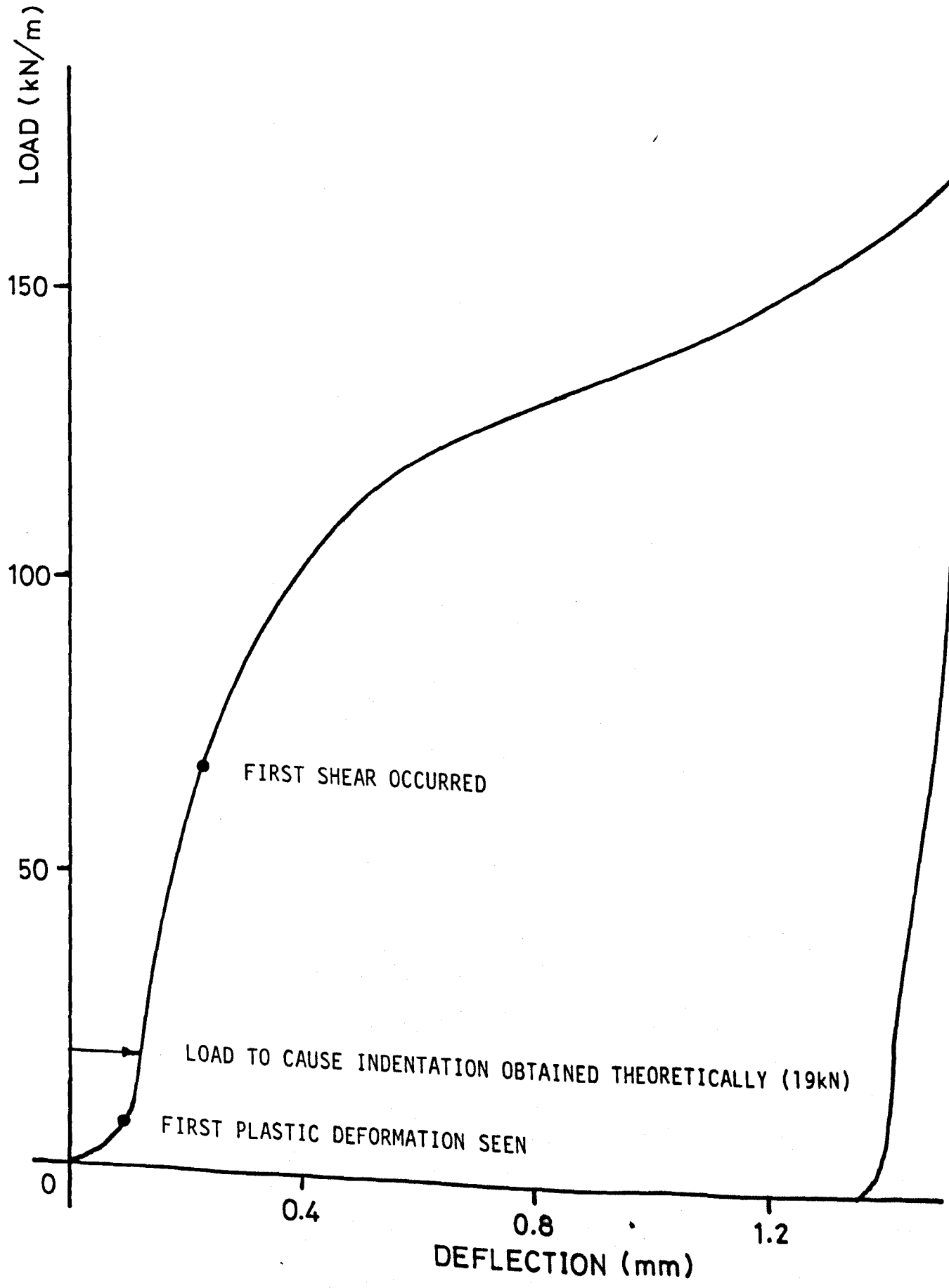

FIG 4.6 COMPARISON OF THEORETICAL INDENTATION LOAD WITH EXPERIMENTAL RESULTS OBTAINED BY HAMLET(90) FOR TWO STRAIGHT RODS IN LINE CONTACT.

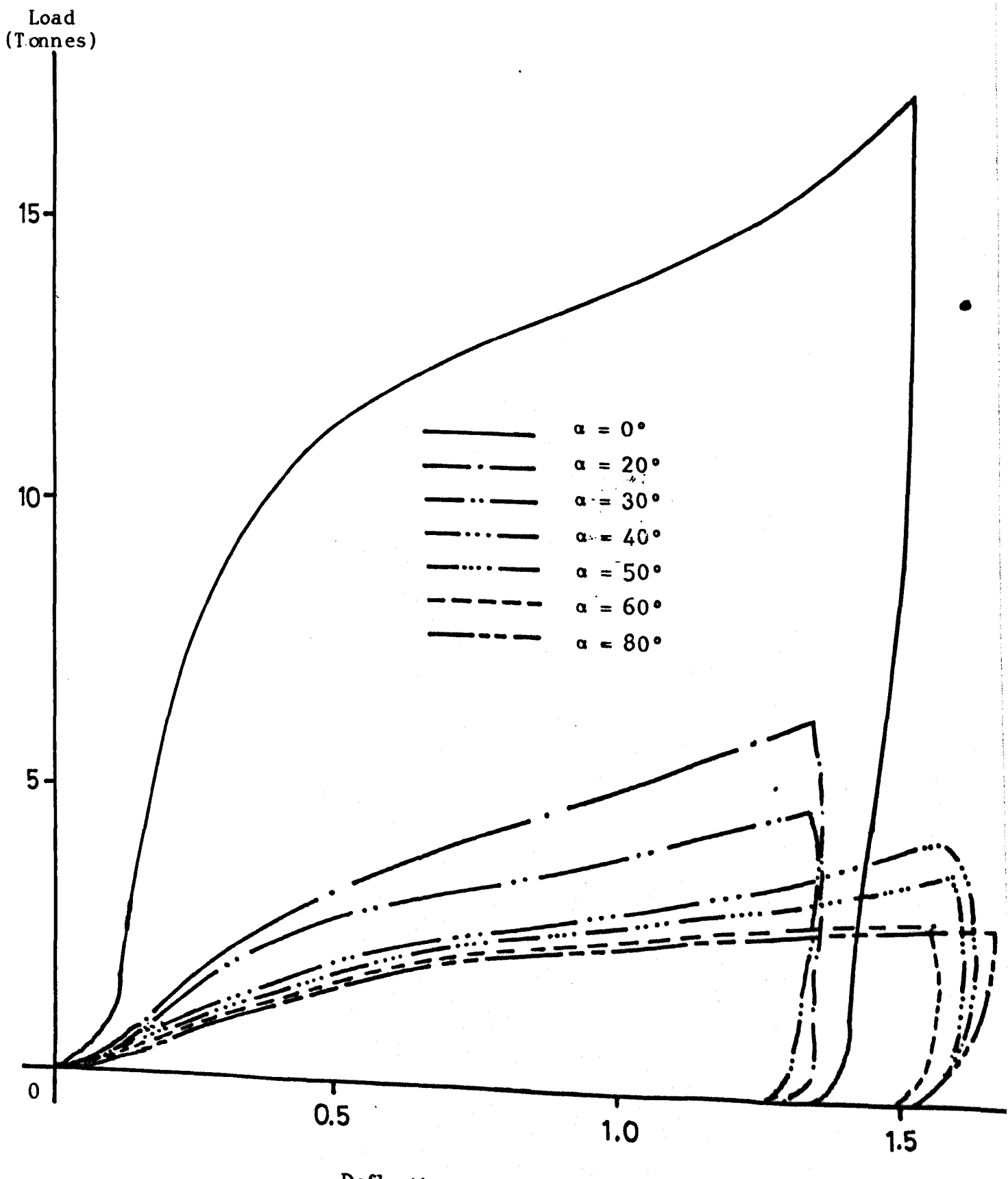

Fig. 4.7 RESULTS OBTAINED BY HAMLET(90) FOR THE CONTACT OF CROSSED-CYLINDERS.

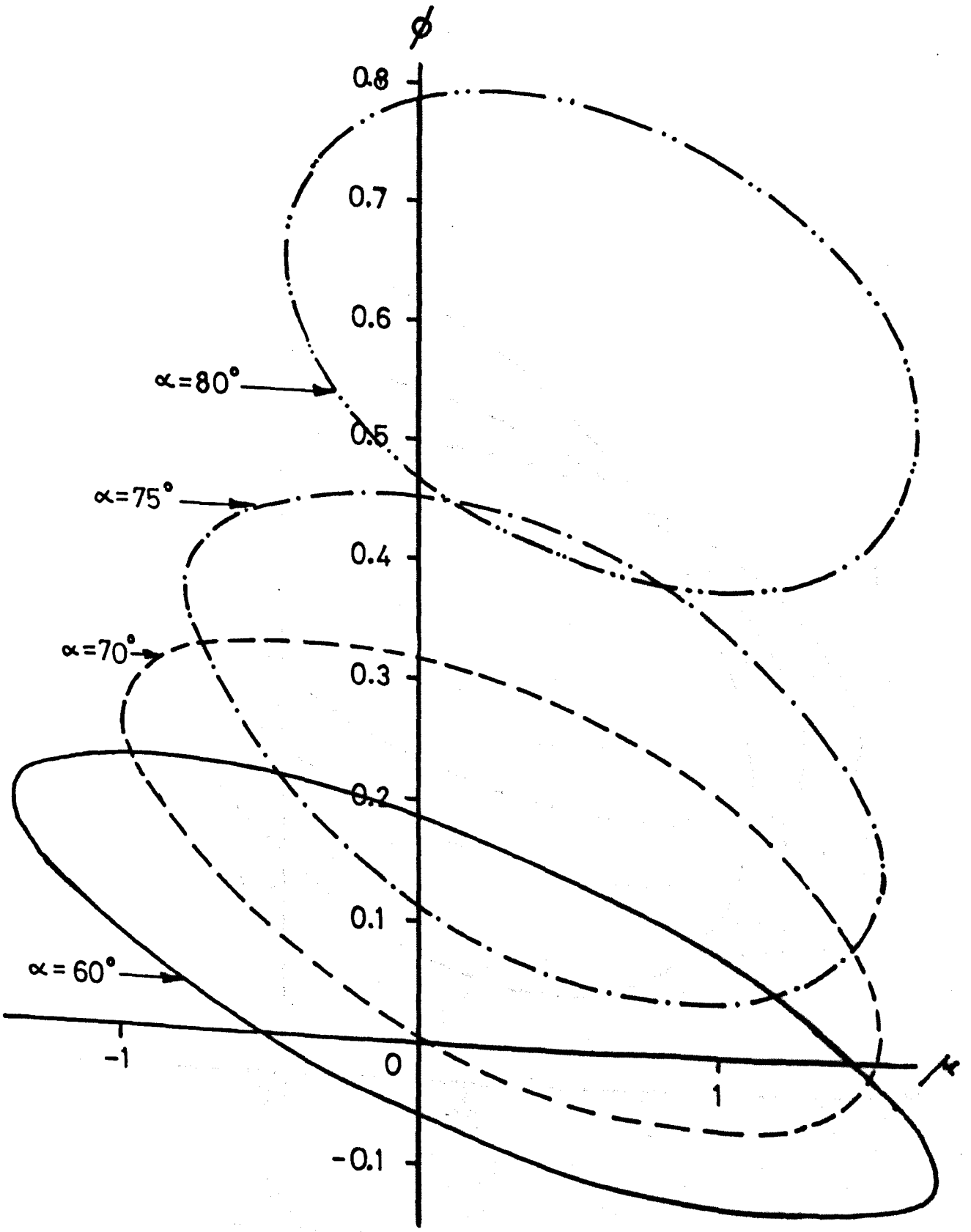

FIG 5.1 EXACT INTERACTION CURVES IN DIMENSIONLESS AXIAL LOAD AND BENDING MOMENT SPACE FOR VARIOUS VALUES OF HELIX ANGLE AND WHEN m=6 (SINGLE STRAND).

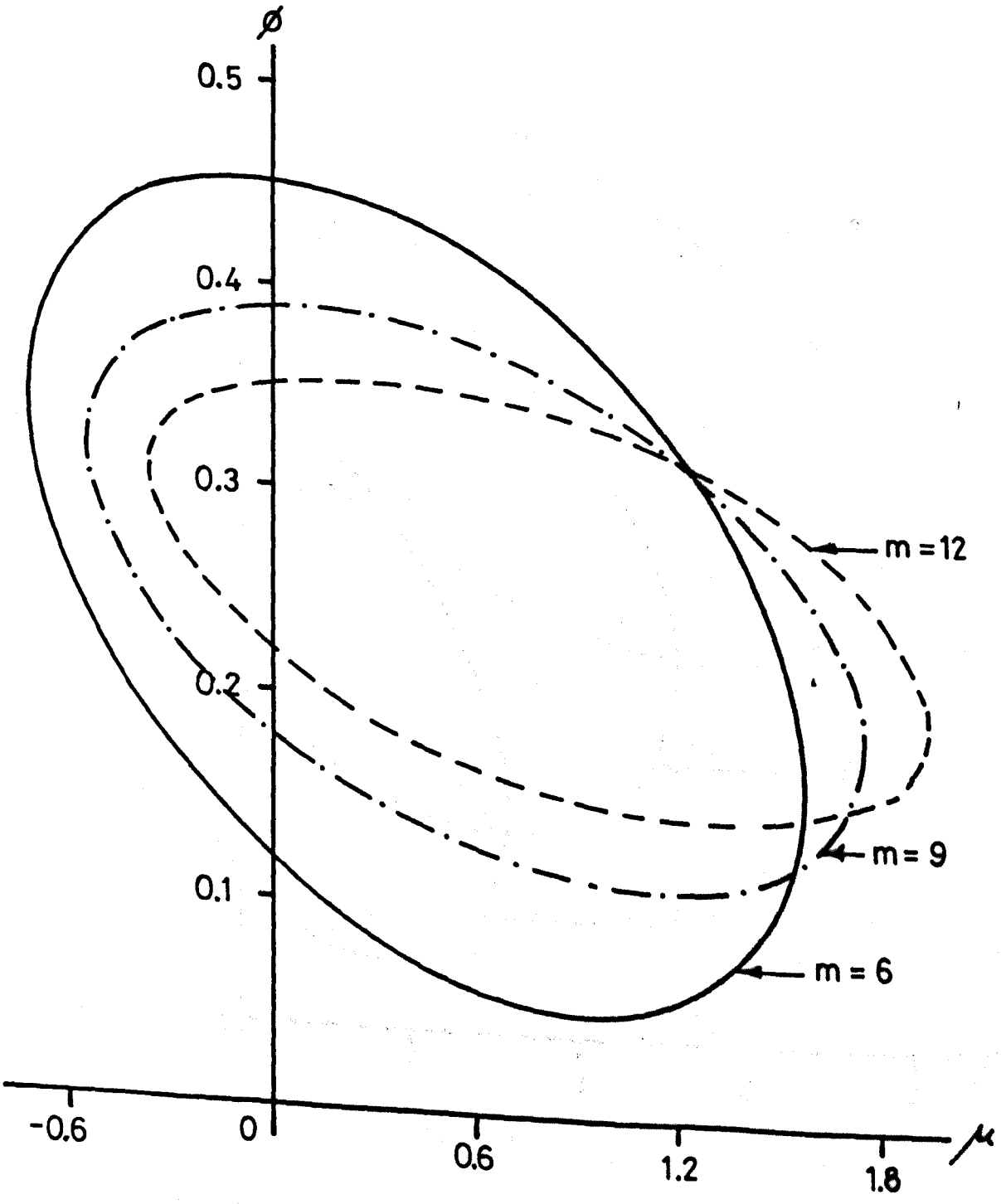

FIG 5.2a EXACT INTERACTION CURVES IN DIMENSIONLESS AXIAL LOAD AND BENDING MOMENT SPACE FOR VARIOUS NUMBERS OF WIRES IN A STRAND AND α=75°. (SINGLE STRAND)

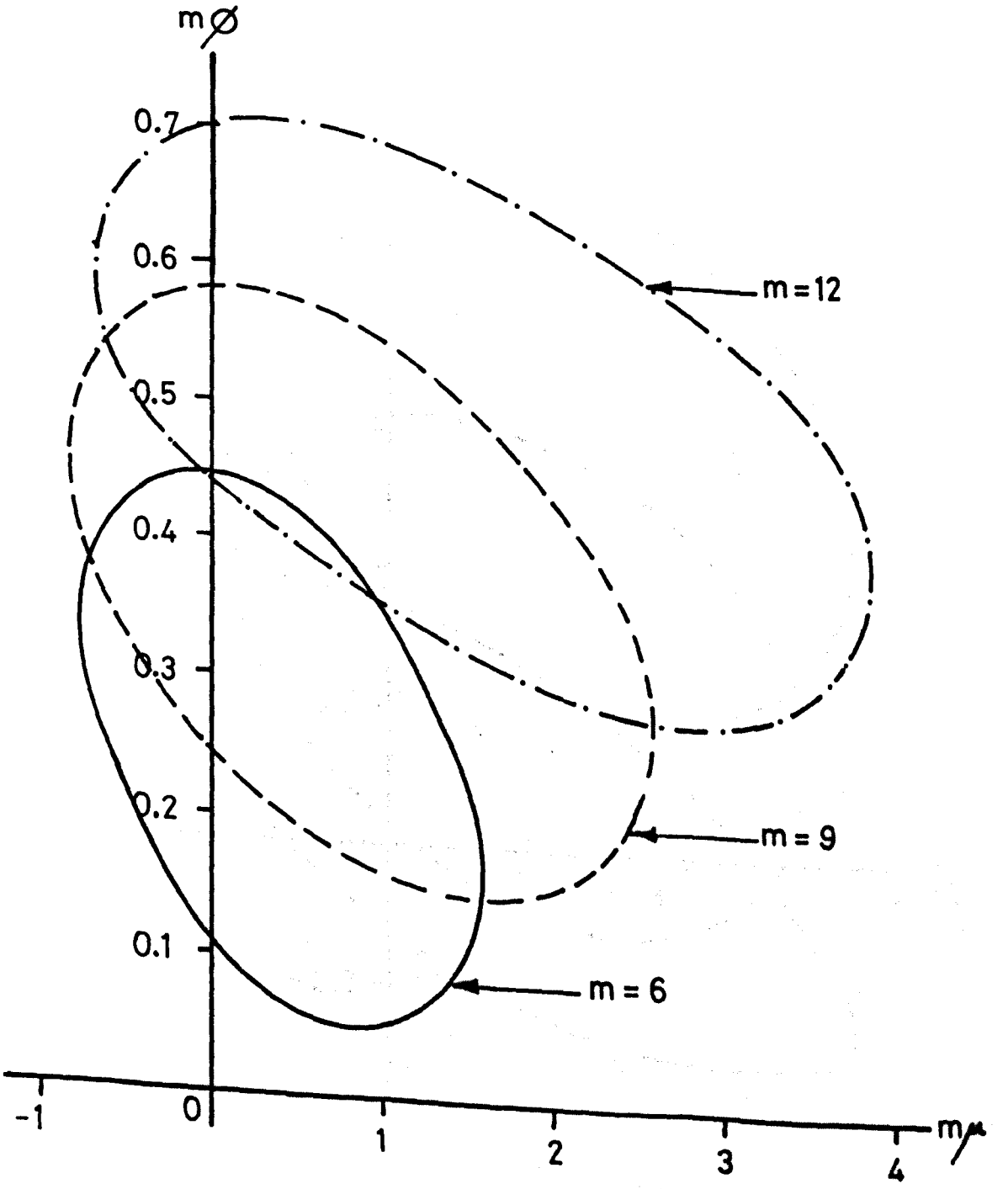

FIG 5.2b EXACT INTERACTION CURVES IN m_ϕ AND m_μ SPACE FOR VARIOUS NUMBERS OF WIRES IN A STRAND AND $\alpha=75°$. (SINGLE STRAND)

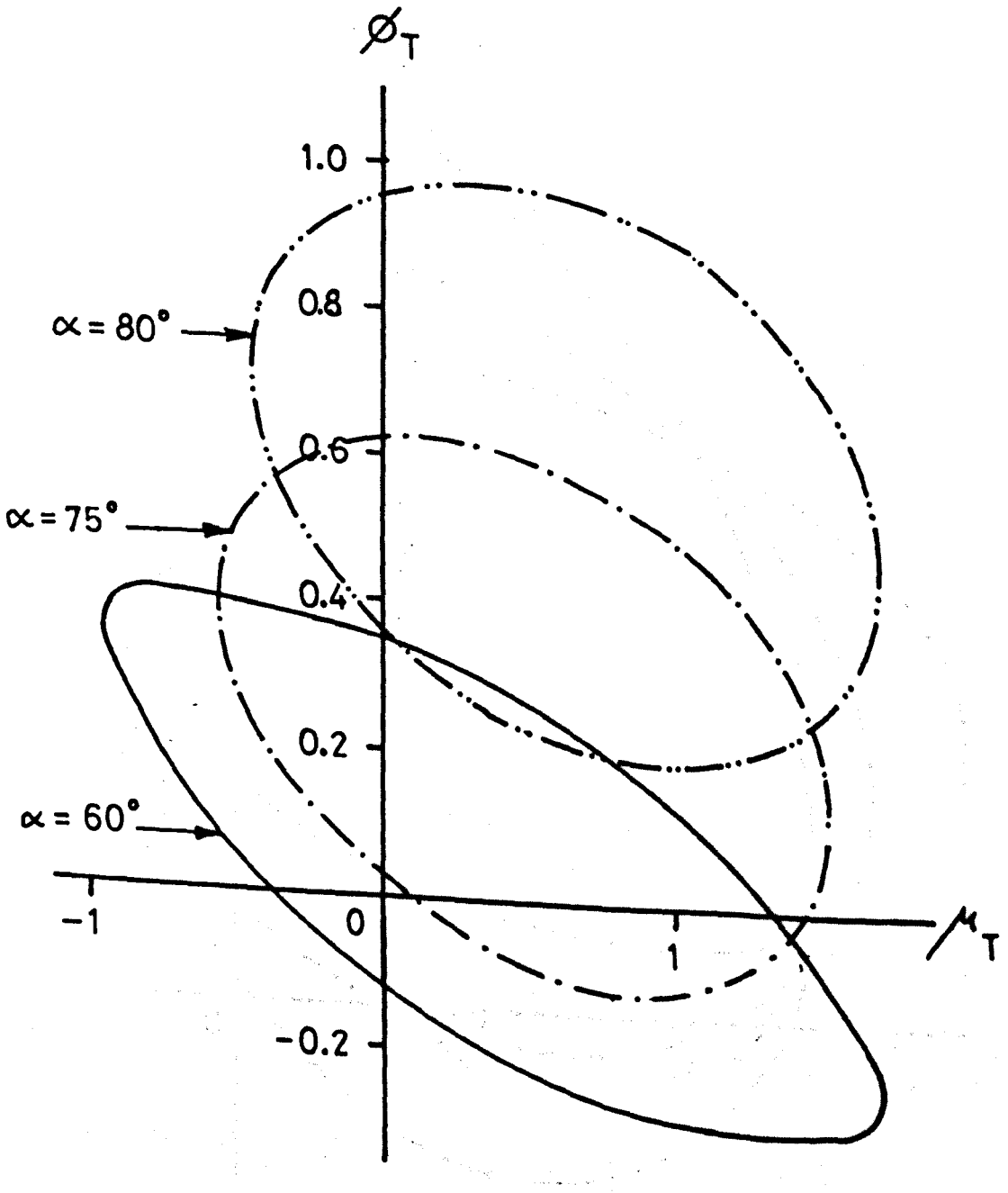

FIG 5.3 EXACT INTERACTION CURVES FOR SINGLE STRAND WITH CORE WIRE FOR VARIOUS VALUES OF HELIX ANGLES AND m=6.

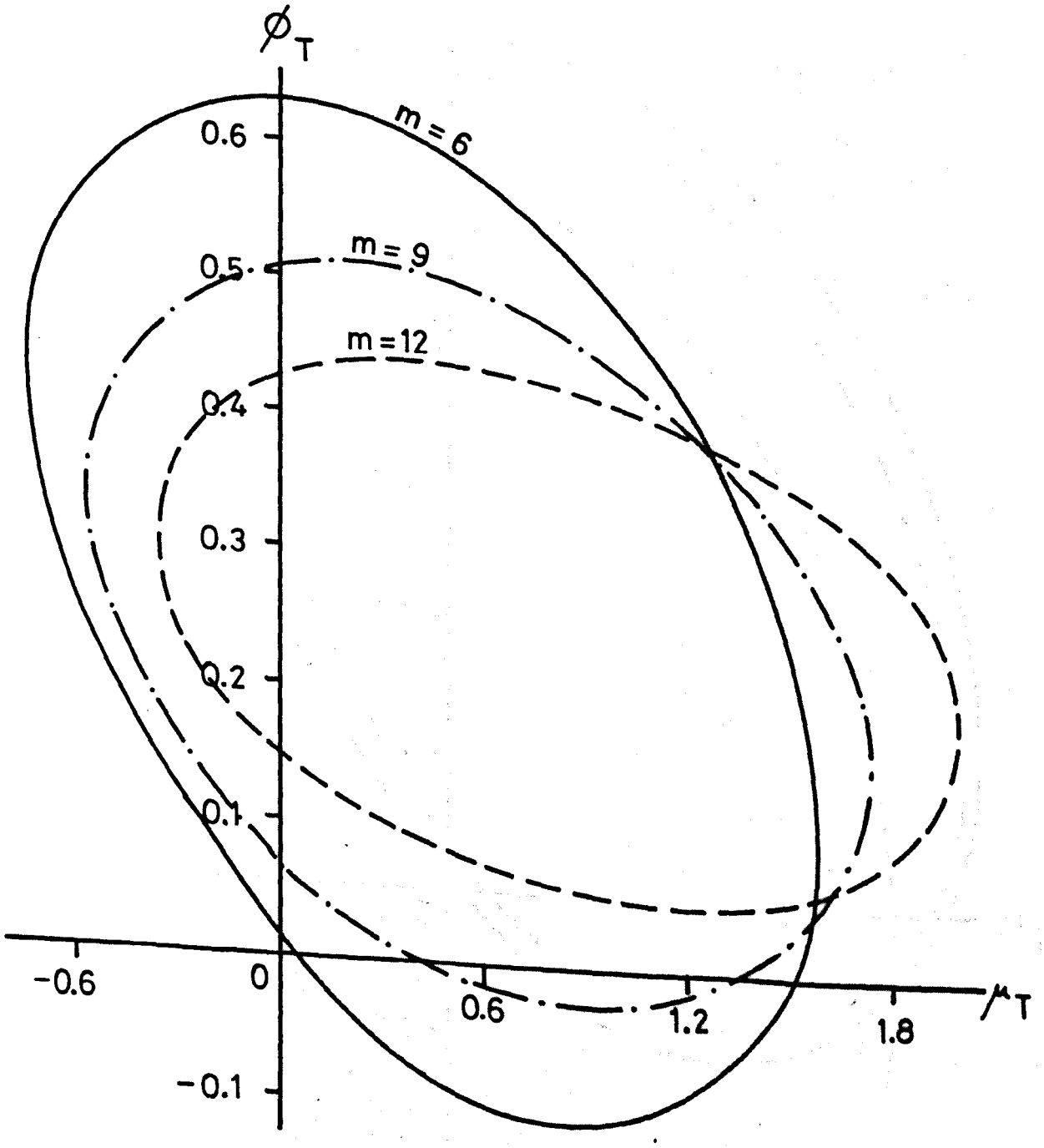

FIG 5.4 EXACT INTERACTION CURVES FOR SINGLE STRAND WITH CORE WIRE WITH VARIOUS NUMBERS OF WIRES IN THE STRAND AND $\alpha=75°$.

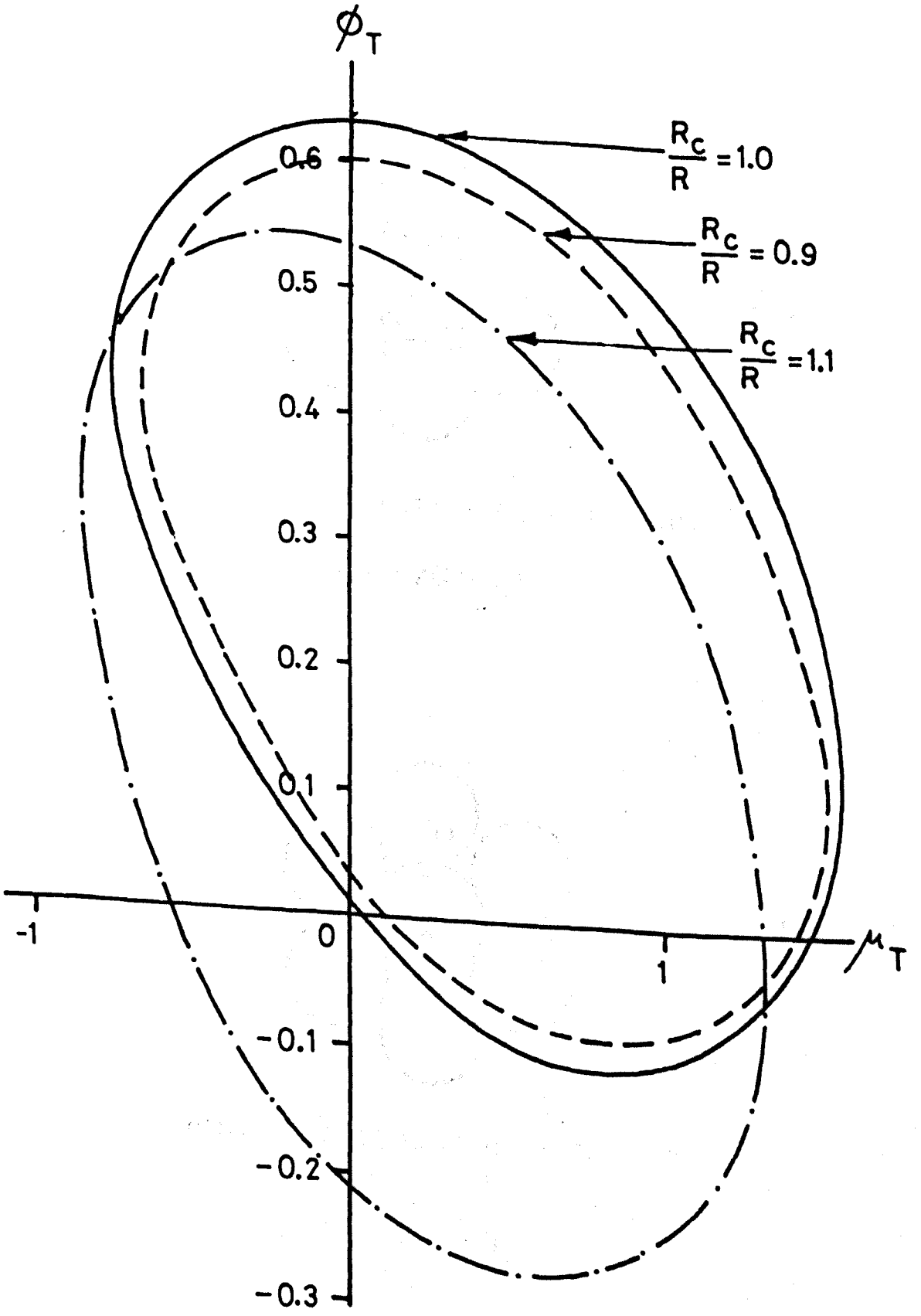

FIG 5.5 EFFECT OF THE SIZE OF CORE WIRE ON THE EXACT INTERACTION CURVES. (m=6 and α=75°)

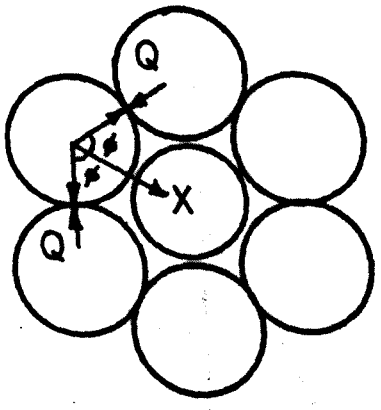

(a)

CORE DIAMETER < DIAMETER OF THE HELICAL WIRE

$$X = -2Q\cos\phi$$

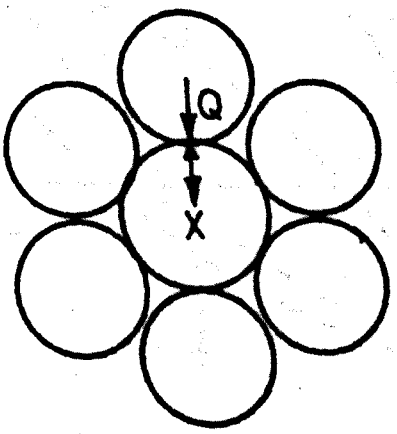

(b)

CORE DIAMETER > DIAMETER OF THE HELICAL WIRE

$$X = -Q$$

FIG 5.6 LINE LOAD RESULTING FROM THE CONTACT FORCE.

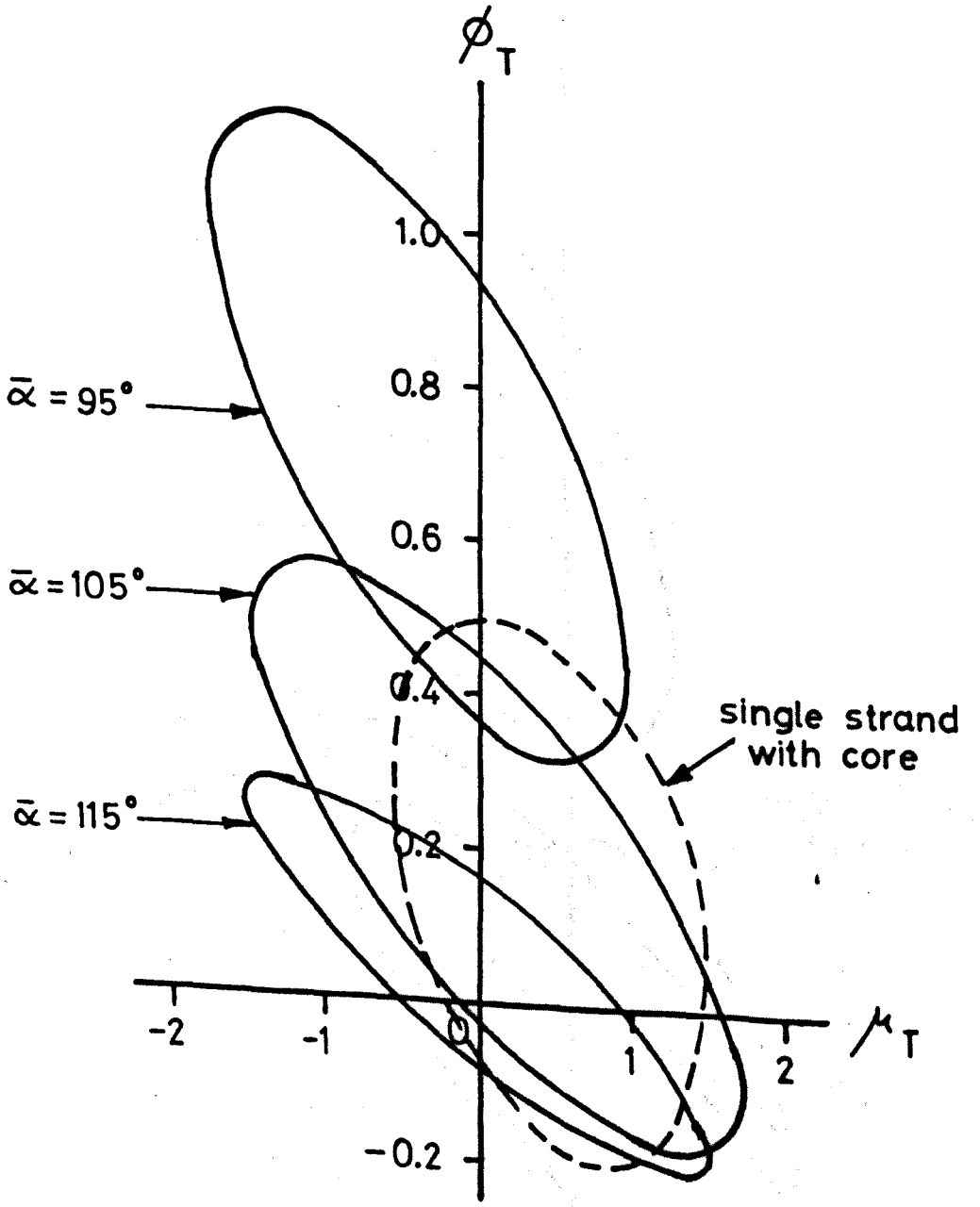

FIG 5.7 EXACT INTERACTION CURVES FOR ROPE WITH TWO LAYERS OF STRAND WHEN α=70°. (WITH CORE WIRE)

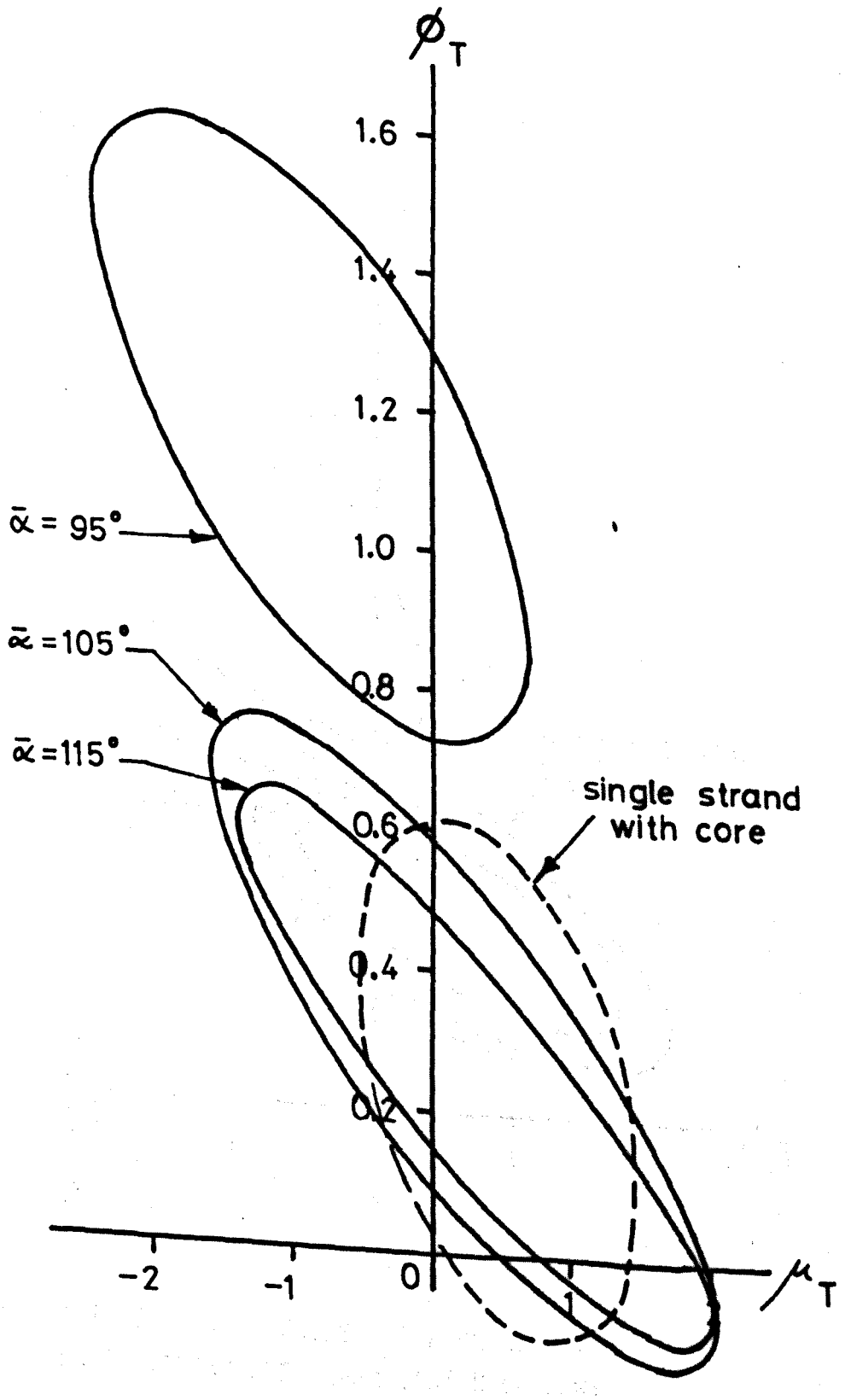

FIG 5.8 EXACT INTERACTION CURVES FOR ROPE WITH TWO LAYERS OF STRAND WHEN $\alpha=75°$.(WITH CORE WIRE)

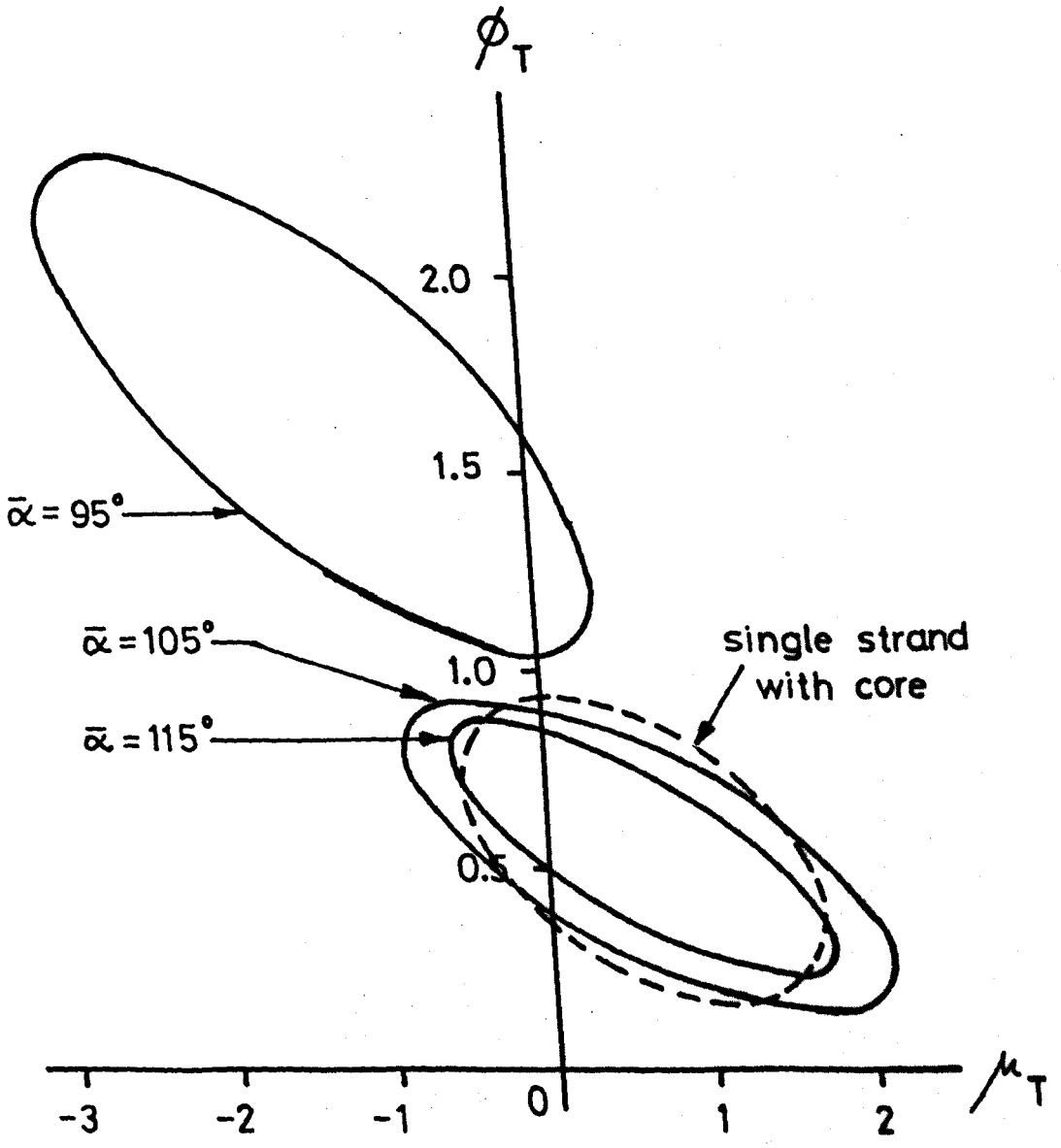

FIG 5.9 EXACT INTERACTION CURVES FOR ROPE WITH TWO LAYERS OF STRAND WHEN α=80°.(WITH CORE WIRE)

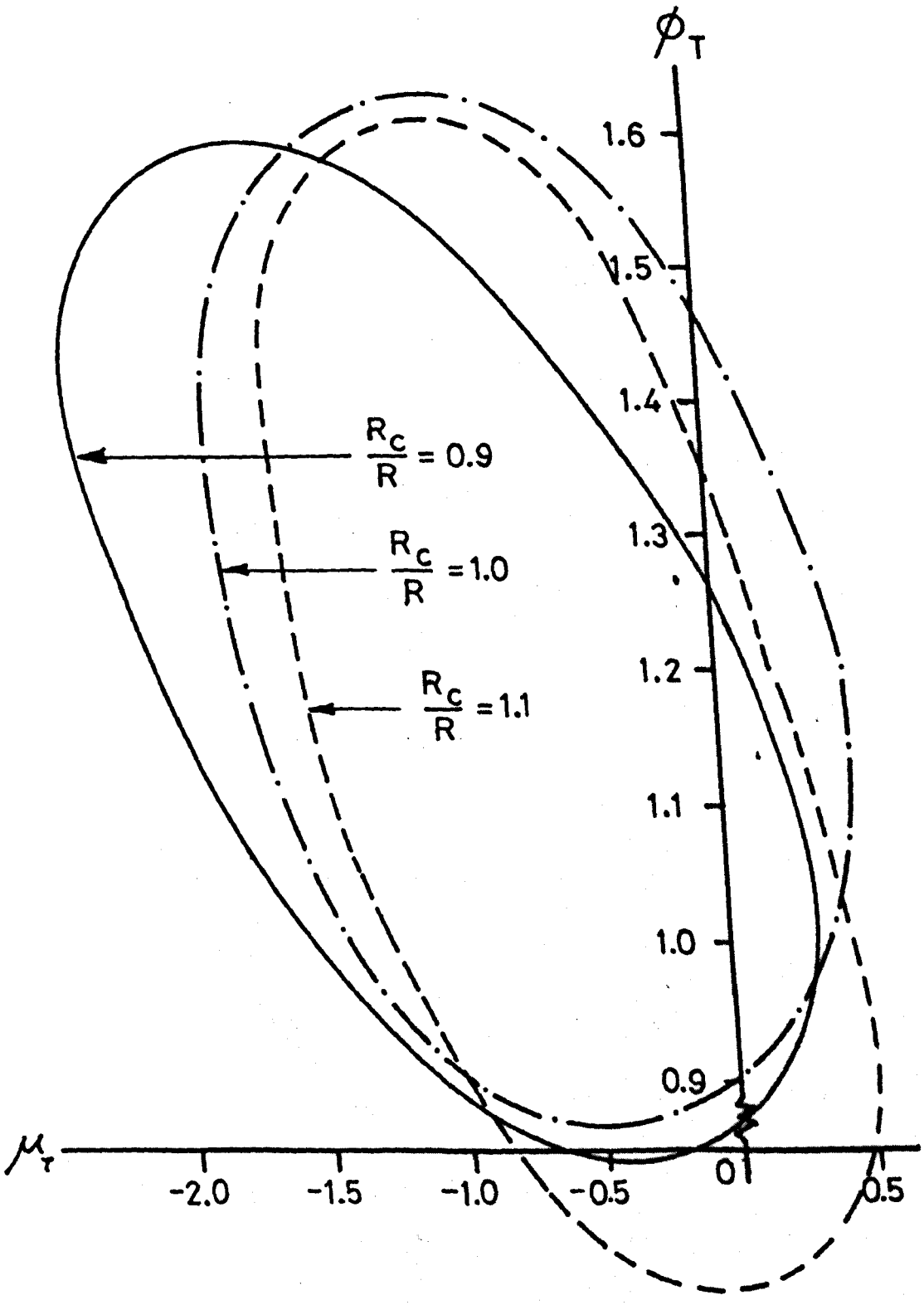

FIG 5.10 EXACT INTERACTION CURVES FOR ROPE WITH TWO LAYERS OF STRAND WITH VARIOUS CORE SIZES.

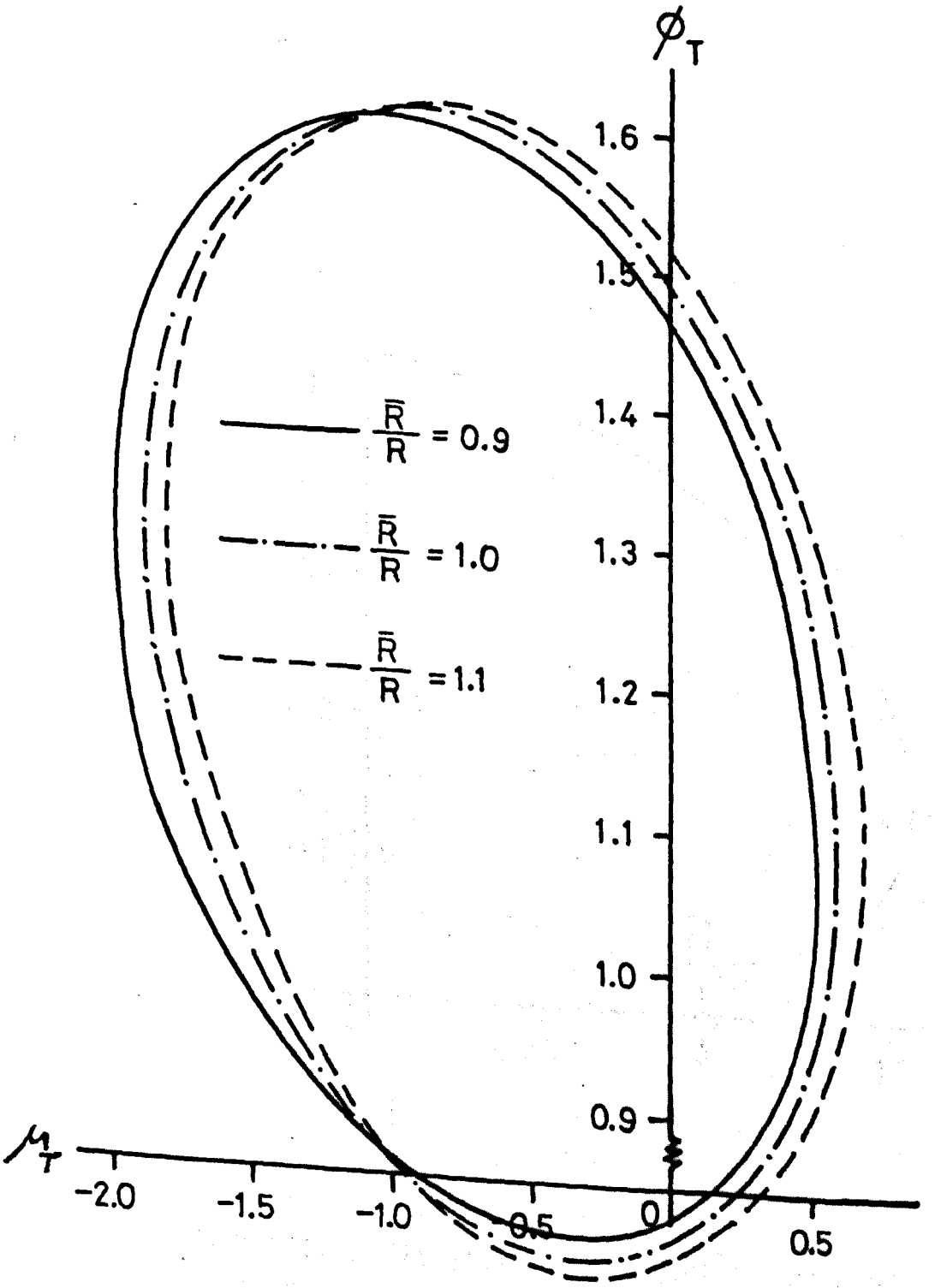

FIG 5.11 EXACT INTERACTION CURVES FOR ROPE WITH TWO LAYERS OF STRAND WITH VARIOUS SIZES OF WIRE IN THE OUTER STRAND. (WITH CORE WIRE)

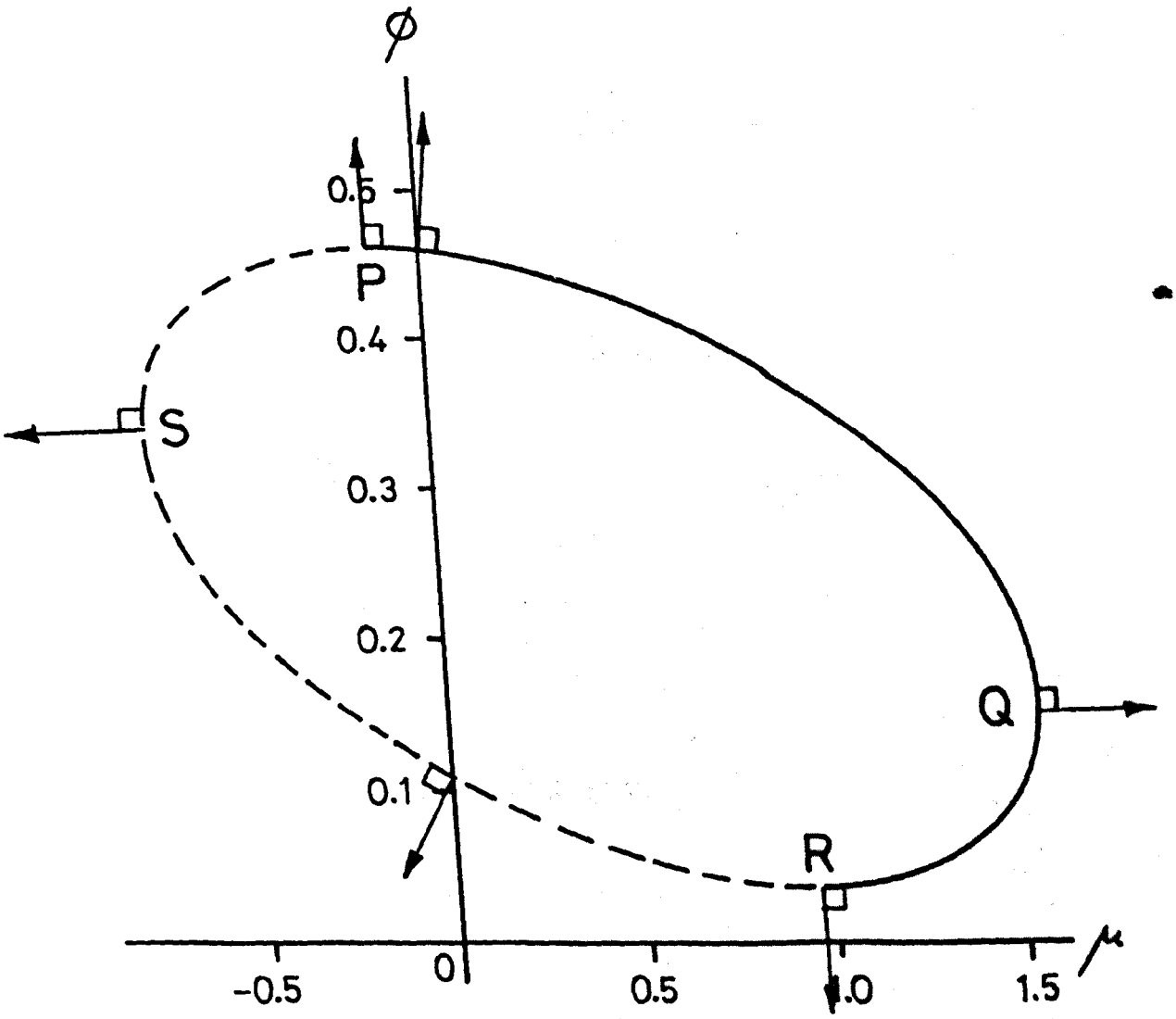

FIG 5.12 NORMALITY OF THE STRAIN RATE VECTOR TO THE YIELD SURFACE. (m=6 ; α=75° ; x=0.01744)

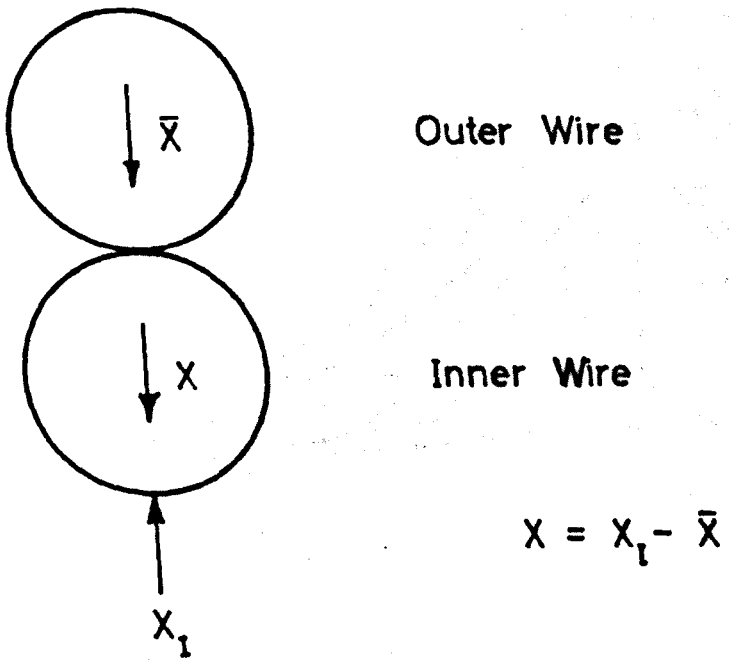

FIG 5.13 RESULTANT NORMAL LINE LOAD.

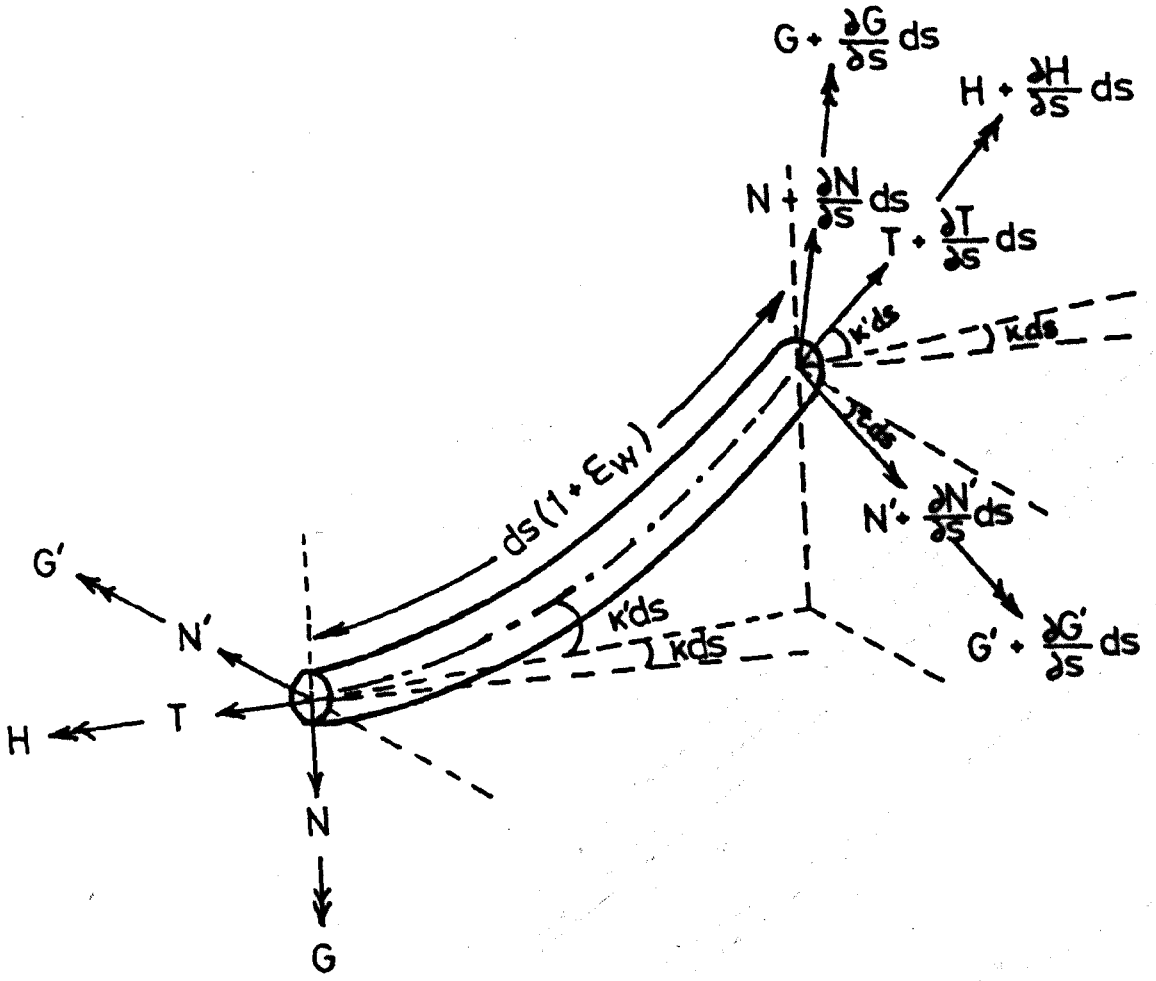

FIG 6.1 EQUILIBRIUM OF FORCES AND MOMENTS.

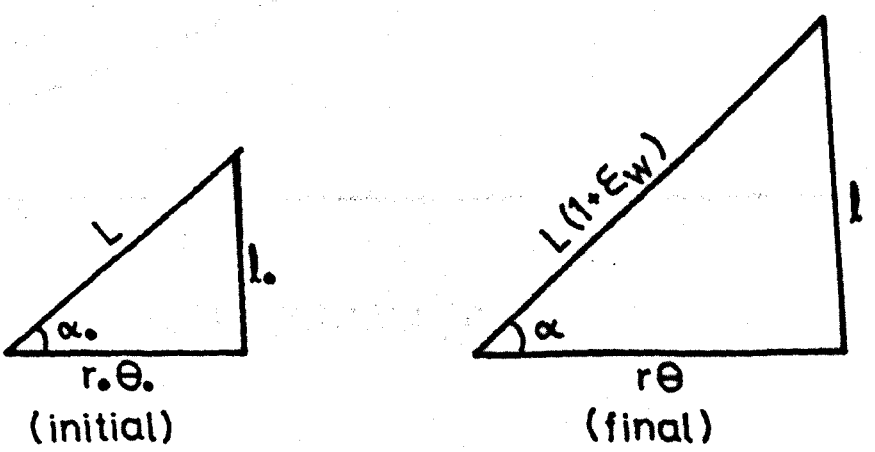

FIG 6.2 HELICAL WIRE CENTRE LINE IN INITIAL AND FINAL CONFIGURATIONS DEVELOPED ON A FLAT PLANE.

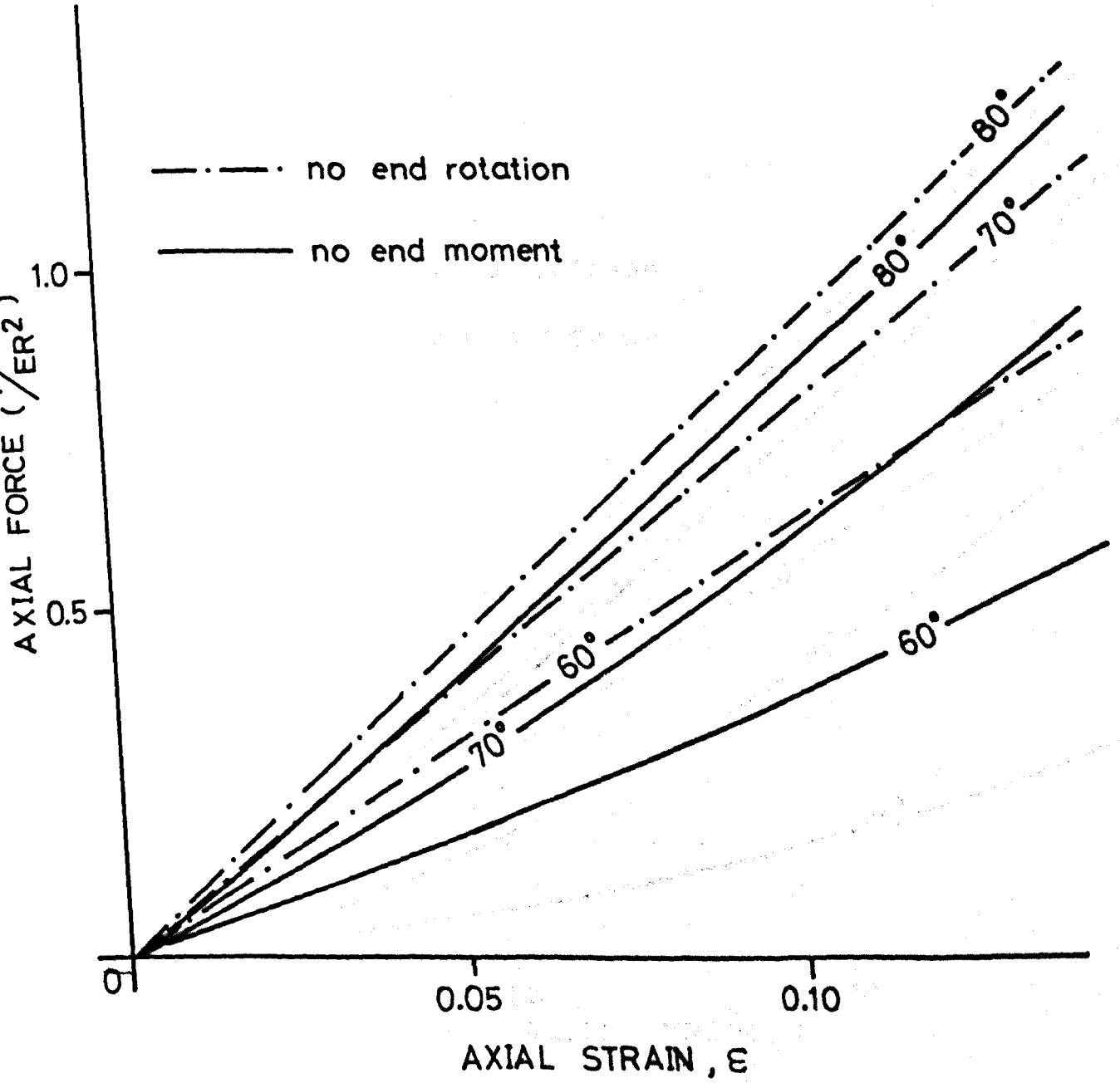

FIG 6.3 NORMALISED AXIAL FORCE AS A FUNCTION OF AXIAL STRAND STRAIN FOR 3-WIRE STRANDS WITH INITIAL HELIX ANGLES 60°, 70° AND 80°.

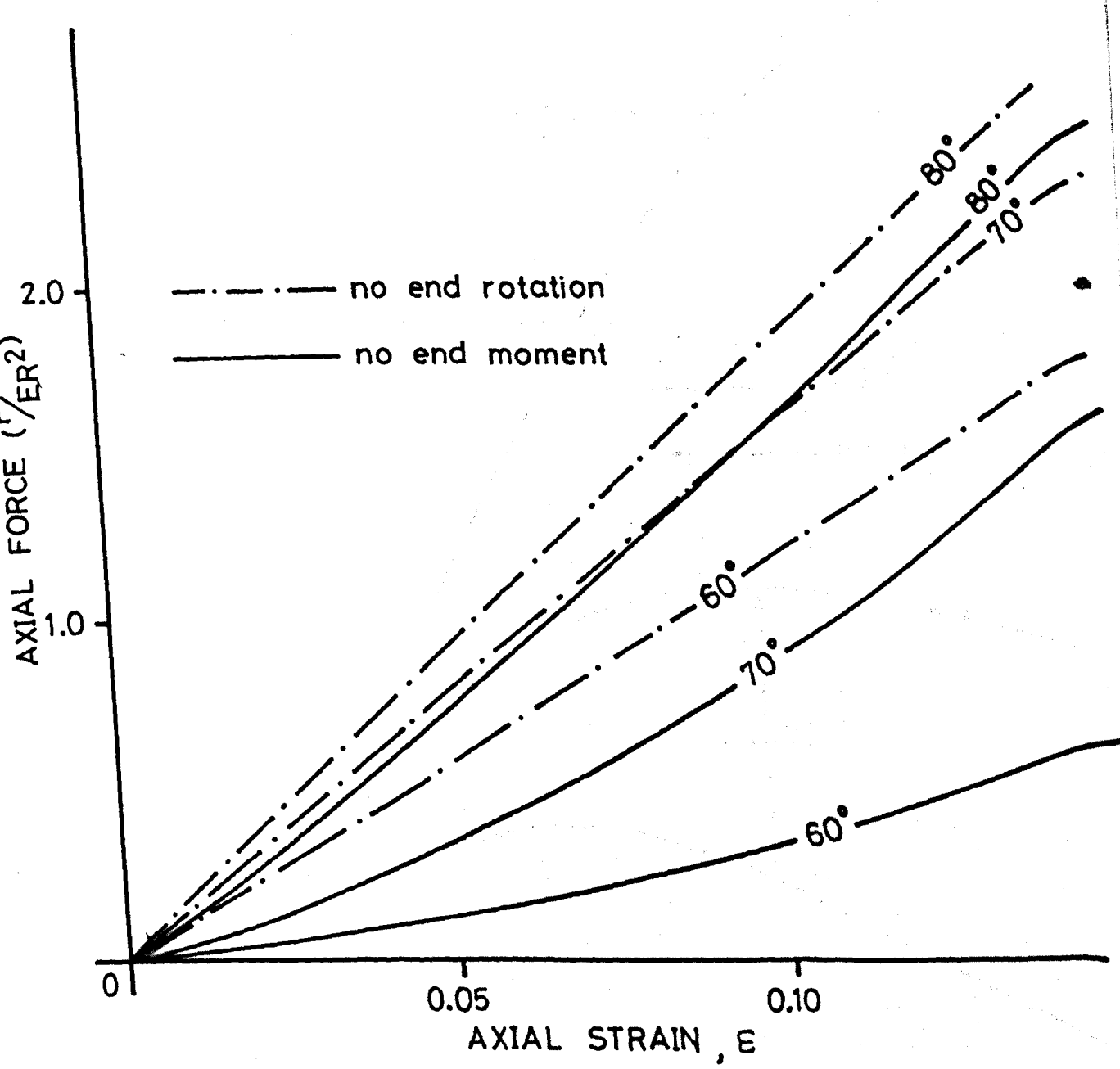

FIG 6.4 NORMALISED AXIAL FORCE AS A FUNCTION OF AXIAL STRAND STRAIN FOR 6-WIRE STRANDS WITH INITIAL HELIX ANGLES 60°, 70° AND 80°.

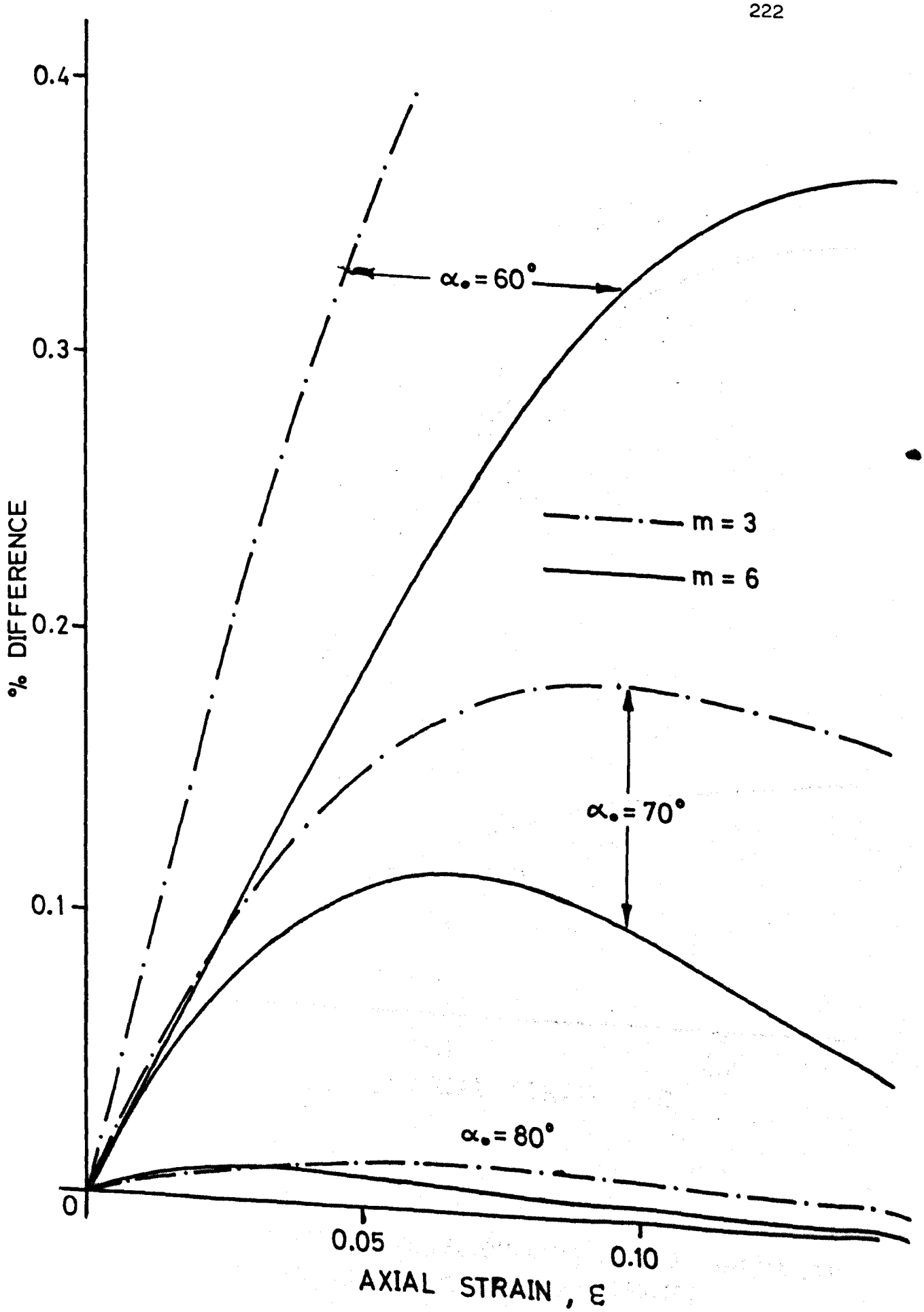

FIG 6.5 PERCENTAGE DIFFERENCE IN AXIAL LOAD OBTAINED BY COSTELLO AND PHILLIPS AND THE PRESENT ANALYSIS - NO END-MOMENT. (ELASTIC)

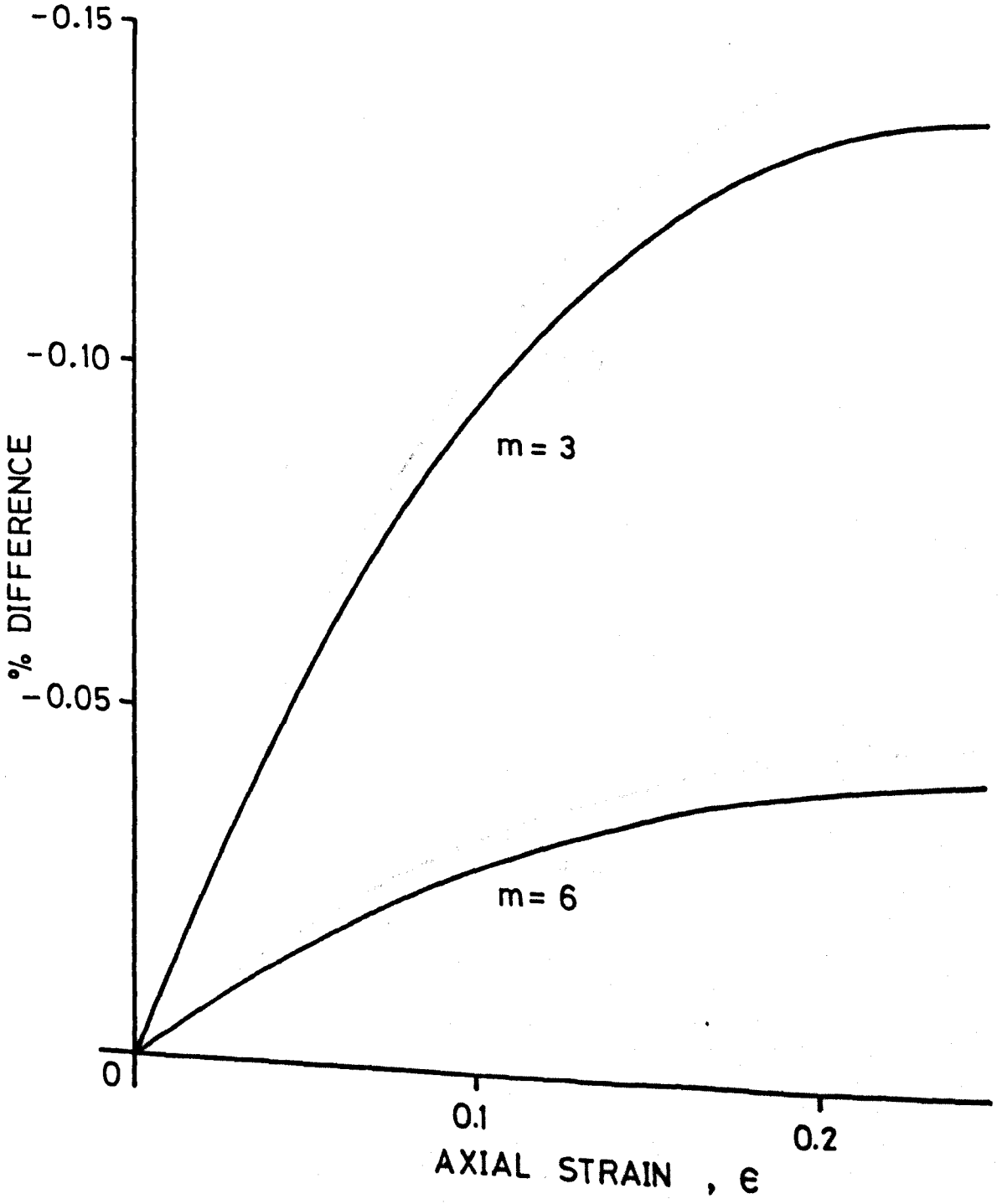

FIG 6.6a PERCENTAGE DIFFERENCE IN AXIAL LOADS OBTAINED BY COSTELLO AND PHILLIPS AND THE PRESENT ANALYSIS - NO END-ROTATION AND INITIAL HELIX ANGLE BEING 60°. (ELASTIC)

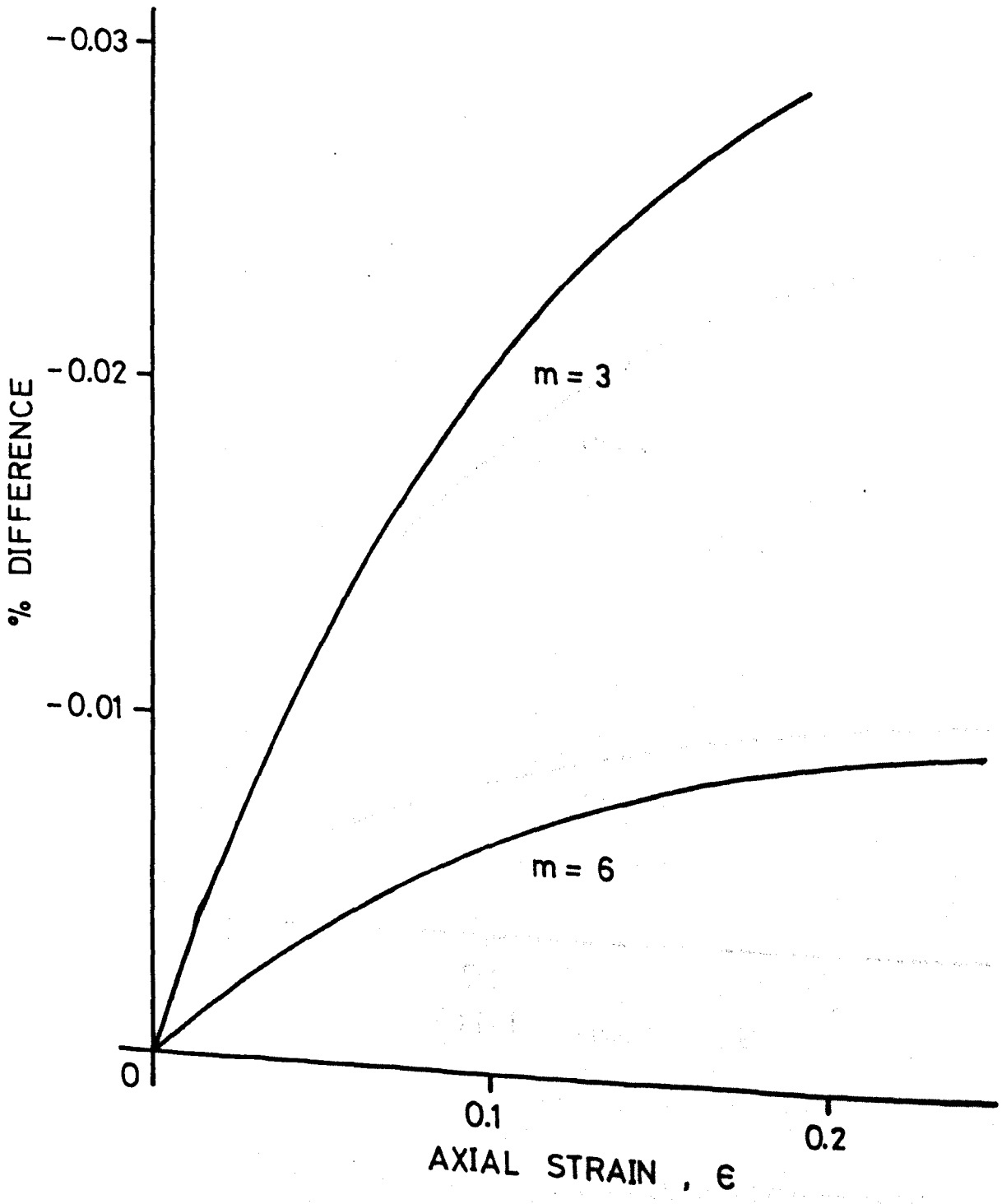

FIG 6.6b PERCENTAGE DIFFERENCE IN AXIAL LOADS OBTAINED BY COSTELLO AND PHILLIPS AND THE PRESENT ANALYSIS - NO END-ROTATION AND INITIAL HELIX ANGLE BEING 70°.(ELASTIC)

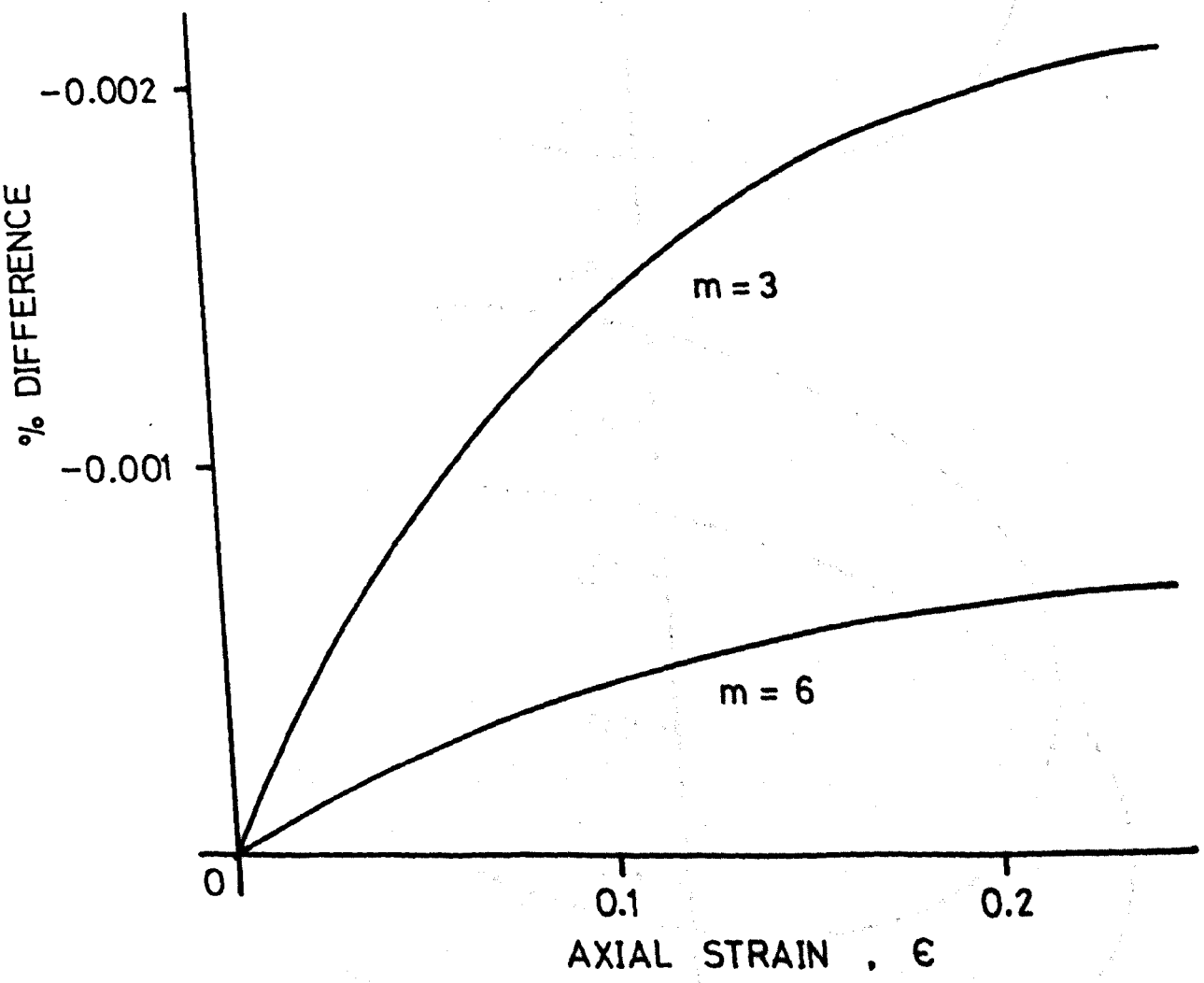

FIG 6.6c PERCENTAGE DIFFERENCE IN AXIAL LOADS OBTAINED BY COSTELLO AND PHILLIPS AND THE PRESENT ANALYSIS - NO END-ROTATION AND INITIAL HELIX ANGLE BEING 80°.(ELASTIC)

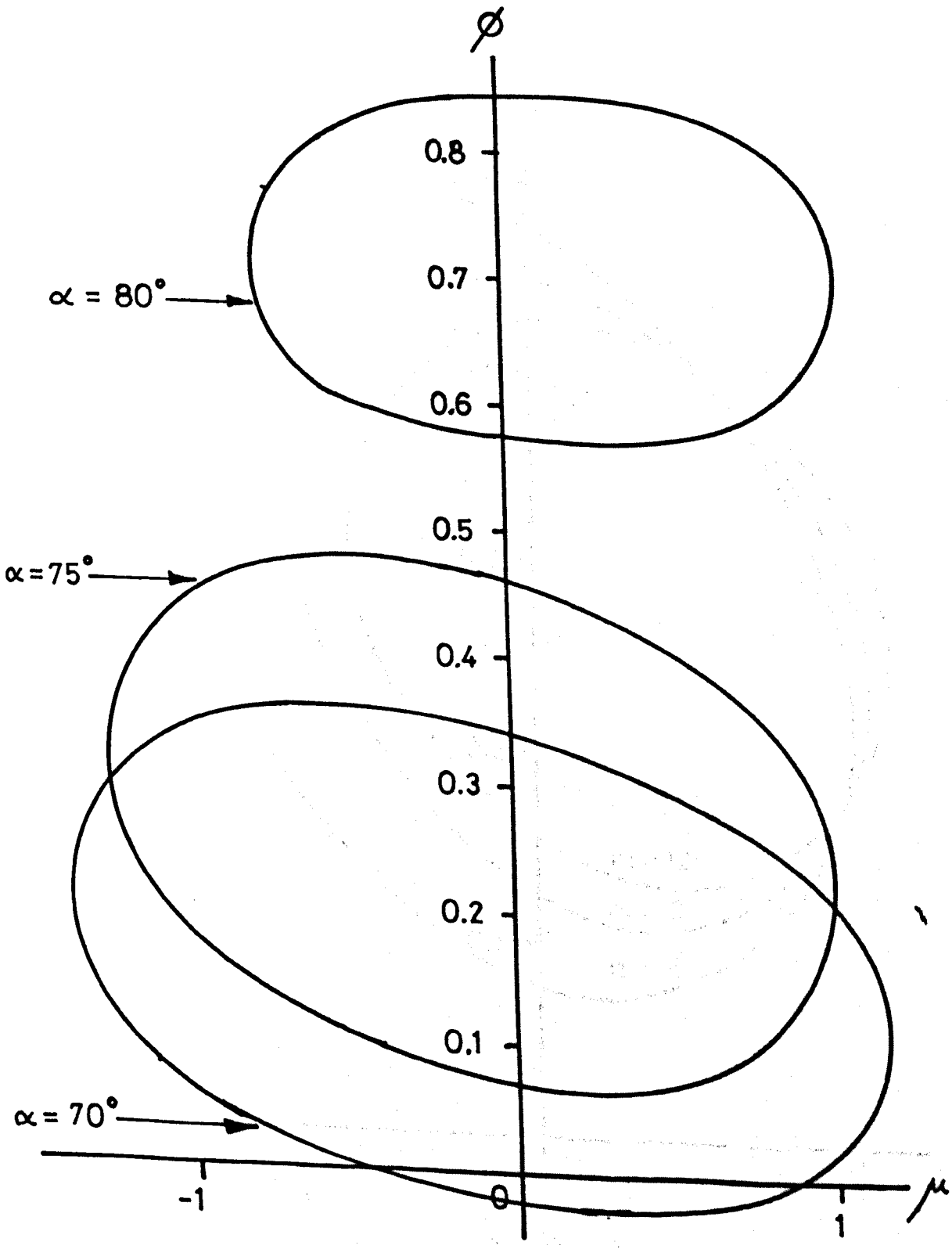

FIG 7.1 INTERACTION CURVES IN DIMENSIONLESS AXIAL LOAD AND BENDING MOMENT SPACE FOR VARIOUS VALUES OF HELIX ANGLES. (m=6 ; ϵ=0.01) - SINGLE STRAND

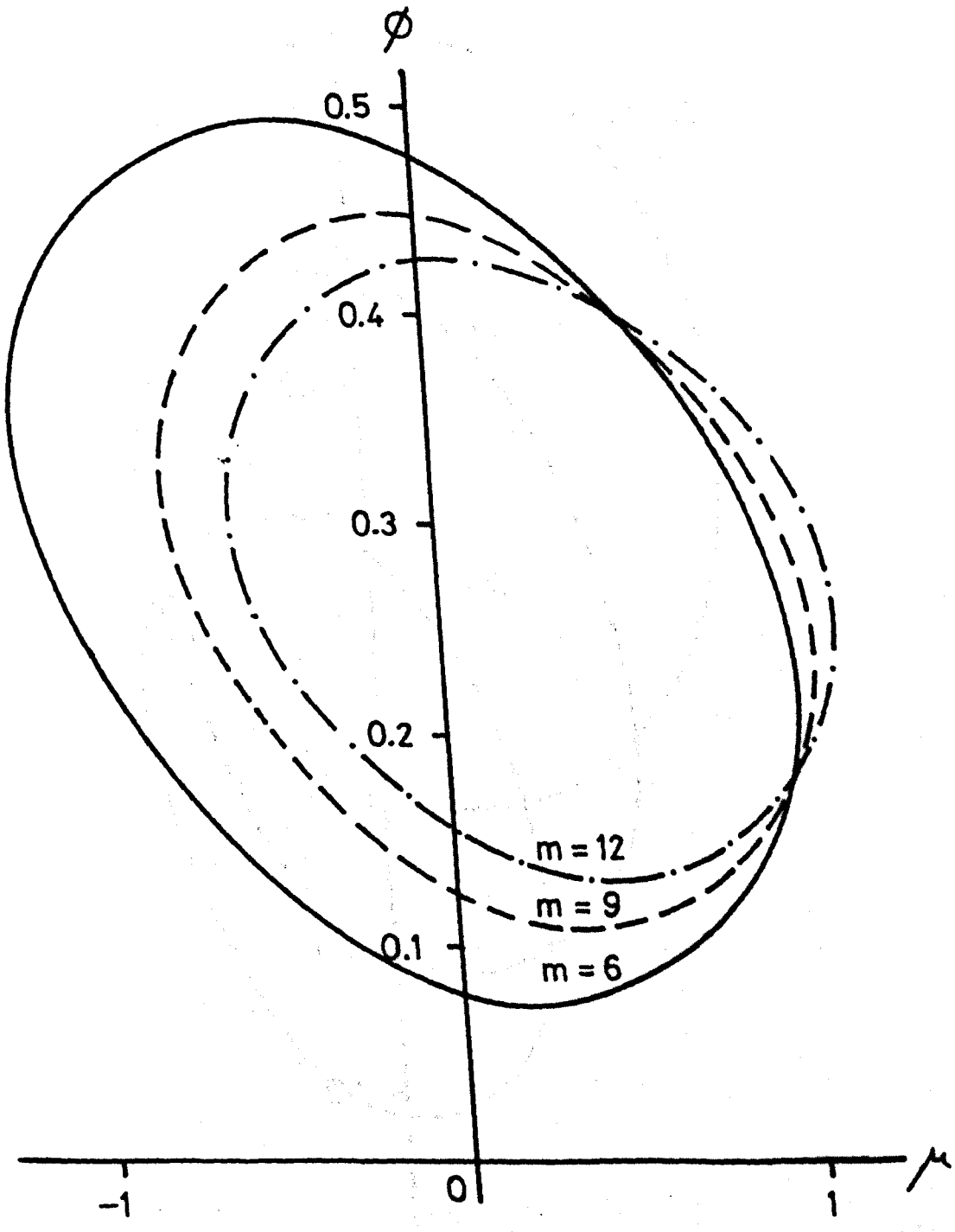

FIG 7.2a INTERACTION CURVES IN DIMENSIONLESS AXIAL LOAD AND BENDING MOMENT SPACE FOR VARIOUS NUMBERS OF WIRES IN THE STRAND. (m=6 ; ϵ=0.01) - SINGLE STRAND

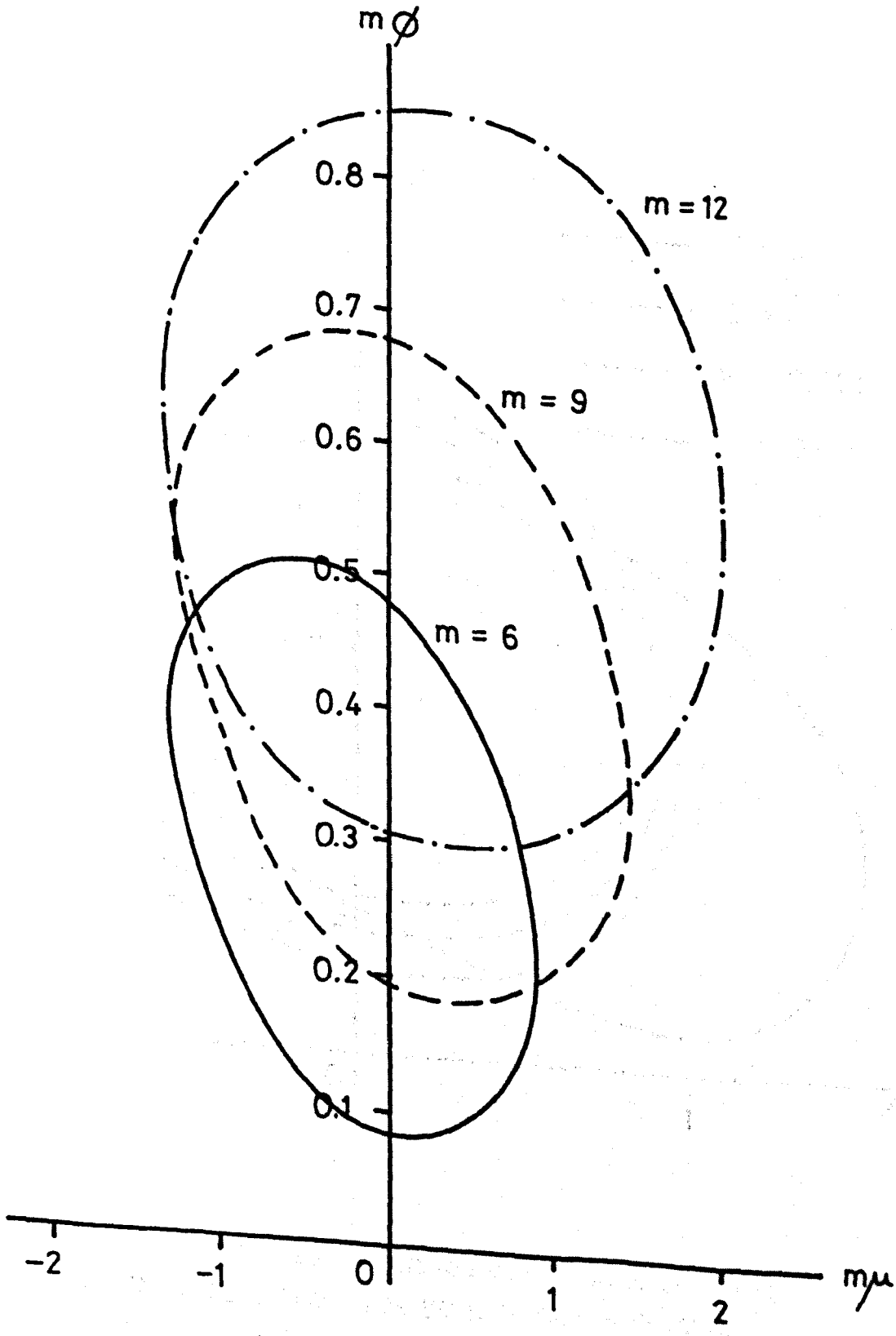

FIG 7.2b INTERACTION CURVES IN mϕ AND mμ SPACE FOR VARIOUS NUMBERS OF WIRES IN A STRAND AND α=75°. (FINITE EXTENSION) - SINGLE STRAND

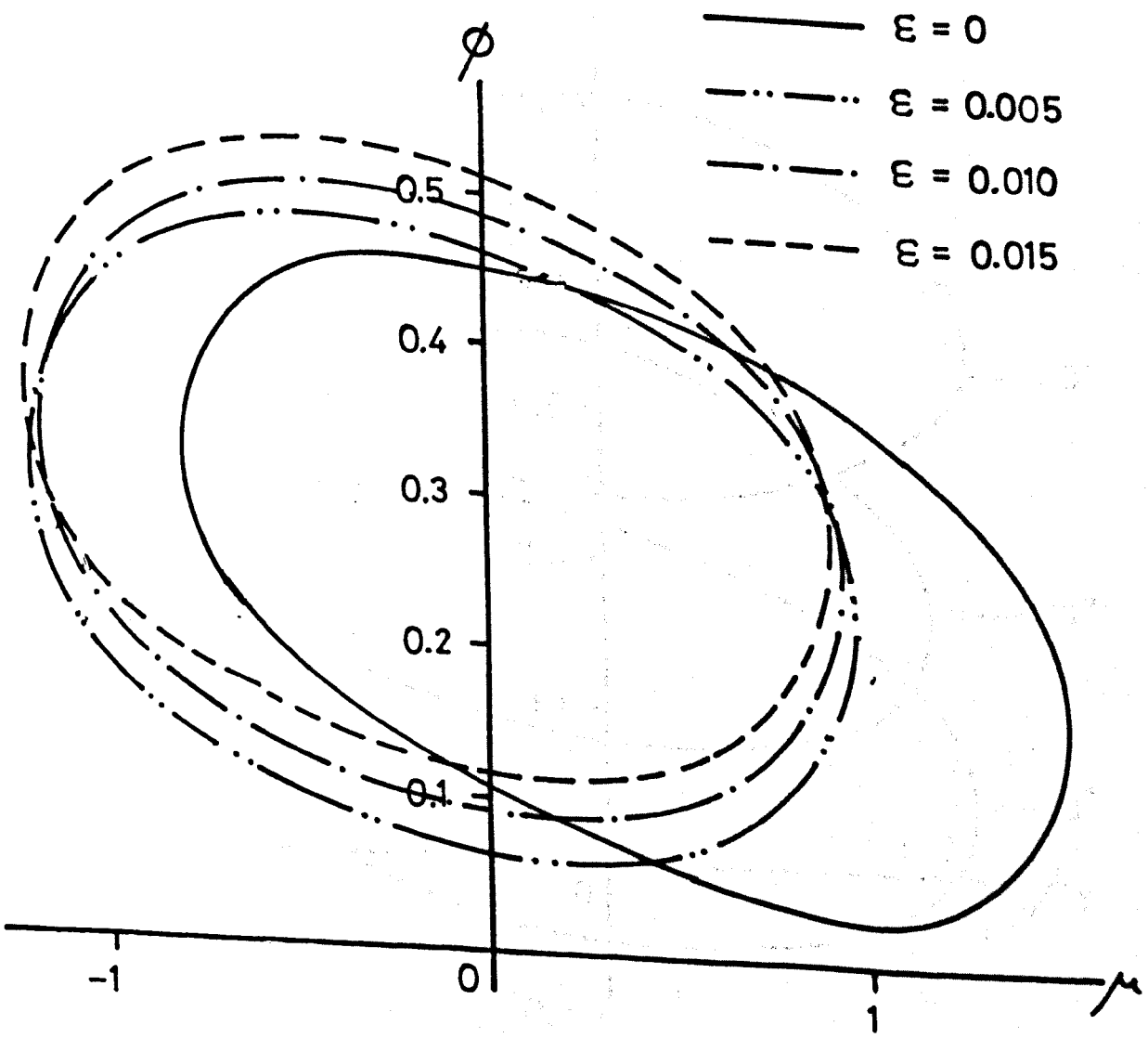

FIG 7.3 INTERACTION CURVES IN DIMENSIONLESS AXIAL LOAD AND BENDING MOMENT SPACE FOR VARIOUS VALUES OF AXIAL EXTENSION. (m=6 ; $\dot{\alpha}$=75°.) - SINGLE STRAND

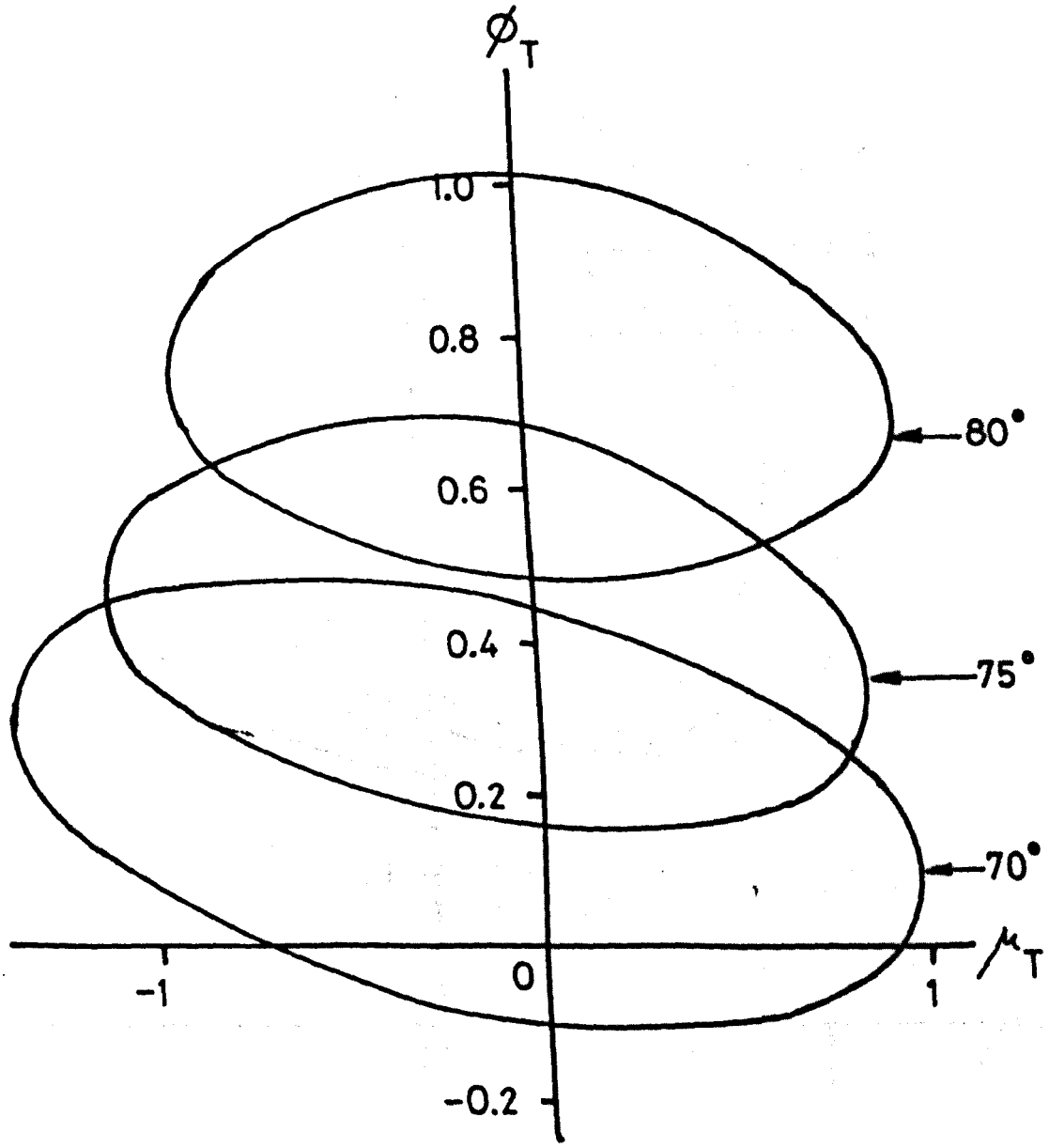

FIG 7.4 INTERACTION CURVES FOR STRAND WITH CORE WIRE.
(m=6 ; ϵ=0.01 ; R_c/R=1.0)

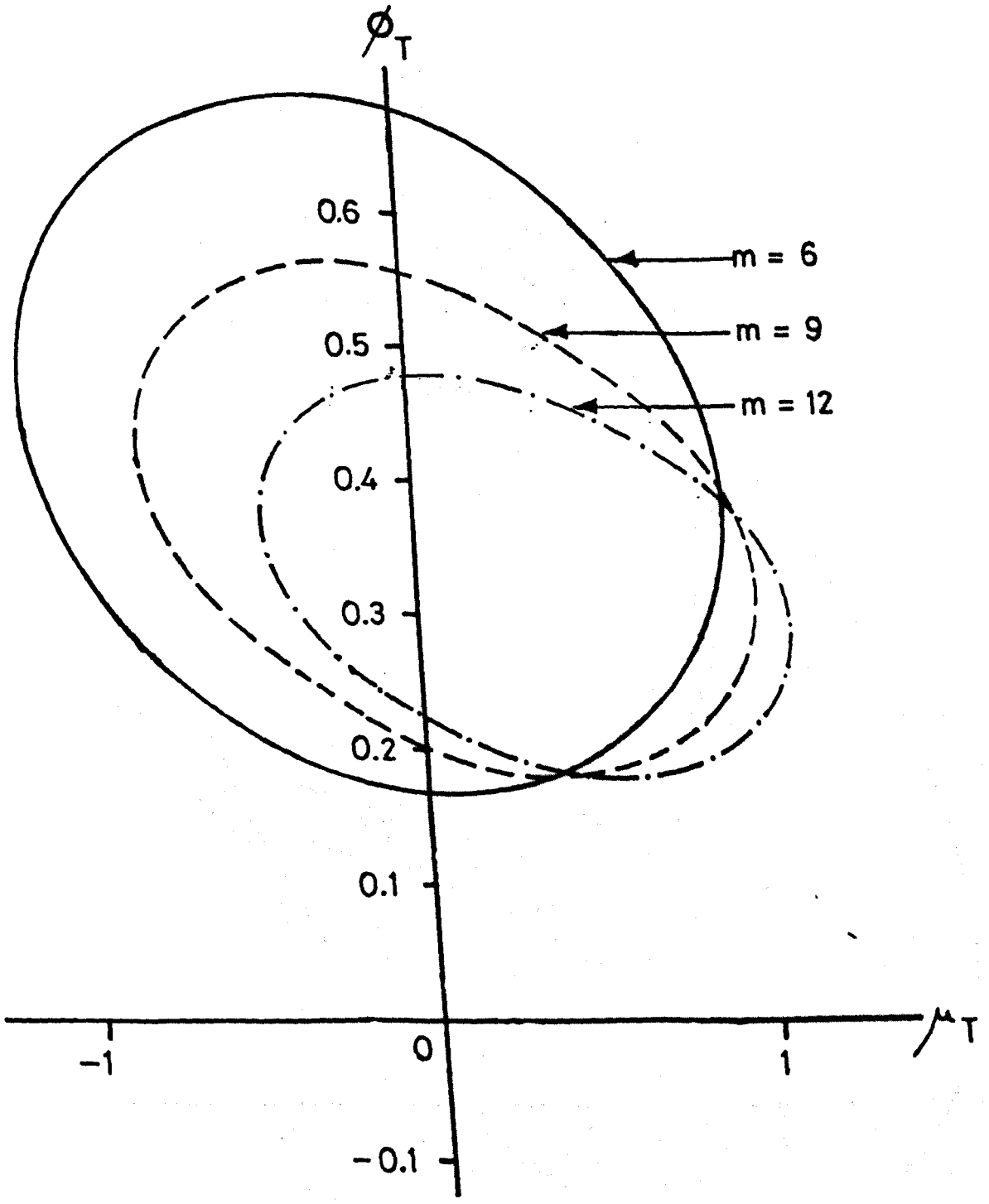

FIG 7.5 INTERACTION CURVES FOR STRAND WITH CORE WIRES WITH VARIOUS NUMBERS OF WIRES IN THE STRAND.
(α=75° ; ϵ=0.01 ; R_c/R=1.0)

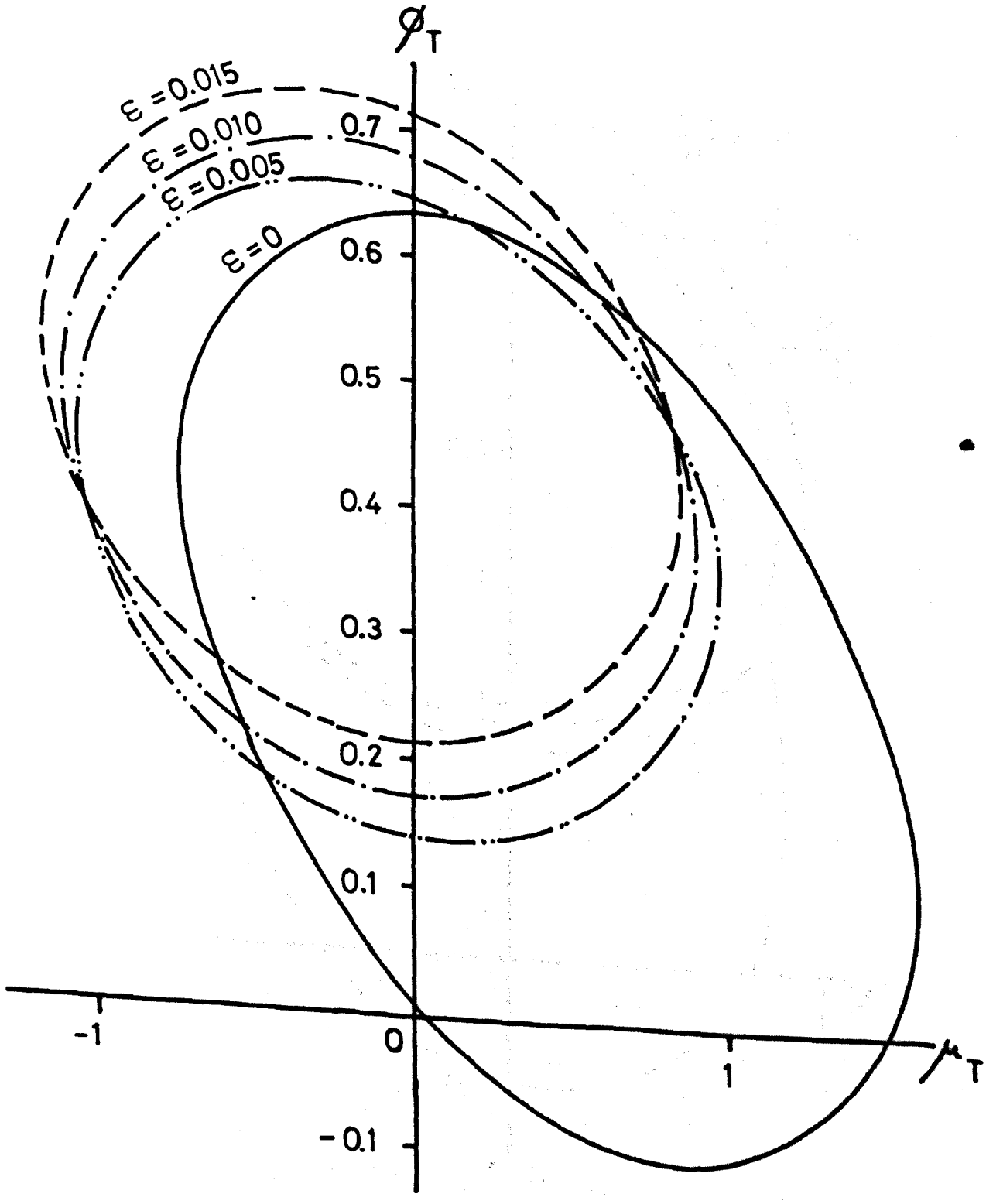

FIG 7.6 INTERACTION CURVES FOR STRAND WITH CORE WIRE WITH VARIOUS VALUES OF AXIAL EXTENSION.
(m=6 ; α=75° ; $R_{c/R}$=1.0)

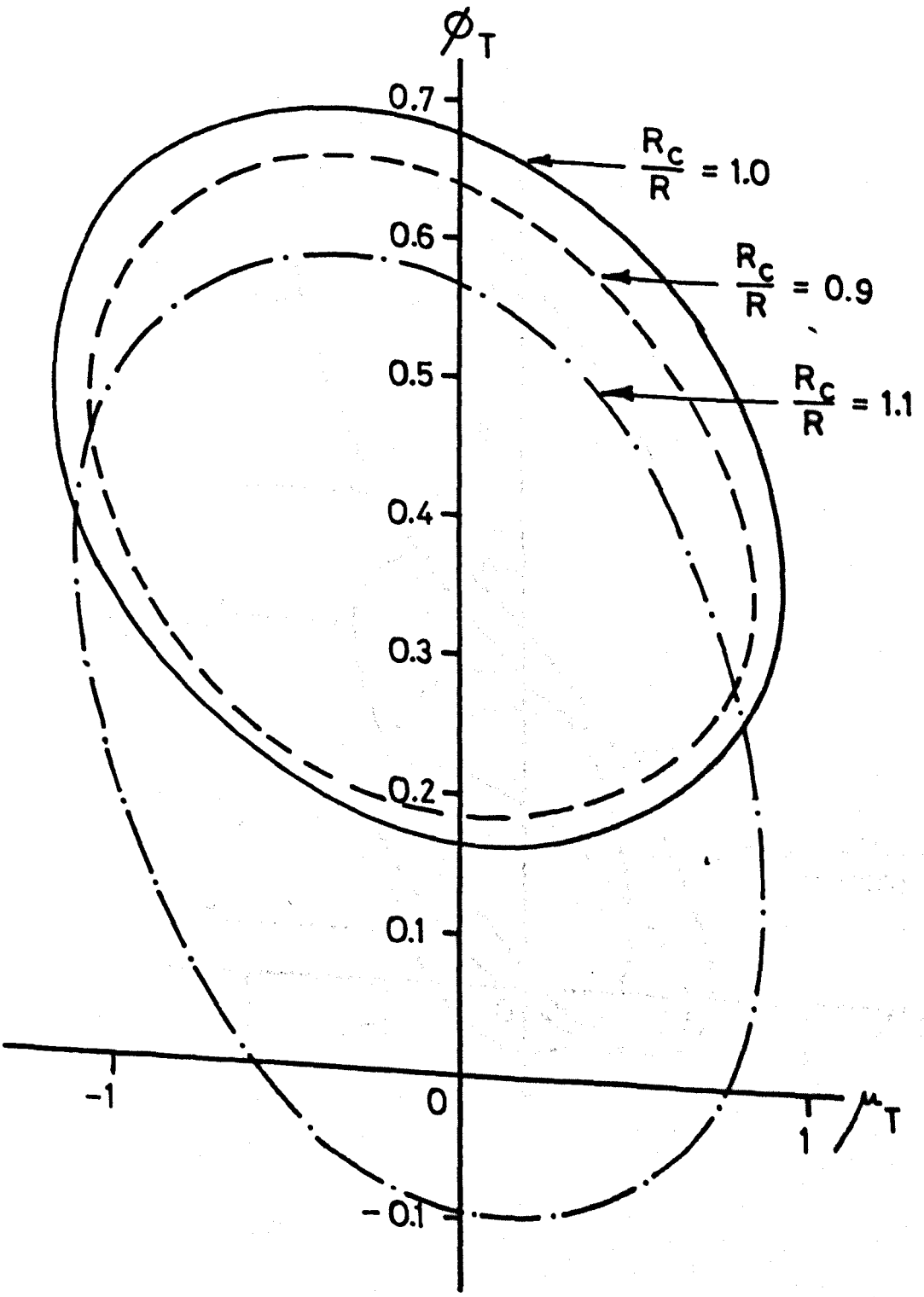

FIG 7.7 EFFECT OF CORE SIZE ON THE INTERACTION CURVES.
(m=6 ; α=75° ; ϵ=0.01)

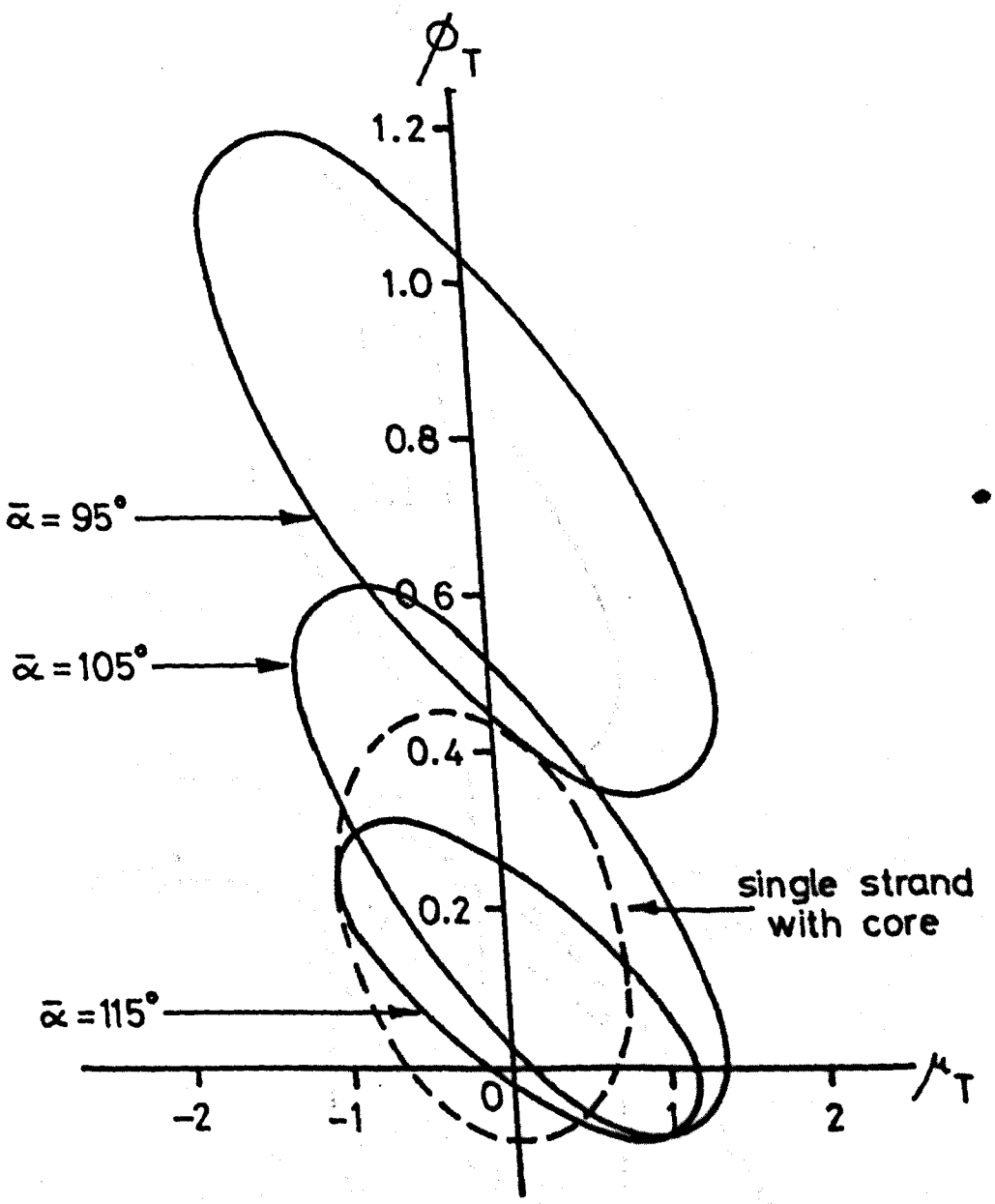

FIG 7.8 INTERACTION CURVES FOR ROPE WITH TWO LAYERS OF STRAND WHEN $\alpha=70°$ (FINITE EXTENSION).- WITH CORE WIRE

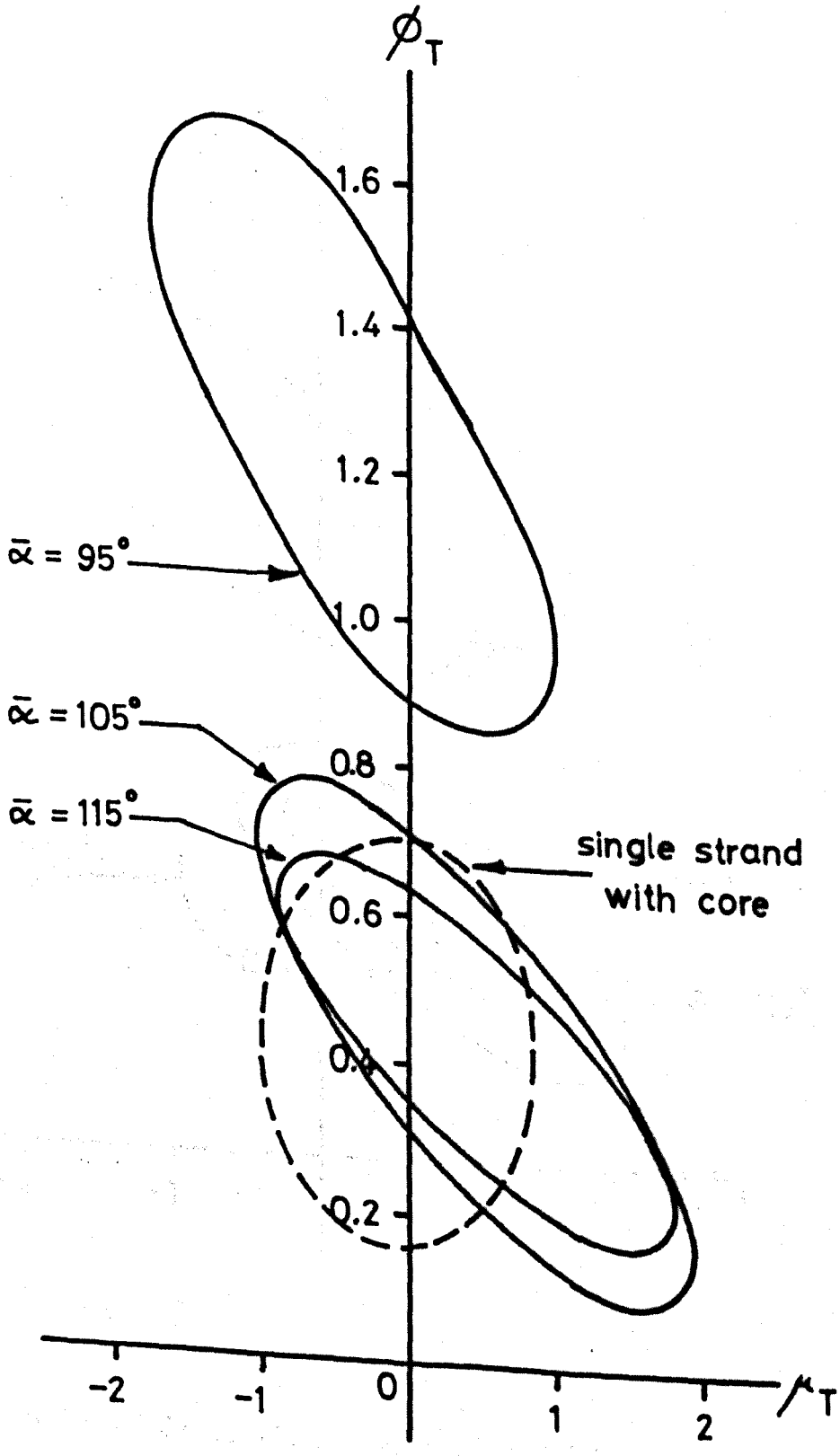

FIG 7.9 INTERACTION CURVES FOR ROPE WITH TWO LAYERS OF STRAND WHEN α=75° (FINITE EXTENSION).
- WITH CORE WIRE

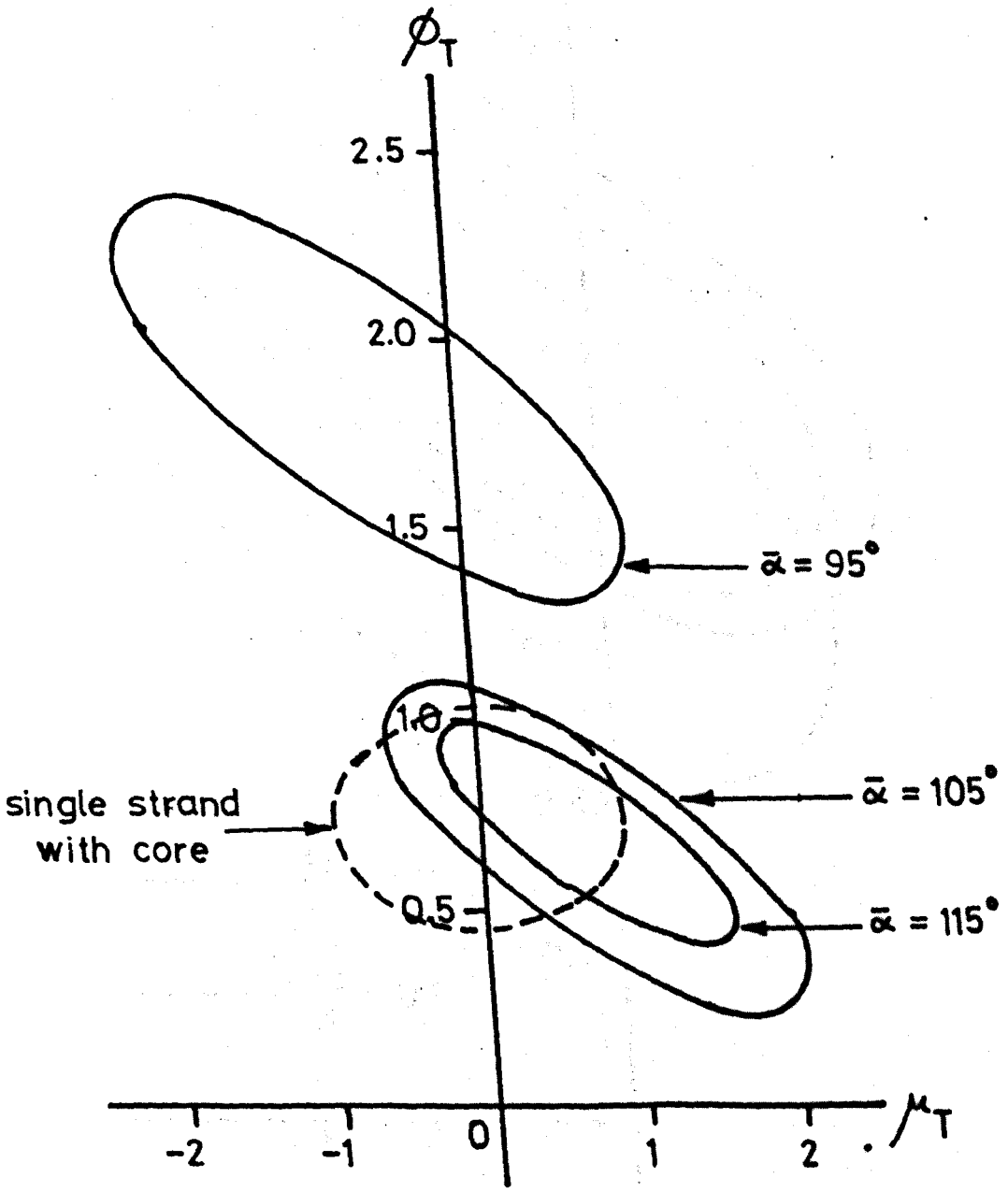

FIG 7.10 INTERACTION CURVES FOR ROPE WITH TWO LAYERS OF STRAND WHEN α=80° (FINITE EXTENSION).
- WITH CORE WIRE

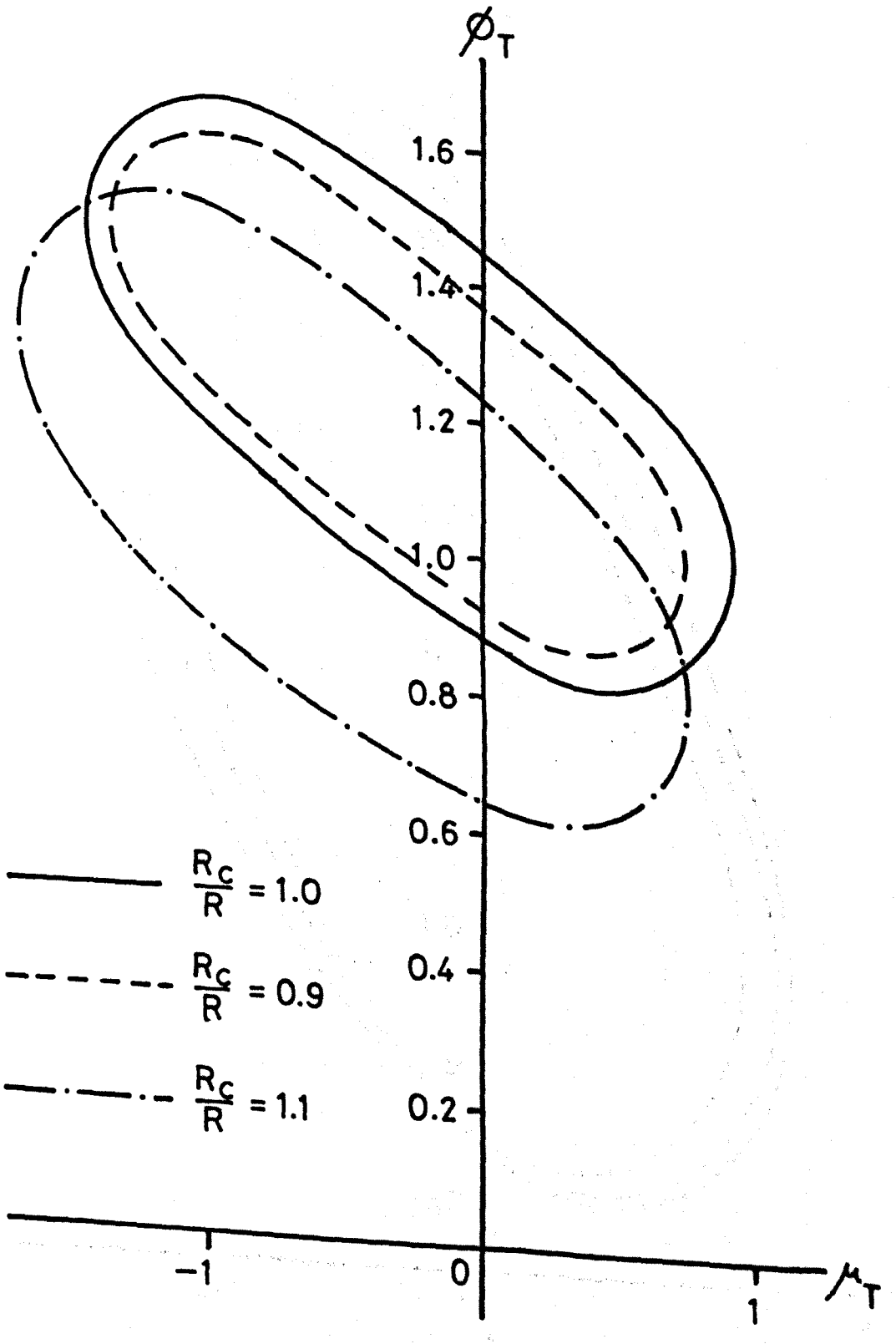

FIG 7.11 INTERACTION CURVES FOR ROPE WITH TWO LAYERS OF STRAND WITH VARIOUS CORE SIZES.
(α=75° ; $\bar{\alpha}$=95° ; $\bar{R}/R$=1.0 ; ϵ=0.01)

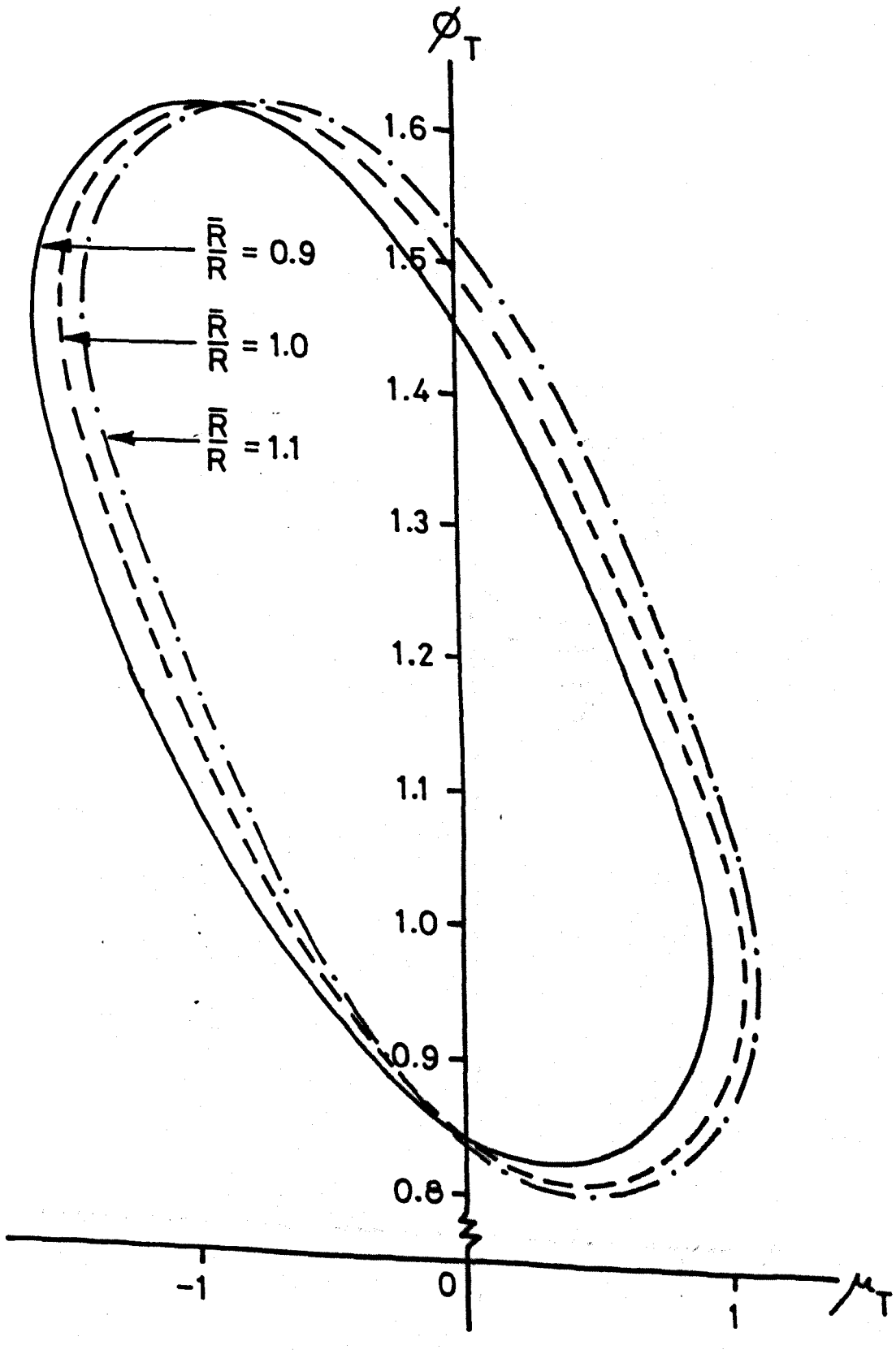

FIG 7.12 EFFECT OF DIFFERENT SIZE OF WIRES IN THE OUTER LAYER ON THE INTERACTION CURVES.
(α=75° ; $\bar{\alpha}$=95° ; R_c/R=1.0 ; ϵ=0.01)

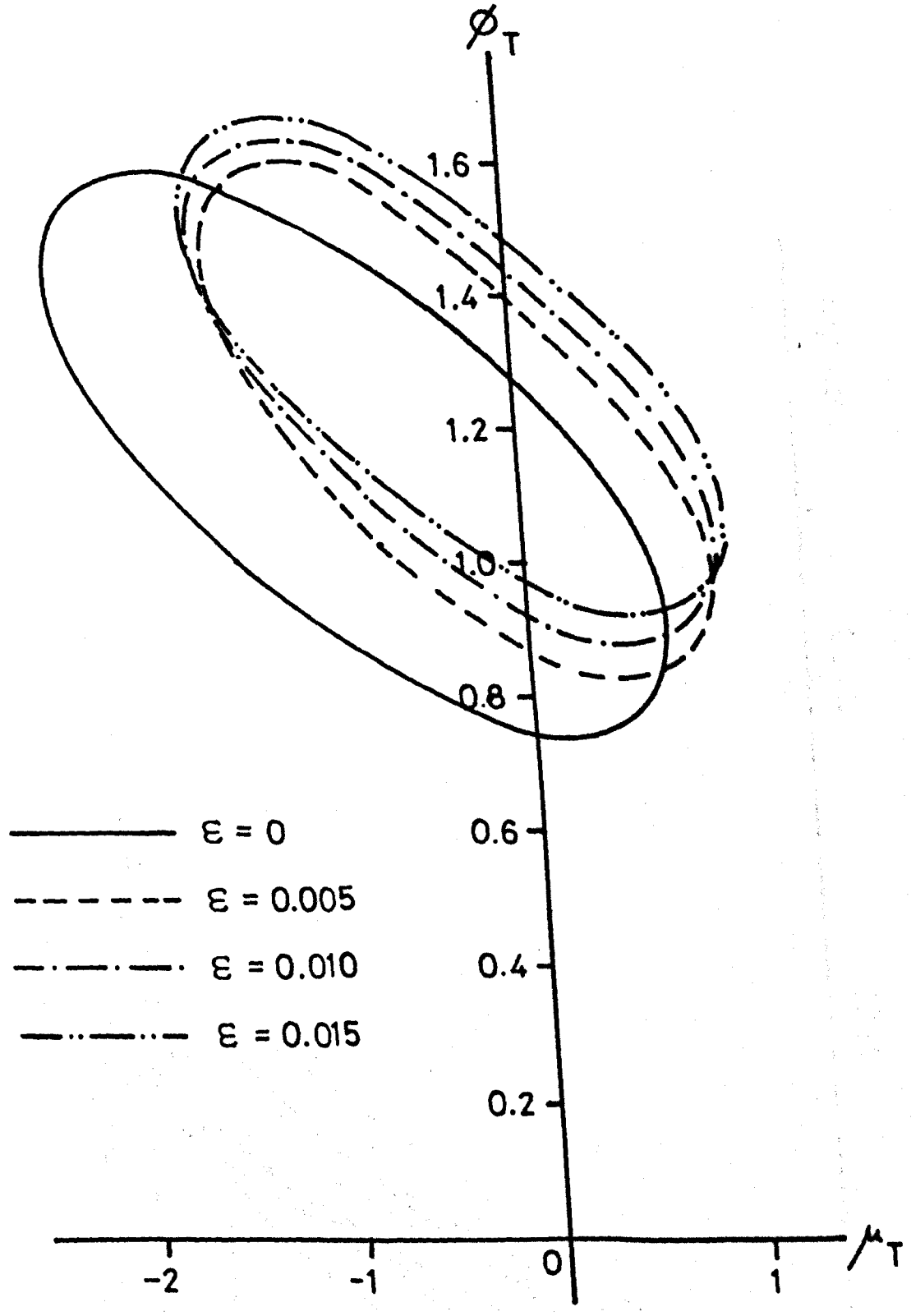

FIG 7.13 INTERACTION CURVES FOR VARIOUS VALUES OF AXIAL EXTENSION. (α=75° ; $\bar{\alpha}$=95° ; $\bar{R}/R$=1.0 ; R_c/R=1.0) - TWO LAYERS OF STRAND WITH CORE WIRE

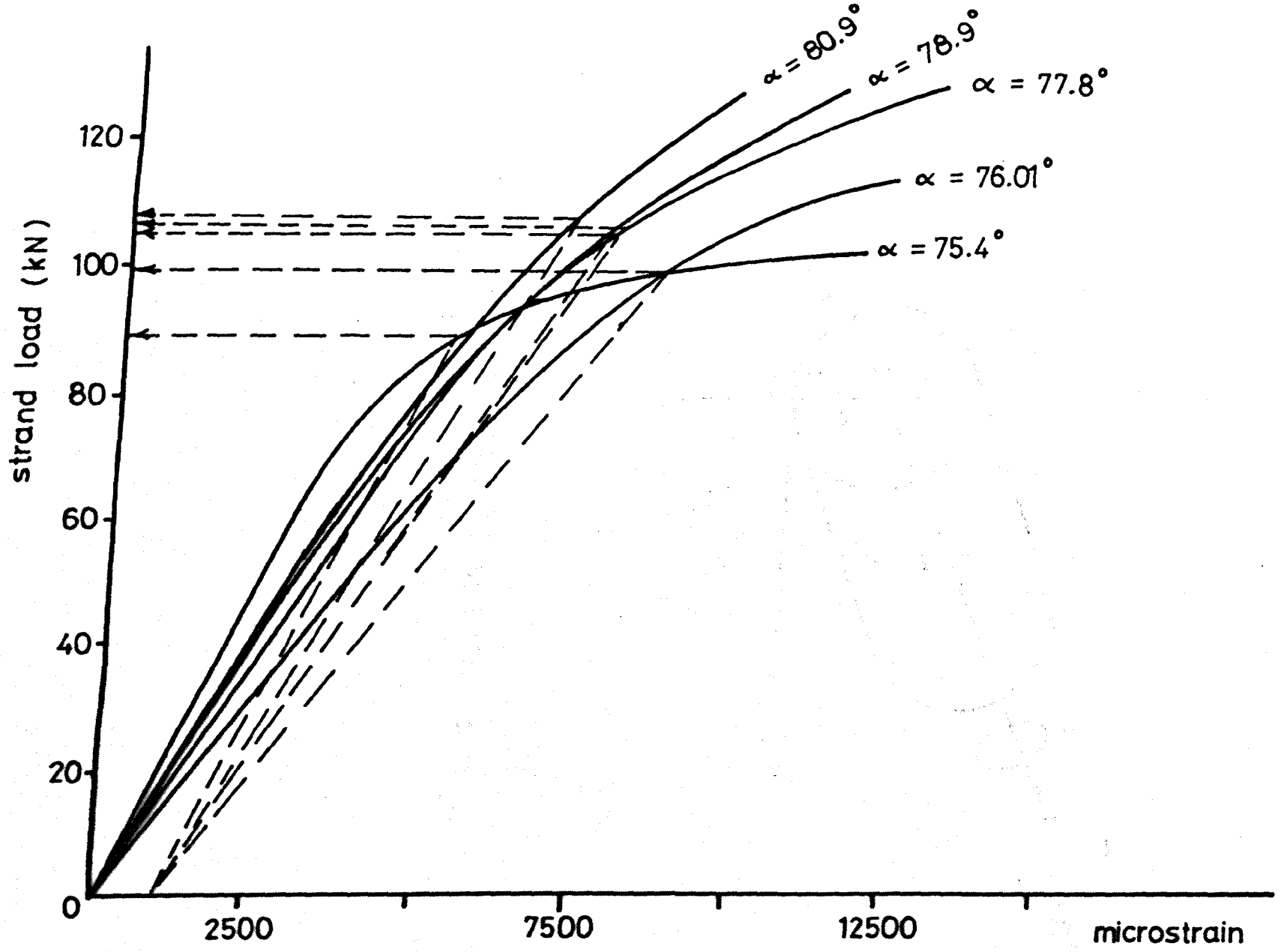

FIG 8.1 EXPERIMENTAL RESULT OBTAINED BY W.S UTTING(92)

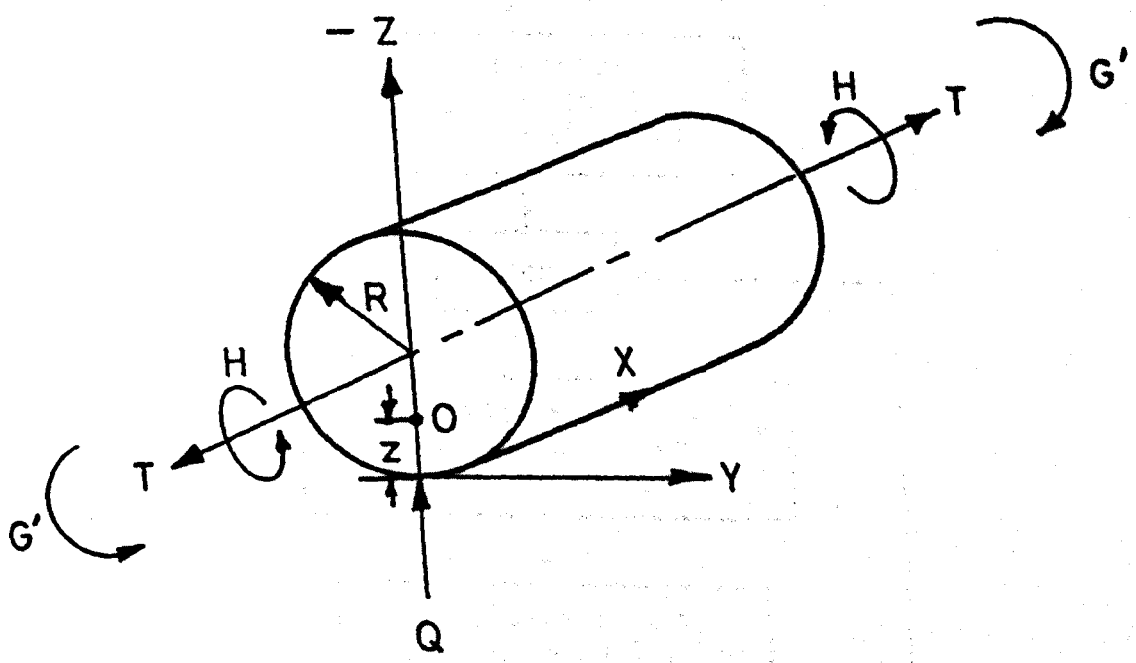

FIG 8.2 SECTION OF A WIRE ACTED UPON BY TENSION, BENDING, TORSION AND CONTACT.

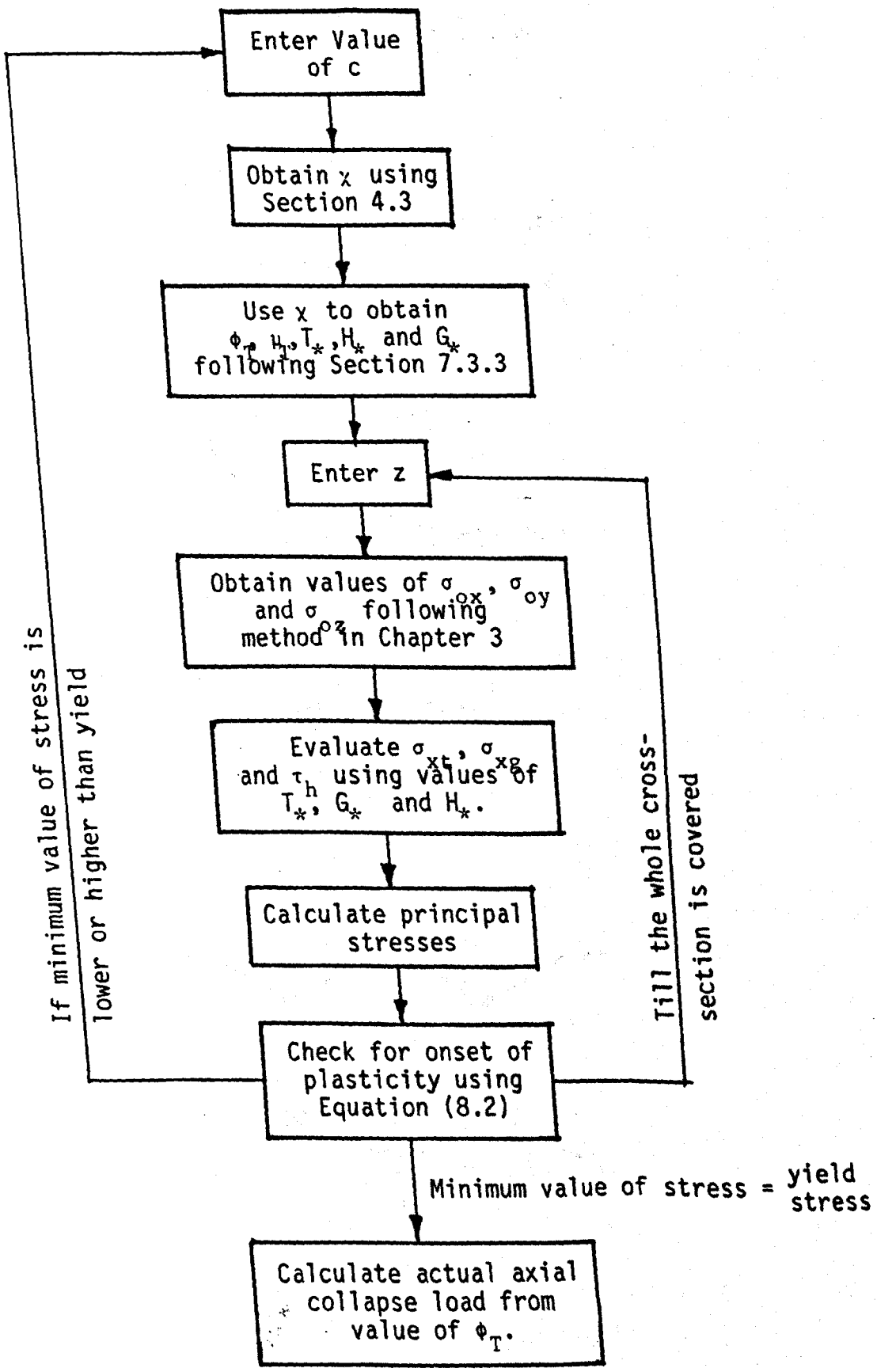

Fig 8.3 BLOCK DIAGRAM SHOWING PROCEDURE OF SOLUTION

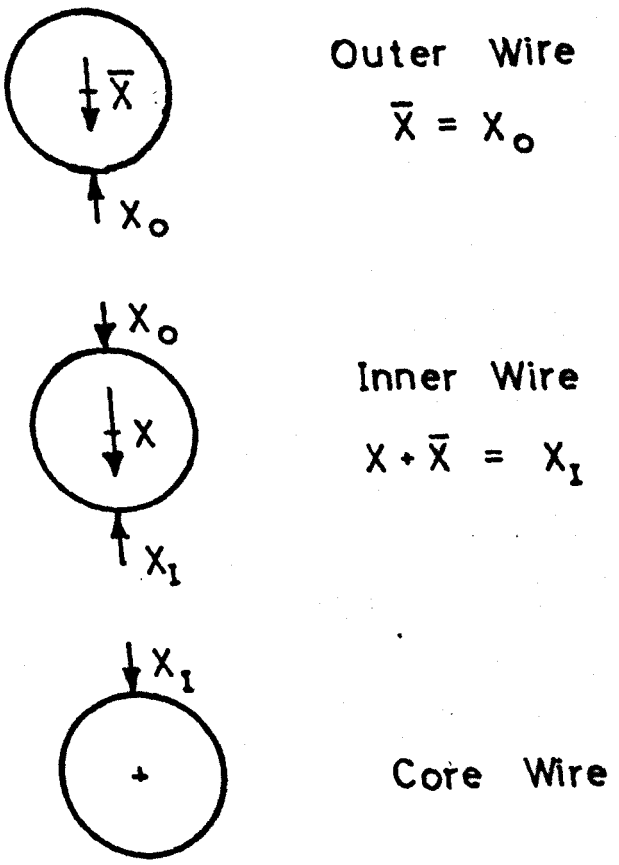

FIG 8.4 LINE LOAD DUE TO CONTACT IN WIRE ROPE WITH TWO LAYERS OF STRAND.

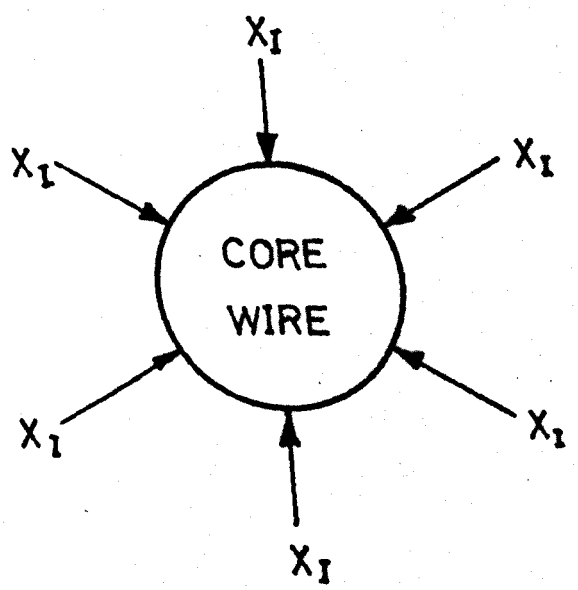

FIG 8.5 CONTACT FORCES EXPERIENCED BY THE CORE WIRE DUE TO CONTACT WITH WIRES IN THE INNER STRAND.